ARISTOTLE UNIVERSITY OF THESSALONIKI
SCHOOL OF ELECTRICAL AND COMPUTER ENGINEERING

STATIC AND DYNAMIC STOCHASTIC NEUTRONIC REACTOR ANALYSIS WITH THERMAL-HYDRAULIC FEEDBACK

DOCTORAL DISSERTATION

ANTONIOS G. MYLONAKIS

SUPERVISOR:
A. CLOUVAS
Professor

ATHENS, September 2017

ARISTOTLE UNIVERSITY OF THESSALONIKI
SCHOOL OF ELECTRICAL AND COMPUTER ENGINEERING

STATIC AND DYNAMIC STOCHASTIC NEUTRONIC REACTOR ANALYSIS WITH THERMAL-HYDRAULIC FEEDBACK

DOCTORAL DISSERTATION

ANTONIOS G. MYLONAKIS

ADVISORY COMMITTEE:
Prof. Clouvas A., Aristotle University of Thessaloniki
Dr Varvayanni M., National Centre for Scientific Research "Demokritos"
Prof. Grigoriadis D.G.E., University of Cyprus

EXAMINATION COMMITTEE:
Prof. Clouvas A., Aristotle University of Thessaloniki
Dr Varvayanni M., National Centre for Scientific Research "Demokritos"
Prof. Grigoriadis D.G.E., University of Cyprus
Dr Catsaros N., National Centre for Scientific Research "Demokritos"
Prof. Tsoukalas L., University of Thessaly
Prof. Stoulos S., Aristotle University of Thessaloniki
Prof. Dr Kodeli I., Jozef Stefan Institute

ATHENS, September 2017

Στους γονείς μου Γιώργο και Αρετή που σε «δύσκολους» καιρούς προσπάθησαν πολύ για να δώσουν στην κοινωνία αξιόλογους ανθρώπους.

ABSTRACT

Some of the most important challenges that the Monte-Carlo based analysis of the nuclear reactor core physics faces nowadays are the insertion of efficient thermal-hydraulic feedback, the extension of the Monte-Carlo method to the study of transient phenomena and the convergence acceleration of the algorithm that is utilised to analyse reactor criticality. These requirements are imposed by the fact that nuclear reactor analysis moves continuously towards a multiphysics direction with demands for higher and higher levels of accuracy combined with high computational cost-effectiveness. This thesis tries to meet these three challenges by suggesting algorithms which can cope with the encountered issues. The programming development of these algorithms along with their initial evaluation are presented and analysed. The results are encouraging showing numerical improvement and increase of the accuracy, as well as leading to the expansion of the current stochastic neutronics. Thus the present findings could contribute to the extension of the Monte Carlo approach for a more global and accurate analysis of the reactor core system with a reasonable computational cost.

"... There is no use burdening yourself with a lot of data.
Once you understand yourself, you understand
human nature and then the rest follows."

— Kurt Gödel

ACKNOWLEDGMENTS

I would like to thank my thesis supervisor Prof. Alexandros Clouvas for giving me the chance to perform this research under the supervision of the School of Electrical and Computer Engineering of the Aristotle University of Thessaloniki and for guiding and correcting this thesis.

I would like to express my gratitude to my thesis co-advisor Dr Melina Varvayanni, Research Director at the National Centre for Scientific Research Demokritos (NCSRD) and to Dr Nicolas Catsaros, Research Director and Head of the Nuclear Research Reactor Laboratory of the NCSRD. Without their guidance and their support, this thesis would not have been possible. They provided me with the necessary environment and tools to perform this research. Additionally, they gave me the chance to travel abroad and acquire a global and open-minded view of science as well as nuclear reactor physics in general.

Furthermore, I would like to express my sincere appreciation to the third member of my advisory committee Prof. Dimokratis G.E. Grigoriadis from the University of Cyprus for his guidance, his help and the useful discussions about scientific and general topics.

Many thanks must go to the members of the computational nuclear technology group of the NCSRD Reactor Laboratory, i.e. Dr Panagiota Savva, Ms Thalia Xenofontos and Ms Nefeli Chrysanthopoulou, for the scientific interaction we had during this period and for their contribution to the creation of a constructive and pleasant working environment.

In addition, I would like to thank Dr Victor Hugo Sanchez Espinoza and Dr Javier Jimenez Escalante from the Institute for Neutron Physics and Reactor Technology of the Karlsruhe Institute of Technology (KIT) for their hospitality in their laboratory, their guidance and cooperation during my four-month stay there.

Of course, I would like to thank my parents, Giorgos and Areti, who supported me in various ways during my studies. I want to thank my brothers Michael and Dimitris for the interesting and useful scientific as well as general discussions during this period.

Last but not least, I would like to express my deepest thank to Christina for her moral support and encouragement during a quite tough period of my life. Her support contributed significantly to the completion of this thesis.

CONTENTS

LIST OF FIGURES

LIST OF TABLES

ACRONYMS

ABN	Approximate Block Newton
BWR	Boiling Water Reactor
CMFD	Coarse Mesh Finite Difference
DR	Dominance Ratio
FA	Fuel Assembly
GMRES	Generalized Minimized Residuals
JFNK	Jacobian Free Newton Krylov
LCRNG	Linear Congruential Random Number Generator
LHS	Left Hand Side
MPI	Message Passing Interface
NRT	Nuclear Reactor Theory
NSKE	Neutron Spatial-Kinetics Equations
NTE	Neutron Transport Equation
NTT	Neutron Transport Theory
OS	Operator Splitting
PDE	Partial Differential Equation
PDEs	Partial Differential Equations
PDF	Probability Density Function
PI	Picard Iteration
PK	Point-Kinetics
PWR	Pressurized Water Reactor
RHS	Right Hand Side
RKE	Reactor Kinetics Equations
RNS	Random Number Sequence
SCF	SUBCHANFLOW
SI	Source Iteration
T-H	Thermal-Hydraulics
VRT	Variance Reduction Technique
XML	Extensible Markup Language

Part I

PROLOGUE

1

INTRODUCTION

Nowadays, the Monte-Carlo analysis of the static reactor core physics is the "bread and butter" for design and safety studies since it can provide a detailed treatment of the core physics in quite reasonable computational cost. The continuous increase of the available computational resources has contributed significantly towards this direction. However, since the demand for a more and more detailed and accurate analysis does not diminish, many scientific problems remain to be solved in this field, some of the most important being:

1. Multi-physics analysis - feedback from other involved physical fields, e.g. thermal-hydraulics, structural mechanics, etc., to the Monte-Carlo transport solution.
2. Dynamic Monte-Carlo neutron transport - pure Monte-Carlo simulation of dynamic neutronics.
3. Convergence acceleration of Monte-Carlo criticality - convergence acceleration of the k-eigenvalue Monte-Carlo source iteration.

These requirements are imposed by the fact that the nuclear reactor analysis moves continuously towards a multi-physical direction with demands for higher and higher level of accuracy combined with high computational cost-effectiveness. This thesis attempts to bring an answer the three problems mentioned above combining the proposal and use of suitable algorithms together with their programming development and their initial evaluation. An essential step is the development of algorithms for pure stochastic dynamic treatment since so far, Monte-Carlo has been involved in dynamics only within the framework of hybrid stochastic/deterministic schemes. Furthermore, the Thermal-Hydraulics (T-H) feedback is a strong requirement due to the strong bond between neutronic and T-H phenomena. However, the static T-H feedback requires special treatment compared with the dynamic one due to the particular nature of the Monte-Carlo k-eigenvalue algorithm. Finally, since Monte-Carlo k-eigenvalue analysis is crucial not only for the analysis of reactor statics but also for core material evolution (e.g. burnup analysis), convergence acceleration remains a significant challenge.

As a first step, this work investigates the insertion of T-H feedback to static Monte-Carlo. So far a "serial" iterative scheme that corresponds to a sequential execution of the involved solvers has been mainly used for the coupling of static Monte-Carlo with T-H. However, within the generalised context of computational physics it has been reported

that the "serial" scheme often fails to converge solution of the unified problem. Initially, a "serial" coupling scheme is developed to scout its behaviour and to validate it against third-party results. Thus, it can be utilised as a reference for comparison of the algorithm proposed by this research. After investigation of the above-mentioned problem, this research proposes the replacement of the previous scheme with an approximate Newton algorithm. The primary motivation for this approach is the interest for an algorithm that could maintain the distinct treatment of the involved fields within a tight coupling context. The selected method, called Approximate Block Newton (ABN), is a version of the Jacobian Free Newton Krylov (JFNK) method suitably modified for the coupling of distinct solvers. After the specification of the algorithmic features, this work investigates the behaviour of the proposed method when the open-source Monte-Carlo neutronics code OpenMC is coupled with the T-H code COBRA-EN, (a T-H code for sub-channel and core analysis) for integrated reactor core analysis utilising both the traditional and the proposed technique, respectively. The performance and the accuracy of the proposed coupling scheme are evaluated and compared with those of the traditional "serial" iterative scheme. The results show a significant numerical improvement that is strongly connected to more accurate results.

Secondly, this thesis investigates the development of a Monte-Carlo dynamic module for analysis of transient phenomena and its implementation in OpenMC. So far, very few attempts to employ the Monte-Carlo method to the analysis of reactor dynamics have been reported. Even more, most of those few attempts make use of several approximations, showing the existence of an open research field of great interest. A straightforward physical treatment of a transient problem requires the assessment of the temporal evolution of the simulated neutrons which is no present in static Monte-Carlo; however this is not adequate. In order to be able to properly analyse transient phenomena, the simulation of delayed neutrons together with other necessary extensions and modifications is needed. The selected method has been recently proposed in the literature and is here inserted in OpenMC following the code's features. Hence, an extra challenge that this work meets is the desire for an optimum embodiment in OpenMC minimising the necessary modifications and maximising the advantage resulting from its existing capabilities. Moreover, the addition of dynamic T-H feedback is investigated. The key points of the developed module as well as the results of the analysis of various numerical experiments are presented and discussed. The results confirm the successful development of the dynamic Monte-Carlo module pointing out its capability for the effective analysis of a variety of reactor core transients.

Finally, an attempt to accelerate the convergence of the Monte-Carlo classical Source Iteration (SI) is presented. Whereas the classical SI guarantees the convergence to the fundamental eigenmode, very often the convergence is slow. In this thesis, an alterna-

tive version of the traditional Monte-Carlo SI algorithm is formulated, developed and analysed aiming to numerically accelerate the Monte-Carlo criticality analysis. More specifically, the JFNK method is adopted in the Monte-Carlo k-eigenvalue context attempting to accelerate the convergence. However, the computationally burdensome nature of a Monte-Carlo algorithm makes a straight forward implementation of this method rather impossible. The problem is overcome by suitably utilising a deterministic diffusion-based SI within the developed algorithm. Since the stochastically derived quantities required by the introduced method are associated with statistical noise (a fact creating questions about the performance of this new concept), the method is initially evaluated in simplified test-cases and compared with the classical SI and the non-linear diffusion accelerated SI. The results are encouraging highlighting a significant potential for the numerical acceleration of the Monte-Carlo SI.

To summarise, the investigation performed in this thesis comprise: the extension of the Monte-Carlo approach to the analysis of dynamic reactor core problems, the insertion of T-H feedback to both statics and dynamics stochastic neutronics and the convergence acceleration of the Monte-Carlo SI. The findings are satisfactory and could contribute to the expansion of the Monte Carlo method for a more global and accurate tool for complete analysis of the reactor core system with a reasonable computational cost.

The organisation of this thesis follows the logic of stating a problem, analysing it and proposing solutions. Thus, the structure includes two levels of categorization of the material. The first/*higher* level comprises the *prologue*, the *problem statement*, the *solutions* and the *epilogue*. The second/lower level is a finer description of each part of the first level. More specifically, the *prologue* includes the introduction; the *problem statement* consists of the theoretical background, the description of the problems to be investigated and the objectives. The part *solutions* has for each problem the following form: state-of-the-art, the approach proposed after the investigation of the problem and numerical experiments for evaluation. Finally, the *epilogue* includes the summary, the conclusion and some ideas for future research.

Part II

PROBLEM STATEMENT

2

THEORETICAL BACKGROUND

The movement of microscopic particles through matter is called particle transport. The mathematical study of the transport of microscopic particles like neutrons, photons, electrons and molecules is called particle transport theory. Since the study of many scientific fields ends up to the study of the transport of microscopic particles, transport theory in general is an important field necessary in various branches of science and engineering. Some of the fields where transport theory plays a crucial role are nuclear reactor theory, astrophysics, plasma physics etc. (Duderstadt and Martin, 1979). Common feature of almost all particle transport problems is that their study leads to the formulation of the transport equation and the need for its solution. This equation is derived by the balance between the generated and the removed particles of interest in a volume.

The study of the behaviour of the neutron population within a medium of matter results in the formulation of the Neutron Transport Equation (NTE). At this point it should be mentioned that the description of the physics of the interaction of neutrons with nuclei is out of the scope of this work. Information on this topic can be found in Krane (1988) and Lamarsh (1966). Nuclear Reactor Theory (NRT) is the branch of science that deals with the study of the behaviour of neutrons in the reactor core by solving the NTE. However, the very complex nature of this equation has actually generated a scientific field called Neutron Transport Theory (NTT). Aim of this field is the solution of the NTE. The mathematical complexity of this equation is very often treated either replacing the original equation by approximate forms or utilising approximations on the solution of the original equation. One very important approximate form is the diffusion equation. However in this case it could be stated that the original nature of particle transport has been altered since now the neutrons diffuse instead of being transported. This simply means that the physical rules that determine the problem are not exactly the same. In addition the solution of NTE is very often achieved utilising stochastic techniques which simulate the physics described by NTE instead of solving the NTE in a mathematical way.

2.1 THE NEUTRON TRANSPORT EQUATION

The central problem of the NRT is to predict the distribution of neutrons in space, energy and time inside the reactor core. In principle this can be done by solving the NTE. This

equation is also called the Boltzmann equation because of its similarity to the expression obtained by L. Boltzmann while studying the kinetic theory of gases. The derivation of the neutron transport equation considers the balance between the generated and the removed neutrons inside a volume. The presentation of the NTE derivation is out of the scope of this work. The reader can find very extensive related information in Davison (1958), Bell and Glasstone (1970) and Duderstadt and Martin (1979).

2.1.1 *The integro-differential form*

One of the forms of the NTE with unknown the angular neutron flux ($\psi(\boldsymbol{r}, \boldsymbol{\Omega}, E)$) is the following:

$$\begin{aligned} \frac{1}{v(E)}\frac{\partial \psi(\boldsymbol{r}, \boldsymbol{\Omega}, E, t)}{\partial t} + \boldsymbol{\Omega} \cdot \nabla \psi(\boldsymbol{r}, \boldsymbol{\Omega}, E, t) + \Sigma_t(\boldsymbol{r}, E, t)\psi(\boldsymbol{r}, \boldsymbol{\Omega}, E, t) = \\ \iint \Sigma_s(\boldsymbol{r}; E', \boldsymbol{\Omega}' \rightarrow E, \boldsymbol{\Omega}; t)\psi(\boldsymbol{r}, E', \boldsymbol{\Omega}', t)d\boldsymbol{\Omega}' dE' \\ + \chi(E) \iint \nu(E')\Sigma_f(\boldsymbol{r}, E', t)\psi(\boldsymbol{r}, E', \boldsymbol{\Omega}', t)d\boldsymbol{\Omega}' dE' \\ + S_{ext}(\boldsymbol{r}, \boldsymbol{\Omega}, E, t) \end{aligned} \tag{2.1}$$

where

$\boldsymbol{r}$	point in $\mathbb{R}^3$ including the spatial coordinates
$\boldsymbol{\Omega}$	unit vector in $\mathbb{R}^3$ showing the direction of the neutron motion
ψ	angular flux connected with the total flux ϕ with the relation $\phi = \int_{4\pi} \psi d\Omega$
E	neutron energy
$\Sigma_t, \Sigma_s, \Sigma_f$	total, scattering and fission macroscopic cross-sections
ν	mean number of neutrons produced per fission
χ	fission energy distribution function
v	neutron speed
S_{ext}	external neutron source

$\Sigma_s(\boldsymbol{r}; E', \boldsymbol{\Omega}' \rightarrow E, \boldsymbol{\Omega}; t)$ expresses the macroscopic scattering cross section for a neutron energy E′ (and $\boldsymbol{r}$, t) times the probability that the scattered particle will change direction from $\boldsymbol{\Omega}'$ to $\boldsymbol{\Omega}$ and energy from E′ to E. The first term of this equation represents the change of the angular flux in time. The second term indicates the net leakage of neutrons from the system whereas the third term represents the number of collisions. The fourth is the scatter-in term, i.e., indicates the neutrons that are scattered in the volume,

the fifth term corresponds to the neutron production by fission events and the last term describes any external neutron source of the system. Eq. (2.1) is an integro-differential equation and is called the three-dimensional, time-dependent, energy-dependent, angle-dependent neutron transport equation, or the 3-D neutron transport equation for short.

2.1.1.1 *Boundary conditions*

The NTE is associated with spatial and temporal boundary conditions. More specifically the spatial boundary conditions of the form:

$$\psi(\boldsymbol{r}, \boldsymbol{\Omega}, E, t) = \tilde{\psi}(\boldsymbol{r}, \boldsymbol{\Omega}, E, t)$$

are utilised where $\boldsymbol{n} \cdot \boldsymbol{\Omega} < 0$ where n is the outward directed vector normal to the surface at the point $\boldsymbol{r}$. Some examples of the usually used boundary conditions are the following:

1. Known surface source
2. Vacuum boundary condition (no incoming neutrons)
3. Reflective boundary condition

In addition, an initial boundary condition must be used. This has the following form:

$$\psi(\boldsymbol{r}, \boldsymbol{\Omega}, E, 0) = \psi(\boldsymbol{r}, \boldsymbol{\Omega}, E)$$

More information about the boundary conditions that accompany the NTE can be found in Bell and Glasstone (1970).

2.1.2 *The integral form*

As mentioned above, Eq. (2.1) is an integro-differential equation. In this paragraph the integral form of the NTE will be given. A pure differential form does not exist as explained in Bell and Glasstone (1970). The integral form can be obtained by the integro-differential form of the NTE with the method of characteristics since it is a linear Partial Differential Equation (PDE) of first order. However it can also be obtained directly from neutron conservation considerations. A very explanatory derivation of the integral NTE can be found in Davison (1958).

The integral NTE with cross-sections constant over time is given by Eq. (2.2):

$$\psi(\boldsymbol{r}, \boldsymbol{\Omega}, E, t) = \int_0^{\infty} e^{-\int_0^s \Sigma(\boldsymbol{r}-s''\boldsymbol{\Omega}, E)\, ds''} q(\boldsymbol{r} - s'\boldsymbol{\Omega}, \boldsymbol{\Omega}, E, t - \frac{s'}{v}) ds' \tag{2.2}$$

where

$$q(\boldsymbol{r}, \boldsymbol{\Omega}, E, t) = \iint \Sigma(\boldsymbol{r}; E', \boldsymbol{\Omega}' \to E, \boldsymbol{\Omega}) \psi(\boldsymbol{r}, E', \boldsymbol{\Omega}', t) d\boldsymbol{\Omega}' dE' + S_{ext}(\boldsymbol{r}, \boldsymbol{\Omega}, E) \tag{2.3}$$

Eq. (2.2) implies that the flux at point $\boldsymbol{r}$ and time t is the sum of neutrons which appeared in the direction $\boldsymbol{\Omega}$ and energy E at all other possible positions $\boldsymbol{r} - s'\boldsymbol{\Omega}$ for all previous time moments $t - \frac{s'}{v}$ multiplied by the exponential attenuation factor. s is the distance of a neutron travelling along the direction $\boldsymbol{\Omega}$ and v is the neutron speed. Further, if the explicit form of q, as given by Eq. (2.3), is introduced into equation Eq. (2.2), it may result in:

$$\psi = \boldsymbol{K}\psi + q' \tag{2.4}$$

where $\boldsymbol{K}$ is the integral operator and q' is a known function assuming that S_{ext} is known. Eq. (2.4) is of the following form:

$$f(\boldsymbol{x}) = Q(\boldsymbol{x}) + \int K(\boldsymbol{x}', \boldsymbol{x}) f(\boldsymbol{x}') dx' \tag{2.5}$$

where $\boldsymbol{x}$ is a point in a multidimensional space, f is a multidimensional function to be determined, Q the source term and $K(\boldsymbol{x}', \boldsymbol{x})$ is the non-negative integral kernel. This is a Fredholm equation of 2nd kind. The solution of this type of equation can be expanded into Neumann series:

$$f = \sum_{i=0}^{\infty} f_i \tag{2.6}$$

where

$$f_0 = q'$$

$$f_{i+1} = \boldsymbol{K} f_i \ , \ i \geqslant 0$$

From this point of view, f_0 is the angular flux of neutrons that have not experienced collisions yet, i.e., the uncollided neutrons that have been introduced by the external source, f_1 is the flux of the neutrons that have been experienced only one collision etc. If Eq. (2.6) converges, it represents a solution to Eq. (2.5). This property is used within the Monte-Carlo method for the solution of Eq. (2.2).

2.1.3 *The k-eigenvalue form*

One of the most important forms of the NTE is the *k*-eigenvalue static (steady-state) form that is associated with the criticality problem. This is one of the focal NRT problems and includes the determination of the *k*-eigenvalue (k_{eff}) that shows the mutliplying nature

of a neutronic system, defining the system as critical (k_{eff} =1), subcritical ($k_{eff} < 1$) or supercritical ($k_{eff} > 1$). The *k*-eigenvalue static form of the integro-differential NTE is:

$$\boldsymbol{\Omega} \cdot \nabla\psi(\boldsymbol{r}, \boldsymbol{\Omega}, E) + \Sigma_t(\boldsymbol{r}, E)\psi(\boldsymbol{r}, \boldsymbol{\Omega}, E) = \iint \Sigma_s(\boldsymbol{r}; E', \boldsymbol{\Omega}' \rightarrow E, \boldsymbol{\Omega})\psi(\boldsymbol{r}, E', \boldsymbol{\Omega}')d\boldsymbol{\Omega}'dE' + \frac{\chi(E)}{k_{eff}} \iint \nu(E')\Sigma_f(\boldsymbol{r}, E')\psi(\boldsymbol{r}, E', \boldsymbol{\Omega}')d\boldsymbol{\Omega}'dE' \tag{2.7}$$

It should be mentioned that also the integral form of the NTE has a *k*-eigenvalue form given in § 2.3.2.

2.1.4 *The spatial-kinetic form*

Eq. (2.1) is a time-dependent equation. However that form does not reflect an important feature that plays crucial role in the time-dependent behaviour of the reactor core, i.e., the separation of the fission generated neutrons in prompt and delayed. This means that some of the fission neutrons, the delayed ones, are not generated immediately but with a time-delay after the fission event. This effect is determining for the reactor core behaviour since it enables the control of the reactor with mechanical devices. More information about this topic can be found in Bell and Glasstone (1970). When this feature is taken into account, the NTE takes the form given by Eq. (2.8) and Eq. (2.9):

$$\begin{aligned} \frac{1}{v(E)}\frac{\partial\psi(\boldsymbol{r}, \boldsymbol{\Omega}, E, t)}{\partial t} + \boldsymbol{\Omega} \cdot \boldsymbol{\nabla}\psi(\boldsymbol{r}, \boldsymbol{\Omega}, E, t) + \Sigma_t(\boldsymbol{r}, E, t)\psi(\boldsymbol{r}, \boldsymbol{\Omega}, E, t) = \\ \iint \Sigma_s(\boldsymbol{r}; E', \boldsymbol{\Omega}' \rightarrow E, \boldsymbol{\Omega}; t)\psi(\boldsymbol{r}, E', \boldsymbol{\Omega}', t)d\boldsymbol{\Omega}'dE' \\ + \chi_p(E)(1 - \beta(E'))\iint \nu(\boldsymbol{r}, E')\Sigma_f(\boldsymbol{r}, E', t)\psi(\boldsymbol{r}, E', \boldsymbol{\Omega}', t)d\boldsymbol{\Omega}'dE' \\ + \sum_j \lambda_j C_j(\boldsymbol{r}, t)\chi_{d,j}(E) + S_{ext}(\boldsymbol{r}, \boldsymbol{\Omega}, E, t) \end{aligned} \tag{2.8}$$

$$\frac{\partial C_j(\boldsymbol{r}, t)}{\partial t} + \lambda_j C_j(\boldsymbol{r}, E) = \iint \beta_j(E')\nu(\boldsymbol{r}, E')\Sigma_f(\boldsymbol{r}, E', t)\psi(\boldsymbol{r}, E', \boldsymbol{\Omega}', t)d\boldsymbol{\Omega}'dE' \tag{2.9}$$

where C is the concentration of the neutron precursors, λ is the precursor decay constant, β is the fraction of the delayed fission neutrons and χ_d is the fission energy distribution function for the delayed neutrons. These variables are associated with the index j which indicates that the neutron precursor particles are separated into distinct groups. The group separation aims to a more practical numerical treatment of the precursors; it would be impossible to handle each precursor particle with its own concentration, decay constant etc. since there are a few hundreds of different ones. Eqs (2.8 and 2.9) are called the Neutron Spatial-Kinetics Equations (NSKE) and provide an exact description of the evolution of the angular flux with time taking into account the delayed neutrons.

An analytical solution of the NTE cannot be achieved in most realistic cases. For this reason the NTE is solved using numerical techniques. In principle the NTE could be solved with straight-forward numerical methods, i.e., through replacing derivatives by finite differences etc. However the complex NTE nature arising form the complex physics of the problem in combination with the complex geometries of the nuclear systems make a straight-forward numerical solution almost impossible. For this reason, the deterministic numerical approach for solving the NTE needs significant approximations. These approximations could be classified in two (2) categories; approximations in physics and numerical approximations. Both categories of approximations aim at the end to reduce the required numerical effort. The first category simplifies the physics and consequently may change the original character of the problem, e.g., diffusion instead of neutron transport. On the other hand, numerical approximations mainly concern the discretization of the phase space of the solution. Very often the discretization is quite coarse leading to significant truncation errors.

Another fundamentally different numerical technique that is employed in the NTE solution is the Monte-Carlo method. The Monte-Carlo method is based on the statistical nature of the evolution of a large population of neutrons and simulates the actual physics that gives rise to the NTE instead of literally solving the NTE. The main advantage of the Monte-Carlo method is that it can treat the geometry and the physics of the problem in a very detailed way. The Monte-Carlo calculated parameters are not associated with truncation error. However they are related with statistical error.

2.2.1 *Deterministic approach*

Deterministic methods are characterized by the NTE discretization in order to obtain an algebraic system of equations with the scalar fluxes as unknowns. A review of deterministic methods is given by Lewis and Miller (1993). One of the primary limitations in deterministic methods is the number of unknowns that can be stored in memory. An important consequence of this limitation is that it creates constraints to the grid resolution. Because the coarser the grid the higher the discretization error, the limitations in the available computer memory may limit the accuracy of deterministic calculations.

The discretization of the NTE concerns geometry, angle, energy and time. The treatment of the NSKE form of the NTE will be described later. The spatial discretization of the NTE consists of the division of the system into a structured or unstructured grid. Very often

the materials that compose a part of the geometry are homogenized in order to reduce the number of spatial unknowns.

The angular treatment is generally performed utilising two different techniques. The P_n method is based on the expansion of the flux in n spherical harmonic functions while the S_n method is based on the discretization of the continuous angular direction to a finite number (n) of discrete directions. The general principle of the P_n method is that the angular dependence of the flux is expanded in a complete set of elementary functions, such as a series of polynomials. Then the flux in NTE is replaced by this expansion and the calculation of the angular dependence is reduced to the calculation of the expansion coefficients. These coefficients determine how much of each polynomial participates to the construction of the function of the flux angular dependence.

In addition an approximation in physics of the problem, called the diffusion approximation, can be used in order to alleviate the need for angular discretization. The diffusion theory is based on the approximation that neutrons' motion is described by Fick's law:

$$\boldsymbol{J} = D\boldsymbol{\nabla}\phi \tag{2.10}$$

where $\boldsymbol{J}$ is the neutron current, D is the diffusion coefficient and ϕ is the total neutron flux. Fick's law states that neutrons diffuse from regions of higher to regions of lower neutron flux. The diffusion equation has the following form:

$$\frac{1}{v(E)}\frac{\partial\phi(\boldsymbol{r},E,t)}{\partial t} = D\nabla^2\phi(\boldsymbol{r},E,t) - \Sigma_\alpha\phi(\boldsymbol{r},E,t) + s_{ext}(\boldsymbol{r},E,t) \tag{2.11}$$

The diffusion approximation is identical to the P_1 method since P_1 means that the angular dependence of the flux in NTE is expanded in only two terms, i.e., the total flux (ϕ) and the current ($\boldsymbol{J}$).

The discretization of energy concerns the transformation of the continuous dependence on energy to a discretized one. For this purpose the multigroup approximation is used. According to the multigroup approximation the energy range is separated into energy groups. Consequently, the continuous energy cross sections should be condensed over each group utilising a weighting function. In order to rigorously preserve reaction rates, the exact angular flux must be applied as the weighting function. This technique eliminates the energy dependence of the cross section but introduces the angular dependence of the resulting multigroup cross section:

$$\Sigma_{t,g}(\boldsymbol{r},\boldsymbol{\Omega}) = \frac{\int_{E_g}^{E_{g-1}}\Sigma_t(\boldsymbol{r},E)\psi(\boldsymbol{r},\boldsymbol{\Omega},E)dE}{\int_{E_g}^{E_{g-1}}\psi(\boldsymbol{r},\boldsymbol{\Omega},E)dE} \tag{2.12}$$

However $\psi(\boldsymbol{r},\boldsymbol{\Omega},E)$ is not known a priori since it is the quantity to be calculated. In addition the angle-dependent collapsed multi-group cross sections cannot be used into

conventional deterministic code frameworks (Lewis and Miller, 1993). For this reason the angular flux weighting function is in practice replaced by an approximate spectrum function, W(E). This function is obtained by preliminary simplified calculations. As a result the cross-sections are condensed as following:

$$\Sigma_{t,g} = \frac{\int_{E_g}^{E_{g-1}} \Sigma_t(E) W(E) dE}{\int_{E_g}^{E_{g-1}} W(E) dE} \tag{2.13}$$

The proper dynamic neutronic analysis concerns the solution of the NSKE. This equation could be solved in a straight forward numerical way replacing the derivatives with finite differences. However the complex nature of the NSKE makes a straight-forward numerical solution almost impossible. This could be noted by roughly estimating the number of unknowns that would be involved in the straight-forward numerical solution of Eqs (2.8 and 2.9). More specifically, a typical discretization of the NSKE would require about $10^3 \times 10^3 \times 10^2$ spatial cells, 50 directions for the angle of neutron's movement, 20 energy groups and about 10^3 temporal steps of about 0.01 s each. Consequently one obtains a number of variables of the order of 10^{11}. Therefore arises the need for significant simplification of the temporal dependence of the flux within NSKE. A very popular approach is the factorization of the flux to an amplitude factor and a flux shape factor:

$$\psi(\boldsymbol{r}, \boldsymbol{\Omega}, E, t) = P(t) s(\boldsymbol{r}, \boldsymbol{\Omega}, E, t) \tag{2.14}$$

where P is the amplitude and $\boldsymbol{s}$ is the spatial distribution of the flux or the shape factor. After some manipulation (Bell and Glasstone, 1970) where also the adjoint flux $\psi^\dagger$ is involved, the NSKE takes the form:

$$\frac{dP(t)}{dt} = \frac{\rho(t) - \beta(t)}{\Lambda(t)} P(t) + \sum_j \lambda_j(t) C_j(t) \tag{2.15}$$

$$\frac{dC_j(t)}{dt} = \frac{\beta_j(t)}{\Lambda(t)} P(t) - \lambda_j(t) C_j(t) \tag{2.16}$$

The formal mathematical definition of all the involved parameters ($\rho(t)$, $\beta_j(t)$, $\beta(t)$, $\Lambda(t)$, $C_j(t)$, $\lambda_j(t)$) according to the derivation of these equations is given in Bell and Glasstone (1970). At this point it should be mentioned that these parameters are somewhat arbitrary. Their physical meaning is also described by Bell and Glasstone (1970). Here it can be mentioned that under some circumstances their meaning is:

ρ	reactivity of the system
β_j	effective (adjoint-weighted) delayed neutron fraction of the j_{th} precursor group
β	total effective (adjoint-weighted) delayed neutron fraction
Λ	effective mean generation time
C_j	effective number of delayed-neutron precursors of the jth group
P	total neutron population

Eqs (2.15 and 2.16) are the Reactor Kinetics Equations (RKE).

No approximations have been made so far in deriving the RKE. However, the development is purely formal only if the flux shape factor can be found for the evaluation of the exact definition of the parameters involved in Eqs (2.15 and 2.16), i.e, ρ, β_j, β, Λ, C_j and P. The exact equation which is satisfied by the shape factor is the following:

$$\begin{aligned}\frac{1}{v(E)}\left[\frac{\partial s}{\partial t}+\frac{1}{P(t)}\frac{P(t)}{dt}s\right]+\boldsymbol{\Omega}\cdot\boldsymbol{\nabla}s+\Sigma s=&\\ &\iint\sum_{x\neq f}\Sigma_x f_x s'\,d\boldsymbol{\Omega}'\,dE'\\ &+\frac{Q}{P(t)}\\ &+\chi_p(E)\iint(1-\beta)\nu(E')\Sigma_f s'\,d\boldsymbol{\Omega}'\,dE'\\ &+\frac{Q_d(\boldsymbol{r},\boldsymbol{\Omega},E,t)}{P(t)}\end{aligned}\tag{2.17}$$

where

$$Q_d=\int_{-\infty}^{t}\iint\nu\Sigma_f(\boldsymbol{r},E',t')P(t')s(\boldsymbol{r},\boldsymbol{\Omega}',E',t')\sum_j\beta_j\chi_{d,j}\lambda_j e^{-\lambda_j(t-t')}\,d\boldsymbol{\Omega}'dE'dt \tag{2.18}$$

where $s'=s(\boldsymbol{r},\boldsymbol{\Omega}',E',t')$. Eqs (2.17 and 2.18) together with Eqs (2.15 and 2.16) constitute a system equivalent to the NSKE. Now, in order to achieve the initial goal of this approach, i.e. the simplification of the NSKE, one of the following approximations regarding the treatment of the shape factor during the solution of the RKE is usually applied.

1. **Point-reactor model** - time-independent shape function.

$$\psi(\boldsymbol{r},\boldsymbol{\Omega},E,t)=P(t)s(\boldsymbol{r},\boldsymbol{\Omega},E) \tag{2.19}$$

2. **Adiabatic approximation** - when the power changes are sufficiently slow, e.g. in xenon and burn-up problems, the time derivatives in Eq. (2.17) can be neglected along with the time variations of P and s in computing the Q_d delayed neutron source. Thus the delayed neutron source is combined with the prompt neutron source and a *k*-eigenvalue calculation can be utilised for the determination of the shape factor at any particular time. This procedure is applicable for sufficiently slow time variations of the reactor power or neutron flux.
3. **Quasi-static approximation** - an improved form of the previous approximation that takes into account the sluggishness of the delayed-neutron precursors in changing the shape factor. In this case Q_d is calculated by Eq. (2.17) and inserted in Eq. (2.18) setting $\frac{1}{v(E)}\frac{\partial s}{\partial t} = 0$. The quantity $P(t)\frac{\partial P(t)}{dt}$ can then be taken from the solution of Eq. (2.17) for the last of a series of time intervals. Accurate shape factors have been obtained by this approximation even for severe space-dependent transients.

This very brief discussion about deterministic methods was made here mainly in order to highlight the substantial number of approximations that are applied in almost every derivation stage of deterministic models as well as in the their numerical solution.

2.2.2 *Stochastic (Monte-Carlo) approach*

The physical process by which a population of particles evolves over time is governed by a number of probability distributions. For instance given a particle travelling through some material, there is a probability distribution for the distance it will travel until its next collision. Then for each collision, there is an associated probability for each possible reaction that could happen with that nucleus. While the behaviour of any single particle is unpredictable, the average behaviour of a large population of particles originating from the same source is well defined. If the above mentioned probability distributions that govern the transport of a particle are known, the process of single particles randomly streaming and colliding with nuclei can be simulated directly using a technique known as Monte Carlo simulation. Because the probability distributions are known from scientific measurements, Monte-Carlo neutronic simulation is possible and nowadays constitutes the most popular tool in the analysis of reactor neutronics. More information can be found in the next section.

2.3 THE MONTE-CARLO METHOD FOR SOLVING THE NEUTRON TRANSPORT EQUATION

The whole work in this thesis is based on Monte-Carlo. Thus one would expect to start this paragraph with the definition of Monte-Carlo. In fact it seems that the term *random* is the only word obligatorily contained in all definitions as Lux and Koblinger (1991) notice. They also suggest one description/definition which (although probably not sufficient) is the following: "*In all applications of the Monte-Carlo method a stochastic model is constructed in which the expected value of a certain random variable is equivalent to the value of a physical quantity to be determined. This expected value is then estimated by the average of several independent samples representing the random variable introduced above. For the construction of the series of independent samples, random numbers following the distributions of the variable to be estimated are used.*"

2.3.1 *Fundamentals of Monte-Carlo for neutron transport*

If p(x) is the Probability Density Function (PDF) of a variable x, $a \leqslant x < b$,

$$\rho = P(x) = \int_a^x p(x)dx \tag{2.20}$$

$$x = P^{-1}(\rho) \tag{2.21}$$

This means that x falls with a frequency p(x)dx within the interval and x + dx. In other words if p_i where i = 1,2,...,n are independent random numbers then the $x = P^{-1}(\rho)$ values are independent realizations of the x random variable. This is actually the basic principle behind Monte-Carlo, i.e., knowing the PDF, the expected value can be calculated using random numbers. As just mentioned heart of the Monte-Carlo method is the generation of random numbers. More specifically the sampling of any probability distribution is based on sampling one or more random numbers uniformly distributed (or equi-distributed) over the interval (0,1) with PDF:

$$p(\xi) = \begin{cases} 1, \xi \in 0 \leqslant \xi < 1 \\ 0, \text{otherwise} \end{cases} \tag{2.22}$$

with expected value

$$M(\xi) = \int_0^1 \xi p(\xi) d\xi = \frac{1}{2} \tag{2.23}$$

The generation of random numbers is done using suitable random number generators called pseudo-random number generators (Brown, 2008). A simple example is the sampling of the distance (R) that a neutron travels between collisions. The PDF is:

$$p(R) = \Sigma(R) \exp(-\int_0^x \Sigma(R')dR') \tag{2.24}$$

Nuclear reactor analysis usually treats geometries consisted of extended regions with homogeneous material. In such homogeneous regions the cross-section can be considered constant ($\Sigma(R') = \Sigma_0$). Hence, Eq. (2.24) can be simplified to:

$$p(R) = \Sigma_0 e^{-\Sigma_0 R} \tag{2.25}$$

Consequently,

$$R = -\frac{1}{\Sigma_0} \ln \rho \tag{2.26}$$

In cases of multi-region problems special techniques are implemented. Analogously to the selection of the path length between collisions, every part of physics that is considered part of neutron's life should be sampled in a similar way, e.g., nucleus for collision, elastic-scattering angle, number of fission particles, fission energy etc.

Initially the whole Monte-Carlo game can be quite straight-forward based on an as precise as possible direct simulation of the physical processes. This method called *analog* Monte-Carlo will necessarily lead to correct results to the extent that the physical laws governing the random-walk of the particles are well known and correctly built into the developed algorithm. In other words the *analog* Monte-Carlo tries to computationally reproduce what would happen in the corresponding physical experiment. In many cases this fact has the following implications:

1. Only a fraction of the emitted particles reaches the region of interest.
2. In the physical measurements if the count rate in a detector is very low, long detection times or many repetitions of the experiment are required to obtain good statistics.

Similarly in the numerical experiments a large number of particle histories has to be simulated in order to reach a reliable estimate of the quantity of interest. However in this case there is a strong constraint that is the limited computational resources. Even in the fastest modern computers the numerical simulation of a long series of collisions and transitions requires an incomparably longer time than the total flight time of a physical particle. In addition a thermal nuclear reactor operating at a neutron flux of 10^{16} neutrons/($cm^2 s$) has a neutron density of 10^{11} neutrons/cm^3. These two facts imply clearly that other manners than the continuous increase of the simulated particles should be found in order to improve the accuracy of the results. This statement leaded

in the generation of the *non-analog* Monte-Carlo. The main aim of the *non-analog* Monte-Carlo is to modify the *analog* Monte-Carlo in order to achieve:

1. More particle simulations with non-zero contributions to the score than in the *analog* simulation.
2. Expected results identical to those of the *analog* Monte-Carlo despite the fact that the used individual scores are different.

The fundamental idea behind the *non-analog* Monte-Carlo is to modify the governing PDF of a random process in order to favour the frequency of some events of interest. However in order to maintain a fair game this modification should be counterbalanced. For this reason Monte-Carlo does not simulate neutrons that are analogous to reality but pseudo-neutrons whose existence is characterized by an associated weight. The value of this weight is initially one (1) but can be suitably altered when the PDF of a physical process is modified.

As one can feel when following logical steps, reliable final results can be obtained only after averaging many individual scores obtained during the individual simulations. This logical argument is formally stated by the Law of large numbers, one of the fundamental theorems of Probability theory. Consider n independent random observations, $\mu_1, \mu_2 .... \mu_n$ of a random variable ϕ. Assuming that the random variable ϕ is a function of t, with a PDF p(t), the expected value of ϕ is defined by

$$M(\phi) = \int \phi(t) p(t) dt \tag{2.27}$$

where t symbolizes a variable by which all the possible random paths can be parametrized. The variance is defined as:

$$D^2(\phi) = M(\phi^2) - [M(\phi)]^2 \tag{2.28}$$

If one estimates the expected value by averaging the n samples through the following relation:

$$M(\phi) \simeq \tilde{\mu}_n = \frac{1}{n} \sum_{i=1}^{n} \mu_i \tag{2.29}$$

then according to the law of large numbers $\tilde{\mu}_n$ approaches the expected value $M(\phi)$ with a probability that approaches 1 as $n \longrightarrow \infty$. Subsequently the central limit theorem establishes that the average of n independent observations of a random variable (with finite mean and variance) approaches a normal distribution. This fact gives us more information about uncertainty that associates the statistical average $\tilde{\mu}_n$. More information can be found in Lux and Koblinger (1991).

Another important matter concerning Monte-Carlo simulation is the generation of pseudo-random numbers. The significance of random number generation can be realized by two

famous quotations: "The generation of random numbers is too important to be left to chance." by Robert R. Coveyou (Oak Ridge National Laboratory) and "Random numbers should not be generated with a method chosen at random." by Donald Ervin Knuth an American computer scientist in his book "The Art of Computer Programming". It is out of the scope of this work to describe the topic of the pseudo-random number generation for particle transport simulation. Information can be found in Brown (2008).

2.3.2 *Solution of the Fredholm-type k-eigenvalue integral neutron transport equation*

The expected number of particles coming out of a collision in a volume element $d\boldsymbol{r}$ about $\boldsymbol{r}$ with an energy between E and E + dE and direction in the solid angle $d\boldsymbol{\Omega}$ about $\boldsymbol{\Omega}$ is written as $\chi(\boldsymbol{r}, \boldsymbol{\Omega}, E)d\boldsymbol{r}d\boldsymbol{\Omega}dE$. During the flight until the next collision the energy and the direction remain constant. The probability that a particle leaving a collision at r′ will enter its next collision in $d\boldsymbol{r}$ about $\boldsymbol{r}$ is given by the transition kernel that is represented by $T(\boldsymbol{r}' \rightarrow \boldsymbol{r}; \boldsymbol{\Omega}, E)d\boldsymbol{r}$. If the 3D form of the transition kernel is transformed to a 1D form using some geometrical manipulations (Fig. (2.1)) (Lux and Koblinger, 1991), T has the form:

$$T(\boldsymbol{r}' \rightarrow \boldsymbol{r}; \boldsymbol{\Omega}, E)d\boldsymbol{r} = \Sigma(R, E)\exp\left(-\tau(R)\right)dR \tag{2.30}$$

where $\tau(R) = \int_0^R \Sigma(R')dR'$ is the optical path distance between $\boldsymbol{r}'$ and $\boldsymbol{r}$. Analogously,

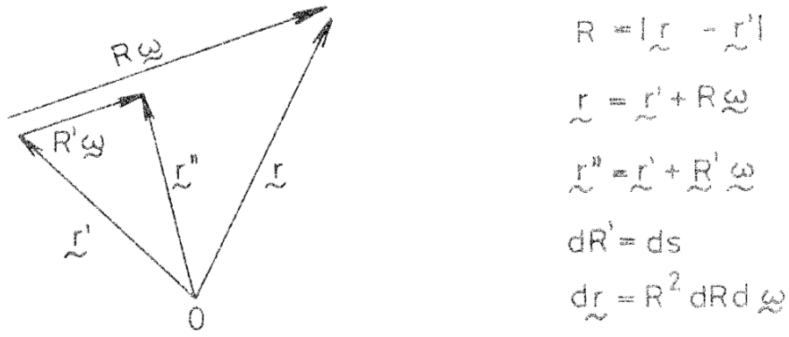

Figure 2.1: Geometrical manipulation for transition kernel transformation (Lux and Koblinger, 1991).

the expected number of particles going into a collision is written as $\psi(\boldsymbol{r}, \boldsymbol{\Omega}, E)d\boldsymbol{r}d\boldsymbol{\Omega}dE$. The collision kernel that describes the total effect of all possible kinds of interactions is given by:

$$C(\boldsymbol{\Omega}', E' \rightarrow \boldsymbol{\Omega}, E; \boldsymbol{r})d\boldsymbol{r} = \frac{\sum_{i=1}^{n}\sum_{j=1}^{m}\nu_{i,j}\Sigma_{i,j}(\boldsymbol{r}; \boldsymbol{\Omega}', E' \rightarrow \boldsymbol{\Omega}, E))}{\Sigma(\boldsymbol{r}, E')} \tag{2.31}$$

Thus, the ingoing collision density is expressed as:

$$\psi(\boldsymbol{r}, E) = \int d\boldsymbol{r}' \chi(\boldsymbol{r}', E) T(\boldsymbol{r}' \to \boldsymbol{r}; E) \tag{2.32}$$

and the outgoing collision density is expressed as:

$$\chi(\boldsymbol{r}, E) = Q(\boldsymbol{r}, E) + \int dE' \psi(\boldsymbol{r}, E') C(E' \to E; \boldsymbol{r}) \tag{2.33}$$

The combination of these two relations gives an integral equation for the ingoing collision density:

$$\psi(\boldsymbol{r}, E) = Q_c(\boldsymbol{r}, E) + \iint dE' d\boldsymbol{r}' \psi(\boldsymbol{r}', E') C(E' \to E; \boldsymbol{r}') T(\boldsymbol{r}' \to \boldsymbol{r}; E) \tag{2.34}$$

where the first collision source Q_c is given by:

$$Q_c(\boldsymbol{r}, E) = \int d\boldsymbol{r}' Q(\boldsymbol{r}', E) T(\boldsymbol{r}' \to \boldsymbol{r}; E) \tag{2.35}$$

The whole Monte-Carlo treatment of particle transport can be carried out in terms of the ingoing collision density. In order to simplify the notation Eq. (2.34) can be written as

$$\psi(P) = Q_c(P) + \int dP \psi(P) K(P', P) \tag{2.36}$$

where P is the general phase space coordinate symbol, i.e. the $(\boldsymbol{r}, \boldsymbol{\Omega}, E)$ coordinates will be symbolized by the single letter P for brevity and K(P',P) is the transport kernel. Noticing Eq. (2.5) it is clear that Eq. (2.36) is a Fredholm type equation of 2nd kind.

The following discussion refers to the Monte-Carlo criticality algorithm which is of special interest but also of special nature. The special nature comes from the fact that this algorithm analyses systems where the neutron source is the fissile/fissionable material and the neutron source intensity depends on the neutron flux and vice versa. Let us now consider $\chi_f(P)dP$ the expected number of fission neutrons produced in dP around P and $K_f(P', P)$ the number of first-generated neutrons produced in dP around P due to one fission at P'. Then Eq. (2.36) takes the form:

$$\chi_f(P) = \frac{1}{k_{\mathit{eff}}} \int dP' \chi_f(P') K_f(P', P) \tag{2.37}$$

where the kernel $K_f(P', P)$ can be factorised as following:

$$K_f(P', P) = C_f(E' \to E; \boldsymbol{r}') T(\boldsymbol{r}' \to \boldsymbol{r}; E) \tag{2.38}$$

where C_f is the fission collision kernel. The factor k_{eff} has been inserted in order to artificially force Eq. (2.37) describing a system in a steady-state even if it is not. If the operator $\int dP' K_f(P', P)$ is represented as F the problem is written as

$$\chi_f = \frac{1}{k_{\mathit{eff}}} F \chi_f \tag{2.39}$$

It is clear that this is an eigenvalue problem. If Eq. (2.39) is integrated over dP, k_{eff} is given by:

$$k_{eff} = \frac{\int dP \int dP' \chi_f(P') K_f(P', P)}{\int dP \chi_f} \tag{2.40}$$

This eigenvalue problem is solved for the largest[1] (fundamental) eigenvalue by a method captured from numerical analysis, the power iteration. In neutron transport it is usually referred to as Source Iteration (SI). SI when adopted in the solution of Eq. (2.39) takes the following form:

$$\begin{aligned} \chi_f^{n+1} &= \frac{1}{k_{eff}^n} F \chi_f^n \\ k_{eff}^{n+1} &= \frac{\int dP F \chi_f^n}{\int dP \chi_f^n} \end{aligned} \tag{2.41}$$

A guess function χ_f^0 is selected as the neutron source and the resulting progeny construct the source for the next generation. The integral operator F represents actually the impact of the physical processes on the fission source χ_f. This impact is simulated by Monte-Carlo.

At this point it should be mentioned that in reactor physics, Monte-Carlo is employed to solve deterministic equations with unknowns the expected values of stochastic variables. Thus Monte-Carlo reactor analysis includes the following steps: first deterministic equations are established for a stochastic process and then a stochastic model is built up to solve the deterministic equations. In the simplest cases the stochastic model leads directly back to the simulation of the basic stochastic process whereas in more refined techniques the physical analogue does not exist anymore; the original physical and final artificial stochastic models can be connected by mathematical manipulations only.

The convergence of SI is determined by the ratio between the first and the fundamental (largest) eigenvalue that is called Dominance Ratio (DR):

$$DR = \frac{k_1}{k_{eff}} \tag{2.42}$$

where $k_{eff} = k_0$. This can be shown by expanding the fundamental fission source to a weighted sum of its eigenvectors since any real function in the domain of F can be expressed as a weighted sum of eigenfunctions. The expansion is:

$$\chi_{f,0} = \sum_i \gamma_i \chi_{f,i} \tag{2.43}$$

If Eq. (2.43) is combined with the first of Eq. (2.41), it results to:

$$\chi_f^{(n)} = \frac{1}{k_{eff}^n} F^n \sum_i \gamma_i \chi_{f,i} \tag{2.44}$$

1 Only the largest eigenvalue has a physical meaning.

In this case the parenthesis denotes that n refers to the iteration index. When no parenthesis n refers to a power. The operator F and the scalar k_{eff}^n are inserted in the sum term

$$\chi_f^{(n)} = \frac{1}{k_{eff}^n} \sum_i \gamma_i F^n \chi_{f,i} \tag{2.45}$$

Because $F\chi_f = k\chi_f$ (eigenvalue/eigenvector relation), Eq. (2.45) can be written as:

$$\chi_f^{(n)} = \sum_i \gamma_i \frac{k_i^n}{k_{eff}^n} \chi_{f,i} \tag{2.46}$$

$$\chi_f^{(n)} = \gamma_0 \chi_{f,0} + (\frac{k_1}{k_{eff}})^n \gamma_1 \chi_{f,1} + (\frac{k_2}{k_{eff}})^n \gamma_2 \chi_{f,2} + \dots \tag{2.47}$$

Since $\left|\frac{k_1}{k_{eff}}\right| > \left|\frac{k_2}{k_{eff}}\right| > \left|\frac{k_3}{k_{eff}}\right| > \dots$, $\chi_f^{(n)}$ converges to $\chi_{f,0}$ when $n \to \infty$. Therefore, it is obvious that the fission source converges slowly in systems with a dominance ratio close to unity (typically loosely coupled multi-component systems and large symmetric systems). Practical problems with a DR close to unity are often met in reactor analysis.

2.3.3 *Variance reduction*

The accuracy of Monte Carlo calculations is mainly restricted by statistical noise. The statistical noise can be decreased using a larger number of histories leading to longer calculation times. However there is a variety of techniques to decrease the statistical fluctuations of Monte Carlo calculations without increasing the number of particle histories. These are known as Variance Reduction Techniques (VRT).

VRT are mostly based on the following ideas:

1. Modify the PDF for physics interactions to favour events of interest.
2. Use splitting/rouletting to increase particles in certain geometric regions of interest.
3. Kill particles in uninteresting parts of problem.

In order to give an idea for VRT let us consider the calculation of the following integral of the function h(x) (Lux and Koblinger, 1991):

$$I = \int_\Gamma \phi(x) h(x) dx \tag{2.48}$$

when $\phi(x)$ is the PDF and Γ the domain of integration. As mentioned above

$$\overline{h} = \frac{1}{N} \sum_{i=1}^{N} h_i \tag{2.49}$$

the mean $\overline{h}$ is an unbiased estimate of I or its expected value is equal to I.

$$\langle \overline{h} \rangle = I \tag{2.50}$$

The variance is defined as

$$\begin{aligned} \langle s^2 \rangle &= \langle (h(x) - I)^2 \rangle = \langle h^2(x) \rangle - 2\langle h(x) \rangle I + I^2 = \\ &= \langle (h^2(x) \rangle - I^2 = \int_\Gamma \phi(x) h^2(x) dx - I^2 \end{aligned} \tag{2.51}$$

An estimate of the variance is given by the empirical variance

$$\overline{s^2} = \frac{N}{N-1} \left[\frac{1}{N} \sum_{i=1}^{N} h^2(x_i) - \overline{h}^2 \right] \tag{2.52}$$

and

$$\langle \overline{s^2} \rangle = s^2 \tag{2.53}$$

Let us now transform the integral to be calculated (Eq. (2.48)) using a function $\phi'(x)$ as following

$$I = \int_\Gamma \frac{\phi(x) h(x)}{\phi'(x)} \phi'(x) dx \tag{2.54}$$

Thus now $\phi'(x)$ is the new PDF and $\frac{\phi(x)h(x)}{\phi'(x)}$ the function to be integrated over Γ. Now an unbiased estimate of the integral is given by the relation:

$$\overline{h} = \frac{1}{N} \sum_{i=1}^{N} \frac{\phi(x_i) h(x_i)}{\phi'(x_i)} \tag{2.55}$$

and an estimate of the variance by the relation:

$$\overline{s^2} = \frac{N}{N-1} \left\{ \frac{1}{N} \sum_{i=1}^{N} \left[\frac{\phi(x_i) h(x_i)}{\phi'(x_i)} \right]^2 - \overline{h}^2 \right\} \tag{2.56}$$

Now the difference between the two variances is

$$\langle \overline{s^2} - \overline{s'^2} \rangle = \langle \overline{s^2} \rangle - \langle \overline{s'^2} \rangle = s^2 - s'^2 = \int_\Gamma h^2(x) \left[1 - \frac{\phi(x)}{\phi'(x)} \right] \phi(x) dx \tag{2.57}$$

If the value of this integral is positive the variance has been reduced with this transformation. However if a not properly selected function $\phi'(x)$ is used, the value can be negative that will imply worse results than in the unmodified case (Lux and Koblinger, 1991).

In the next paragraph a hint of how to properly select functions for the transformation of an integral is given. The empirical variance for sufficiently large N takes the form:

$$\overline{s'^2} = \langle \overline{s'^2} \rangle \cong \langle \left(\frac{1}{N} \sum_{i=1}^{N} \frac{\phi(x_i) h(x_i)}{\phi'(x_i)} - I \right)^2 \rangle = \frac{1}{N} \int_\Gamma \left[\frac{\phi(x) h(x)}{\phi'(x)} \right]^2 \phi'(x) dx - \frac{1}{N} I^2 \tag{2.58}$$

It is obvious that if $\phi'(x) = \frac{\phi(x)h(x)}{I}$ then the value of Eq. (2.58) will be zero. However, this ideal construction of $\phi'(x)$ means that the value of I is already known. But then there is no reason to develop all this procedure; this means that that value is not usually known a priori. The conclusion is that a function $\phi'(x)$ that approximates satisfactorily $\frac{\phi(x)h(x)}{I}$ is to be found. This is an example of how a function to be integrated can be modified in order to improve the calculation of the integral without inserting a bias in the calculation.

3

PROBLEMS, CHALLENGES & OBJECTIVES OF THIS THESIS

Nowadays the Monte-Carlo static analysis of the reactor core is constantly gaining ground for design and safety studies since it can provide a detailed treatment of the reactor core in quite reasonable computational cost. The continuous increase of the available computational resources has contributed significantly towards this direction. However since the demand for more and more detailed and accurate analysis does not stop, many scientific problems remain to be solved in this field, some of the most important being:

1. **Multi-physics analysis** - feedback from the other involved physical fields, e.g. Thermal-Hydraulics (T-H) to the Monte-Carlo solution of NTE.
2. **Dynamic analysis** - pure Monte-Carlo solution of the NSKE.
3. **Convergence acceleration of static Monte-Carlo** - convergence acceleration of the k-eigenvalue Monte-Carlo Source Iteration (SI).

These requirements are imposed by the fact that the nuclear reactor analysis moves continuously towards a multi-physical direction with demands for higher and higher level of accuracy combined with a high computational cost-effectiveness. This thesis attempts to answer the three problems mentioned above combining the proposal and use of suitable algorithms together with their programming development and their initial evaluation. An essential step towards complete Monte-Carlo analysis of the reactor core is the development of algorithms for pure stochastic dynamic treatment. So far Monte-Carlo is involved in dynamics only within the framework of hybrid, i.e stochastic/deterministic, schemes. Furthermore the T-H feedback is a strong requirement due to the tight bond between neutronic and T-H phenomena. However, the static T-H feedback requires a special treatment comparing to the dynamic one due to the special nature of the Monte-Carlo k-eigenvalue algorithm. Finally since the Monte-Carlo criticality/k-eigenvalue analysis is crucial not only for the analysis of reactor statics but also for burnup analysis, convergence acceleration remains a significant challenge. These are the main problems/challenges handled in this thesis.

In the past, the main trend in nuclear reactor core analysis was to analyse each part of the involved physics separately using distinct solvers. According to this philosophy, the static-critical neutronic behaviour of the reactor core is analysed either solving Eq. (2.7) or simulating the corresponding physics in a stochastic (Monte-Carlo) way. In both cases the T-H conditions are considered fixed. Similarly the T-H behaviour of the reactor core is analysed using a variety of T-H solvers in various levels (system level, sub-channel, computational fluid dynamics). In this case the neutronic conditions (power distribution) are considered as known. However in a nuclear reactor core the various existing physical phenomena of different nature are interrelated. In this sense the neutronic and T-H phenomena are strongly bonded; the microscopic neutron cross sections of the core materials are dependent on the temperature. This interrelation induces the need for multi-physics calculations, i.e. calculations which can compute the parameters of interest taking these interactions into consideration. The need for sophisticated computational tools capable of performing multi-physical treatment of the reactor core becomes even more important for the GENIV reactor concepts proposed in the Generation IV International Forum since these concepts are characterised by unique features and high complexity.

After spatial discretization Eq. (2.7) can be written in the following matrix form:

$$\boldsymbol{\Phi} = \frac{1}{k_{eff}} \boldsymbol{F}\boldsymbol{\Phi} \tag{3.1}$$

where $\boldsymbol{F}$ is an operator combining all the mechanisms that are involved in neutron transport and $\boldsymbol{\Phi}$ is the vector containing the scalar fluxes. When this equation is solved as is, in a standalone way, the temperature and density fields are considered as given. Thus the dependence of neutronics on T-H is not properly handled.

If the dependence on T-H conditions is desired to be taken into account, the problem described by Eq. (3.1) can be represented as:

$$\boldsymbol{f}(\boldsymbol{x}, \boldsymbol{y}) = \boldsymbol{0} \tag{3.2}$$

where $\boldsymbol{x}$ contains the vector of fluxes $\boldsymbol{\Phi}$ and the scalar k_{eff} while $\boldsymbol{y}$ contains the temperature and density fields. The T-H problem that corresponds to the calculation of the temperature and density fields is written as

$$\boldsymbol{g}(\boldsymbol{x}, \boldsymbol{y}) = \boldsymbol{0} \tag{3.3}$$

Therefore a global solution of the problem described by Eq. (3.2) and Eq. (3.3) is desired. If it is assumed that the solution of the sub-problems $\boldsymbol{f}$ and $\boldsymbol{g}$ is segregated, i.e., $\boldsymbol{x}$ is

the solution of $\boldsymbol{f}$ and $\boldsymbol{y}$ is the solution of $\boldsymbol{g}$, the problem can be written in the following way:

$$\boldsymbol{f}(\boldsymbol{x}, \widetilde{\boldsymbol{y}}) = \mathbf{0} \tag{3.4}$$

$$\boldsymbol{g}(\widetilde{\boldsymbol{x}}, \boldsymbol{y}) = \mathbf{0} \tag{3.5}$$

where the tilde represents the coupling terms. Assuming mono-disciplinary solvers available for the solution of each sub-problem that is considered as a fixed-point problem, the global problem takes the following form:

$$\boldsymbol{x} = \mathsf{N}(\boldsymbol{x}, \widetilde{\boldsymbol{y}}) \tag{3.6}$$

$$\boldsymbol{y} = \mathsf{T}(\widetilde{\boldsymbol{x}}, \boldsymbol{y}) \tag{3.7}$$

where N and T represent the action of the Neutronic and the T-H solver on the vectors $\boldsymbol{y}$ and $\boldsymbol{x}$, respectively. Now an important decision on the exact method that will be utilised for the numerical solution of this problem should be made.

The Monte-Carlo method is extensively used for static analysis mainly because it allows for the detailed geometrical and continuous energy treatment of the analysed model. Stochastically, the integral form of Eq. (2.7) (see § 2.3.2) is solved utilising the Monte-Carlo SI (Lux and Koblinger, 1991) in order to calculate the fundamental eigenpair.

Very often within the generalised context of computational physics, the *loose* coupling approaches face difficulties in obtaining convergence of the overall problem, as referred for example by Gill et al. (2017), Yeckel et al. (2009) and Yeckel et al. (2010). For this reason the issue of *developing a coupling algorithm that could maintain the distinct treatment of the Monte-Carlo neutronic and the T-H fields within a tight coupling context* arises.

3.2 DYNAMIC MONTE-CARLO ANALYSIS

The static Monte-Carlo analysis is extensively employed as standalone and/or coupled with other tools since it can provide thorough description and analysis of the neutronic model of the reactor. At this point a scientific "gap" arises; although the pure Monte-Carlo method could analyse transient phenomena (normal or accidental) without making use of significant approximations, it has not extensively been employed yet in this domain. In case that pure Monte-Carlo could be applied to the solution of the the problem described by Eqs (2.8 and 2.9), it might lead to a very detailed and accurate treatment of reactor dynamics.

Due to the general multi-physics orientation of Nuclear Reactor Theory (NRT) an extra challenge is the insertion of T-H feedback to the pure Monte-Carlo dynamic neutronics.

The homogeneous (source-free) Neutron Transport Equation (NTE) can be written in the following form:

$$\frac{\partial \phi}{\partial t} + E\phi + C\phi = S\phi + M\phi \tag{3.8}$$

along with the initial condition $\phi(0) = \phi_0$. E is the leakage operator (loss term), C is the collision operator (loss term), S is the scatter-in operator (gain term) and M is the fission multiplication operator (gain term). Eq. (3.8) can be written in the following form:

$$\frac{\partial \phi}{\partial t} = L\phi \tag{3.9}$$

where L is the transport operator that combines the action of all the above-mentioned operators. Eq. (3.9) describes the dynamic neutronic problem for a constant temperature field and can be solved by a pure neutronic solver. However the transport operator depends on temperature T and thus:

$$\frac{\partial \phi}{\partial t} = L(T)\phi \tag{3.10}$$

When the temperature is to be taken into account in the solution of the NTE, the integrated neutronic/T-H problem should be solved. When neutronics is solved with Monte-Carlo which inherently differs from the form of the typical deterministic solvers, several fundamental algorithmic questions about the multi-physics solution arise.

Therefore another significant challenge is the *development of effective pure Monte-Carlo techniques for the dynamic analysis of the reactor core together with T-H feedback*.

3.3 CONVERGENCE ACCELERATION OF THE MONTE-CARLO SOURCE ITERATION

The solution of the *k*-eigenvalue form of the NTE is traditionally performed utilizing the SI that calculates the *k*-eigenvalue and the eigenvector. In Monte-Carlo the *k*-eigenvalue problem is solved using the Monte-Carlo SI. The integral form of the NTE is presented in § 2.1.2 and § 2.3.2. The *k*-eigenvalue, integral NTE can be written in the following simplified way:

$$\chi_f(\boldsymbol{r}) = \frac{1}{k_{eff}} F\chi_f(\boldsymbol{r}) \tag{3.11}$$

where F is the integral operator providing the expected number of fission neutrons produced per unit volume from the contribution of the neutrons of all other volumes of the space.

It is clear that this is an eigenvalue problem. Numerically this problem is classically solved utilising the SI. The spatially discretized SI can be written as:

$$\boldsymbol{\chi}_f^{n+1} = \frac{1}{k_{eff}^n} \boldsymbol{F}\boldsymbol{\chi}_f^n \tag{3.12}$$

where:

$$k_{eff}^{n+1} = \frac{\int \boldsymbol{F}\chi_f^n \, d\boldsymbol{r}}{\int \chi_f^n \, d\boldsymbol{r}} = k_{eff}^n \frac{\int \chi_f^{n+1} \, d\boldsymbol{r}}{\int \chi_f^n \, d\boldsymbol{r}} \tag{3.13}$$

and n denotes the nth iterative step. In § 2.3.2 it has been shown that when the Dominance Ratio (DR) $\simeq 1$ the convergence of SI is slow; the closer to the unity the slower the convergence of the algorithm. Typically this situation is met in loosely coupled multi-component systems and large symmetric systems (Dufek, 2007).

The convergence of the fission source is a crucial point because it affects the accuracy of the results. That is, statistically calculated results from a poorly converged fission source are significantly biased. This is the reason why the convergence of the source should be confirmed in order to avoid the contribution to the statistics of cycles (or batches or iterations) that do not correspond to the converged region. Although progress towards the acceleration of the k-eigenvalue Monte-Carlo SI has been made, the problem has not been entirely solved yet. For this reason, *the improvement of the convergence of the Monte-Carlo k-eigenvalue iterative process* has been recently listed among the most important and challenging problems in computational neutron transport as stated by Cho and Chang (2009) and Martin (2012).

3.4 OBJECTIVES

The aim of this thesis is to investigate the problems mentioned above and to propose solutions/answers. At this point it should be highlighted that here, the term *solution* has three aspects, i.e. physics, numerics, computation (Fig. (3.1)). Although the central objective is the accurate solution of the physical problem, this should be combined with high computational cost-effectiveness. The satisfaction of these two primary goals generates the need for a solution that combines the accurate analysis of physics as well as the accurate and efficient numerical treatment and computational implementation. Numerics can improve both accuracy and cost-effectiveness improving the performance of the algorithm that solves the physical problem. Computation is also related to the accuracy through the translation of physics and numerics into the machine language and with cost-effectiveness through the manner that this translation is done.

An important prerequisite of this research is the selection of a Monte-Carlo neutronic solver[1] that can serve as a platform for research and development of the methodologies that will arise. The selected Monte-Carlo solver should combine at least the following features:

1. k-eigenvalue transport capability.

1 Hereinafter it will referred to as Monte-Carlo solver.

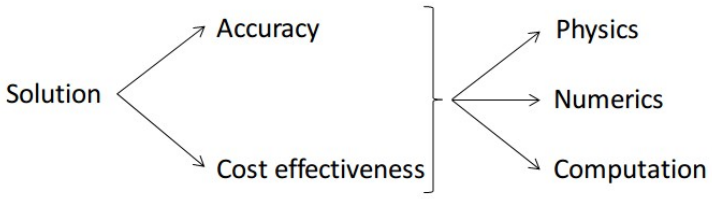

Figure 3.1: Aspects of the term *solution* in this thesis.

2. Effective parallelism pattern.
3. Access to the source code.

The evaluation and selection procedure is a preliminary part of this thesis.

The first part of this thesis concerns the investigation of a coupling algorithm that could maintain the distinct treatment of the Monte-Carlo neutronics and the T-H fields within a tight coupling context (see § 3.1). So far a "serial" iterative scheme that is the simplest and most straight-forward way to couple two solvers is almost exclusively used according to literature research. Initially such a scheme will be developed in order to investigate the problem and understand its weaknesses. Afterwards, ways that might improve these drawbacks will be investigated. The final step consists of the programming development of the proposed algorithm together with its evaluation.

The second part of this thesis regards the investigation and development of a Monte-Carlo module for the analysis of reactor core transient. As regards physics, the temporal evolution of the simulated neutrons along with the adequate simulation of the delayed neutrons are the basic requirements for a straight-forward Monte-Carlo treatment of a transient problem. Thus, the first step is the selection of the method that will provide the features mentioned above. As a second step, an algorithm that will insert that method to the Monte-Carlo statistical context should be designed. The third step is the efficient programming development following the host code's features, trying to minimise the necessary modifications and to maximise the advantage resulting from its existing capabilities. The fourth step includes the investigation and the development of a T-H feedback capability to the transient module. This step consists of the algorithmic/numerical investigation, the algorithm's flowchart design and the programming implementation. The last step is the evaluation of each part of the developed algorithm.

The last part of this thesis is an attempt to accelerate the convergence of the Monte-Carlo classical SI iteration. This work will focus on the possibility for pure numerical acceleration (elaborating on the numerical mechanism) since attempts to accelerate the Monte-Carlo convergence indirectly, by "biasing" physics or by improving each source iteration guess autonomously, are met in literature. Thus, the author has the sense that there is still unused numerical power that could be exploited. The first step will be the

investigation and the development of a numerical technique that could achieve the goal of acceleration. Afterwards the programming development together with its evaluation follow.

To summarise, the main objectives of this thesis are the extension of Monte-Carlo to the analysis of dynamic reactor core problems, the insertion of T-H feedback to both statics and dynamics as well as the convergence acceleration of the Monte-Carlo source iteration. The findings could contribute to the expansion of the Monte Carlo approach to a more global and accurate tool for complete analysis of the system "reactor core" with a reasonable computational cost.

Part III

SOLUTIONS

4

STATIC MONTE-CARLO WITH THERMAL-HYDRAULIC FEEDBACK

4.1 STATE-OF-THE-ART

Generally, within the scientific community of computational physics, there is a keen interest for efficient and flexible techniques which can solve systems of equations in some segregated fashion. Quite efficient methods are those that allow the distinct treatment of the involved physical problems by black-box solvers, alleviating the need for modification of their algorithms. The main advantage of this kind of methods is that they can link existing highly sophisticated solvers to treat complex multi-physics and multi-scale problems aiming to a higher level of accuracy than that achieved by each solver separately. Furthermore this philosophy can reduce dramatically the required effort for development-verification which can extraordinarily increase when tools are designed and developed from scratch.

So far most of the attempts to couple Monte-Carlo with Thermal-Hydraulics (T-H) solvers for coupled static analysis have used a kind of serial coupling. Some examples of this type of coupling can be found in Joo et al. (2004), Waata (2005), Ivanov and Avramova (2007), Seker et al. (2007), Grieshemer et al. (2008), Hu and Rizwan-Uddin (2008), Kotlyar et al. (2011), Cardoni (2011), Li et al. (2012), Chaudri et al. (2012), Li and Wang (2012), Bettencourt (2013), Espel et al. (2013), Guoa et al. (2013), Bernnat et al. (2014), Wu and Kozlowski (2015). This kind of coupling can be considered as a Picard Iteration (PI) (it is also referred to as a block Gauss Seidel iteration) and can be described by Eq. (4.1) and Eq. (4.2) where only the exchanged variables appear since the internal variables at the current iteration are inaccessible and are treated as invisible.

$$\boldsymbol{x}^{k+1} = N(\boldsymbol{y}^{k}) \tag{4.1}$$

$$\boldsymbol{y}^{k+1} = T(\boldsymbol{x}^{k+1}) \tag{4.2}$$

Or it can be described by just writing:

$$\boldsymbol{y}^{k+1} = T(N(\boldsymbol{y}^{k})) \tag{4.3}$$

N and T represent the neutronics and the T-H solvers that receive as inputs the vectors $\boldsymbol{y}$ and $\boldsymbol{x}$, respectively. The T-H information (part of the output of the T-H solver that passes

to neutronics) is symbolised by a vector $\boldsymbol{y}$ while $\boldsymbol{x}$ represents the neutronics output that acts as input of T-H. The index k denotes the iterations of this method.

At this point it should be mentioned that the solvers N and T should not be considered as the actual neutronics and T-H solver respectively. In fact they are conceptual solvers that include the real solvers plus all the additional required operations on the calculated results such as normalizations.

The main advantage of this method is that it can be performed quite easily by independent solvers. On the other hand the main drawback is that PI does not guarantee the convergence. In such coupling schemes under-relaxation techniques are often utilised in order to improve the numerical performance (Dahlquist G., 1974).

4.2 SELECTION OF A MONTE-CARLO SOLVER AS THE PLATFORM FOR RESEARCH AND DEVELOPMENT IN THIS THESIS

An essential prerequisite of this thesis is the selection of a Monte-Carlo solver that can serve as a platform for research and development of the methodologies that will arise in this research. The OpenMC (Romano and Forget, 2013) Monte-Carlo solver has selected to play this role. The reasons are that OpenMC fulfils the requirements defined in § 3.4. OpenMC is a new, open source, Monte-Carlo transport solver written in the modern Fortran programming language. It provides the capability for k-eigenvalue (criticality) and fixed-source analysis. The principal reason that this code has been selected for the research and development procedure within this thesis is that it is open-source and therefore it can facilitate the developing process without any constraint. The fact that it is written in modern Fortran using "type" structures and other advanced programming features is another reason that makes OpenMC an attractive platform. Also it is characterised by some other notable features such as a very efficient parallelism pattern that allows excellent scalability up to some hundreds of thousands of processors for even k-eigenvalue calculations (Romano and Forget, 2013). Furthermore its input files are written in the Extensible Markup Language (XML) format rather than in arbitrary solver-dependent text formats which are used by most of the other codes, simplifying the development of models significantly.

4.3 DEVELOPING A CLASSICAL SERIAL MONTE-CARLO/THERMAL-HYDRAULIC COUPLING SCHEME

In this introductory section of this chapter a classical serial iterative Monte-Carlo/T-H coupling scheme is developed. This scheme will be used for an initial study of the

coupled Monte-Carlo/T-H problem. Also it will act as the reference for any other approach proposed by this work. OpenMC is coupled with the COBRA-EN solver (Basile et al., 1999). COBRA-EN is a sub-channel solver, written in Fortran 77, which computes the T-H parameters of nuclear fuel assemblies or whole cores for both steady-state and transient conditions. An important issue in coupled neutronic/T-H calculations is the feedback information which is exchanged between the neutronic and the T-H field. As a result, the mapping between neutronics and T-H plays a critical role in that procedure. Furthermore the cross-section upgrading procedure as well as the convergence of the iterative scheme are additional important steps of the integrated scheme.

In this work a one-to-one mapping between the axial and radial nodalization of the two coupled solvers is implemented. The data transfer between the solvers is controlled by a program, written in Fortran, in combination with some BASH-scripts. The developed control program is also responsible for the handling of the cross-section evolution within the iterative scheme and for checking the convergence. The simplified flowchart of the OpenMC/COBRA coupled scheme can be seen in Fig. (4.1). Since OpenMC is a new solver under continuous development, it is desirable to use it without modifying its source aiming mainly to an easy replacement by newer versions. For this purpose it is preferable to limit its interaction with other solvers in exchanging data through the input-files. This point also makes understandable the importance of the XML format which is adopted by the input files of OpenMC. For a robust and easily controlled mapping between neutronic and T-H solvers, extra XML-elements can be used in the input file of OpenMC where the materials are specified. These extra XML-elements do not interrupt the parsing of the file by OpenMC, and at the same time, they are used by the developed routines which transfer data and control other parameters. Finally it should be mentioned that since COBRA uses channel-oriented cells whereas OpenMC uses pin-oriented, the surrounding coolant temperatures and densities of each rod in OpenMC are deduced by averaging throughout all the sub-channels surrounding that rod in COBRA.

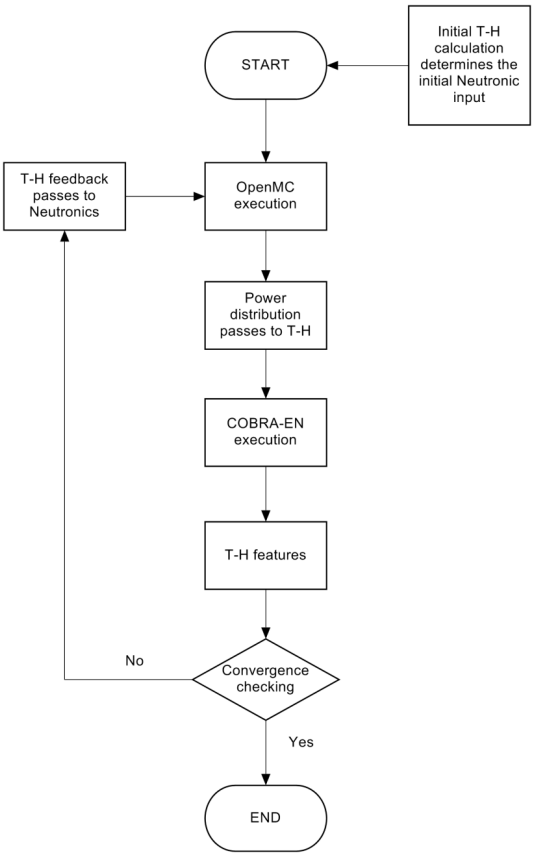

Figure 4.1: A simplified flowchart of the serial OpenMC/COBRA coupled scheme.

The method of pseudo-materials, originally introduced by Bernnat et al. (2000), has been adopted to handle the Doppler broadening of the cross-sections within the coupled scheme. More information about the method of pseudo materials as applied in here can be found in § 4.5.2. Due to the iterative coupling approach between the neutronic and T-H solver, a large number of iterations may be needed until convergence is achieved. The local fuel temperature was selected to be the convergence parameter following a well-established practice according to the bibliography (e.g. Ivanov et al. (2013)). Thus, the difference of the local fuel temperature is checked using the following convergence criterion:

$$\| \frac{T_k - T_{k-1}}{T_{k-1}} \|_\infty < \epsilon \tag{4.4}$$

where ϵ is the convergence parameter and k the iteration index. When Eq. (4.4) is satisfied for each axial region of each fuel rod, the calculation stops. Additionally the literature shows that the implementation of an under-relaxation method on the fuel temperature might accelerate the convergence of such coupling schemes. Here an under-

relaxation scheme applied on the T-H vector is tested. This scheme has the following form:

$$y_i^{weighted} = (1-\omega)y_i - \omega y_{i-1} \tag{4.5}$$

y_i is the ith component of the T-H vector containing the fuel and the coolant temperatures together with the coolant densities. and ω is the under-relaxation parameter.

4.3.1 *Test-case 4-1: Benchmarking and investigation*

In this section a benchmark that has been proposed in the bibliography for a code-to-code intercomparison of coupled neutronic/T-H tools is analysed. This benchmark concerns a single Boiling Water Reactor (BWR) multi-region fuel pin whose detailed description can be found in Ivanov et al. (2012). More precisely this configuration consists of a single BWR uranium-based fuel pin surrounded by water that acts at the same time as coolant and moderator. At the top and bottom there is a reflector made of the material of the cladding. The fission-rate, the fuel and the coolant temperature and density are the variables that are exchanged between neutronics and T-H. At this point it should be mentioned that terms *fission-rate* and *power* are referred to interchangeably for the remainder of this chapter since the power can be easily calculated from the fission-rate. The cladding temperature remains fixed within the coupled calculation. The temperature treatment in the neutronic side is done utilising the method of pseudo-materials. In both the neutronic and the T-H model, 38 axial regions have been used. In the radial direction the neutronic model uses reflective boundary conditions whereas at the axial edges vacuum boundaries have been implemented. Two calculations are performed with OpenMC/COBRA, i.e., one without under-relaxation and one with $\omega = 0.5$. The convergence criterion is $\epsilon = 0.8\%$. The results are validated against an MCNP/COBRA computation obtained from bibliography (Vazquez, 2014). MCNP (*A general Monte Carlo N-Particle Transport Code, Version 5. Volume I: Overview and Theory*) is a Monte-Carlo neutronic solver. At this point it should be mentioned that in Figs (4.2-4.4) the left graphs have been captured from Vazquez (2014) whereas the right ones depict direct comparisons between the present results and the corresponding findings derived from the left graphs.

The results obtained with OpenMC/COBRA are in satisfactory agreement with the MCNP/COBRA ones (Vazquez, 2014) as can be seen in Figs (4.2-4.4). The difference observed in the power profile (Fig. (4.2)) can be considered as small in this case where a code-to-code comparison is performed. Actually this difference is attributed to the corresponding discrepancy in the axial density profiles calculated by the T-H part of the coupled tools. This fact has also been highlighted by Ivanov et al. (2012); the T-H solvers

make use of various (semi-)empirical correlations and thus the different combinations of these correlations can easily introduce discrepancies in the coupled results. Other factors that could cause differences are the number of the simulated neutron histories, the convergence criterion, the numerical grid used for the calculation of the radial fuel temperature profile, the formula used for the calculation of the effective fuel temperature, etc. Table (4.1) presents some of the two coupling schemes key features used for this calculation.

Table 4.1: Test-case 4-1: Comparison of some key features of the two coupling schemes.

	Statistics (active/skipped/ histories per batch)	Convergence criterion (ϵ) (Eq. (4.4))	Void fraction correlation	Effective fuel temp.
This work	300/100/500000	0.8%	Armand	Rowland (§ 4.6.1)
Vazquez (2014)	350/-[1]/500000	0.3%	Armand	Averaged values

When under-relaxation is applied the convergence is indeed accelerated while at the same time the calculated parameters remain almost identical as depicted in Figs (4.5-4.9).

The main conclusion of this section is that a classical "serial" coupling algorithm between OpenMC and COBRA has been successfully developed. The role of this numerical tool in the present research is twofold: firstly it is used for an initial scouting of the problem and its features. Secondly, it is used as a reference for the new proposed approach that has been developed, not only for result-validation but also for the evaluation of the numerical performance of the introduced method.

1 This value has not been reported in the reference.

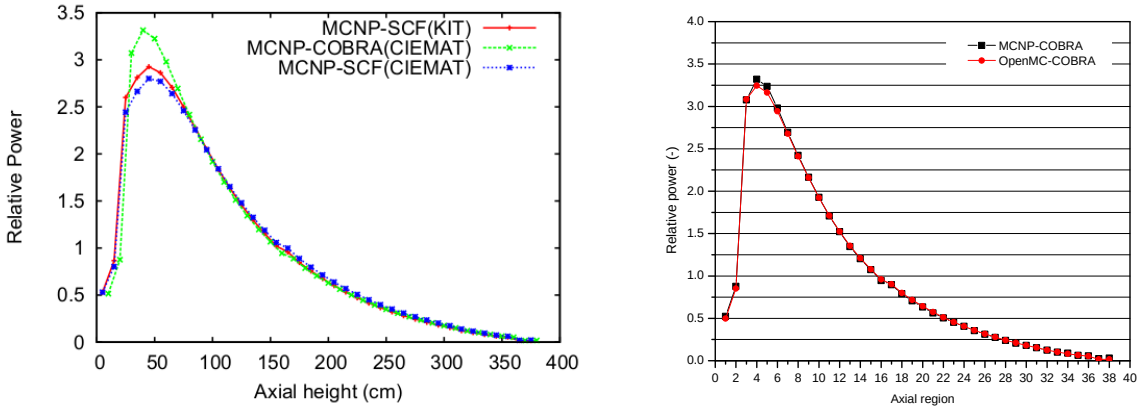

Figure 4.2: Test-case 4-1: Converged relative power axial profile given by serial OpenMC/COBRA vs MCNP/COBRA (Vazquez, 2014).

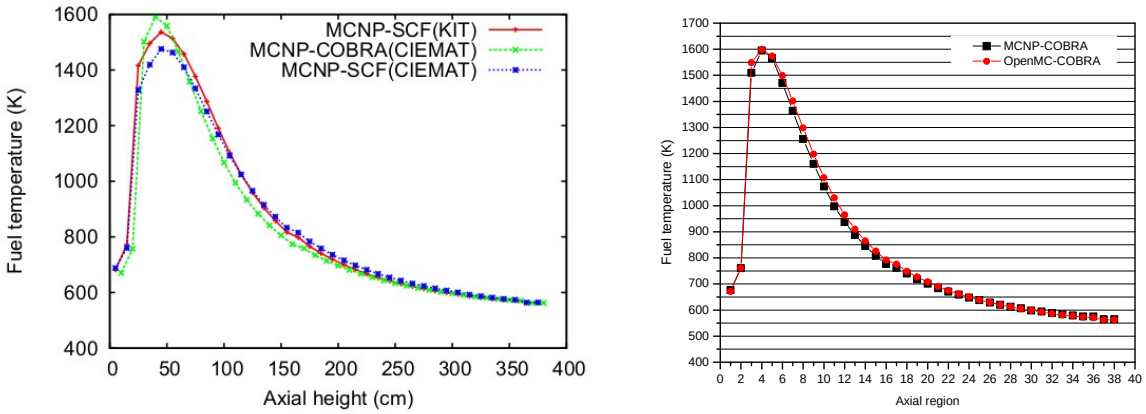

Figure 4.3: Test-case 4-1: Converged fuel temperature axial profile given by serial OpenMC/COBRA vs MCNP/COBRA (Vazquez, 2014).

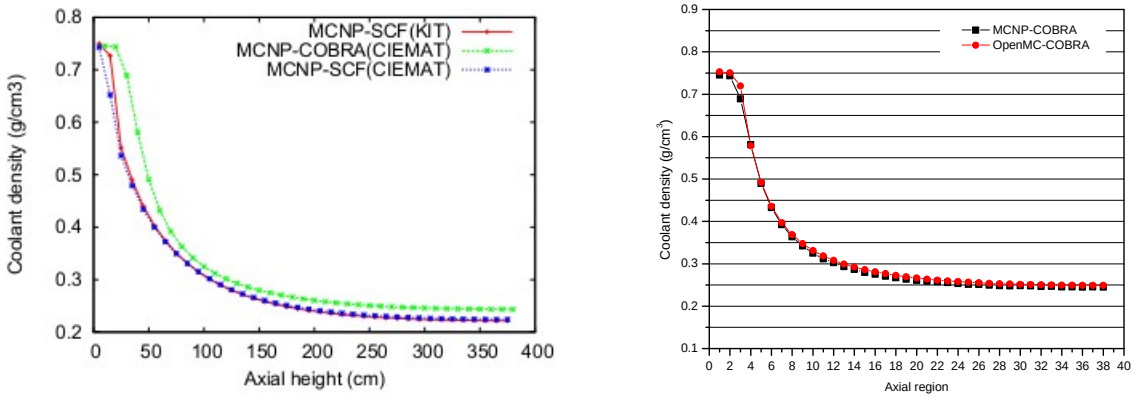

Figure 4.4: Test-case 4-1: Converged coolant density axial profile given by serial OpenMC/COBRA vs MCNP/COBRA (Vazquez, 2014).

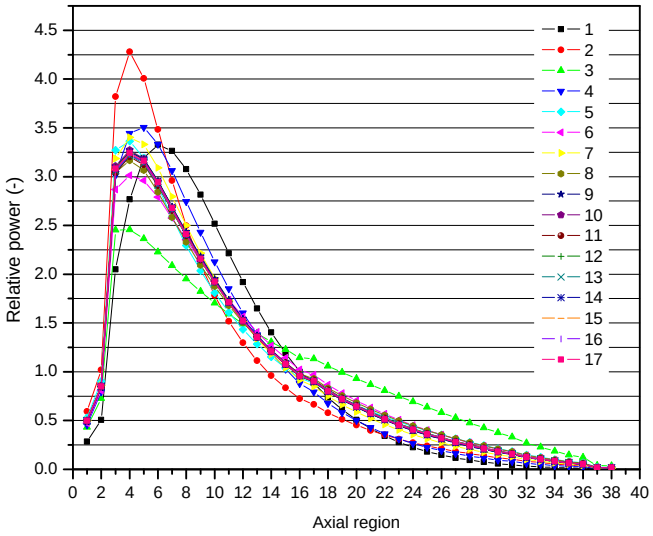

Figure 4.5: Test-case 4-1: Relative normalized power evolution within the serial iterative coupled calculation (no under-relaxation).

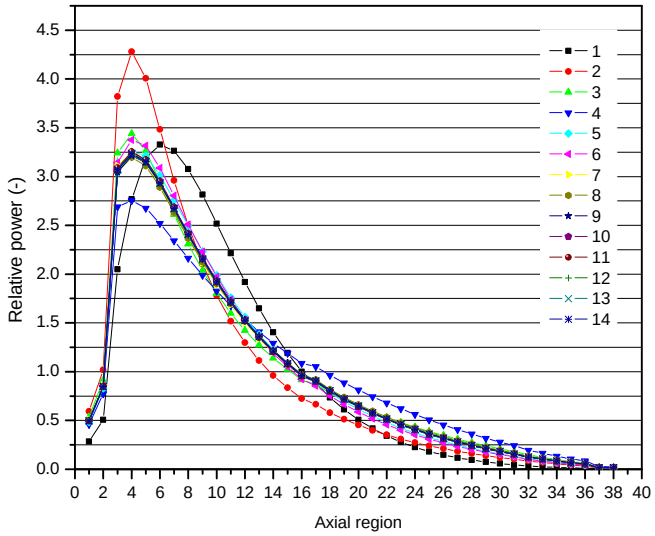

Figure 4.6: Test-case 4-1: Relative normalized power evolution within the serial iterative coupled calculation with under-relaxation ($\omega = 0.5$).

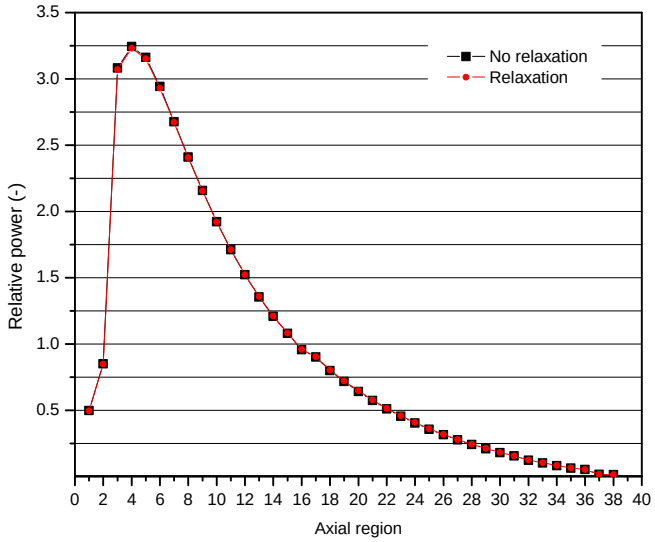

Figure 4.7: Test-case 4-1: Converged (serial algorithm) relative power axial profile with and without under-relaxation.

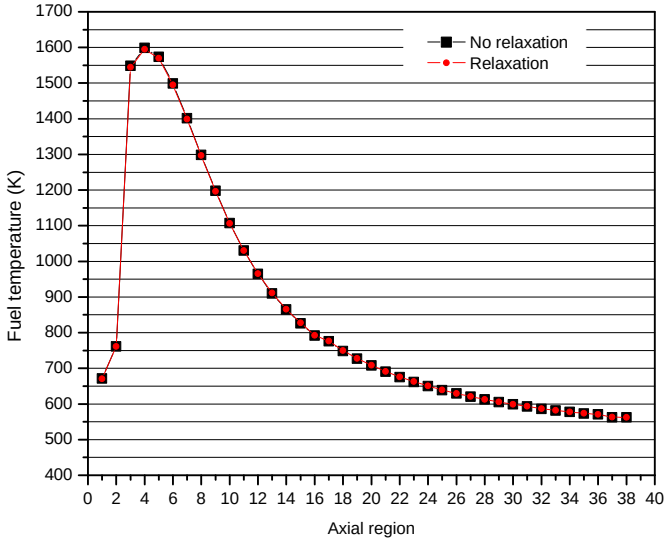

Figure 4.8: Test-case 4-1: Converged (serial algorithm) fuel temperature axial profile with and without under-relaxation.

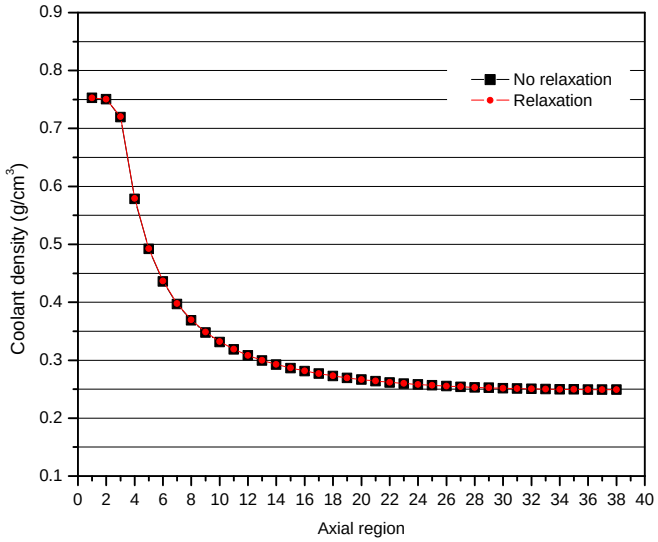

Figure 4.9: Test-case 4-1: Converged (serial algorithm) coolant density axial profile with and without under-relaxation.

Newton methods for the solution of non-linear systems are characterized by fast convergence and simultaneous solution of the flux, eigenvalue, temperature, and density unknowns, a feature that is desirable in tightly coupled systems. However, a Newton method is not appropriate when neutronics is analysed with a Monte-Carlo solver. More specifically, the fact that a Newton method requires the calculation of the Jacobian matrix is a substantial limitation even when it is adopted in pure deterministic environments. However the stochastic and computationally burdensome nature of a Monte-Carlo solver makes the implementation of the original Newton method practically impossible and theoretically rather unclear.

A method that is an approximation of the original Newton method and tries to alleviate the problem of the creation of the "expensive" Jacobian matrix is the Jacobian Free Newton Krylov (JFNK) method (Knoll and Keys, 2004). JFNK substitutes the construction of the Jacobian matrix by the calculation of the effect of the Jacobian matrix on a vector. However, even in this form, a Newton method would be suitable for the coupling of two distinct solvers provided that quite extensive modification would be applied to their source codes to calculate the required residuals (which is again unclear for Monte-Carlo). Although JFNK is not adopted in this work it is briefly described since it is the basis of the Newton-based method that is finally utilised.

4.4.1 *Newton iteration*

A sequence of non-linear systems can written as $\boldsymbol{F}(\boldsymbol{y}) = \mathbf{0}$. The Newton iterative method can be utilised for the solution of this system of non-linear equations. A multivariate expansion of $\boldsymbol{F}(\boldsymbol{y}) = \mathbf{0}$ about a current point $\boldsymbol{y}^k$ would give:

$$\boldsymbol{F}(\boldsymbol{y}^{k+1}) = \boldsymbol{F}(\boldsymbol{y}^k) + \boldsymbol{F}'(\boldsymbol{y}^k)(\boldsymbol{y}^{k+1} - \boldsymbol{y}^k) + \text{higher order terms} \tag{4.6}$$

Neglecting the higher order terms and setting the Right Hand Side (RHS) equal to zero the Newton linearised form of the non-linear system is derived:

$$\boldsymbol{J}(\boldsymbol{y}^k)\delta\boldsymbol{y}^k = -\boldsymbol{F}(\boldsymbol{y}^k) \tag{4.7}$$

$$\boldsymbol{y}^{k+1} = \boldsymbol{y}^k + \delta\boldsymbol{y}^k, \text{ for } k = 0, 1... \tag{4.8}$$

where $\boldsymbol{y}$ is the vector of the unknowns, $\boldsymbol{y}^0$ is the initial guess, $\boldsymbol{F}(\boldsymbol{y}^k)$ is the vector of the non-linear residuals, $\boldsymbol{J} = \boldsymbol{F}'(\boldsymbol{y}^k) = \frac{\partial \boldsymbol{F}}{\partial \boldsymbol{y}}$ is its associated Jacobian matrix, and $\delta\boldsymbol{y}$ is the Newton correction vector. For a system of n unknowns each element (i, j) of the Jacobian matrix is given by:

$$J_{i,j} = \frac{\partial F_i}{\partial y_j}$$

Thus the Jacobian matrix has the following form:

$$\boldsymbol{J} = \begin{bmatrix} \frac{\partial F_1}{\partial y_1} & \frac{\partial F_1}{\partial y_2} & \cdots & \frac{\partial F_1}{\partial y_n} \\ \frac{\partial F_2}{\partial y_1} & \frac{\partial F_2}{\partial y_2} & \cdots & \frac{\partial F_2}{\partial y_n} \\ \vdots & \vdots & \ddots & \vdots \\ \frac{\partial F_n}{\partial y_1} & \frac{\partial F_n}{\partial y_2} & \cdots & \frac{\partial F_n}{\partial y_n} \end{bmatrix}$$

When a Monte-Carlo solver is used to analyse neutronics, it is rather unclear how each element $J_{i,j} = \frac{\partial F_i}{\partial y_j}$ would be constructed. For a straight forward construction, the complete set of equations that describe the problem would be required.

Of course, the major drawback of a general Newton iterative method is that the calculation of each element of the Jacobian matrix by using analytic techniques or discrete derivatives is quite computationally "expensive". Also solving the possibly large linear system of Eq. (4.7) by using Gauss elimination can be very expensive since a significant number of iterations are needed. In such cases Krylov methods are highly recommended as they can significantly reduce the computational load since they can overcome these two problems. The Krylov methods are briefly described in the next paragraph.

The Newton iteration (Eqs (4.7 and 4.8)) continues until the achievement of a sufficient drop in a suitably chosen indicator like the norm of the non-linear residual Eq. (4.9) and/or the Newton update Eq. (4.10):

$$\frac{\| \boldsymbol{F}(\boldsymbol{y}^k) \|}{\| \boldsymbol{F}(\boldsymbol{y}^0) \|} \leqslant \epsilon_1 \tag{4.9}$$

$$\| \delta \boldsymbol{y}^k \| \leqslant \epsilon_2 \tag{4.10}$$

where ϵ_1 is a suitably specified limit of the Left Hand Side (LHS) of Eq. (4.9) while ϵ_2 is a specified limit of the LHS of Eq. (4.10).

4.4.2 *Krylov iteration*

The main feature of Krylov methods which makes them suitable for use in the JFNK methods is that they need only matrix-vector products and so the creation of the expensive Jacobian matrix can be avoided. The general idea behind the Krylov method is that it generates a chain of orthonormal vectors that are used as a basis of the subspace $\boldsymbol{K}_j$:

$$\boldsymbol{K}_j = \text{span}(\boldsymbol{r}_0, \boldsymbol{J}\boldsymbol{r}_0, \boldsymbol{J}^2\boldsymbol{r}_0, ..., \boldsymbol{J}^{j-1}\boldsymbol{r}_0) \tag{4.11}$$

This basis is used for the construction of the solution of a linear system $\boldsymbol{J}\delta\boldsymbol{y} = -\boldsymbol{F}$ where $\boldsymbol{r}_0 = \boldsymbol{J}\delta\boldsymbol{y}_0 + \boldsymbol{F}$ is the initial linear residual. The solution of the linear system, in

this case $\delta \boldsymbol{y}$, is constructed as a linear combination of the Krylov vectors (Eq. (4.11)) and can be written as:

$$\delta \boldsymbol{y}_j = \delta \boldsymbol{y}_0 + \sum_{i=0}^{j-1} \beta_i (\boldsymbol{J})^i \boldsymbol{r}_0 \tag{4.12}$$

where j is the Krylov iteration index. The scalars β_i determine "how much" of each basis vector will participate to the construction of the solution. In a Krylov method they are calculated in a least square sense in order to minimize the magnitude of the linear residual vector $\| \boldsymbol{J}\delta \boldsymbol{y}_j + \boldsymbol{F} \|_2$ (Saad and Schultz, 1986).

The matrix-vector products required by Krylov methods can be approximated by the following relation which is actually a first-order Taylor series expansion approximation to the Jacobian ($\boldsymbol{J} = \boldsymbol{F}'(\boldsymbol{y}) = \frac{\partial \boldsymbol{F}}{\partial \boldsymbol{y}}$) times a vector (Knoll and Keys, 2004) :

$$\boldsymbol{J}\boldsymbol{\nu} = \frac{\boldsymbol{F}(\boldsymbol{y} + \varepsilon \boldsymbol{\nu}) - \boldsymbol{F}(\boldsymbol{y})}{\varepsilon} \tag{4.13}$$

where $\boldsymbol{\nu}$ is a vector and ε is a small perturbation parameter. The perturbation parameter ε is used for the calculation of the finite difference Eq. (4.13). It should be mentioned that if its value is too large, the derivative is poorly approximated and if it is too small the result of the finite difference is contaminated by floating-point round-off error. Therefore the selection of ε should maintain a balance of these two trade-offs. An extensive discussion about the selection of the parameter ε is given in Knoll and Keys (2004).

Although more than one Krylov methods exist, Generalized Minimized Residuals (GMRES) (Saad and Schultz, 1986) is one of the most popular.

4.4.3 *Adapting the Approximate Block Newton method to a Monte-Carlo/T-H context*

In this paragraph the way that the Approximate Block Newton (ABN) method is adapted to a Monte-Carlo/T-H context is described. The extensive derivation and description of the ABN method are presented by Yeckel et al. (2009). The ABN method could be seen as a modified version of the JFNK method oriented to the coupling of individual single-physics solvers. In other words it is an approximation of JFNK that tries to remove the features of JFNK that make its implementation in the coupling of distinct solvers difficult or even impossible.

Here two individual solvers, a neutronic solver called N and a T-H solver called T, are considered. The term solver includes the actual internal solver plus the necessary transformations of the results, as mentioned above. The starting point of this method is the PI-based iteration of Eq. (4.3):

$$\boldsymbol{x}^{k+1} = N(T(\boldsymbol{x}^k)) \tag{4.14}$$

This equation is a more compact way to write the system of Eqs (4.1 and 4.2). A converged solution $\boldsymbol{x}^*$ means $\boldsymbol{x}^{k+1} = \boldsymbol{x}^k = \boldsymbol{x}^*$. Eq. (4.14) could also be written in the following residual form:

$$\boldsymbol{F}(\boldsymbol{x}) = \boldsymbol{x} - N(T(\boldsymbol{x})) = \boldsymbol{0} \tag{4.15}$$

This is a problem of finding the root $\boldsymbol{x}^*$. In other words, this statement is nothing else than the requirement for convergence to the solution $\boldsymbol{x}^*$, i.e. when convergence is achieved there is no difference between successive updates of the solution ($N(T(\boldsymbol{x}^*) = \boldsymbol{x}^*$ or $\boldsymbol{x}^* - N(T(\boldsymbol{x}^*) = \boldsymbol{0}$). Eq. (4.15) can be solved with a Newton method:

$$\boldsymbol{J}(\boldsymbol{x})\delta\boldsymbol{x} = -\boldsymbol{F}(\boldsymbol{x}) \tag{4.16}$$

where the Jacobian matrix is given by the following relation

$$\boldsymbol{J} \equiv \frac{\partial \boldsymbol{F}}{\partial \boldsymbol{x}} = \boldsymbol{I} - \frac{\partial[N(T(\boldsymbol{x}))]}{\partial \boldsymbol{x}} \tag{4.17}$$

where $\boldsymbol{I}$ is the identity matrix. The construction of the second term of the RHS of Eq. (4.17) and thus the Jacobian matrix formulation element by element could be done by perturbing independently each element of the solution vector and then solving T and N to compute each element of $\frac{\partial[N(T(\boldsymbol{x}))]}{\partial \boldsymbol{x}}$. However it is obvious that the cost of such an approach would be prohibitive. In order to solve this linear system and at the same time to avoid the creation of the Jacobian matrix $\boldsymbol{J}$, a Krylov method is implemented. As mentioned above a Krylov solver is based on matrix-vector multiplication. Thus the requirement for calculation of $\boldsymbol{J}$ can be substituted by the calculation of matrix-vector products. The second term of the RHS of Eq. (4.17) is a directional derivative in the direction of $\boldsymbol{\nu}$. Thus the Jacobian matrix-vector products can be approximated by finite differences of the form:

$$\boldsymbol{J}\boldsymbol{\nu} = \boldsymbol{I}\boldsymbol{\nu} - \frac{\partial[N(T(\boldsymbol{x}))]}{\partial \boldsymbol{x}}\boldsymbol{\nu} \approx \boldsymbol{\nu} - \frac{1}{\varepsilon}(N(T(\boldsymbol{x} + \varepsilon\boldsymbol{\nu})) - N(T(\boldsymbol{x}))) \tag{4.18}$$

where $\boldsymbol{\nu}$ is a Krylov vector and ε is a perturbation parameter.

Thus the ABN iteration is performed following the below-mentioned steps:
Starting from the current guess of the solution vector $\boldsymbol{x}^k$, a PI-analogous step is executed as:

$$\boldsymbol{y}^{PI} = T(\boldsymbol{x}^k) \tag{4.19}$$

$$\boldsymbol{x}^{PI} = N(\boldsymbol{y}^{PI}) \tag{4.20}$$

where the upperscript PI indicates that this step corresponds to a PI iterative step and generates the solution update that a PI iteration would give. Afterwards a vector of residuals is constructed as:

$$\boldsymbol{F} = \boldsymbol{x}^k - \boldsymbol{x}^{PI} \tag{4.21}$$

Subsequently, the following system is solved:

$$\boldsymbol{J}\delta\boldsymbol{x}^{k} = -\boldsymbol{F} \tag{4.22}$$

For each iteration of the linear solver a matrix-vector product is constructed using the approximation:

$$\boldsymbol{J}\boldsymbol{\nu} \approx \boldsymbol{\nu} - \frac{1}{\varepsilon}(N(T(\boldsymbol{x}^{k} + \varepsilon\boldsymbol{\nu})) - \boldsymbol{x}^{PI}) \tag{4.23}$$

Once the solution $\delta\boldsymbol{x}^{k}$ is calculated, the neutronic solution is updated:

$$\boldsymbol{x}^{k+1} = \boldsymbol{x}^{k} + \delta\boldsymbol{x}^{k} \tag{4.24}$$

and finally the T-H solution is updated:

$$\boldsymbol{y}^{k+1} = T(\boldsymbol{x}^{k+1}) \tag{4.25}$$

When convergence has been achieved the iteration stops.

At this point three remarks should be made. Firstly, in this work the input of the T-H solver is updated using only neutronic information, i.e., the power distribution. Thus Eq. (4.25) is identical to Eq. (4.19). However, if the T-H input is updated based also on T-H calculated information, these two equations take the form $\boldsymbol{y}^{update} = T(\boldsymbol{x}, \boldsymbol{y})$. More specifically, Eq. (4.25) would take the form: $\boldsymbol{y}^{k+1} = T(\boldsymbol{x}^{k+1}, \boldsymbol{y}^{k})$ while Eq. (4.19) takes the form: $\boldsymbol{y}^{PI} = T(\boldsymbol{x}^{k}, \boldsymbol{y}^{k})$. Thus it is clear that when this difference is applied an extra T-H calculation is needed. Secondly, it is clear that the upperscript PI indicates that Eq. (4.19 and 4.20) correspond to a PI iterative step that generates the solution update that a PI iteration would give. From this point of view the ABN method could be considered as a correction to the PI method aiming to accelerate the convergence.

4.5 THE DEVELOPED COUPLING SCHEME

4.5.1 *Numerical tools*

In this work the ABN method has been adopted for coupling the Monte-Carlo solver OpenMC (Romano and Forget, 2013) and the T-H subchannel solver COBRA-EN (Basile et al., 1999). OpenMC is an open source Monte-Carlo solver written in modern Fortran (see § 4.2). COBRA-EN is a sub-channel analysis solver written in Fortran 77, which computes the T-H parameters in nuclear fuel rod bundles or cores for both steady state and transient conditions. It can be used for the thermal-hydraulic analysis of water, liquid metal and gas cooled reactors.

The GMRES Krylov method (Saad and Schultz, 1986) has been chosen to solve the linear system of Eq. (4.22). The implementation of the GMRES Krylov solver was done using

Algorithm 1 The introduced coupling scheme based on the ABN method

Find a neutronic guess $\boldsymbol{x}^0$

do $k = 0$, (Number of Newton iterations-1)

Calculate $\boldsymbol{y}^{PI}$ running T-H based on $\boldsymbol{x}^k$

Calculate $\boldsymbol{x}^{PI}$ running neutronics based on $\boldsymbol{y}^{PI}$

Construct the residual: $\boldsymbol{F} = \boldsymbol{x}^k - \boldsymbol{x}^{PI}$

Solve the linear system: $\boldsymbol{J}\delta\boldsymbol{x}^k = -\boldsymbol{F}$ (Krylov linear solver)

- - - - - - - - - - - - - *Internal operation of the Krylov solver*- - - - - - - - - - - - -

do $j = 1$, Number of Krylov iterations

...

Call an external subroutine that provides the matrix-vector approxim.:

Perturb the neutronic solution: $\boldsymbol{x}^j_{per} = \boldsymbol{x}^k + \varepsilon\boldsymbol{\nu}$

Calculate $\boldsymbol{y}^{PI,j}_{per} = T(\boldsymbol{x}^j_{per})$ running T-H based on $\boldsymbol{x}^j_{per}$

Calculate $\boldsymbol{x}^{PI,j}_{per} = N(\boldsymbol{y}^{PI,j}_{per})$ running neutronics based on $\boldsymbol{y}^{PI,j}_{per}$

Calculate the jth matrix-vector product: $\boldsymbol{J}\boldsymbol{\nu}^j = \boldsymbol{\nu}^j - \frac{1}{\varepsilon}(\boldsymbol{x}^{PI,j}_{per} - \boldsymbol{x}^{PI})$

...

end do

- -

Update the Neutronic solution: $\boldsymbol{x}^{k+1} = \boldsymbol{x}^k + \delta\boldsymbol{x}^k$

Update the T-H solution: $\boldsymbol{y}^{k+1} = N(\boldsymbol{x}^{k+1})$

end do

the PETSc library (*PETSc*). Also, the FoX XML library (Walker, 2014) was used to control the XML-elements in the input of OpenMC during the Newton and the Krylov iterative process. XML was also utilised for the initial generation of the input files of OpenMC. The coupling scheme was developed in Fortran.

4.5.2 *Practical implementation*

At this point it should be mentioned that there are two options for setting up the coupling scheme. According to the formulation of the method in section § 4.4.3, a neutronic-based scheme was developed, i.e. a vector of non-linear residuals (Eq. (4.21)) is built with the differences between fission-rates. An alternative option would be the development of a T-H based coupling scheme. This means that the residual $\boldsymbol{F}$ would contain information generated by T-H, e.g. the differences of fuel and coolant temperatures, coolant densities and any other variable that is considered part of the T-H vector $\boldsymbol{y}$ between successive evaluations. However in that case the different kinds of the involved T-H variables (fuel/coolant temperature, coolant density) would lead to a larger and possibly more complicated linear system. On the other hand as the neutronics-generated information includes only fission-rates, a smaller linear system should be solved. As a result a neutronic set-up is chosen here as the first stage of investigating this method.

The neutronic-based implementation of the algorithm is described in this paragraph. For the first step, an initial guess ($\boldsymbol{x}^0$) of the neutronic fission-rate distribution is required. For the next kth iterations the initial guess is the solution update calculated each time by the previous iteration. Given this initial guess a T-H calculation runs in order to generate the PI-based T-H conditions ($\boldsymbol{y}^{\mathrm{PI}}$). The OpenMC input is now updated with the new T-H conditions, a Monte-Carlo calculation runs and a new PI-based neutronic profile ($\boldsymbol{x}^{\mathrm{PI}}$) is generated. Now, a vector ($\boldsymbol{F}$) that contains the differences between the new ($\boldsymbol{x}^{\mathrm{PI}}$) and the old ($\boldsymbol{x}^{\mathrm{k}}$) fission-rate values is created (Eq. (4.21)). Thus $\boldsymbol{F}$ is the vector of the non-linear residuals. As a result, the linear system of Eq. (4.22) can now be solved. Of course, to avoid the construction of the matrix $\boldsymbol{J}$ as explained in § 4.4.3, the GMRES solver from the PETSc library is utilised. The implementation of the GMRES solver in PETSc provides the capability for a matrix-free solution of a linear system by calling an external subroutine in each iteration. This user-defined subroutine calculates the matrix-vector product (Eq. (4.23)). After a user-defined number of linear iterations or after a user-defined drop of a selected norm, the linear solver stops. The solution of the linear system $\delta\boldsymbol{x}$ is used to update the fission-rate distribution-solution that corresponds to the previous ABN step. As a final step, the T-H solution is updated running COBRA using as input the updated neutronic solution.

As mentioned above the matrix-vector products are constructed by a user-defined subroutine that is called in each step of the linear solver. Before the description of the construction of the matrix-vector product, a few words about the vector $\boldsymbol{\nu}$ should be said. Generally, Eq. (4.23) corresponds to the product of a matrix $\boldsymbol{J}$ and a general vector, i.e., no matter what this vector is. In a Krylov context this is a vector generated in each iteration of the linear solver and hereinafter it will be referred to as a Krylov vector. This Krylov vector is the new vector (member of the orthonormal Krylov basis, see § 4.4.2) generated in the current linear iteration by the Arnoldi method of orthogonalization (Saad and Schultz, 1986). This procedure concerns the internal operation of the linear solver. This vector is generated internally by the Krylov solver and is an input of the external subroutine that calculates the matrix-vector product. Observing Eq. (4.23) it is evident that the matrix-vector product is constructed as the difference between two vectors, i.e., the Krylov vector $\boldsymbol{\nu}$ (first term of RHS) and another one (second term). The second RHS term is a difference between the neutronic solution that would be generated if $\boldsymbol{x}^k$ would be perturbed by $\varepsilon\boldsymbol{\nu}$ and the PI-based guess ($\boldsymbol{x}^{PI}$) of the current iteration. In other words the old solution $\boldsymbol{x}^k$ is first perturbed giving $\boldsymbol{x}^k + \varepsilon\boldsymbol{\nu}$. This perturbed fission-rate profile is now used to run COBRA and then the new COBRA output ($T(\boldsymbol{x}^k + \varepsilon\boldsymbol{\nu})$) is used to update the OpenMC input. Finally, OpenMC runs using as input the vector $T(\boldsymbol{x}^k + \varepsilon\boldsymbol{\nu})$ and a new neutronic profile $N(T(\boldsymbol{x}^k + \varepsilon\boldsymbol{\nu}))$ is generated. Now the vector $\frac{1}{\varepsilon}N(T(\boldsymbol{x}^k + \varepsilon\boldsymbol{\nu}))$ is subtracted by the Krylov vector and the current matrix-vector product is generated. The introduced coupling scheme is illustrated in Algorithm (1). It should be mentioned that the role of the perturbation parameter ε needs to be investigated. Since a Monte-Carlo solver is used to analyse neutronics, it should be assured that the perturbation of the neutronic vector is larger than the statistical uncertainty to avoid poor approximation of the directional derivatives (Eq. (4.18)). In this work an experimentally found value ε=0.001 has been used. The procedure used to determine this value is similar to the one described by Yeckel et al. (2010).

Another important issue is the mapping between Monte-Carlo and T-H. Here, a one-to-one spatial mapping between the two solvers is implemented. The variables which are exchanged between neutronics and T-H are the fission-rate (power), the fuel/coolant temperature and the coolant density. Since COBRA uses channel-oriented cells whereas OpenMC uses pin-oriented ones, the surrounding coolant temperatures and densities of each rod in OpenMC are deduced by averaging throughout all the sub-channels surrounding that rod in the T-H field.

Concerning the treatment of the cross-section variation with temperature, the method of pseudo-materials has been adopted within this coupling scheme. According to this approach, each material in OpenMC is defined as a mixture of two pseudo-materials. The temperatures of the two pseudo-materials which compose the actual one corre-

spond to the upper (T_{high}) and lower (T_{low}) bounds of the particular interval in which the actual temperature (T), obtained from T-H, is lying. The linear-linear version of the method approximating the cross-section (Σ) of a material at the current temperature (T) is given by Eqs (4.26 - 4.28). In this work the JEFF 3.1.2 library (*Jeff-3.1.2*) in ACE format has been used, where cross-sections are provided at the 100K-1000K range with a 100K increment and 1200K, 1500K and 1800K. Only for the first numerical experiment, the NJOY code (MacFarlane and Muir, 1999) has been used to generate the missing libraries from 1000K to 2000K with an increment of 100K.

$$\Sigma(T) = w_{low}\Sigma(T_{low}) + w_{high}\Sigma(T_{high}) \tag{4.26}$$

$$w_{high} = \frac{T - T_{low}}{T_{high} - T_{low}} \tag{4.27}$$

$$w_{low} = 1 - w_{high} \tag{4.28}$$

As regards the thermal-scattering data for the moderator, the libraries provided by JEFF 3.1.2 are used. In this case the thermal-scattering library of each axial region corresponding to the temperature closest to the one of the moderator is used.

Finally, the results of the introduced ABN-based coupling scheme are compared with those of a PI-based coupling scheme. The latter is the one described in § 4.3. The only difference is that, in this work, a norm of the fission-rate distribution is monitored for convergence rather than that of the fuel temperature distribution.

4.6 NUMERICAL EXPERIMENTS

Since a new approach for Monte-Carlo/T-H coupled analysis is introduced, the aim of this section is twofold: to perform a first-step validation of the results of the proposed method and to highlight the possible advantages vs. the "traditional" method. For this reason the numerical experiments that are used here should be complex enough to highlight the potential numerical advantages of the introduced method and at the same time simple enough to allow for an initial validation. It should be noted that a very complicated test case might lead to failure of the goal of validation since constraints in accuracy could be induced by potentially significant differences in numerical performance.

Two configurations are analysed to evaluate the developed coupling scheme. For each model two numerical experiments were performed, one using the PI method and another using the ABN method. Before analysing the results it should be mentioned that, due to the Monte-Carlo neutronic solver utilisation, the computational cost of any other part of the algorithm is overshadowed by the Monte-Carlo runs. Therefore the computational cost of the algorithm is evaluated counting the number of Monte-Carlo runs.

Convergence will be monitored by measuring the update norm of both methodologies:

$$e_1 = \| \boldsymbol{x}^{k+1} - \boldsymbol{x}^{k} \|_2 \tag{4.29}$$

as well as the norm of the intermediate PI update within a ABN-step or, in other words, the norm of the non-linear residual vector:

$$e_2 = \| \boldsymbol{F}(\boldsymbol{x}^{k}) \|_2 = \| \boldsymbol{x}^{PI} - \boldsymbol{x}^{k} \|_2 \tag{4.30}$$

In addition, in order to evaluate the convergence of the linear solver per ABN-step the norm of the linear residual vector is also evaluated.

$$e_3 = \| \boldsymbol{r}^{j} \|_2 = \| -\boldsymbol{J}\delta\boldsymbol{x}^{j} - \boldsymbol{F} \|_2 \tag{4.31}$$

The subscript 2 indicates the Euclidean norm (l^2) in all cases. Finally, the multiplication factor will also act as an indicator of the convergence.

In this type of computational schemes the algorithm usually stops immediately after a pre-defined drop of one or more norms. However in this work the computations are let to proceed for a specified number of iterations aiming to evaluate the stability of the norms without stopping them by setting specific criteria.

Of course, the convergence criteria should be realistic since the drop of the corresponding norms is limited by the statistical uncertainty and thus by the used statistics (number of simulated histories). Established knowledge in performing Monte-Carlo/T-H analysis will provide empirically realistic values. One solution that could be possibly used to reach arbitrarily large drop of norms is the progressive increase of the used neutron histories per Newton step. Such an approach could also contribute to the avoidance of very "expensive" iterative steps when the solution is far from convergence. In addition relaxation schemes could be combined possibly with the Newton iteration in order to stabilize it. An investigation of such approaches could be a future research step. At this stage it is more interesting to see the relative difference in the performance of the two methods.

4.6.1 *A single fuel pin numerical experiment*

The first numerical experiment concerns a single BWR fuel pin whose detailed description can be found in Ivanov et al. (2012). More precisely this configuration consists of a single BWR uranium-based fuel pin surrounded by water that acts at the same time as coolant and moderator. At the top and bottom, there is a reflector made of the material of the cladding. The key features can be seen in Table 4.2. The fission-rate, the fuel and the coolant temperature and density are the parameters that are exchanged iteratively

between neutronics and T-H. The cladding temperature remains fixed within the coupled calculation. The temperature treatment in the neutronic side is done utilising the method of pseudo-materials. In both the neutronic and the T-H model, 38 axial regions have been used. In the radial direction, the neutronic model uses reflective boundary conditions whereas at the axial edges vacuum boundaries have been implemented. In COBRA the Armand-Messena correlation (Basile et al., 1999) is used for the calculation of the void fraction. For radial heat transfer, 5 radial nodes have been used for the calculation of the fuel temperature in each axial region. The effective fuel temperature, which passes to the neutronic model, is calculated with the Rowland formula (Rowlands, 1962) by post-processing the COBRA results. According to this formula the single value of the fuel temperature that corresponds to each axial region $T_{f,effective}$ is calculated as:

$$T_{f,effective} = \frac{4}{9}T_{f,center} + \frac{5}{9}T_{f,edge} \tag{4.32}$$

where $T_{f,center}$ is the temperature at the center of the fuel pin while $T_{f,edge}$ is the temperature at the radial edge.

Table 4.2: Main characteristics of the BWR single pin (first row) and the 1/8 symmetric PWR FA (second row) model.

Active length	Pellet radius	Pin radius	Inlet cool. temp.	Mass flow rate	Total power	Pressure
3.80m	0.5225cm	0.6125cm	553K	1120 kg/m^2 s	70kW	7.01MPa
3.66m	0.4100cm	0.4750cm	556.25K	3500 kg/m^2 s	2.149MW	14.91MPa

Table 4.3: Test-cases 4-1 & 4-2: Main calculation parameters.

Model	Coupling method	Monte-Carlo statistics batches/skipped/histories	Iterations (for ABN, Newton/ Krylov per Newton
Single-Pin	PI	400/100/500k	15
Single-Pin	ABN	400/100/500k	5/2
PWR-FA	PI	400/100/500k	15
PWR-FA	ABN	400/100/500k	5/2

4.6.1.1 *Results*

Fig. (4.10) illustrates the convergence of ABN vs PI for the single-pin BWR problem. It is clear that ABN outperforms PI in both convergence speed and computational cost. More

specifically, it can be observed that ABN reaches the limit of 3×10^{-4} in the 5th Newton iteration (=15 OpenMC runs). On the other hand PI after 15 iterations (=15 OpenMC runs) does not satisfy this limit and it seems that it stagnates in the area of 6×10^{-4}. In addition it can be seen that even at the 4th Newton iteration (=12 OpenMC runs) the vector norm e_1 is very close to the level of 3×10^{-4} whereas at the same time the 12th PI iteration lies above the limit of 10^{-3}. As mentioned above the part of the ABN algorithm after Eq. (4.20) is actually a correction to the current PI update. The l^2 norm of the intermediate PI update within each Newton step vs the l^2 norm of the final ABN update of each Newton step is illustrated in Fig. (4.11). It can be seen that in each Newton step the l^2 norm of the ABN correction is lower than the l^2 norm of the ABN-PI correction which confirms that ABN method outperforms the simple PI method because of the higher quality of the Newton correction. The fact that ABN converges quite fast is also reflected in the convergence of the linear solution per Newton step. More specifically, Fig. (4.12) illustrates a rapid drop of the linear residual norm (e_3); e_3 decreases by orders of magnitude from Newton step to Newton step indicating that the global problem gradually converges. The fact that the linear solution converges very fast can be explained noticing the formulation of this method and the inherent manipulation of the usage of the involved solvers (Yeckel et al. (2009),Yeckel et al. (2010)). The derivative of the non-linear residual vector, or in other words, the Jacobian matrix, does not differ from the identity matrix significantly if the perturbation is not too large. This form of the ABN matrix-vector products inserts a kind of inherent preconditioning of the linear system.

The multiplication factor calculated by ABN based on the T-H solution of the 5th Newton iteration is 1.25790 ± 0.00008 whereas the one calculated by PI in the 15th iteration is 1.25786 ± 0.00008. The difference is 4 pcm. The convergence of the calculated multiplication factor is depicted in Figs (4.13 and 4.14). According to The ABN-calculated multiplication factor converges almost immediately compared with PI where the convergence is achieved after 10 iterations where a quite large oscillation is observed. A zoom-in shows that there is an oscillation of ~50 pcm in the last 3 ABN iterations. In the last 6 PI iterations there is an oscillation of a maximum range of ~160 pcm. This again highlights the faster ABN global convergence but also suggests that the convergence should be monitored using additional criteria based on the multiplication factor. The fission-rate profiles calculated by the two methods are illustrated in Fig. (4.15 and 4.16). Although Fig. (4.16) shows that the maximum difference in the calculated fission-rate profile is 1.72%, that is not negligible, this difference is observed in layers that produce negligible power levels. Thus it is probably caused by the higher statistical uncertainty of those regions. Secondly, this difference might be attributed to the limited numerical efficiency of the PI method. To investigate this statement the PI is let to run for 3 extra

iterations, i.e., 18 in total. Now the power profile of the 5th ABN iteration is compared with the one of the 18th PI iteration. Fig. (4.17) illustrates the relative difference. The maximum value is now 0.838%, and the statement mentioned above is confirmed. Also, the area of relatively higher difference is concentrated again in the upper axial levels that are characterised by low power production also indicating the contribution of the statistical uncertainty to this difference.

Figs (4.18-4.23) show the T-H sub-solution and the comparison between the two methods; there is no significant difference. More specifically the maximum difference in coolant density and fuel temperature between ABN and PI and is 0.1% and 0.22%, respectively. The coolant temperature is the least sensitive parameter showing a negligible difference between the two methods.

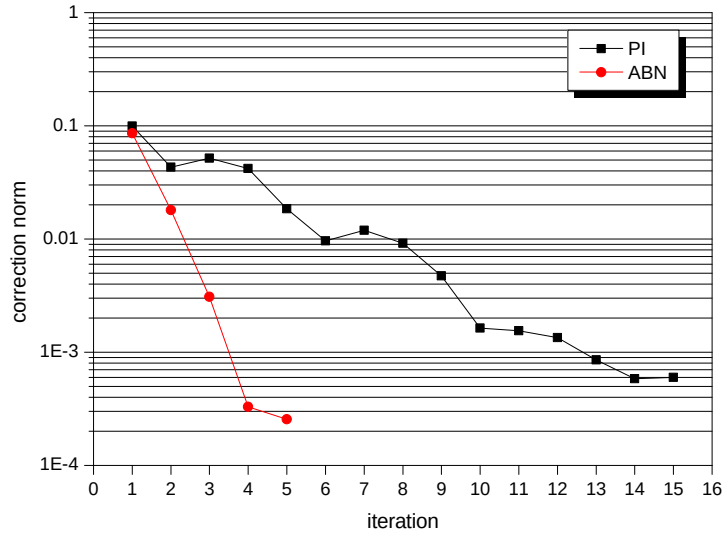

Figure 4.10: Test-case 4-2: Correction norm ($\| \boldsymbol{x}^{k+1} - \boldsymbol{x}^{k} \|_2$) of ABN vs PI method.

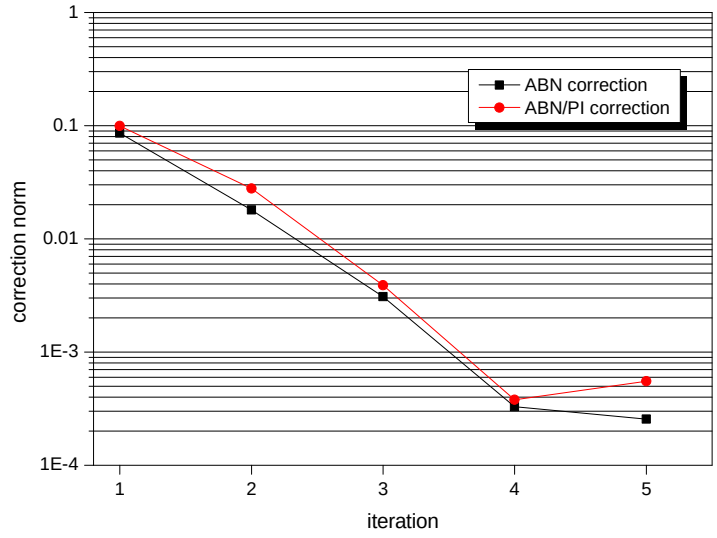

Figure 4.11: Test-case 4-2: Final ABN ($\| x^{k+1} - x^k \|_2$) vs intermediate PI ($\| x^{PI} - x^k \|_2$) correction within ABN iterations.

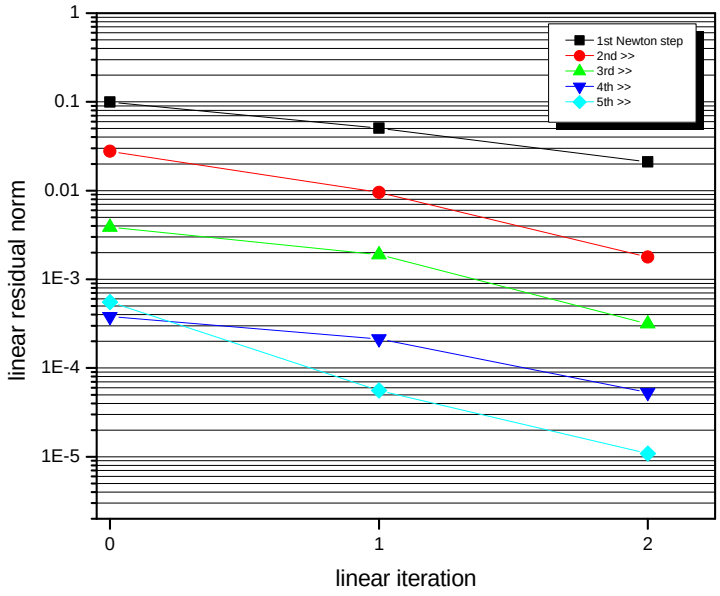

Figure 4.12: Test-case 4-2: Convergence of the linear solver ($\| J\delta x^j + F \|_2$).

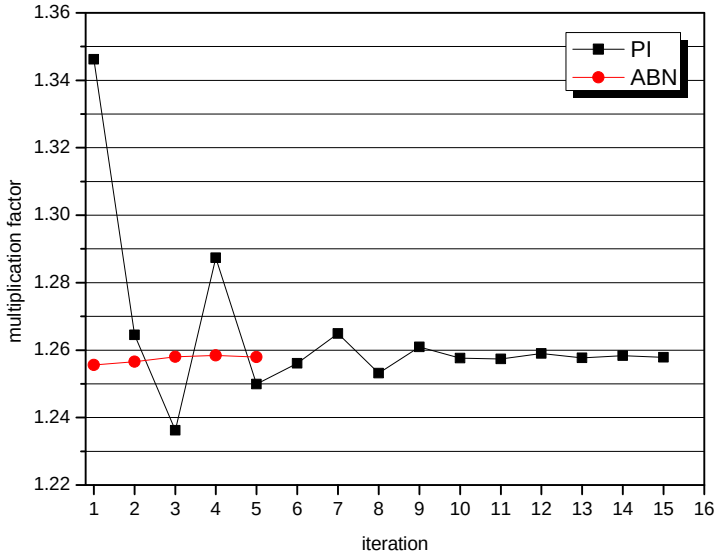

Figure 4.13: Test-case 4-2: Convergence of the multiplication factor.

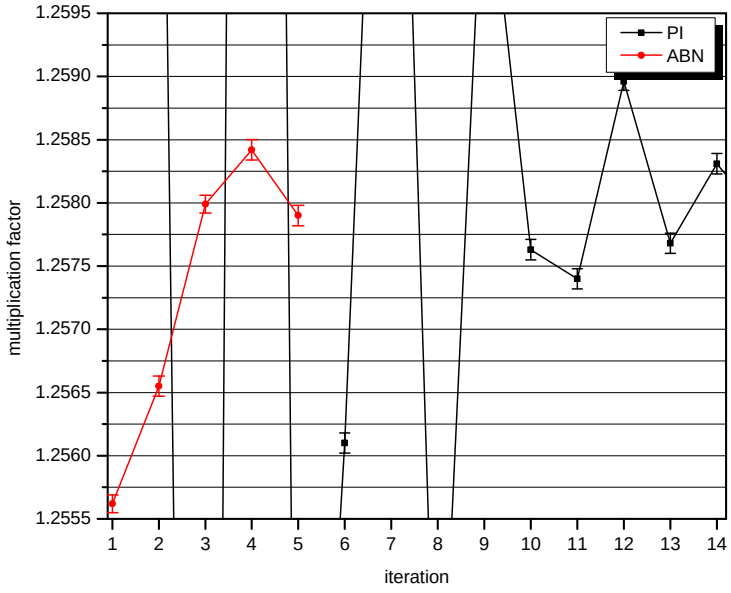

Figure 4.14: Test-case 4-2: Convergence of the multiplication factor (zoom-in).

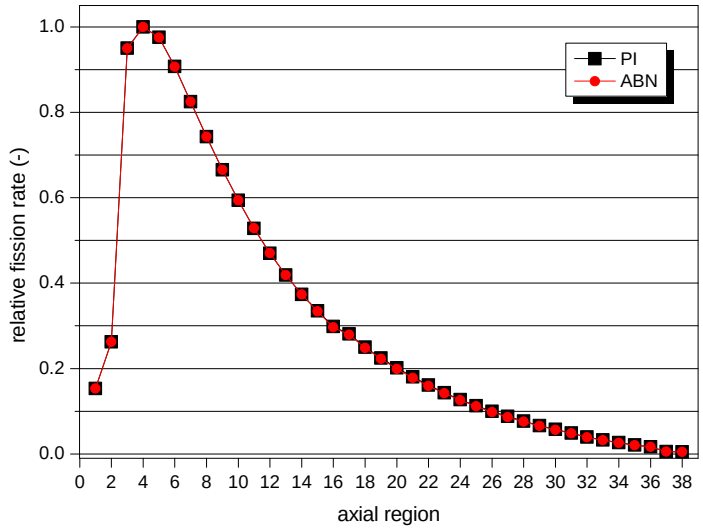

Figure 4.15: Test-case 4-2: Axial relative to max fission-rate distribution.

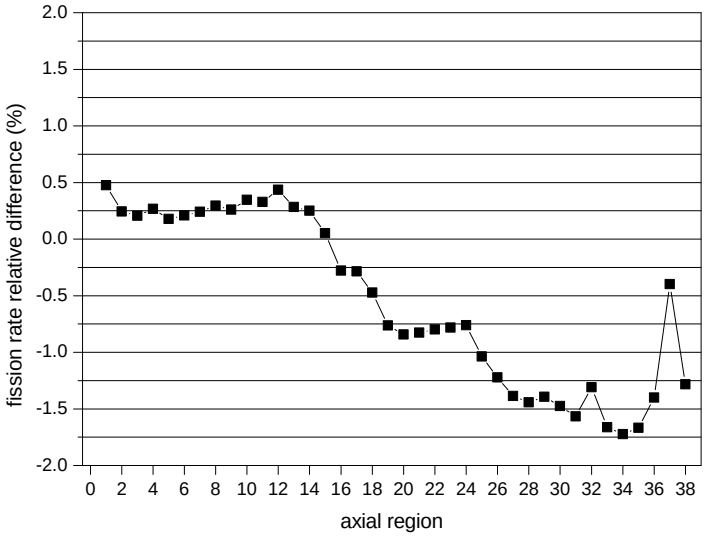

Figure 4.16: Test-case 4-2: Relative difference ($\frac{\text{ABN}-\text{PI}}{\text{PI}} \times 100$) between ABN (5th) and PI (15th) fission-rate profile.

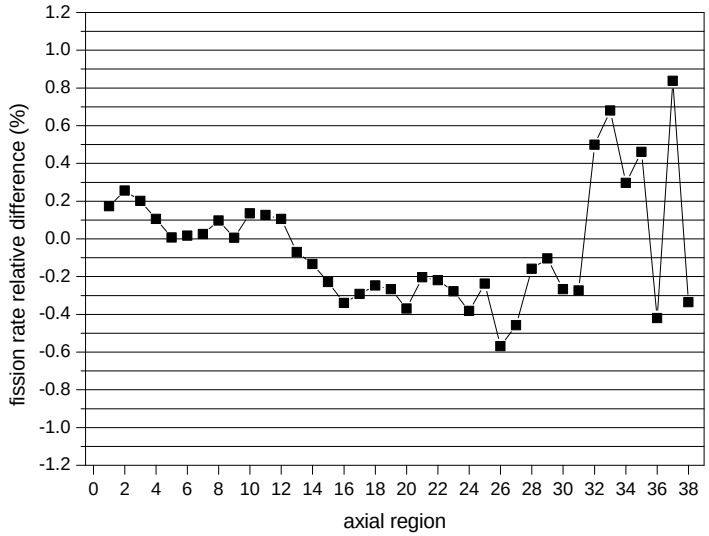

Figure 4.17: Test-case 4-2: Relative difference ($\frac{\text{ABN}-\text{PI}}{\text{PI}} \times 100$) between ABN (5th) and PI (18th) fission-rate profile.

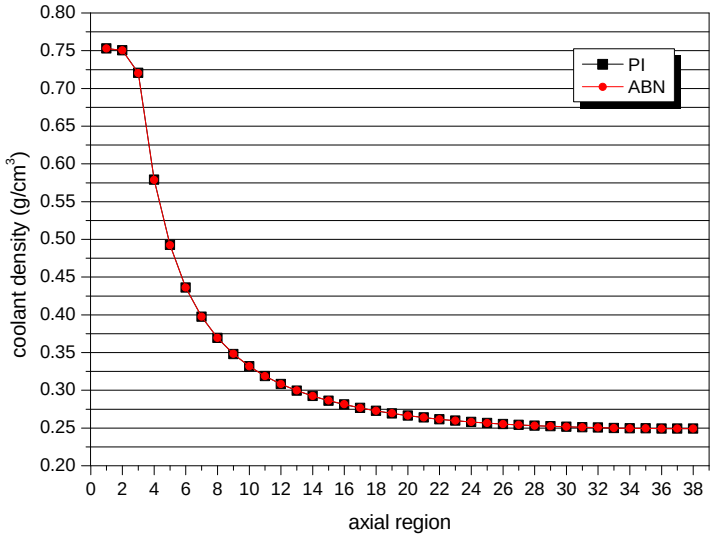

Figure 4.18: Test-case 4-2: Coolant density profile.

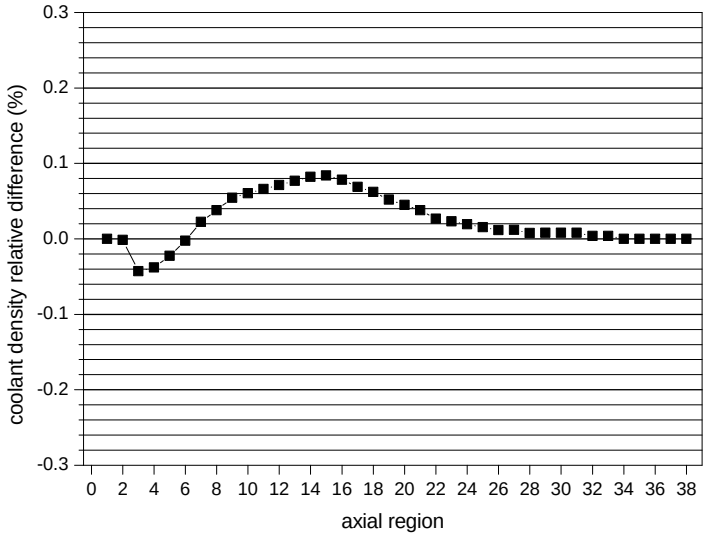

Figure 4.19: Test-case 4-2: Relative difference ($\frac{\text{ABN}-\text{PI}}{\text{PI}} \times 100$) between ABN and PI coolant density profile.

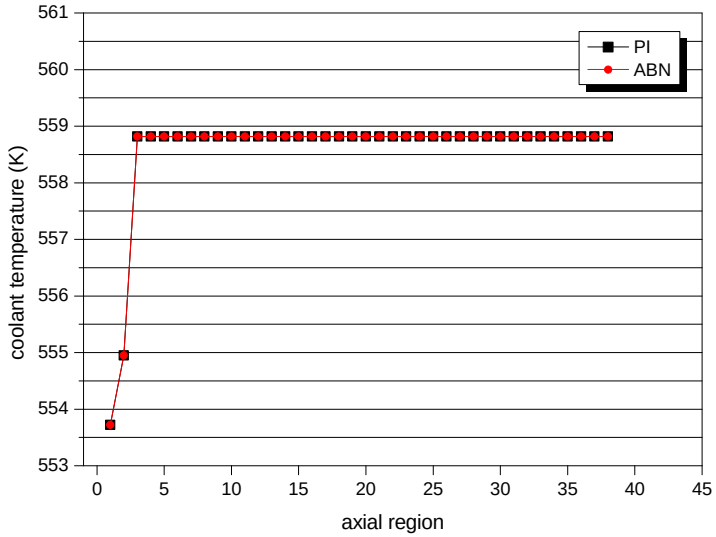

Figure 4.20: Test-case 4-2: Coolant temperature profile.

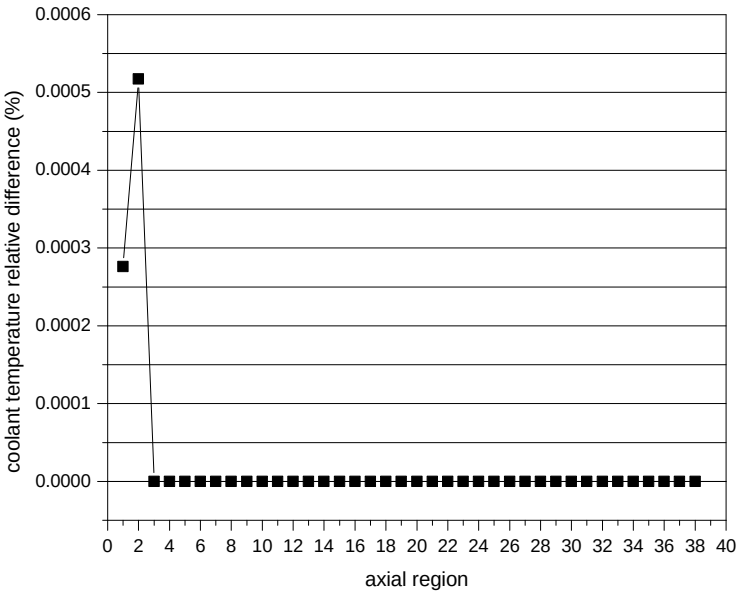

Figure 4.21: Test-case 4-2: Relative difference ($\frac{\text{ABN}-\text{PI}}{\text{PI}} \times 100$) between ABN and PI coolant temperature profile.

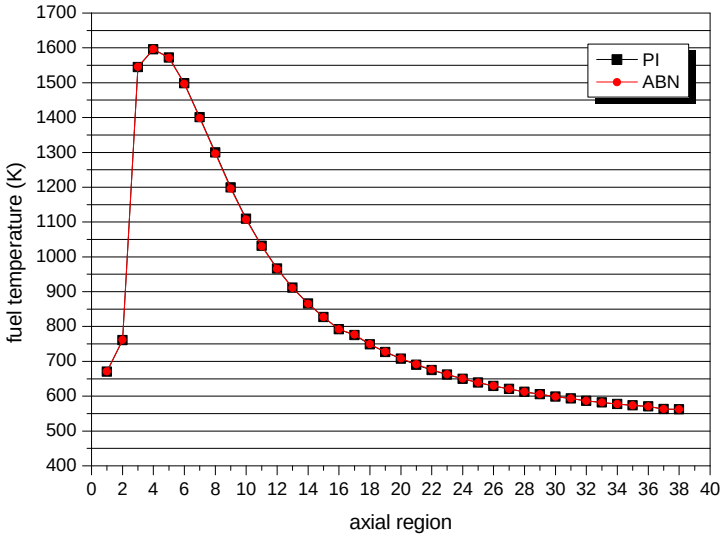

Figure 4.22: Test-case 4-2: Fuel temperature profile.

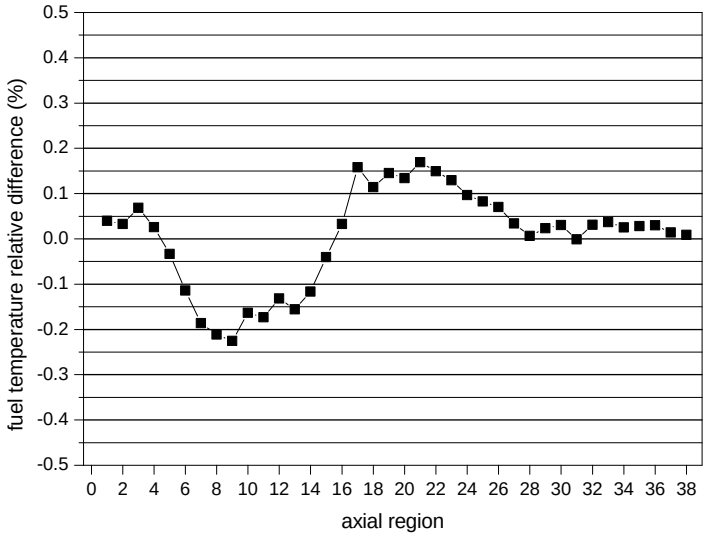

Figure 4.23: Test-case 4-2: Relative difference ($\frac{\text{ABN}-\text{PI}}{\text{PI}} \times 100$) between ABN and PI fuel temperature profile.

4.6.2 *Test-case 4-3 & 4-4: A Fuel Assembly numerical experiment*

The second experiment concerns the analysis of a pin-by-pin PWR FA configuration. A model of a PWR FA, captured from Hoogenboom et al. (2011), is analysed using OpenMC/COBRA. In this coupled calculation a 1/8 symmetric FA model has been used in both OpenMC and COBRA. It consists of 45 pins (39 fuel pins and 6 guide tubes) each one axially divided into 20 nodes. In both the neutronic and the T-H calculations the model has been axially separated in only 20 regions since the PWR coolant is characterised by much lower density gradients than the case of a BWR. In the radial direction the OpenMC model uses reflective boundary conditions whereas at the axial edges vacuum boundaries have been implemented. The homogeneous model (Basile et al., 1999) has been selected for the calculation of the void fraction. The key features of the model analysed here can be seen in Table 4.2. It should be mentioned that all the graphs presenting the calculated physical quantities of the FA use a 1/4 symmetric part of the FA.

4.6.2.1 *Results*

Fig. (4.24) illustrates the convergence of ABN vs PI for the PWR FA problem. It seems that the convergence of the ABN is superior because the l^2 norm of the Newton correction

is moving at a level lower than 10^{-4} at the 3rd iteration (=9 OpenMC runs) and then it slightly oscillates around this level. On the other hand, PI shows a quite oscillatory behaviour and only the minima of this oscillation satisfy drop below this level. Even after 20 iterations (=20 OpenMC runs) PI fails to achieve a stable behaviour. Similarly to the previous case Fig. (4.25) shows that in each Newton step the l^2 norm of the ABN correction is lower than the l^2 norm of the ABN-PI correction. This problem is possibly "easier" in numerical terms than the previous one since both methods reach their convergence limits (connected with the used Monte-Carlo statistics) quite fast and then they stagnate. This hypothesis is also confirmed by Fig. (4.26) where the convergence of the linear solver is illustrated; it can be noticed that after the first Newton step the linear solver oscillates for the remaining Newton steps without indicating a gradually (in successive Newton steps) larger drop of the linear residual norm (e_3).

The multiplication factor calculated by ABN in the 7th Newton iteration is 0.99694$\pm$ 0.00006 whereas the one calculated by PI in the 20th iteration is 0.99702 $\pm$ 0.00008 . The difference is 8 pcm. As regards the neutronic solution Fig. (4.27) shows the relative fission-rate distribution calculated with ABN. The maximum difference between ABN and PI is 3.5%. Fig. (4.28) depicts the relative difference between the fission-rate distributions calculated by the two coupling algorithms in some axial levels. The difference of 3.5% is relatively high but it is again concentrated on levels with very low power production and thus higher statistical uncertainty (Fig. (4.28)). Further analysis shows that differences above 1% are concentrated only on the lower and upper part of the FA, due to the low power levels of these regions. This is confirmed by Figs (4.29, 4.30, 4.31, 4.32, 4.33, 4.34 and 4.35). The coolant density distribution is illustrated in Fig. (4.36) whereas the coolant density relative difference between the two methods is presented in Fig. (4.37). The agreement is very satisfactory with a maximum absolute difference value ~0.07%. The coolant temperature distribution is illustrated in Fig. (4.38). Fig.(4.39) confirms that this is the least sensitive parameter within the iterative coupled solutions with maximum difference between the two methods ~ 0.02%.

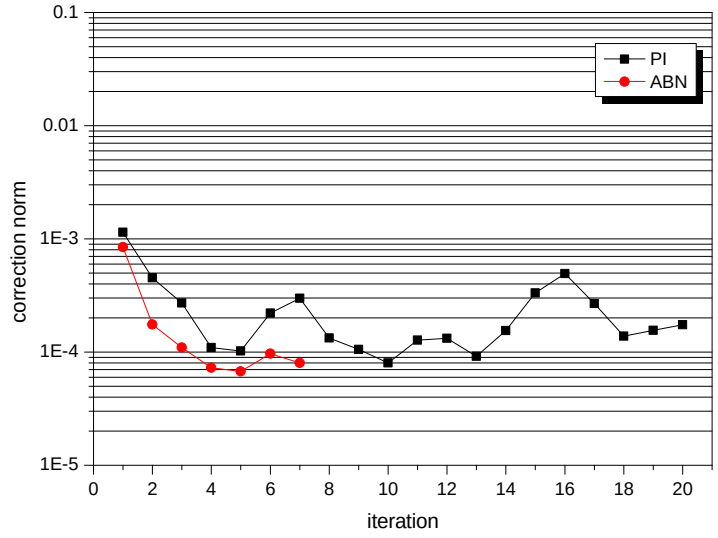

Figure 4.24: Test-case 4-3: Correction norm ($\| \boldsymbol{x}^{k+1} - \boldsymbol{x}^{k} \|_2$) of ABN vs PI method.

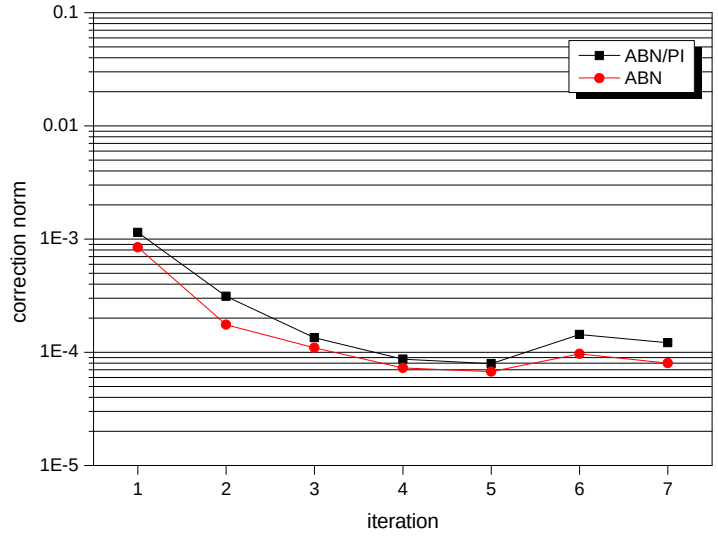

Figure 4.25: Test-case 4-3: ABN ($\| \boldsymbol{x}^{k+1} - \boldsymbol{x}^{k} \|_2$) vs PI ($\| \boldsymbol{x}^{PI} - \boldsymbol{x}^{k} \|_2$) correction within ABN method.

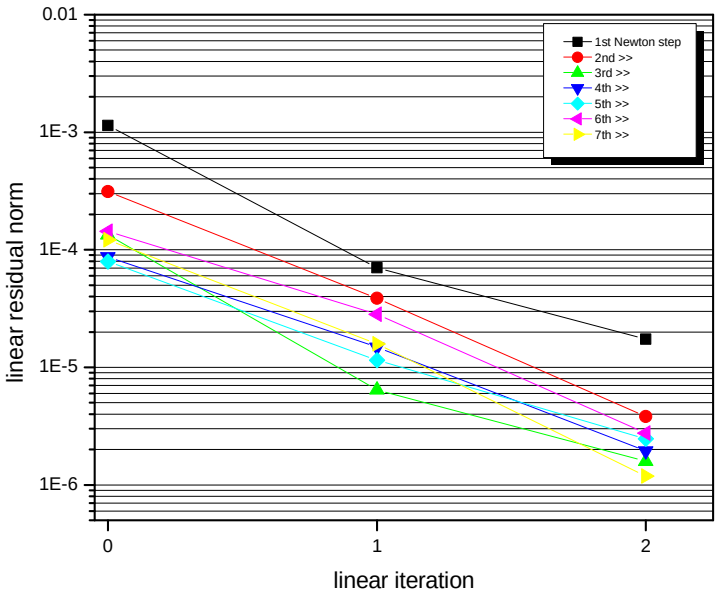

Figure 4.26: Test-case 4-3: Convergence of the linear solver ($\| \boldsymbol{J}\delta\boldsymbol{x}^j + \boldsymbol{F} \|_2$).

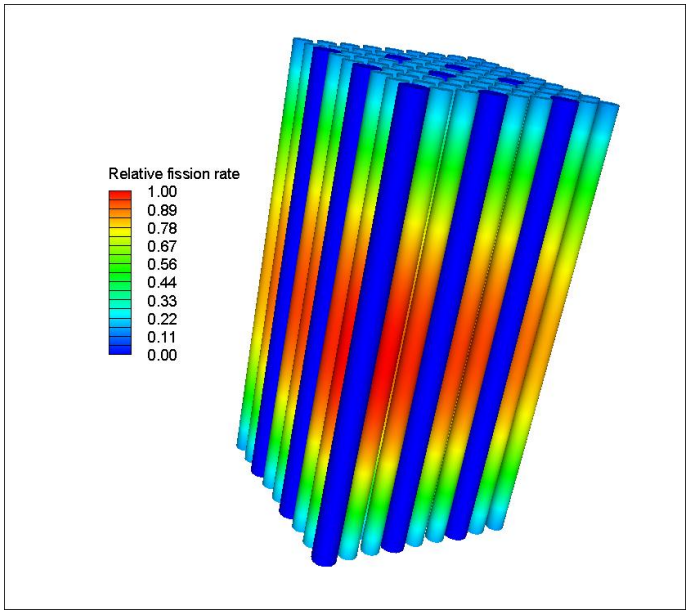

Figure 4.27: Test-case 4-3: Relative (to the max) fission-rate distribution.

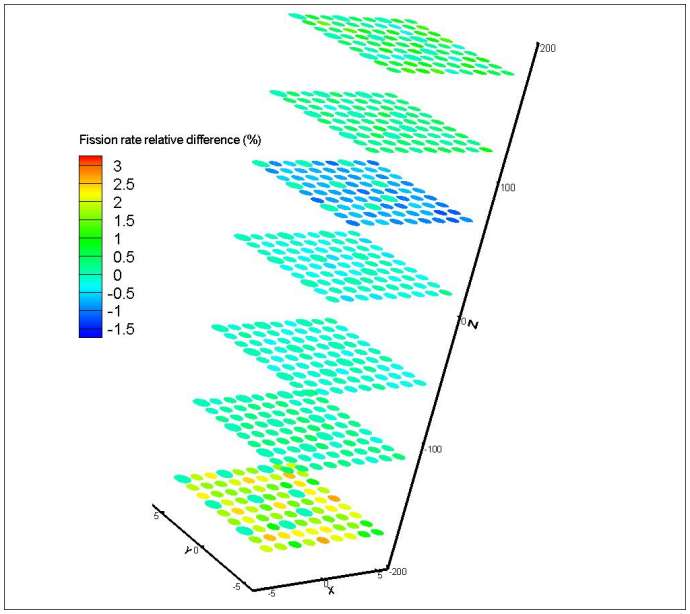

Figure 4.28: Test-case 4-3: Relative difference $(\frac{\text{ABN}-\text{PI}}{\text{PI}} \times 100)$ between ABN and PI fission-rate distribution.

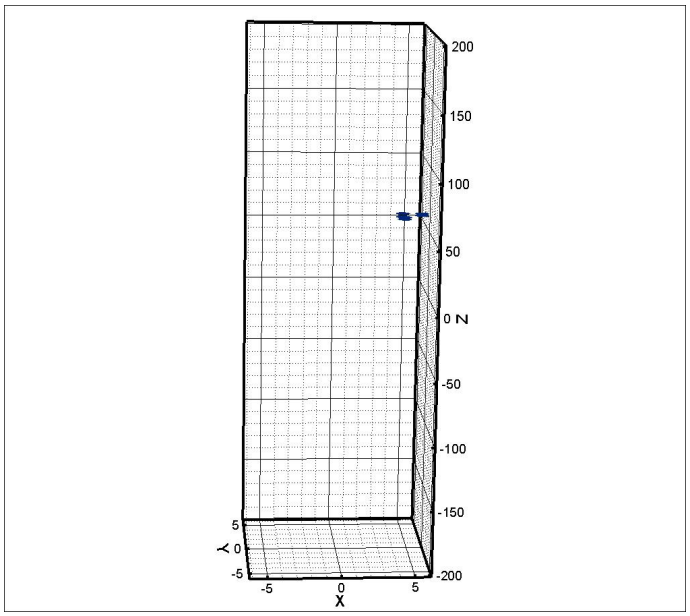

Figure 4.29: Test-case 4-3: Isosurface of fission-rate relative difference $\frac{\text{ABN}-\text{PI}}{\text{PI}}$= -1.218%.

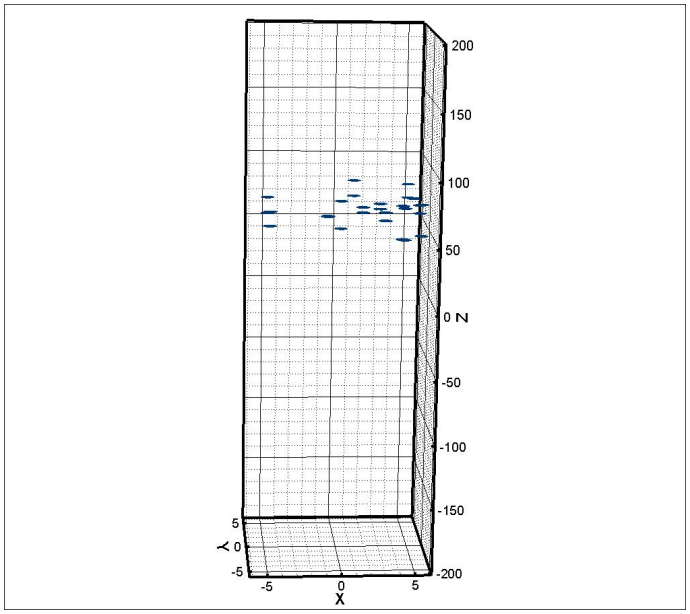

Figure 4.30: Test-case 4-3: Isosurface of fission-rate relative difference $\frac{\mathrm{ABN}-\mathrm{PI}}{\mathrm{PI}}$= -1.031%.

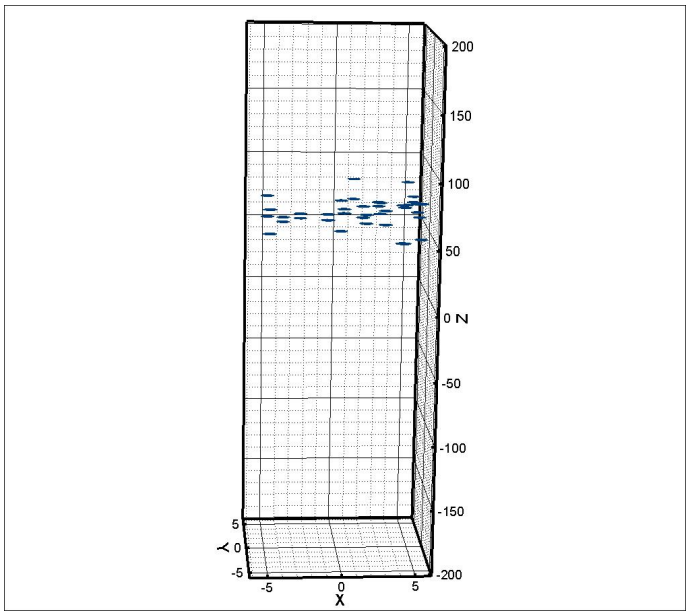

Figure 4.31: Test-case 4-3: Isosurface of fission-rate relative difference $\frac{\mathrm{ABN}-\mathrm{PI}}{\mathrm{PI}}$= -0.984%.

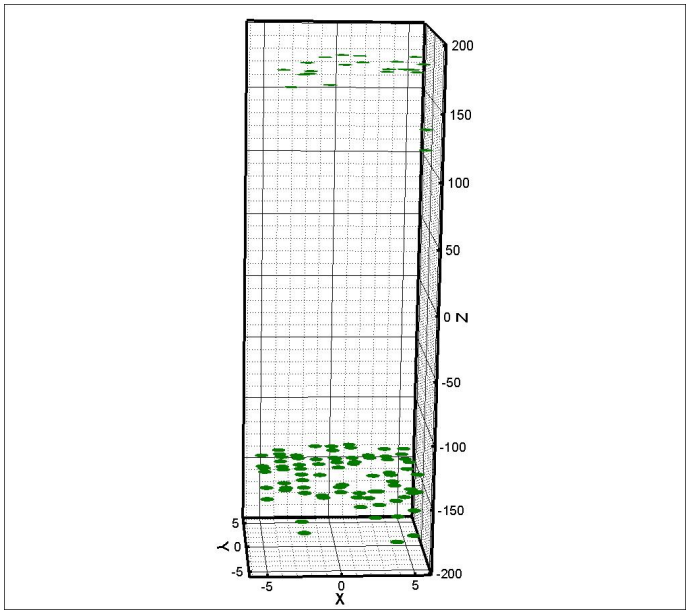

Figure 4.32: Test-case 4-3: Isosurface of fission-rate relative difference $\frac{\mathrm{ABN}-\mathrm{PI}}{\mathrm{PI}} = 1\%$.

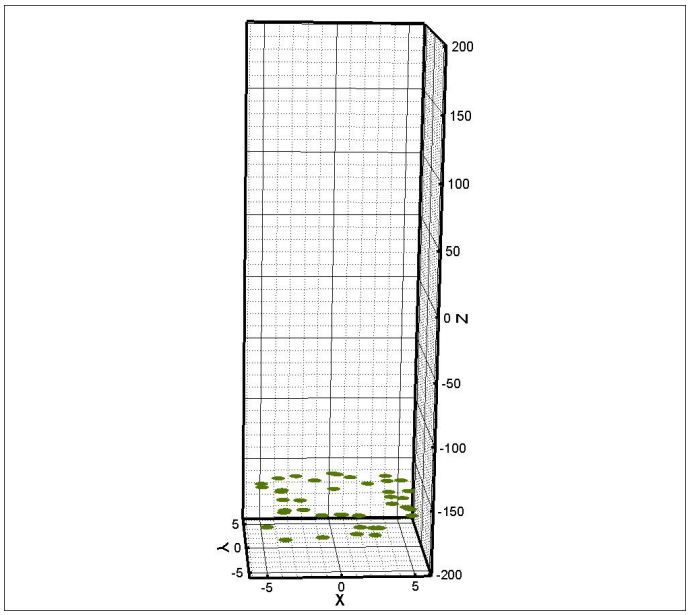

Figure 4.33: Test-case 4-3: Isosurface of fission-rate relative difference $\frac{\mathrm{ABN}-\mathrm{PI}}{\mathrm{PI}} = 1.835\%$.

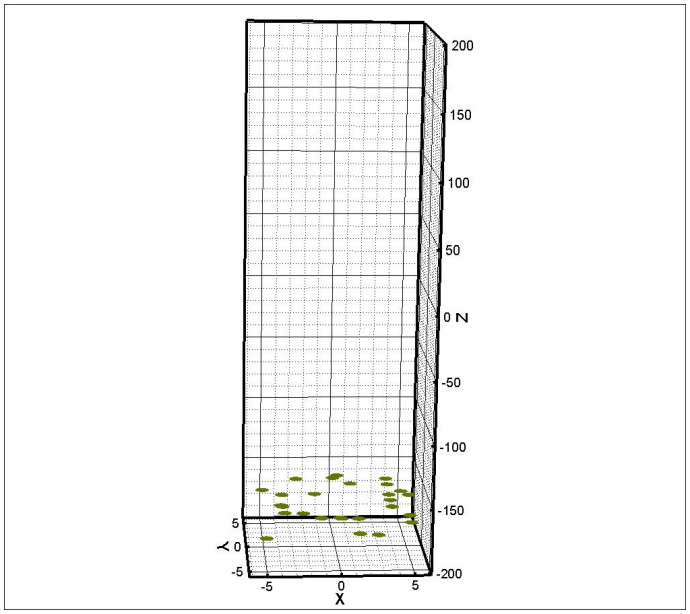

Figure 4.34: Test-case 4-3: Isosurface of fission-rate relative difference $\frac{\mathrm{ABN}-\mathrm{PI}}{\mathrm{PI}} = 2\%$.

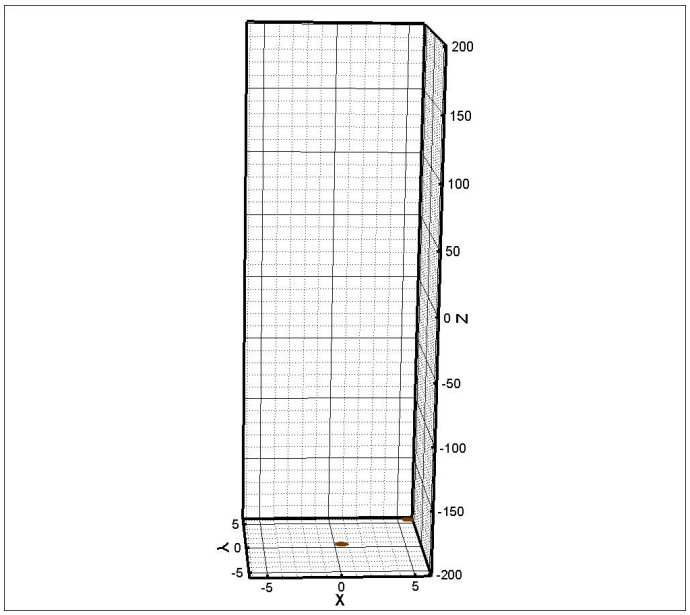

Figure 4.35: Test-case 4-3: Isosurface of fission-rate relative difference $\frac{\mathrm{ABN}-\mathrm{PI}}{\mathrm{PI}} = 2.8356\%$.

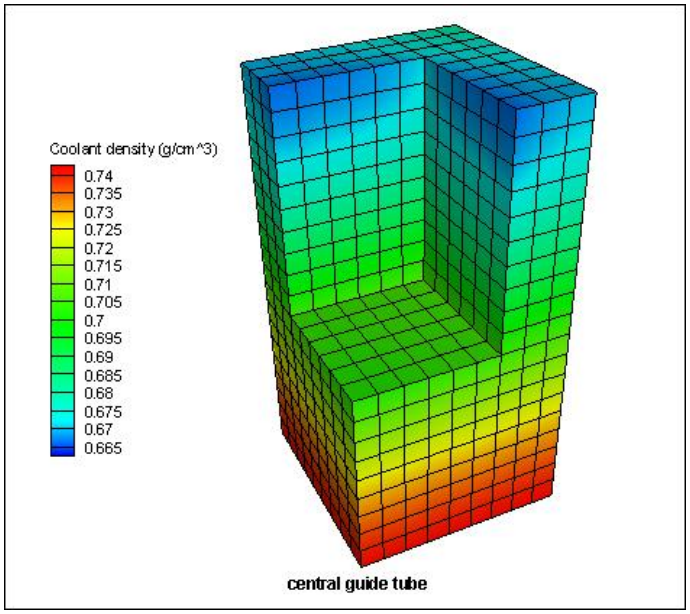

Figure 4.36: Test-case 4-3: Coolant density distribution.

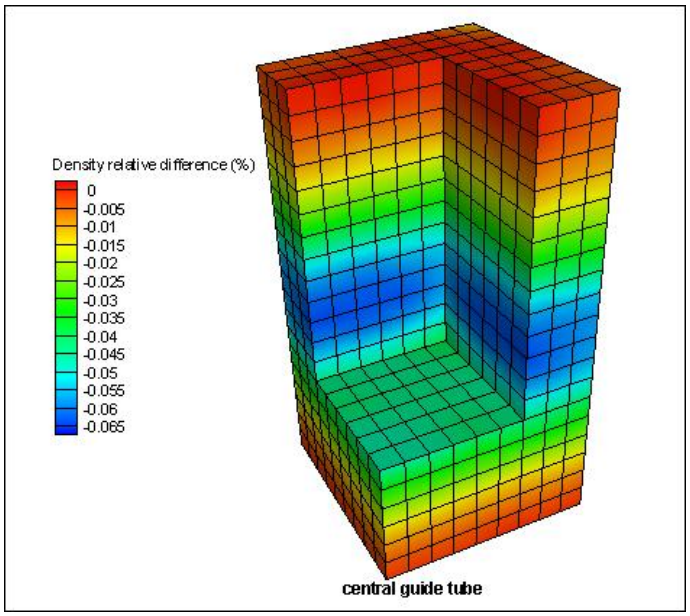

Figure 4.37: Test-case 4-3: Relative difference $(\frac{\mathrm{ABN}-\mathrm{PI}}{\mathrm{PI}} \times 100)$ between ABN and PI coolant density distribution.

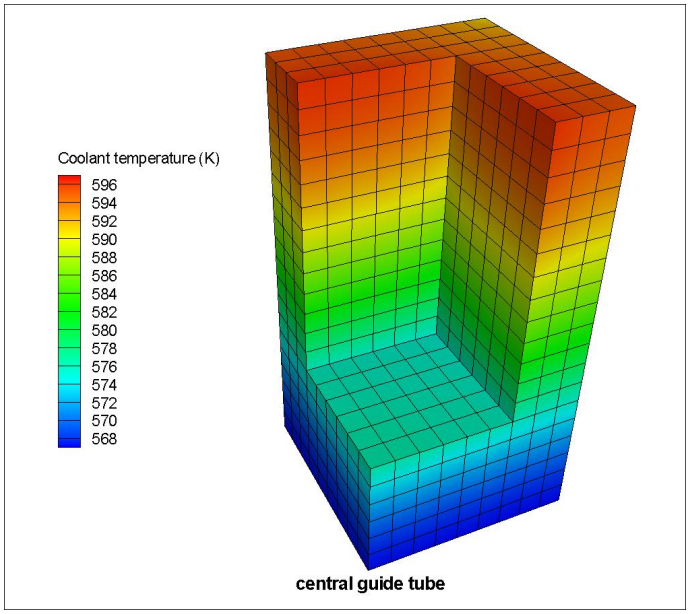

Figure 4.38: Test-case 4-3: Coolant temperature density.

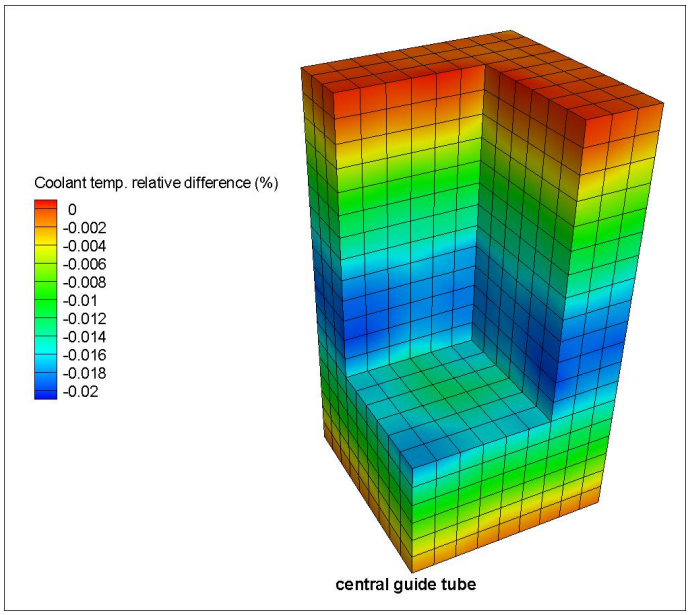

Figure 4.39: Test-case 4-3: Relative difference $(\frac{\mathrm{ABN}-\mathrm{PI}}{\mathrm{PI}} \times 100)$ between ABN and PI coolant temperature distribution.

Because this numerical experiment converges very fast compared with the previous one (probably due to the much lower coolant-moderator density gradients), the coolant-moderator pressure is now decreased to the value used in the single-pin test-case, i.e., P=7.01 MPa; this is done in order to achieve an increase in the void fraction and conse-

quently stronger density gradients. In addition the atom density of U-235 has been increased for the same reason. Then the performance of the two methodologies is re-evaluated. In addition an extra PI calculation was run using the following under-relaxation scheme:

$$\boldsymbol{x}_{relax}^{k+1} = \boldsymbol{x}^{k} + \omega(\boldsymbol{x}^{k+1} - \boldsymbol{x}^{k}) \tag{4.33}$$

where ω is the under-relaxation parameter. Table (4.4) shows the main numerical characteristics of these extra calculations. Now ABN is performed again with a maximum number of Krylov linear iterations per Newton iteration equal to 2. However the linear residual norm e_3 (Eq. (4.31)) is measured and a specific limit (tol_{e_3}) is specified. Consequently, linear iterations (not more than 2 in this case) are performed until the imposed limit is satisfied. Fig. (4.40) illustrates the convergence of ABN vs PI (with and

Table 4.4: Main calculation parameters of the modified FA numerical experiment.

Model	Coupling method	Monte-Carlo statistics batches/skipped/ histories	Iterations (for ABN, Newton/ Krylov per Newton
FA-modif.	PI with no relax.	400/100/500k	18
FA-modif.	PI with relax. ($\omega = 0.5$)	400/100/500k	24
FA-modif.	ABN	400/100/500k	8/2 and $tol_{e_3} = 10^{-5}$

without relaxation) for the modified FA problem. It is obvious that ABN outperforms both PI approaches in both convergence and computational cost. More specifically, it seems that ABN stabilises around the level of 4×10^{-5} after 5 Newton iterations (=15 OpenMC runs). On the other hand PI without relaxation is characterised by a quite oscillatory behaviour even after 18 iterations (=18 OpenMC runs). As regards PI with relaxation, it is clear that outperforms significantly PI without relaxation reaching higher convergence levels. However it is outperformed by the ABN approach failing to show as stable behaviour as ABN does. (Fig. (4.40)). Although it temporarily achieves a higher norm drop, it afterwards exhibits an oscillatory behaviour. The fact that ABN stabilises after 5 iterations is also confirmed by the behaviour of the Krylov linear iteration that is depicted in Fig. (4.41). More specifically, for the first 7 Newton iterations, 2 Krylov iterations are performed whereas for the last Newton iteration only one linear iteration is adequate to satisfy the imposed linear convergence limit (tol_{e_3}).

Fig. (4.42) shows the convergence of the multiplication factor. Again it can be noticed that the ABN-calculated multiplication factor converges immediately, i.e., after 2 iterations (=6 OpenMC executions). PI without relaxation needs 9 iterations (=9 OpenMC

executions) whereas PI with relaxation needs 5 iterations (=5 OpenMC executions). The multiplication factor calculated by PI without relaxation in the 18th iteration is 0.94491 ± 0.00006 whereas PI with relaxation in the 24th gives 0.94491 ± 0.00007. The ABN calculated multiplication factor is 0.94467 ± 0.00007; The difference between ABN and both PIs is 0.00024 ± 0.00010, i.e. zero is more than 2 standard deviations away from the difference. Thus this point needs further investigation. The latter shows that the value given by the PI with relaxation at the 23rd iteration, i.e., one iteration before, is 0.94470 ± 0.00007, much closer to the ABN value. This is a hint that the difference mentioned above between ABN and PI is caused by the unstable behaviour of PI. For supporting this hypothesis the difference of the multiplication factor between successive iterations is plotted in Fig. (4.43). This graph shows that after some iterations ABN corrects the multiplication factor less than both PIs confirming its more stable behaviour. Finally, this is evident when the multiplication factors only from the converged region of each method are plotted. Fig. (4.44) shows clearly that the PI calculated multiplication factor oscillates significantly while the ABN shows a much more stable behaviour. These remarks indicate that it is the insufficient PI numerics that creates large differences between successive iterations and thus it could lead to misinterpretation. In other words these PI oscillations show that the establishment of criteria that consider just the drop of the norms of some variables can be insufficient.

Fig. (4.45) shows the relative fission-rate distribution calculated by ABN. It can be seen that due to the higher density gradients the peak of the fission-rate has significantly moved towards the lower part of the configuration where the coolant/moderator density is larger than that of the lower levels. Fig. (4.46) shows the relative difference of the fission-rate distributions between ABN and PI with relaxation for some axial levels. The maximum absolute difference is ~ 3.37%. Observing Fig. (4.46) it is again clear that this relatively large difference occurs at the very upper axial levels that correspond to a negligible power production and thus to a higher statistical uncertainty. Fig. (4.47) depicts the coolant density distribution and Fig. (4.48) the relative difference between ABN and PI that is negligible.

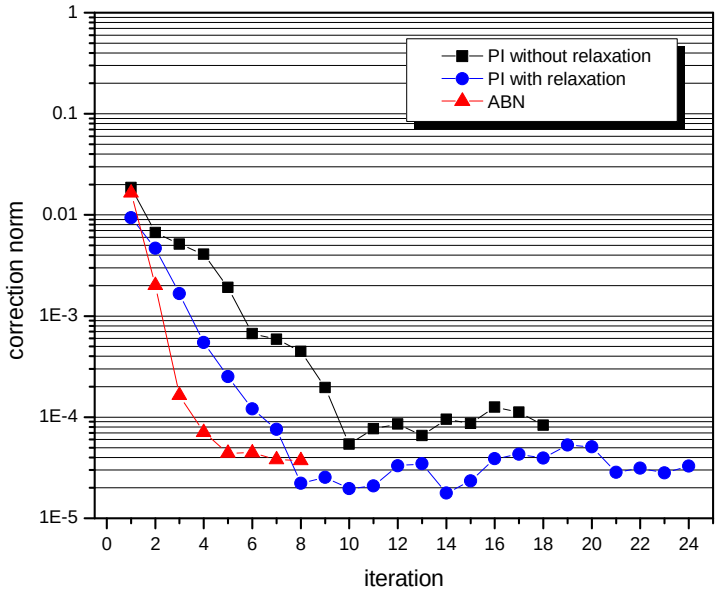

Figure 4.40: Test-case 4-4: Correction norm ($\| \boldsymbol{x}^{k+1} - \boldsymbol{x}^{k} \|_2$) of ABN vs PI (with and without relaxation) method.

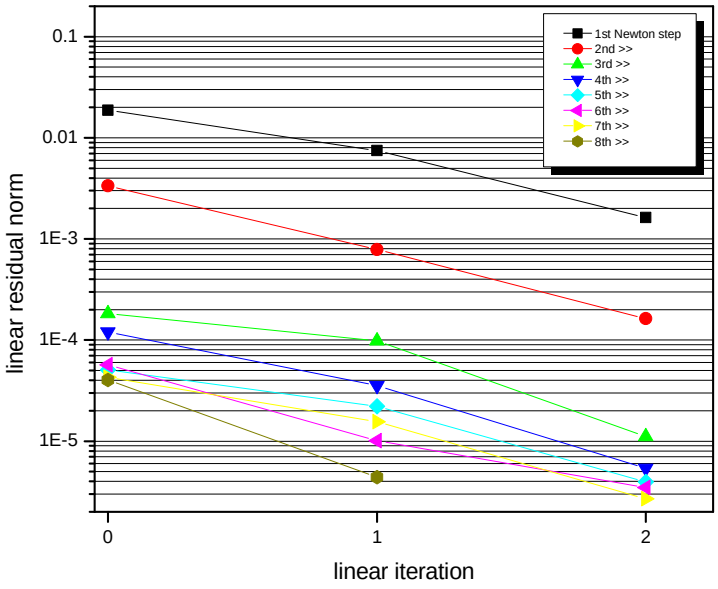

Figure 4.41: Test-case 4-4: Convergence of the Krylov linear solver ($\| \boldsymbol{J}\delta\boldsymbol{x}^{j} + \boldsymbol{F} \|_2$).

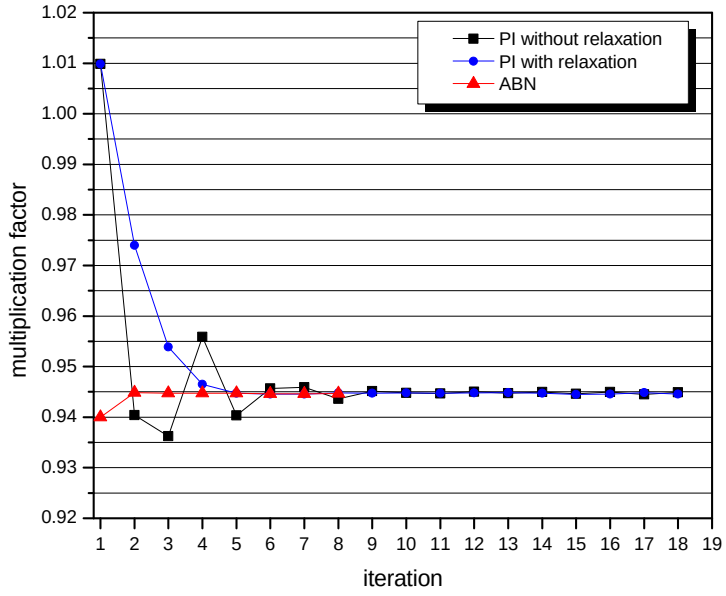

Figure 4.42: Test-case 4-4: Multiplication factor within iterations.

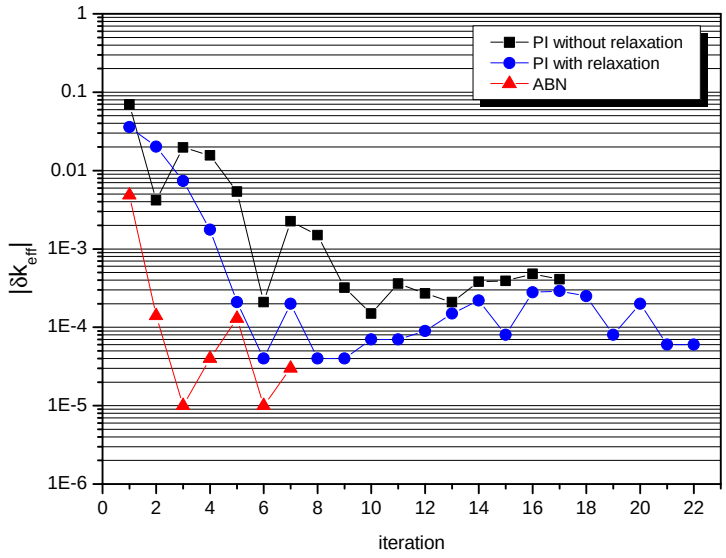

Figure 4.43: Test-case 4-4: Multiplication factor correction within iterations.

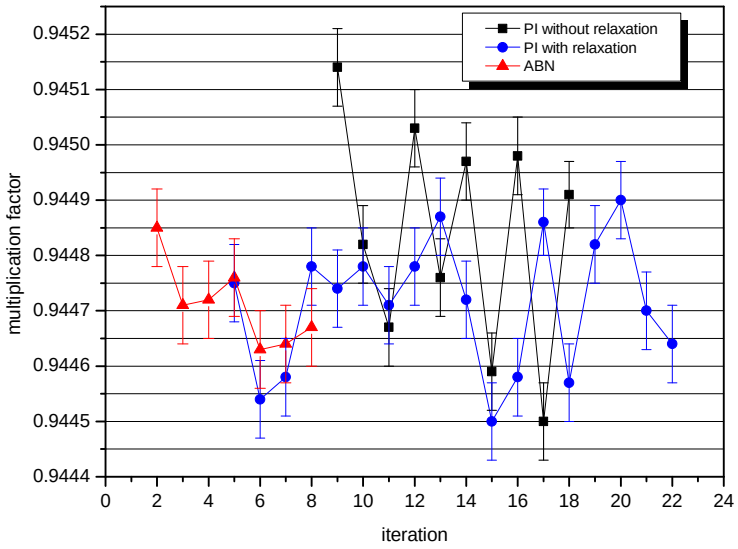

Figure 4.44: Test-case 4-4: Multiplication factor within iterations (zoom-in).

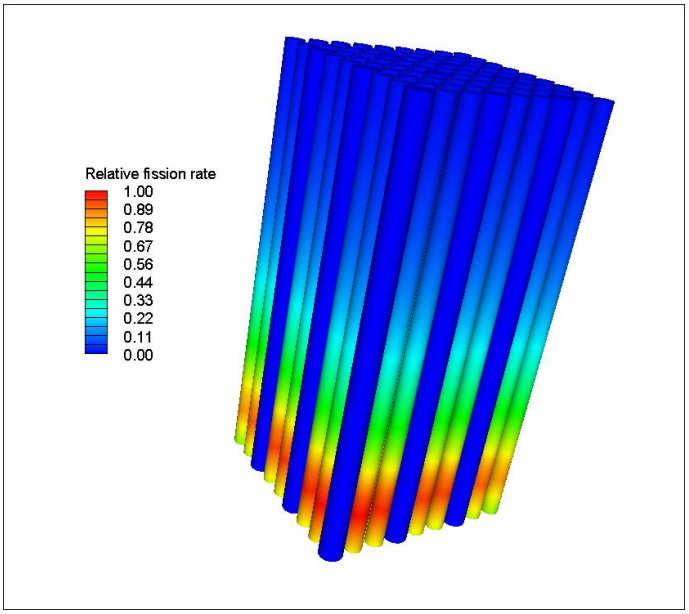

Figure 4.45: Test-case 4-4: Relative (to the max) fission-rate distribution.

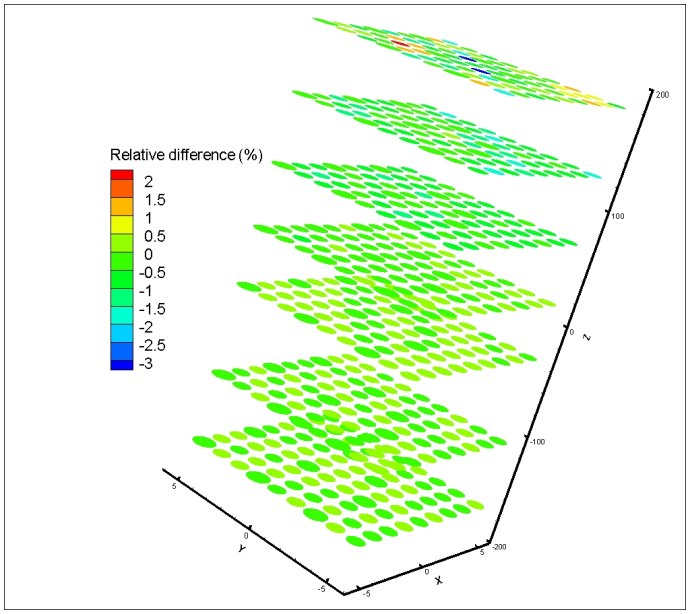

Figure 4.46: Test-case 4-4: Relative difference $(\frac{\text{ABN}-\text{PI}}{\text{PI}} \times 100)$ between ABN and PI coolant density distribution.

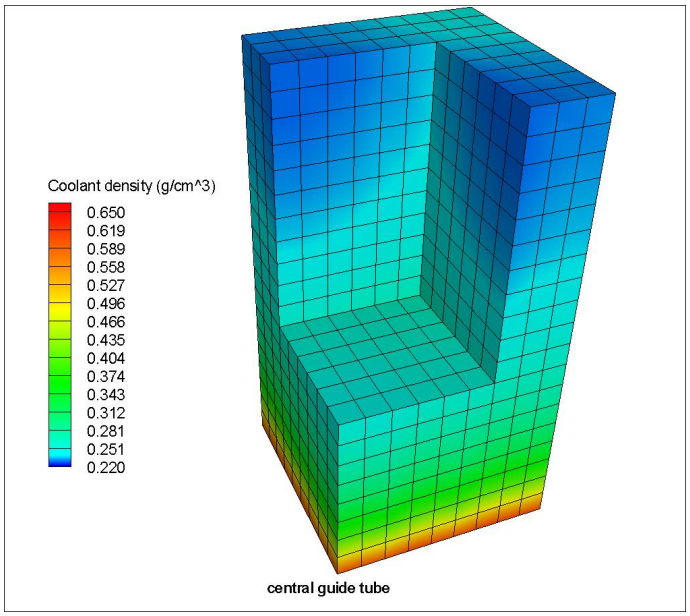

Figure 4.47: Test-case 4-4: Coolant density distribution.

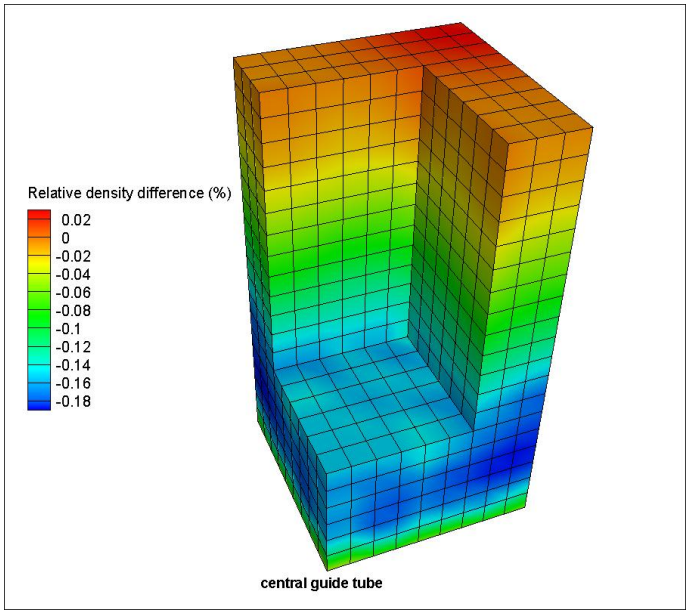

Figure 4.48: Test-case 4-4: Relative difference $(\frac{\text{ABN}-\text{PI}}{\text{PI}} \times 100)$ between ABN and PI coolant density distribution.

At this point it should be mentioned that the convergence of the ABN iteration can be linked to the one of the Krylov iteration by the following relation

$$\| \boldsymbol{J}^{k} \delta \boldsymbol{x}^{k} + \boldsymbol{F}(\boldsymbol{x}^{k}) \|_2 < \gamma \| \boldsymbol{F}(\boldsymbol{x}^{k}) \|_2 \tag{4.34}$$

where γ is a forcing term. Details about the role of this forcing term can be found in Dembo et al. (1982). Here it must be stated that a proper compromise should be sought between the convergence level of the Krylov iteration and the one of the Newton iteration. The improper balance between the convergence of these two iterative procedures can result in "over-solving". Practically this means that a very low γ has been used in quite early Newton steps implying that a very accurate linear solution has been obtained to a quite inaccurate Newton correction. "Oversolving" can affect the convergence of the Newton iteration negatively. Discussion about this issue can be found in Shadid et al. (1997) and Tuminaro et al. (2002). The analysis of the connection of these two norms was out of the scope of this work and constitutes subject for future research.

Another matter that might contribute to the reduction of the computational cost is the progressive increase of the used neutron histories. Such an approach could reduce the number of neutron histories simulated in iterative steps where the solution is far from the convergence. The determination of the number of neutron histories could be combined somehow with the norms mentioned above for problem-dependent and accurate control of such a process.

Initially, a classical "serial" coupling algorithm between OpenMC and COBRA is successfully developed in the framework of this work. The role of this tool here is twofold: firstly it is used for an initial scouting of the problem and its features. Secondly, it is used as a reference for the new proposed approach that has been developed; this holds not only for result-validation but also for the evaluation of the numerical performance of the introduced method. After the analysis of a simple benchmark problem, the results are validated against numerical results found in the bibliography.

Afterwards, this work describes an attempt, possibly the first one to the author' s knowledge, for considering a Monte Carlo-neutronic/T-H coupling scheme based on a Newton-type method. Initially, a discussion on the potential numerical methodologies for a tighter Monte-Carlo/T-H coupling is presented. The ABN algorithm seems to be an interesting candidate since it combines a tighter coupling algorithm with higher convergence rates and at the same time maintains the independence of the coupled solvers. Thus the ABN algorithm is adapted in a Monte Carlo-neutronic/T-H coupling context. Afterwards, the OpenMC Monte-Carlo solver is coupled with the COBRA-EN T-H solver using the introduced approach. The performance of the developed scheme is tested in two reactor physics problems and is compared with that of the traditional "serial" coupling method, called PI. The results show that ABN outperforms the PI method in both the convergence speed and the computational cost. This is reflected in the convergence of the unified problem, i.e., the fission-rate distribution, the T-H parameters and the multiplication factor. The fact that the computational cost is low enough enabling the usage of Monte-Carlo-based matrix-vector products is due to the rapid convergence of the linear system solution. This property is attributed to the formulation of the method. The derivative of the non-linear residual vector, or in other words, the Jacobian matrix, does not differ from the identity matrix significantly if the perturbation is not too large. This form of the ABN matrix vector products inserts a kind of inherent preconditioning of the linear system. Furthermore, it is concluded that the observed PI numerical oscillations may lead to the inefficiency of the simple norm drop-based convergence criteria. Also, it seems that the improvement comparing to the traditional PI scheme is more significant in BWR-type problems, probably because they are characterised by larger moderator density gradients which might complicate the numerical solution of the problem.

It will be interesting to test the performance of the introduced approach in the analysis of problems of larger scale. Also, possible improvements of the numerical performance like preconditioning of the linear system would be interesting to consider. Furthermore, the role of the involved numerical parameters, e.g. the perturbation pa-

rameter, should be investigated to optimise all the involved iterative procedures as well as their combination. The introduced approach could be combined possibly with the progressive increase of the used neutron histories per Newton step or the usage of relaxation schemes to reach arbitrarily large drop of norms. Last but not least a comparison between neutronic-based and T-H-based set-ups could be performed. These issues constitute a subject of further investigation.

5

MONTE-CARLO FOR DYNAMIC REACTOR CORE ANALYSIS

5.1 STATE-OF-THE-ART

Nowadays, the computational nuclear reactor analysis is moving towards a detailed analysis of the reactor core system in a multi-physics context (Zerkak et al., 2015). In this framework, the Monte-Carlo method is extensively employed standalone and/or coupled with other tools (see § 4.1) since it can analyse thoroughly the neutronic model of the nuclear reactor core. At this point a scientific "gap" arises. While reactor dynamics is of great interest, the Monte-Carlo method that could analyse it without making use of significant approximations is not extensively employed in this domain. As the transient analysis is an important issue concerning the reactor safety and design, various techniques mainly deterministic or hybrid, i.e., deterministic/Monte-Carlo, are employed. However a common feature of almost all of them is that they make use of various approximations and they are strongly problem-dependent.

From the family of deterministic methods, Point-Kinetics (PK) is the most common and the simplest method to perform transient analysis. However, it inherently includes significant approximations. Also a variety of space- and time-dependent deterministic methods have been widely developed and utilised including however approximations that concern mostly the discretization of space, time, angle and energy. On the other hand Monte-Carlo is only involved in hybrid kinetics analysis. This has been achieved by coupling the Monte-Carlo method for the calculation of the shape function with PK schemes for the calculation of the time evolution of the reactor power. Such approaches are the adiabatic and the quasi-static approximation (Vazquez (2014), Dulla et al. (2008), and Goluoglu et al. (1998)).

The almost inexistence of pure dynamics Monte-Carlo tools reveals the presence of an "open" research field of great interest. Recently, a method that analyses in a pure Monte-Carlo way the physical phenomena that are involved in the transient behaviour of a reactor core has been published by Sjenitzer and Hoogenboom (2011), Sjenitzer (2013) and Sjenitzer and Hoogenboom (2013) and constitutes the starting point for this work. Of course, the primary constraint of performing large scale Monte-Carlo simulations is the prohibitive computational cost as mentioned, for example, by Martin (2012). This argument is stronger when time-dependent problems are considered. However according to Martin (2012), when speaking about static analysis, literature results show

that Monte-Carlo simulation is moving towards finer and finer resolution within a more and more realistic computational cost. The results presented by Sjenitzer (2013) indicate that this conclusion might be transferred in the field of Monte-Carlo dynamic analysis.

5.2 THE DEVELOPED DYNAMIC SOLVER

This part of the thesis aims to develop and investigate a pure Monte-Carlo numerical tool able to analyse the kinetic neutronic behaviour of a nuclear system. Such a tool could serve as a platform for research and development on this interesting but also quite challenging field. The approach followed here is an attempt to insert in the Monte-Carlo method the simulation of all the physical neutronic phenomena that determine the dynamic behaviour of the reactor. This approach is selected considering that this study constitutes an initial step into a field that has not yet been mapped sufficiently. Therefore, more sophisticated techniques can be investigated in a next step.

The present research follows a step-by-step development of the above-mentioned numerical tool. In the first stages quite many approximations are adopted since they can limit the number of factors that could complicate the verification-validation process. Progressively these approximations are removed and replaced by more accurate approaches. To make easier the distinction between the original form of OpenMC and the extended form of OpenMC developed in this work, the latter hereinafter will be referred to as OpenMC^{+}.

5.2.1 *Challenges comparing to static Monte-Carlo*

The static form of the existing Monte-Carlo algorithms considers all the fission neutrons as prompt. In some cases, a distinction in the energy spectrum is just made. Thus, it is clear that the proper analysis of a reactor transient requires the encapsulation of the impact of the precursors as a source of delayed neutrons in the corresponding time scale (see § 2.1.4). However, it is obvious that the main constraint towards this direction will be the necessary simultaneous numerical treatment of phenomena of different time-scales, i.e. the neutron lifetime is approximately 10^{-4} s for a light water reactor and 10^{-7} s for a fast reactor whereas the precursor lifetime can go up to 10^{2} s. This will induce variance in the statistical estimation of the desired quantities. A promising technique that tries to alleviate this problem has been presented by Sjenitzer and Hoogenboom (2013) and is used in this work to overcome the problem mentioned above. From the side of physics, another important point that needs special treatment is the generation of the initial source of particles. From the side of numerics and computation,

the temporal evolution of the particles, the variance reduction and the population control, the dynamic tallying, dynamic changes of the model and the parallelization of the algorithm are points that need special attention.

5.2.2 *General description of the transient module*

In this paragraph the general flowchart of the developed computational scheme is described. Since a reactor transient usually follows the perturbation of the reactor core steady-state, an initial static criticality calculation is performed to create the critical neutron source that corresponds to the reactor steady-state. Using that neutron source a prompt and a precursor source distribution is generated utilising the proper analogy between them. When the source is ready, the simulation starts. At the beginning of each time-step, the decay process of the precursors is simulated. It should be noted that according to Sjenitzer (2013), each precursor is forced to produce a delayed neutron within each time-step without dying after that, for reasons that will be explained below. Within each time step the neutrons coming from the previous step and the ones generated by the precursor decay, at the beginning as well as within the current time-step, are simulated. The simulation within each time-step is done in a generation-by-generation context. During a time-step a fission event may generate prompt and delayed neutrons. If a delayed neutron is going to be produced, a precursor is firstly generated and saved in the proper bank and then its decay process is simulated. This results in a forced birth of a delayed neutron within the remaining time interval of the current time-step. If a neutron crosses the time boundary of the current time-step, it is stored to continue its simulation in the next step.

The development of this new module was based on the fixed-source scheme of OpenMC following the general flowchart of that module; as a result, the simulation of the whole phenomenon is performed in each batch [1]. Since OpenMC calculates statistics considering each batch as a single realisation of the random variable, the selected approach is compatible and can take advantage of the already existing tallying capabilities which are extended to provide the necessary monitoring in time. To be able to apply changes that could initiate a transient such as the movement of a control rod or the modification of the material density, a suitable subroutine has been developed. This subroutine gives the ability to define a variety of dynamic changes by properly combining the construction of the geometry/materials input and the definition of the dynamic change. Another modification is the extension of the existing structured mesh by adding an extra dimension. This feature provides the ability to track the desired quantities in time.

1 The terms Monte-Carlo batch and Monte-Carlo cycle are used interchangeably in this work.

As a result, each tallied quantity can be calculated in the desired spatial and temporal resolution. Algorithm (2) presents a simplified overview of the developed module.

Algorithm 2 A simplified-general overview of the developed module

```
START
Generate transient source
BATCH loop
Initialize batch
  TIME-STEP loop
  Simulate initial precursors for the current time-step
  Scan for scheduled changes in materials and/or geometry
    PARTICLE-tracking loop
      PHYSICS loop Simulate particle's physics
      ...
      IF particle crosses the time boundary
      Store it for simulation in the next time-step
      EXIT loop
      END IF
      ...
      IF fission occurs
      Generate prompt neutrons + precursor
      Simulate precursor + generate delayed neutron
      EXIT loop
      END IF
      ...
      END PHYSICS loop
    END PARTICLE-tracking loop
  END TIME-STEP loop
Finalize batch/Process tallies
END BATCH loop
Calculate statistics
END
```

5.2.3 *Initial particle source*

The initial particle source is generated by an initial k-eigenvalue calculation. For a good description of the initial neutron distribution, a sufficient number of neutron histories should be selected. In the case of OpenMC, the convergence of the neutron source in

a *k*-eigenvalue calculation can be evaluated by monitoring the Shannon entropy in a suitably defined spatial mesh.

Two ways can be used for the generation of the initial particle source. The first option is to transform the converged critical neutron source in a mixed particle source composed of neutrons and precursors using Eq. (5.1). The second option is to sample the prompt neutron and the precursor population utilising an appropriate tally estimators during the *k*-eigenvalue calculation (Sjenitzer, 2013). In the first development stage, OpenMC$^+$ utilises the first approach since it is considered adequate for the simulation of simplified homogeneous problems. The prompt neutron fraction in position r (one-group) is calculated by the following relation:

$$\frac{n_0(r)}{n_0(r)+C_0(r)} = \frac{\frac{1}{\upsilon}\phi(r)}{\frac{1}{\upsilon}\phi(r)+\frac{\beta}{\lambda}\nu\Sigma_f\phi(r)} = \frac{1}{1+\frac{\beta}{\lambda}\upsilon\nu\Sigma_f} \tag{5.1}$$

where r is the position in space, n_0 is the initial population of the prompt neutrons, C_0 is the initial population of the precursors, β is the delayed neutron fraction, λ is the precursor decay constant, υ is the neutron speed, ν is the average number of fission neutrons per fission event, Σ_f is the macroscopic fission cross section and ϕ is the total flux. The variables β, ν, Σ_f are spatially dependent but in small homogeneous cases suitably averaged values may be a reasonable approximation. It should be noticed that this relation is valid only for cases with constant neutron energy but here is considered as a reasonable approximation.

The converged fission source of a *k*-eigenvalue calculation differs from the flux source especially in the energetic domain because the former is mainly composed of neutrons of high energy, while the latter contains also moderated neutrons. This results in the insertion of variance in the dynamic calculation. For this reason, the second development stage includes the utilisation of tallies that sample the prompt neutron and precursor source during the Monte-Carlo *k*-eigenvalue calculation. More specifically the tally used to sample neutrons has the following form:

$$n_0(\boldsymbol{r}, E) = \int_{4\pi} \frac{\phi_0(\boldsymbol{r}, \boldsymbol{\Omega}, E)}{\upsilon(E)} d\boldsymbol{\Omega} \tag{5.2}$$

The precursors are sampled developing a tally of the form:

$$C_{i,0}(\boldsymbol{r}) = \int_{4\pi}\int_0^\infty \frac{\beta_i(\boldsymbol{r}, E)\nu(\boldsymbol{r}, E)\Sigma_f(\boldsymbol{r}, E)}{\lambda_i}\phi_0(\boldsymbol{r}, \boldsymbol{\Omega}, E) dE d\boldsymbol{\Omega} \tag{5.3}$$

where i corresponds to the number of the precursor group. ϕ_0 is the flux that is sampled by an already existing tally. The tallies for prompt neutrons and precursors are based on the post-processing of the flux tally. The tallies are accumulated over a superimposed spatial/energetic mesh. Afterwards, proper ratios between prompt neutrons

and precursors inside each mesh cell as well as between the populations of each cell over the total population of the whole configuration are calculated. The number of the particles per mesh cell is calculated by normalising the above-mentioned ratios to the total number of the particles to be simulated. Finally neutrons and precursors are randomly generated inside each mesh cell. Special attention is paid to the precursors since they have to be generated in the part of the spatial cell where fissionable material exists. This technique for the initial particle source generation was selected since it does not imply significant modifications to the OpenMC *k*-eigenvalue solver.

5.2.4 *Precursors*

In the first development stage only one precursor group is used. This choice has been made in order to reduce the factors that could complicate the validation process. Also, doing that, the precursor decay constant can deliberately be set to a chosen value to facilitate the comparison with the analytical solution of the PK equations for one precursor group (Duderstadt and Martin, 1979).

The second step considers the treatment of as many precursor-groups as provided by the nuclear data library. Two methods are envisaged for this purpose:

1. The analogue treatment of each precursor group.
2. The treatment of only one precursor group that would encapsulate inherently the information concerning all the groups (combined precursor).

The analogue treatment of each precursor group is a more straight forward approach and can be implemented more easily in this work. In OpenMC, in each fission event, when a delayed neutron is emitted, the family of this delayed neutron is firstly determined to select a proper energy. At this point OpenMC was modified to extract the precursor decay constant (λ_i) from the nuclear data library. λ_i together with the delayed neutron fraction (β_i) are provided to the precursor that is subsequently created. Then the precursor is simulated and a delayed neutron is emitted in the system with the proper time delay. The second approach, that is extensively described in Sjenitzer (2013), is also implemented as an alternative option since it aims to reduce the variance that is inserted by the treatment of precursors which are characterised by different decay constants.

The simulation of the precursors is based on the precursor decay probability given by the following relation:

$$p(t) = \lambda_i e^{-\lambda_i (t - t_0)} \tag{5.4}$$

where $p(t)$ is the decay probability of the precursors, λ_i is the decay constant for the ith precursor group, t is the current time and t_0 the moment of the generation of the

precursor. The p(t) probability is used to simulate stochastically the behaviour of the precursors. However a straight-forward simulation of the precursors would introduce significant variance. This is an implication of the relatively large precursor life-time that would cause a low generation rate of delayed neutrons in a Monte-Carlo limited statistics context. This problem can be alleviated when the technique of forced precursor decay proposed by Legrady and Hoogenboom (2008) is used. According to this method a precursor is not killed after a decay event but it continues to exist. In the meantime it is forced to generate a delayed neutron in each time-step. Of course, the fact that the precursor stays artificially alive should be properly counterbalanced to keep the game fair. This is done using a precursor time weight (w_t) which reflects the probability of a precursor to exist after a certain time interval following its generation. It should also be mentioned that another weight, i.e., the main statistical weight (w_m), is used and reflects the statistical importance of the precursor. The decay probability of combined precursor can be defined as following:

$$p_{comb}(t) = \sum_i \frac{\beta_i}{\beta} \lambda_i e^{-\lambda_i (t-t_0)} \tag{5.5}$$

For a combined precursor the time weight is derived by the main one according to the following relation:

$$w_t = w_m \sum_i \frac{\beta_i}{\beta} e^{-\lambda_i (t-t_0)} \tag{5.6}$$

The index i refers to the precursor group. As mentioned before, each precursor is forced to decay in each time-step to increase the number of the generated delayed neutrons. To counterbalance this artificial action the weight (w_d) of the generated delayed neutron is calculated by the following relation:

$$w_d = w_m \frac{p_{comb}(t)}{\overline{p(t)}} = w_m \Delta t \sum_i \frac{\beta_i}{\beta} \lambda_i e^{-\lambda_i (t-t_0)} \tag{5.7}$$

where $p(t), \overline{p(t)}$ and Δt are the real decay probability in each time-step, the artificial decay probability and the length of each time-step. In this work the artificial probability $(\overline{p(t)})$ is chosen to be the uniform probability distribution $\overline{p(t)} = \frac{1}{\Delta t}$ as proposed by Sjenitzer (2013). This strategy results in a continuous accumulation of new precursors and the creation of precursors of low statistical importance. For this reason, Russian roulette is played to reduce, in a fair way, the number of these precursors of low statistical significance.

A point that requires special treatment and should be mentioned here is the fact that the steady-state distribution and thus the probability for creation of each precursor group differs from the one that characterises a fission event. This happens due to the different group-based precursor decay constants. More specifically a fission event will generate a

precursor of group i with probability simply β_i/β. However the precursors of different groups decay with different speeds (because of the different precursor decay constants) resulting in a steady-state group distribution that is given by the following relation:

$$\frac{C_{i,0}}{C_0} = \frac{\beta_i}{\beta}\frac{\lambda^b}{\lambda_i} \tag{5.8}$$

where λ^b is an inversely weighted decay constant (Sjenitzer, 2013) defined as:

$$\lambda^b \equiv \frac{\beta}{\sum_i \frac{\beta_i}{\lambda_i}} \tag{5.9}$$

This is taken into account during the generation of the initial precursor source by suitably modifying the delayed neutron fraction.

5.2.5 *Remaining needs*

The most important remaining needs of the under-development module are the following:

1. Neutrons' clock - Time boundary crossing
2. Variance reduction
3. Population control
4. Tallying
5. Dynamic changes of the model

All these matters are discussed in this section.

A clock which shows the time evolution within each time-step is connected with each simulated neutron. The time evolution is calculated based on the kinetic energy and the pre-calculated distance of each movement of the neutron. The boundary crossing is handled in a way analogous to that used for the handling of the spatial boundary crossing in a static Monte-Carlo solver. In static Monte-Carlo two distances are defined for each movement of a particle, i.e. the collision path length and the boundary path length (Brown, 2008). After a comparison the smallest is always chosen. In this case a new extra length is inserted, i.e. the time-boundary length. Now, after a comparison of these three lengths, the movement corresponding to the smallest length is chosen. If for example the smallest length is the time-boundary length, the neutron is advanced to the new spatial position which corresponds to the time-boundary and then is stored; its simulation continues in the next time-step.

In this work the in-built variance reduction scheme of OpenMC has been adopted. According to this scheme, called "survival-biasing", the absorption reactions are prohib-

ited from occurring. Instead of that, at every collision, the weight of the neutron is suitably reduced by the probability of the occurrence of an absorption event, i.e.

$$w' = w(1 - \frac{\sigma_a(E)}{\sigma_t(E)}) \tag{5.10}$$

The variance reduction is also accompanied with the use of Russian roulette. The Russian roulette "kills" the neutrons of very low statistical importance.

The particle population control is necessary for three reasons:

1. The enforced precursor decay results in the creation of delayed neutrons of low statistical importance.
2. Neutrons of low statistical importance create precursors of low statistical significance.
3. When the variance reduction is activated, additional neutrons with low weight may appear.

With purpose to avoid the simulation of particles of low statistical importance, the Russian roulette (Brown, 2008) is played for each neutron based on its statistical weight at the starting point of its simulation and for precursors, at the beginning of each time-step using the time-weight and affecting the main (statistical) weight.

The tallying capabilities of OpenMC have been extended to monitor the temporal evolution of the measured quantity. For this purpose a new time-bin that can measure the desired quantity in time has been created. Moreover, to achieve flexibility, the in-built structured spatial mesh has been extended to include a time dimension. As a result the model can be easily monitored in the desired spatial and temporal resolution.

The capability of dynamically changing the analysed model is necessary to simulate the progressive movement of a control rod, the change in the density of the coolant etc. For this reason a new subroutine has been developed capable of performing the necessary changes at the desired time-step. More specifically at the beginning of each time-step the code scans for any scheduled change and if changes are found, they are applied. The change can be instantaneous, i.e. it is performed at the beginning of only one time-step, or progressive, i.e. it is performed progressively in more than one time-steps based on a defined step. This capability allows for the modelling of a variety of changes provided that the geometry/material model and the desired changes are designed and defined in a proper (consistent) way.

5.2.6 *Task parallelism*

The parallelization of Monte-Carlo algorithms is crucial for the simulation of realistic problems. The parallelization of the developed module is rather straight forward since

there is independence between batches of particles analogous to that of a fixed-source Monte-Carlo algorithm. This argument is justified because the particle source has been generated in advance (k-eigenvalue calculation) and is identical for each batch. The parallel scheme utilised in the developed module is based on the Message Passing Interface (MPI) (*MPI website*).

A somewhat tricky point for a parallel Monte-Carlo algorithm is the reproducibility of the results, i.e., independency of the number of the employed processors. This feature is important especially for development purposes. This difficulty comes from the following fact: for reproducibility, each neutron should be simulated with the same Random Number Sequence (RNS) no matter the number of the employed processors. However this is impossible when each processor has access only to its own neutrons. Then the id number of the same neutron varies with the number of the employed processors. In case of the in-house Linear Congruential Random Number Generator (LCRNG) of OpenMC the id number of the neutron is used as a seed (ξ_0) to generate the corresponding RNS (ξ_i). Thus a different id means a different RNS. An RNS is calculated using the following recurrence relation:

$$\xi_{i+1} = (g\xi_i + c) \bmod M \tag{5.11}$$

where g, c, and M are constants. The choice of these constants has a profound effect on the quality and performance of the generator, so they should not be chosen arbitrarily (*OpenMC website* and Brown, 2008).

Here the reproducibility is achieved using a master-worker context during the generation of the initial particle source. During that procedure the master process that generates the source provides each particle with a unique id number. This id number is used as the seed ξ_0 that is provided to the in-built LCRNG (Eq. (5.11)) in order to generate the corresponding RNS. This means that each neutron has the same id number no matter the specific worker process that will simulate its life. A point that requires particular attention regarding reproducibility concerns the generation of fission neutrons. Each fission neutron is assigned the id of its predecessor. However because the RNS should be continued and not restarted, the number of random numbers that have been generated per seed is kept to be available when that fission neutron is simulated continuing the RNS of its predecessor. At this point the skip-ahead capability of the LCRNG plays an important role. When the RNS would restart from the point that it had stopped and in case that all the previous random numbers should be regenerated to reach the desired point, then the computational cost would increase significantly taking also into account the long time-histories due to the time evolution of the analysed phenomenon. The skip-ahead capability makes it possible to skip a population of N already generated random numbers with a cost of $O(\log_2 N)$, instead of O(N) that would otherwise be needed (*OpenMC website*). As mentioned above the initial source generation is done

within a master-worker context. Afterwards the particle population is separated and provided to each worker. Subsequently each worker continues its task independently and the communication is limited in the tally synchronisation process at the end of the simulation of each particle batch.

5.2.7 *Kinetic parameters*

In order to be able to compare the Monte-Carlo calculated results with a PK solution it is required to calculate the kinetic parameters of the analysed system, i.e., the effective delayed neutron fraction (β_{eff}) and the mean neutron generation time (Λ). One method that can be used for the calculation of β_{eff} is the Prompt method (Meulekamp and Marck, 2006) according to which the value of β_{eff} can be approximated by the following relation:

$$\beta_{eff} \approx 1 - \frac{k_p}{k} \tag{5.12}$$

where k_p is the multiplication factor of the system when the average total number of released fission neutrons per fission is equal to the average number of prompt neutrons released per fission, i.e. $\nu = \nu_p$ and $\chi = \chi_p$ and k is the actual multiplication factor of the system. For this purpose, and because this capability might be generally useful, a capability to perform criticality analysis by considering $\nu = \nu_p$ and $\chi = \chi_p$ has been developed as part of OpenMC$^+$ in the framework of this research. This enables the calculation of β_{eff} in two steps, i.e. through performing two criticality calculations. For the calculation of Λ and for comparison of the calculated β_{eff} value, Tripoli-4 (Petit et al., 2008, Truchet et al., 2015) is employed.

5.3 NUMERICAL EXPERIMENTS - ONE PRECURSOR GROUP

In this section four (4) numerical experiments are performed aiming to the preliminary verification and validation of the module. These experiments concern some very simplified configurations designed for the testing of the various features of the developed module. The results are compared with an analytical solution of the PK equations for one delayed neutron group and relatively small reactivity insertion (Duderstadt and Hamilton, 1976):

$$P(t) = P_0\left(\frac{\beta}{\beta-\rho}e^{\frac{\lambda\rho}{\beta-\rho}t} - \frac{\rho}{\beta-\rho}e^{\frac{\rho-\beta}{\Lambda}t}\right) \tag{5.13}$$

where P_0 is the initial power, β is the delayed neutron fraction, ρ is the reactivity, λ is the precursor decay constant, Λ is the mean neutron generation time, and t is the time. In all cases, the JEFF 3.1.2 (*Jeff-3.1.2*) nuclear data library has been used.

5.3.1 *Test-case 5-1: A simple bare configuration with insertion of positive reactivity*

A simplified homogeneous energy-dependent example is analysed here. This example consists of a parallelepiped which is composed of pure U-235. The density and the dimensions are suitably selected in order to achieve a critical state. The dimensions are $10 \times 20 \times 24$ cm. Initially the density has a value of $4.49495\ 10^{-2}\ \frac{atoms}{barn-cm}$. A criticality calculation for this configuration using 5000 batches, 300 skipped and $1.5\ 10^{6}$ neutrons per batch, gives $k_{eff} = 0.99998 \pm 0.00001$; the configuration is almost critical. Afterwards a dynamic analysis is performed for 10 s using a time-step of 0.1 s. For the first 2.9 s the configuration remains critical and for $t = 2.9$ s, i.e the beginning of the 30th time-step, the density increases instantaneously to $4.509\ 10^{-2}\ \frac{atoms}{barn-cm}$ inducing a positive reactivity of $\rho =\sim 246$ pcm. The evolution of the phenomenon is monitored for the remaining time interval. The precursor decay constant is equal to 0.0784 s^{-1}. For comparison, Eq. (5.13) is used.

For the calculation of β_{eff} one extra *k*-eigenvalue calculation with the new functionality of OpenMC^{+} that ignores delayed neutrons has been performed. This gave $k_p = 0.99363 \pm 0.00001$. By using the prompt method, β_{eff} is found equal to 0.00635 ± 0.00002. Table (6.1) shows the two calculated β_{eff} and the Tripoli calculated Λ. Notice that with these values the exponent of the second term in the parenthesis of Eq. (5.13) equals $-6.73\ 10^{5}\ t$ and therefore the corresponding term is negligible at any time. Two tallying meshes (x,y,z,t), one with $1 \times 1 \times 1 \times 100$ and one with $10 \times 10 \times 10 \times 100$ cells have been used for the accumulation of the necessary tallies. Fig. (5.1) illustrates the temporal evolution of the total fission-rate during the transient phenomenon associated with the standard deviation. The maximum standard deviation is 1.93%. Fig. (5.2) shows a comparison of the Monte-Carlo calculated relative fission-rate with the PK analytical solution; as can be seen, a very satisfying agreement is found. Both the prompt jump and the afterwards behaviour are very well-predicted by Monte-Carlo. Fig. (5.3) shows some frames (5.3a, 5.3b, 5.3c, 5.3d, 5.3e) of the temporal evolution of the spatial fission-rate distribution. Figs (5.3a and 5.3b) correspond to the steady state region before the insertion of reactivity. Fig. (5.3c) illustrates the increase of the fission-rate that corresponds to the prompt jump and Figs (5.3d and 5.3e) depict the increase of the fission-rate following the prompt jump. As expected the fission-rate is higher towards the centre of the bare parallelepiped comparing to the edges where the leakage is quite high. The total wall-clock time of this transient calculation, using $1.5\ 10^{6}$ initial neutrons, prompt and delayed, per batch and 100 transient neutron batches, was 2.94 h utilising 48 MPI-processes on 48 physical cores. In this calculation 200 tally-bins were accumulated. Since the number of tally-bins may significantly affect the computational cost, it should be taken into account in comparisons. It should be mentioned that a significant

part of the total wall-clock time was spent in the synchronisation process of the desired tallies. More specifically 0.83 h was the time needed for tally synchronisation at the end of the statistical batches corresponding to the 28% of the total wall-clock time. At this point it should be noted that further study is necessary to determine the problem-type dependent, necessary statistics that allows generating satisfying results with the lowest possible computational cost.

Fig. (5.4) shows the temporal evolution of the fission-rate as calculated with 48 and 96 MPI-processes respectively. The independence of the number of the utilised MPI-processes for the analysis of the problem can be easily noticed. As regards parallel scalability, Fig. (5.5) depicts the parallel speed-up ratio, relative to the 1-processor case, achieved for a range of 1 - 48 physical cores. In this case the speed-up is based on the total wall-clock time required for the transient calculation. It can be seen that the higher the number of processors the more the divergence of the observed speed-up from the ideal one. One of the sources of this behaviour is probably the tally-synchronization at the end of each batch. It would be interesting to implement the in-built "no reduce" tallying option and investigate its effect to the scalability. This option considers the accumulated score in one batch on a single processor as an independent realisation for the tally random variable and, as a consequence, the tallies are not reduced across processors in a parallel calculation. Further investigation on possible ways which could improve the scalability of the dynamic Monte-Carlo algorithm would be useful.

Finally the same problem is analysed for a time interval of 15 s. Now at t = 9.9 s the inserted reactivity is extracted and the configuration returns in a new critical state. Fig. (5.6) illustrates the temporal evolution of the total fission-rate during the transient phenomenon associated with the standard deviation. The maximum standard deviation is 1.93%. Fig. (5.7) shows a comparison of the Monte-Carlo calculated relative fission-rate with the PK analytical solution; as can be seen, a very satisfying agreement is found. Both the prompt jump and the afterwards behaviour are very well-predicted by Monte-Carlo. Also the new critical state of higher power agrees with the one predicted by the PK solution.

Table 5.1: Test-case 5-1: Kinetic parameters.

	Delayed neutron fraction β_{eff} (Prompt-method)	Mean neutron generation time Λ (s)
Tripoli-4	0.00628 ± 0.000004	$5.78E{-}9 \pm 5E{-}13$
OpenMC	0.00635 ± 0.00002	-

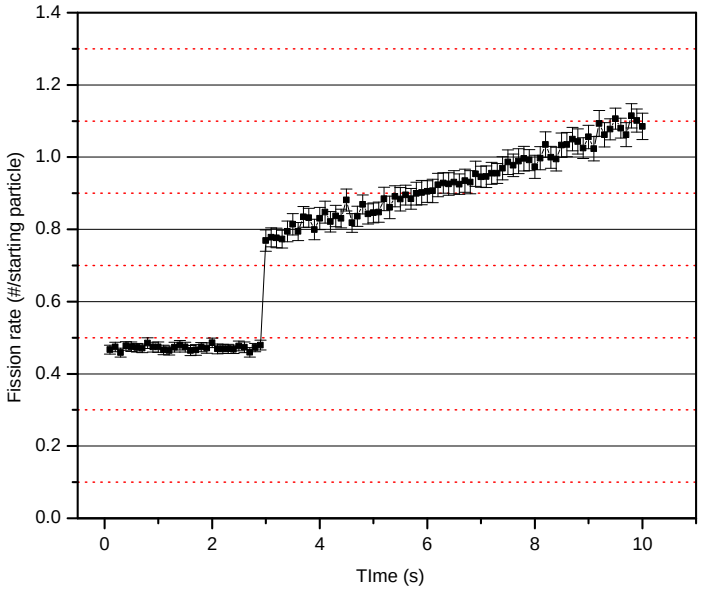

Figure 5.1: Test-case 5-1: Temporal evolution of the total fission-rate $\left[\frac{\text{fissions}}{\text{starting particle}}\right]$ with standard deviation.

5.3.2 *Test-case 5-2: A simple reflected configuration with insertion of positive reactivity*

In order to thermalize the previous numerical experiment the bare cuboid is now surrounded by a water reflector 8 cm thick. In order to achieve criticality the material density is now 0.032645 $\frac{\text{atoms}}{\text{barn}-\text{cm}}$. The dimensions of the internal parallelepiped remain constant. This configuration using 1000 batches, 300 skipped and 1.5 10^6 neutrons per batch gives $k_{\mathit{eff}} = 1.00002 \pm 0.00003$; the configuration is almost critical. When density increases to 0.0327895 $\frac{\text{atoms}}{\text{barn}-\text{cm}}$ there is an insertion of reactivity $\rho =\sim 247$ pcm. The precursor decay constant is again taken $\lambda = 0.0784\ s^{-1}$. The phenomenon is monitored for 10 s and for comparison Eq. (5.10) is used.

For the calculation of β_{eff} the same method as in the previous case is adopted. The extra calculation gave $k_p = 0.99303 \pm 0.00003$. As a result using the prompt method, β_{eff} is found 0.00699 ± 0.00006. Table (6.2) shows the calculated β_{eff} and the Tripoli calculated Λ; the second term in the parenthesis of Eq. (5.13) is again negligible at any time.

A tallying mesh of the form (x, y, z, t) with $1 \times 1 \times 1 \times 100$ cells regarding only the internal region of fissile material has been used for the accumulation of the necessary tallies. The total wall-clock time of this transient calculation, using 1.5 10^6 initial neutrons per batch and 100 transient neutron batches, was 10.6 h utilising 96 MPI-processes

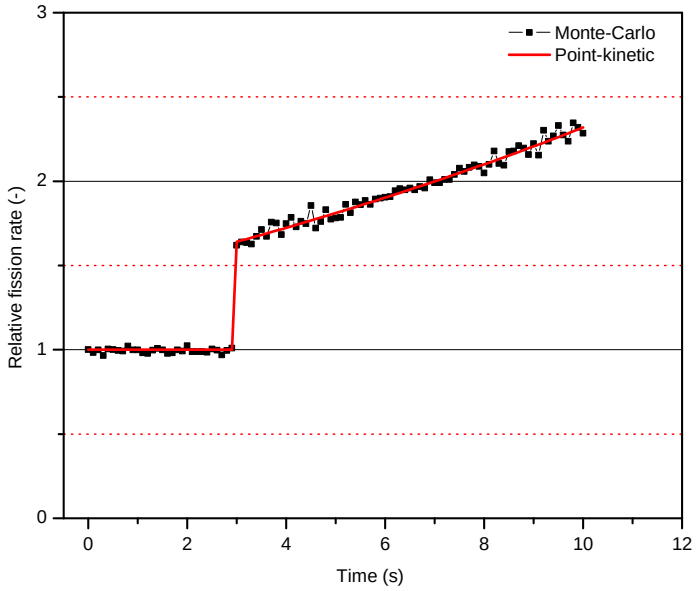

Figure 5.2: Test-case 5-1: Monte-Carlo calculated relative fission-rate vs PK analytical solution.

on 48 physical cores. The computational time of this case is significantly larger than the one of the previous case mainly due to the different nature of these two configurations. That is the much larger mean generation time (Λ) leads to much longer neutron histories compared with Test-case 5-1. Fig. (5.8) shows the temporal evolution of the total fission-rate with the associated standard deviation. The maximum standard deviation is 1.74%. Fig. (5.9) illustrates a comparison between the Monte-Carlo calculated fission-rate evolution and the PK analytical solution. The agreement is considered very satisfactory. Fig. (5.10) shows the temporal evolution of the fission-rate for the two test cases. It can be seen that while the inserted reactivity is almost the same, the different nature of the configuration, i.e. fast vs. thermalized, that is reflected in the values of the kinetic parameters, results in a different behaviour. That is a more rapid increase of the fission-rate occurs in the first case since the higher effective delayed neutron fraction in the second case decreases the speed of the fission-rate, i.e. the power, increase.

At this point it should be mentioned that terms *power*, *fission-rate* and *flux* are referred to interchangeably for the remainder of this chapter since the power can be easily calculated from the fission-rate, which can be obtained from the flux.

Table 5.2: Test-case 5-2: Kinetic parameters.

	Delayed neutron fraction β_{eff} (Prompt-method)	Mean neutron generation time Λ (s)
Tripoli-4	0.00712 ± 0.00001	1.19E−5 ± 5E−9
OpenMC	0.00699 ± 0.00006	-

5.3.3 *Test-case 5-3: A simplified sub-critical bare configuration*

The third test-case consists of a simplified energy-dependent homogeneous parallelepiped which is composed of pure U-235. Now the density and the dimensions are suitably selected to achieve a sub-critical state. The dimensions are $10 \times 20 \times 24$ cm and the initial density has a value of 0.044809 $\frac{atoms}{barn-cm}$. This configuration, after performing a *k*-eigenvalue calculation with 1000 batches, 300 skipped and $1.5{\cdot}10^6$ neutrons per batch, gives $k_{eff} = 0.99745 \pm 0.00002$; the configuration is indeed subcritical. The evolution of the fission-rate is monitored for a time interval of 30 s. The time-step is t=0.1 s and the precursor decay constant is equal to 0.0784 s^{-1}. Fig. (5.11) illustrates the temporal evolution of the fission-rate during the transient phenomenon associated with the Monte-Carlo statistical uncertainty. The maximum standard deviation is 1.90%. Fig. (5.12) shows a comparison of the Monte-Carlo calculated relative fission-rate with the PK calculated one, where a very satisfactory agreement is noticed. In this calculation 100 batches with $1.5{\cdot}10^6$ initial neutrons (prompt and delayed) per batch were used. Utilising 96 MPI-threads on 48 physical cores and accumulating $3{\cdot}10^5$ tally-bins the total wall-clock time was 3.11 h. Although a quite large number of tallies is accumulated during this calculation, the sub-critical nature of the configuration leads to a relatively low computational cost in comparison with the previous test-cases.

5.3.4 *Test-case 5-4: A simple bare configuration with power level reduction*

The fourth test-case concerns the same geometric and material configuration as in the previous cases. The density and dimensions are suitably selected in order to achieve a critical state; the dimensions are $10 \times 20 \times 24$ cm and the initial density has a value of 0.0449495 $\frac{atoms}{barn-cm}$. This configuration, after performing a *k*-eigenvalue calculation with 1000 batches, 300 skipped and $1.5{\cdot}10^6$ neutrons per batch, gives $k_{eff} = 0.99998 \pm 0.00001$; the configuration is almost critical. In this case, during the first 2.9 s of the analysed phenomenon, the model is in a steady-state. For t = 2.9 s the density decreases

to 0.04509 $\frac{atoms}{barn-cm}$ inducing a negative reactivity of ~ 246 pcm. The configuration remains in this subcritical state until t = 9.9 s. For t = 9.9 s the inserted negative reactivity is removed by re-adjusting the density of the material, and the model returns in a critical state again. The time-step and the precursor decay constant are equal to those of the first test-case.

Fig. (5.13) illustrates the temporal evolution of the fission-rate during the transient phenomenon associated with the Monte-Carlo statistical uncertainty. The maximum standard deviation is 1.78%. Fig. (5.14) shows a comparison of the Monte-Carlo calculated relative fission-rate with the PK calculated one, where a very satisfying agreement is noticed. Both the prompt-jump as well as the afterwards behaviour is well-predicted. Fig. (5.15) shows some frames of the temporal evolution of the fission-rate spatial distribution. The first two frames (Figs (5.15a and 5.15b)) are taken from the time interval of the initial steady-state before the insertion of reactivity. The next two (Figs (5.15c and 5.15d)) frames concern the subcritical state after the insertion of reactivity and the last one (Fig. (5.15)) corresponds to the new critical state after the re-adjustment of density. It can be seen that the second critical state (t=9.9-15 s) corresponds to a lower power level than the initial one that is an expected result.

In this calculation 100 batches with $1.5 \cdot 10^6$ initial neutrons (prompt and delayed) per batch. Utilising 48 threads, in 24 physical cores, and accumulating $1.5 \cdot 10^5$ tally-bins the total wall-clock time was 3.57 h. It should be mentioned that the total wall-clock time of this test-case is significantly lower than the one of the supercritical problems. This is because in subcritical cases the number of the simulated particles decreases continuously with time.

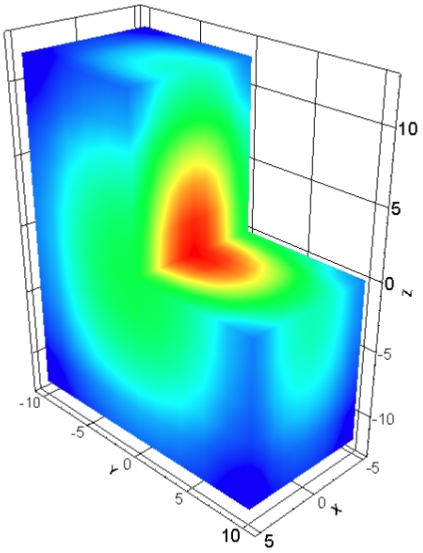

(a) t = 0.1 s

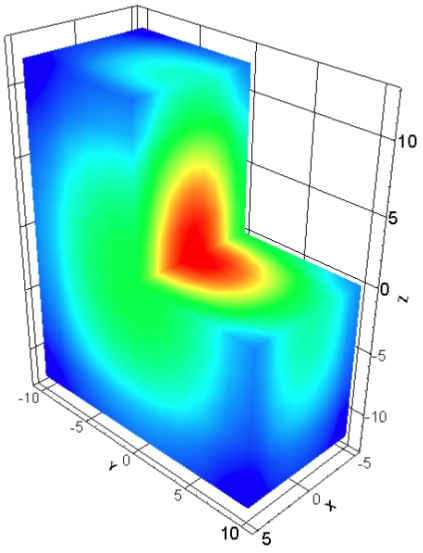

(b) t = 2.9 s

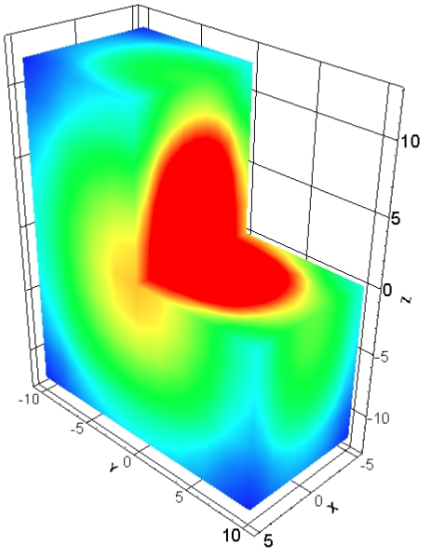

(c) t = 3.0 s

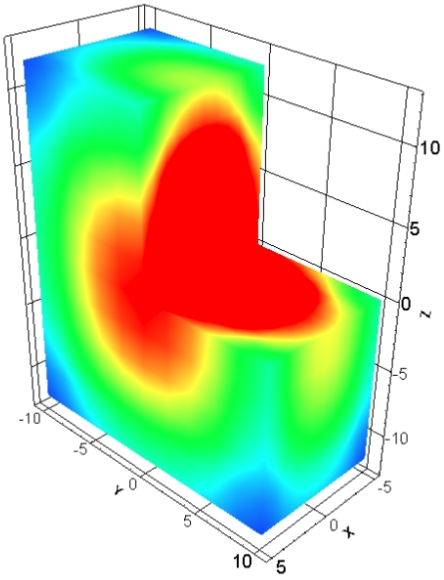

(d) t = 7.0 s

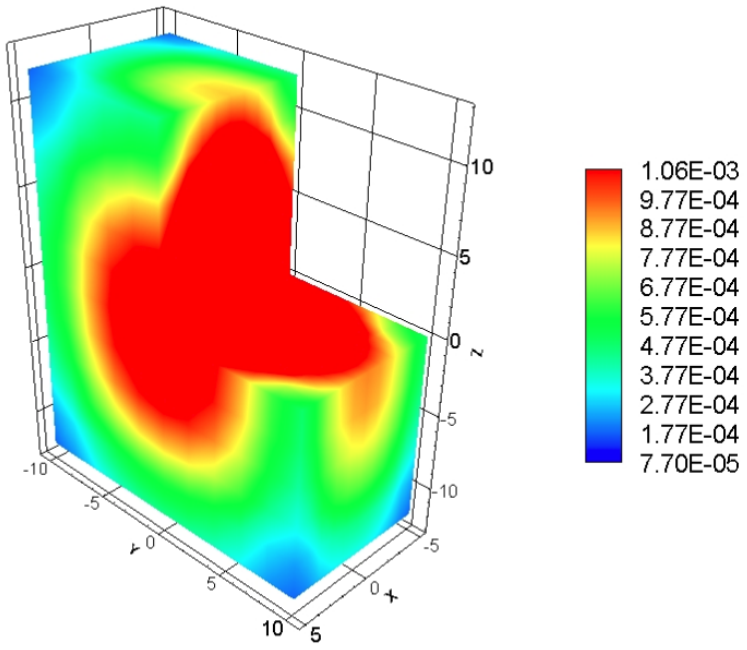

(e) t = 10.0 s

Figure 5.3: Test-case 5-1: Monte-Carlo calculated temporal/spatial fission-rate distribution $\left[\frac{fissions}{starting\ particle}\right]$.

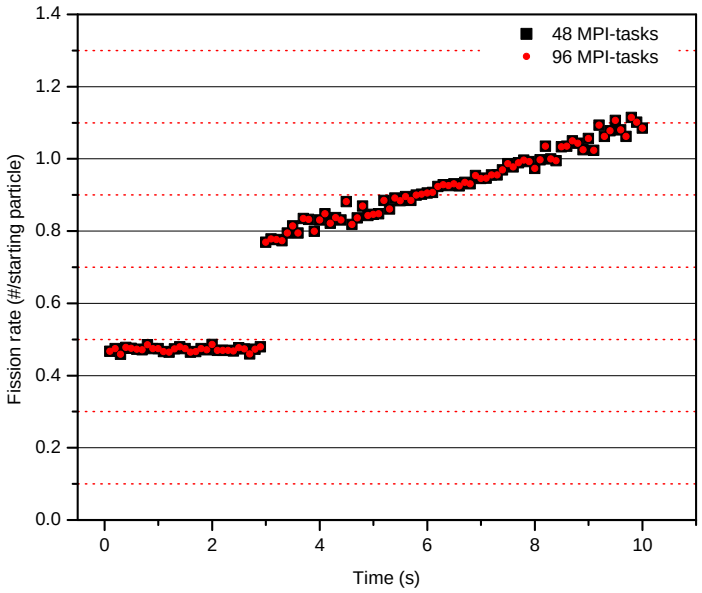

Figure 5.4: Test-case 5-1: Comparison of the Monte-Carlo solution for different number of MPI-tasks.

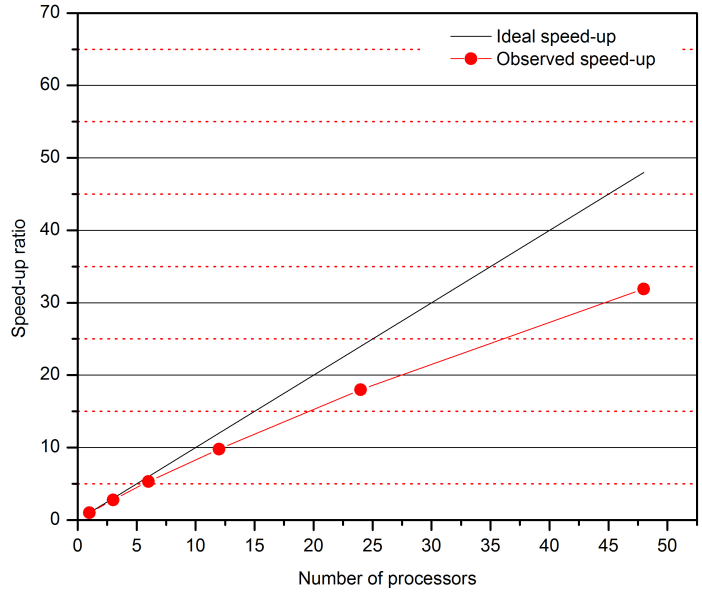

Figure 5.5: Test-case 5-1: Observed vs ideal speed-up ratio.

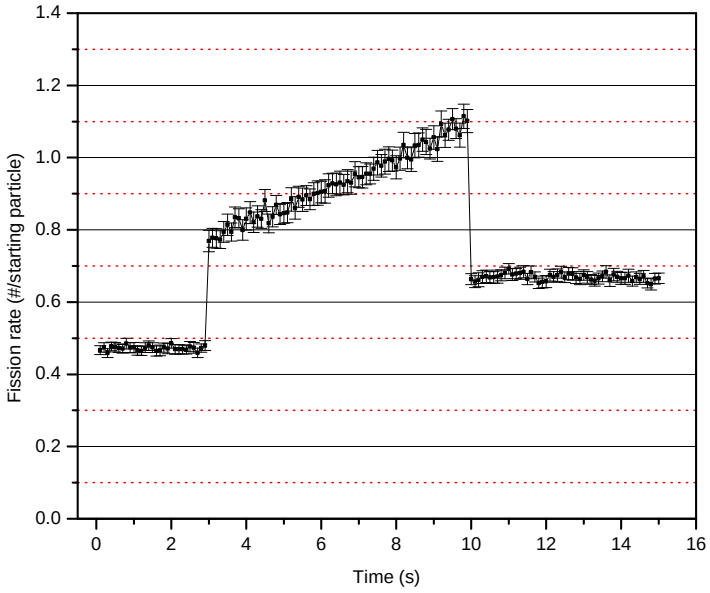

Figure 5.6: Test-case 5-1: Temporal evolution of the total fission-rate $\left[\frac{\text{fissions}}{\text{starting particle}}\right]$ with standard deviation.

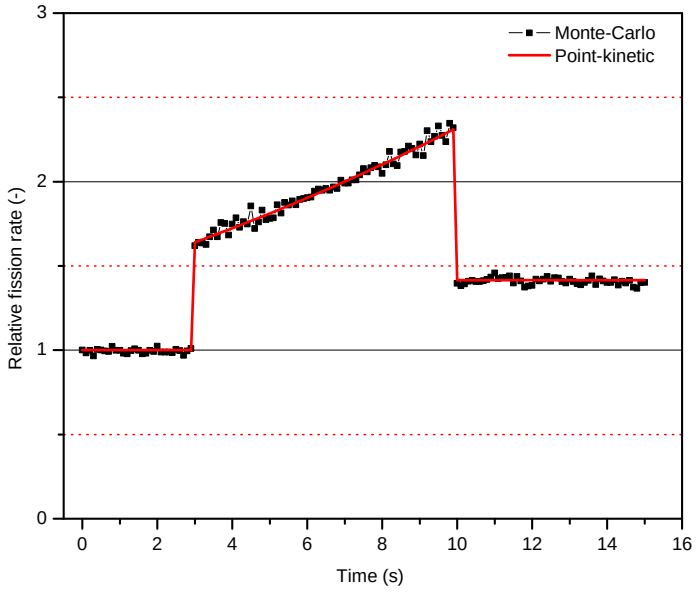

Figure 5.7: Test-case 5-1: Monte-Carlo calculated relative fission-rate vs PK analytical solution.

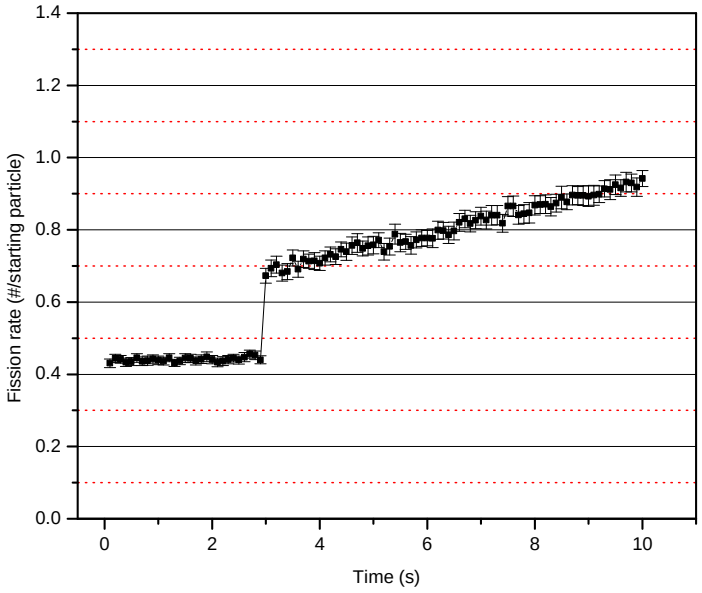

Figure 5.8: Test-case 5-2: Temporal evolution of the total fission-rate $\left[\frac{\text{fissions}}{\text{starting particle}}\right]$ with standard deviation.

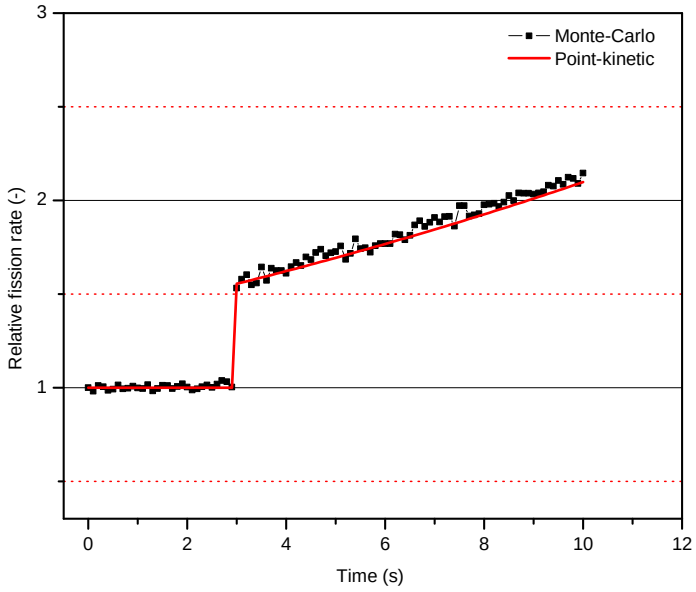

Figure 5.9: Test-case 5-2: Monte-Carlo calculated relative fission-rate vs PK analytical solution.

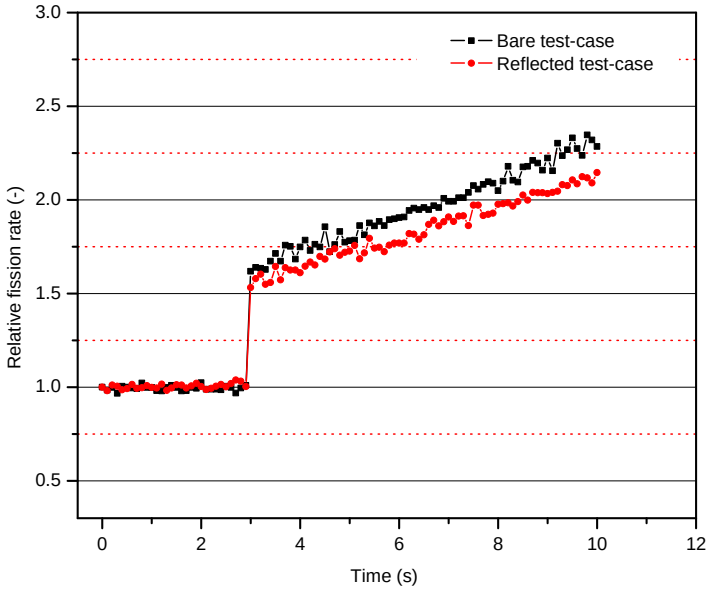

Figure 5.10: Test-case 5-1 & 5-2: Comparison of the Monte-Carlo calculated fission-rate for two different configurations.

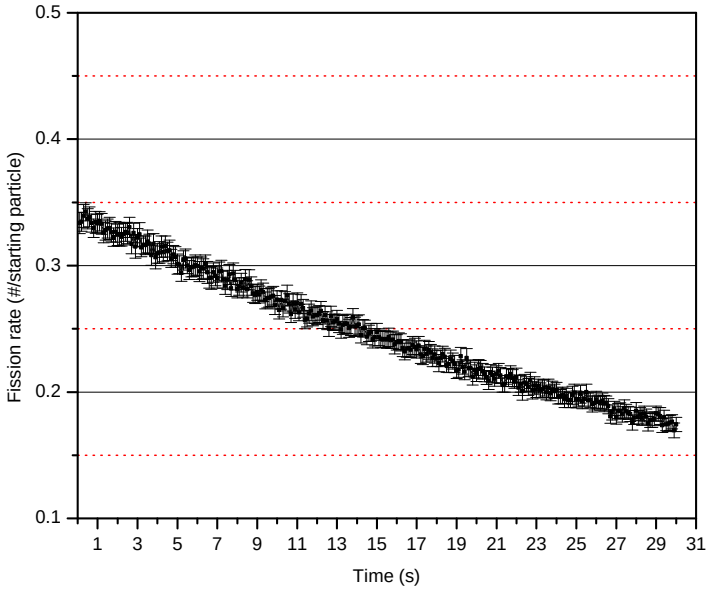

Figure 5.11: Test-case 5-3: Temporal evolution of the total fission-rate $\left[\frac{\text{fissions}}{\text{starting particle}}\right]$ with standard deviation.

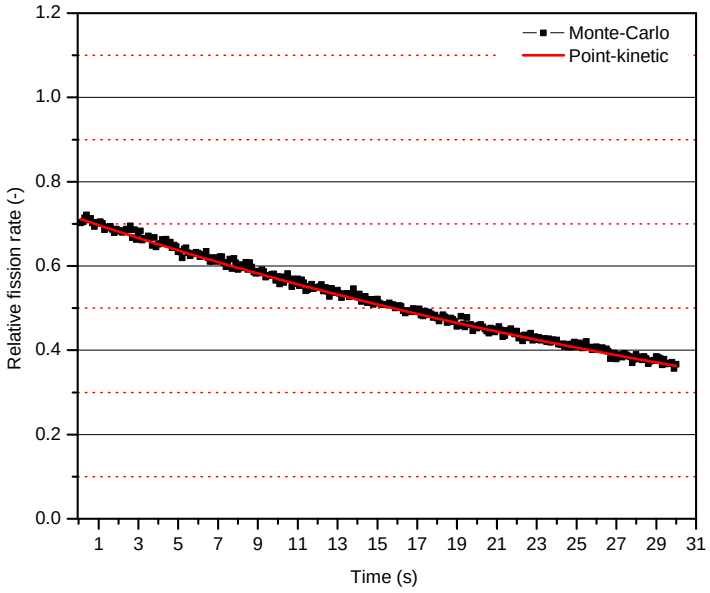

Figure 5.12: Test-case 5-3: Monte-Carlo calculated relative fission-rate vs PK analytical solution.

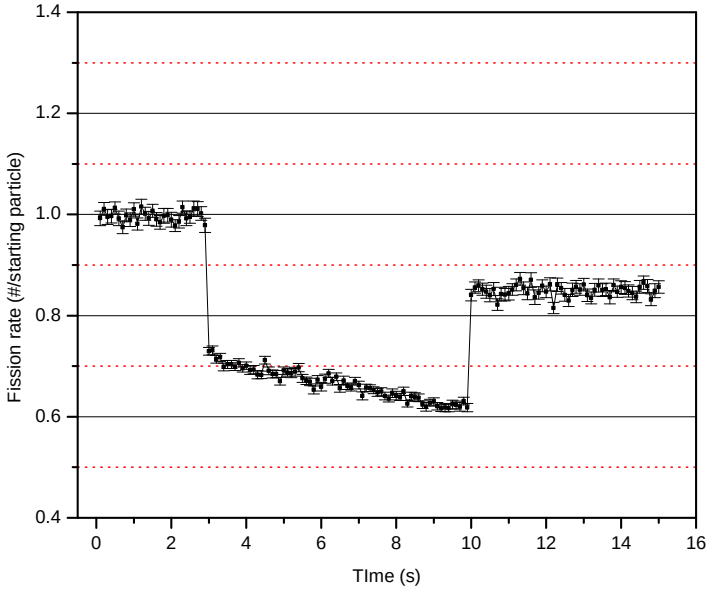

Figure 5.13: Test-case 5-4: Temporal evolution of the total fission-rate $\left[\frac{\text{fissions}}{\text{starting particle}}\right]$ with standard deviation.

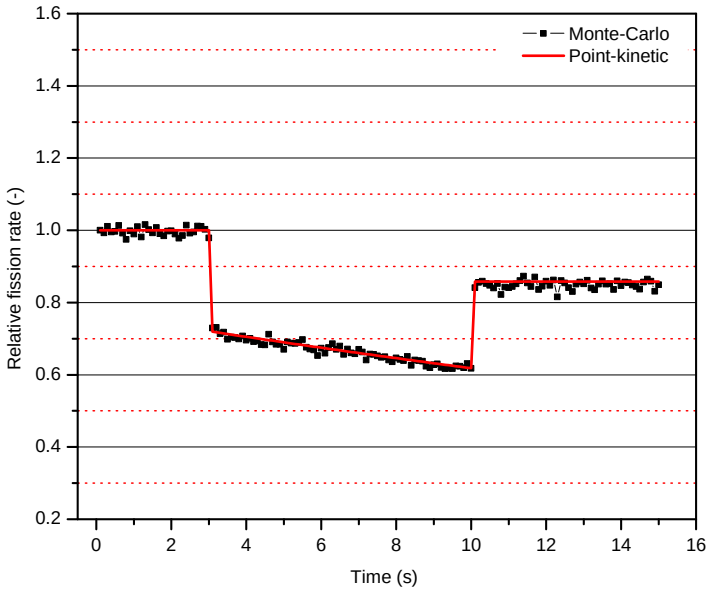

Figure 5.14: Test-case 5-4: Monte-Carlo calculated relative fission-rate vs PK analytical solution.

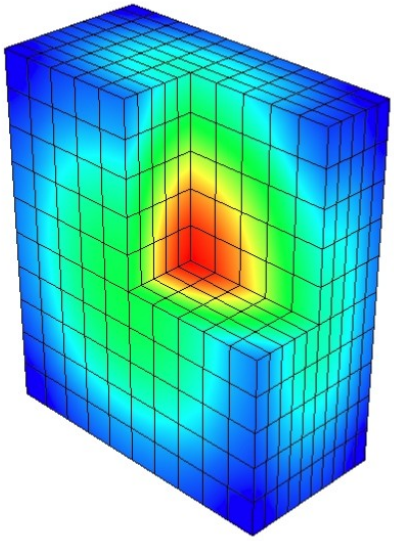

(a) t = 0.1 s

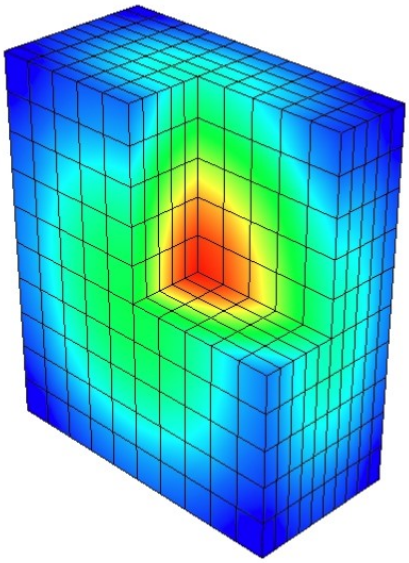

(b) t = 2.9 s

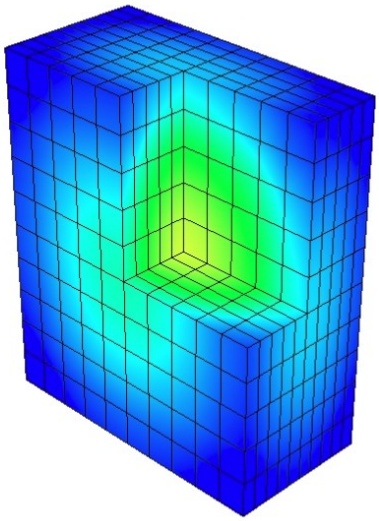

(c) t = 3.0 s

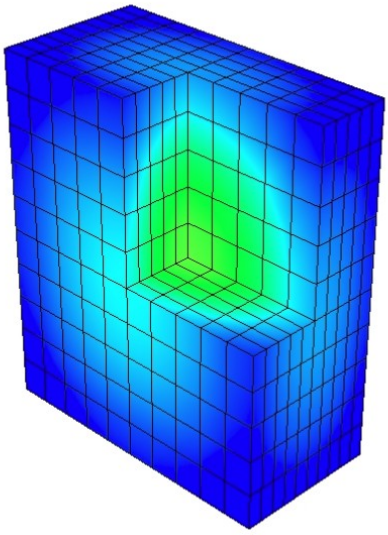

(d) t = 9.9 s

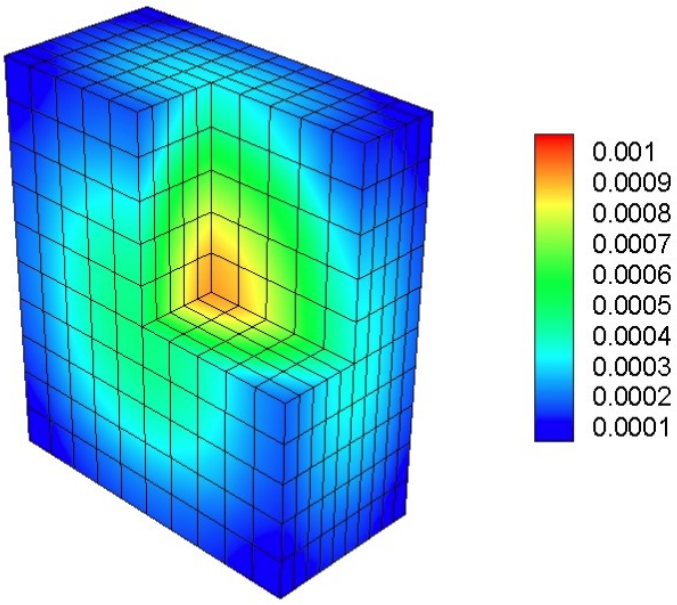

(e) t = 15.0 s

Figure 5.15: Test-case 5-4: Monte-Carlo calculated temporal/spatial fission-rate distribution $\left[\frac{\text{fissions}}{\text{starting particle}}\right]$.

5.4 NUMERICAL EXPERIMENTS - MULTI-GROUP PRECURSORS

In this section three (3) numerical experiments are analysed aiming to verify and validate the module when more than one precursor groups are used. More specifically the multigroup precursor treatment as well as the sampling of the transient source (prompt neutrons + precursors) using suitable tallies (Eqs (5.2 and 5.3)) during the initial *k*-eigenvalue calculation should be verified. The first experiment is the same with that of § 5.3.1 while the second one concerns a pin-by-pin Fuel Assembly (FA) analysis of a transient induced by a control rod movement. In all cases the JEFF 3.1.2 (*Jeff-3.1.2*) nuclear data library has been used. The results are compared with a numerical solution of the PK equations obtained with the simple explicit forward-Euler method.

5.4.1 *Test-case 5-5: A simplified bare configuration with insertion of positive reactivity*

The same configuration with § 5.3.1 is analysed using the 8-group precursor format provided by the Jeff-3.1.2 nuclear data library (*Jeff-3.1.2*). The dynamic analysis of this configuration is performed for 5 s using a time-step of 0.1 s. For the first 0.9 s the

configuration remains critical and for $t = 1.0$ s the density increases instantaneously to $4.50245 \cdot 10^{-2} \frac{atoms}{barn-cm}$ inducing positive reactivity $\rho =\sim 130$ pcm. The evolution of the transient is monitored for the remaining time interval.

In the beginning two calculations are performed with 50 batches and 10^6 initial neutrons per batch. The first one is performed without using combined precursors whereas in the second this capability has been activated. The maximum standard deviation of the total fission-rate in the first calculation is 3.47%. When combined precursors are used the maximum standard deviation is reduced to 3.14%. The reduction of the maximum standard deviation confirms that the combined precursor technique can reduce the statistical variance induced by the treatment of particles associated with significantly different time constants.

Afterwards the same calculation is performed with 100 batches and 10^6 neutron histories per batch at the beginning of the transient. Utilising 96 MPI tasks on 48 physical cores and accumulating 50 tally-bins the total wall-clock time was 1.04 h. Fig. (5.16) illustrates the temporal evolution of the fission-rate associated with the standard deviation. Fig. (5.17) shows a comparison of the Monte-Carlo calculated relative fission-rate with a PK solution; as can be seen a satisfactory agreement is found. Both the prompt jump and the afterwards behaviour are predicted with Monte-Carlo.

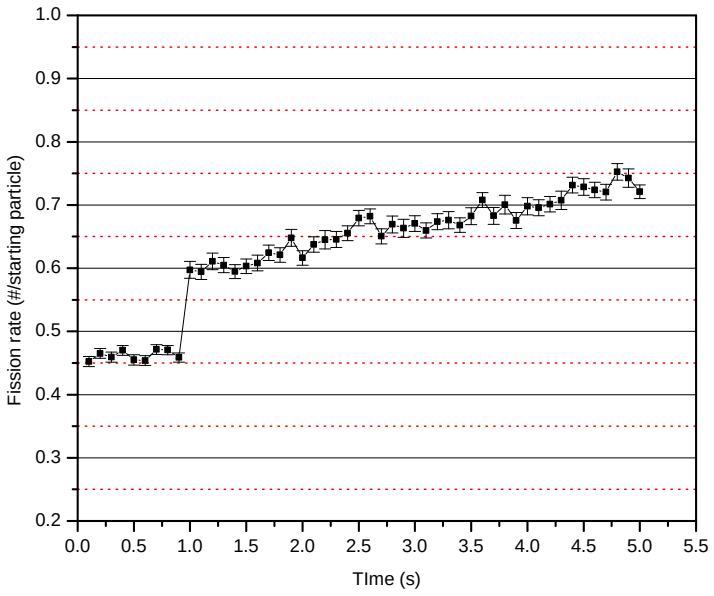

Figure 5.16: Test-case 5-5: Temporal evolution of the total fission-rate with standard deviation. $\left[\frac{fissions}{starting\ particle}\right]$.

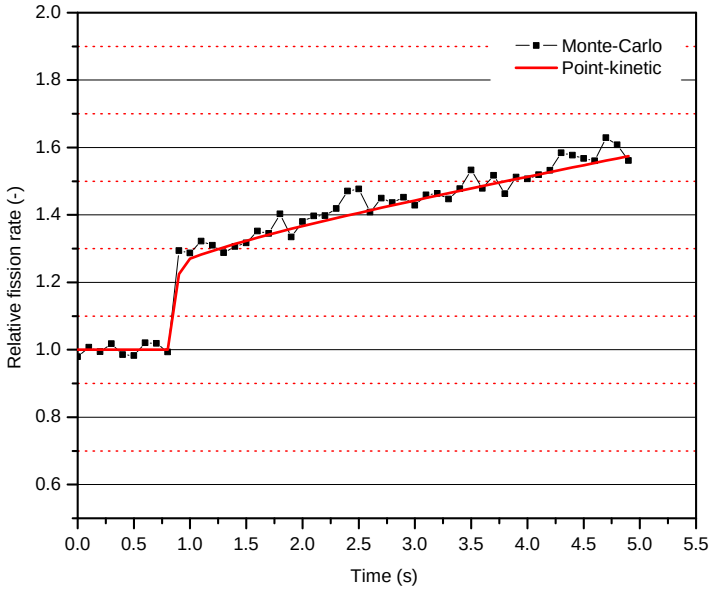

Figure 5.17: Test-case 5-5: Monte-Carlo calculated relative fission-rate vs PK.

5.4.2 *Test-case 5-6: A pin-by-pin 17×17 FA transient induced by control-rod movement - with reflective boundaries*

In this section a control-rod induced transient in a 17×17 UO_2 FA is analysed. The FA model has reflective boundary conditions in the periphery. At the axial edges of the water reflectors, vacuum boundaries have been implemented. This FA model is captured from the whole-core Monte-Carlo benchmark presented by Hoogenboom et al. (2011). A horizontal cross section of the model is illustrated in Fig. (5.18). The main difference is that here, partially inserted control rods are located in the water-filled guide tubes. In addition, the material compositions have been modified; for this reason they are presented in appendix a.

Initially the critical height of the inserted control rods is specified. Afterwards three (3) different scenarios are analysed. In all of them the configuration remains critical for the first 0.3 s. Subsequently three different transients occur.

In the first case, at t=0.3 s, the control rods are extracted in one step to a new level. The inserted reactivity at that level has been calculated ~477 pcm (0.9998 → 1.00475). The evolution of the power is monitored for a time interval of 2.5 s. This dynamic calculation has been performed using 60 batches and 10^6 initial neutrons per batch. The

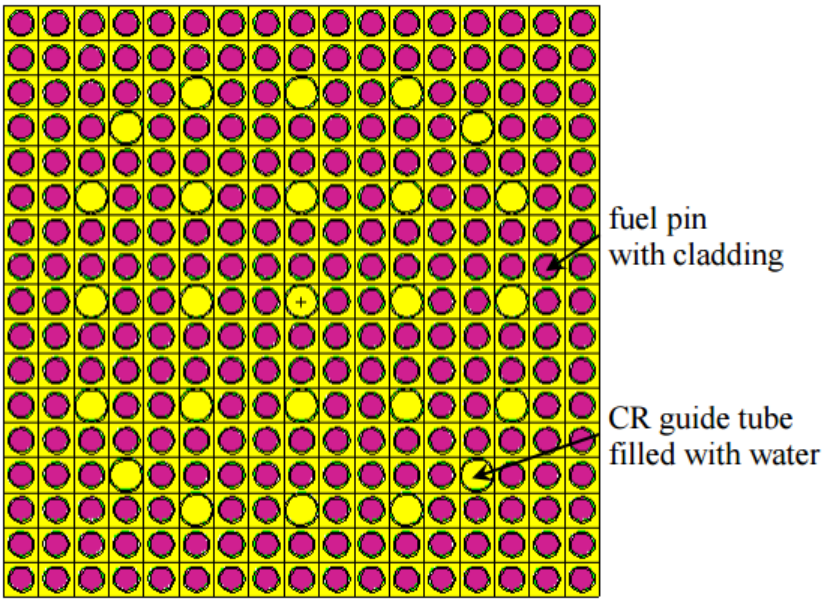

Figure 5.18: Horizontal cross section of the 17×17 FA model.

calculated temporal evolution of the total fission-rate along with the standard deviation is illustrated in Fig. (5.19). The maximum statistical error is 3.45%. Then it is compared with PK; Fig. (5.20) shows a satisfactory agreement.

In the second case the movement of the control rods is implemented progressively; between t=0.3 s - 0.5 s. The evolution of the power is monitored for a time-interval of 2.3 s. This dynamic calculation has been performed using 20 batches and 10^6 initial neutrons per batch. Utilising 96 MPI-tasks on 48 physical processors the total wall-clock computational time was 9.07 h. The maximum statistical error is 5.67%. This significant increase of the statistical error compared with the first case is mostly attributed to the smaller number of used batches, i.e. 20 instead of 60. A comparison with PK shows a satisfactory agreement (Fig. (5.21)).

In the third case the same problem is analysed but now, at t=1.9 s, the control rods are entirely inserted in one step and the scram is monitored in the remaining time interval. This dynamic calculation has been performed using 20 batches and 10^6 initial neutrons per batch. When a tallying mesh (x,y,z,t) with 1×1×1×25 cells is used, the utilisation of 48 MPI-tasks on 48 physical processors gives 7.05 h total wall-clock time. The maximum statistical error is 5.54%. A comparison between the Monte-Carlo and the PK solution is illustrated in Fig. (5.22). It is noteworthy that while the solutions show a satisfactory agreement before scram, afterwards there is a significant deviation. This can be attributed to the fact that the point-reactor model approximation (§ 2.2.1)

has been here utilised in the PK numerical solution. According to this model the flux is given by the following relation:

$$\psi(\boldsymbol{r}, \boldsymbol{\Omega}, E, t) = P(t)\boldsymbol{s}(\boldsymbol{r}, \boldsymbol{\Omega}, E) \tag{5.14}$$

In other words the flux shape $s(\boldsymbol{r}, \boldsymbol{\Omega}, E)$ is considered constant with time. However, after a scram, the flux shape is significantly distorted and this approximation does not work anymore. In such cases the utilisation of the quasi-static model would be a more reasonable approximation.

The spatial/temporal fission-rate behaviour has been calculated with a tallying mesh (x,y,z,t) with 9×9×20×25 cells utilising 20 batches and 10^6 neutron (prompt and delayed) histories per batch. Figs (5.23, 5.24, 5.25 and 5.26) show the fission-rate (power) spatial distribution for some specific moments. The rapid increase of the power after the partial extraction of the control rods as well as the decrease after the full insertion of the rods are evident. Figs (5.27, 5.28, 5.29 and 5.30) illustrate the fission-rate (power) spatial distribution for some specific axial levels at some specific moments. The power increase towards higher axial levels can be noticed as well as the scram that causes significant power reduction.

Figs (5.31 - 5.34) illustrate the spatial distribution of the fission-rate statistical-error. At this point it should be mentioned that in Monte Carlo the statistical-error increases when the tally-volume decreases; in a smaller tally-volume a smaller number of events is expected to be recorded. Figs (5.31 - 5.34) show that the statistical error is higher in the upper regions of low power production. The large errors appeared in areas of negligible power production are of no significance. In addition Figs (5.31 - 5.34) depict that at the very upper regions the statistical error is zero. This happens because in these areas there is practically no power production at all; no events are recorded. In the areas of significant power production, i.e. the areas of interest, the statistical error is relatively small. If it is taken into account that only 20 batches were used for this calculation, it is clear that there is a significant potential to reduce the error by increasing the number of batches.

Figs (5.35, 5.36 and 5.37) depict more clearly the fission-rate (power) spatial distribution in some specific axial levels for some specific moments. It is noteworthy that in Fig. (5.35) the power peak appears in the center of the FA whereas in Figs (5.36 and 5.37) in the periphery. This is explained by the fact that in the axial level z=-112.73 cm the guide tubes are filled with water causing higher moderation rates near them. On the other hand in the axial levels z=-112.73 cm and z=-100.65 cm the guide tubes are filled with the control-rod material. Thus areas of high neutron absorption are located near them.

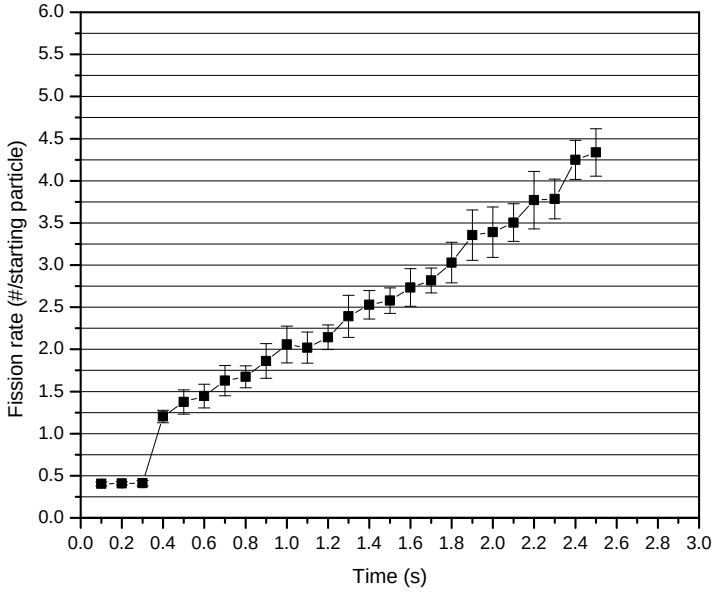

Figure 5.19: Test-case 5-6: Temporal evolution of the total fission-rate with standard deviation $\left[\frac{\text{fissions}}{\text{starting particle}}\right]$.

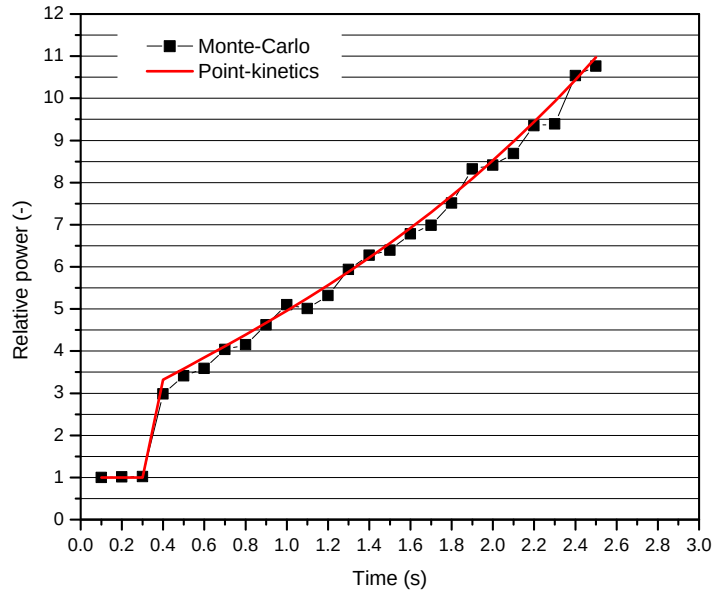

Figure 5.20: Test-case 5-6: Monte-Carlo calculated relative fission-rate vs PK.

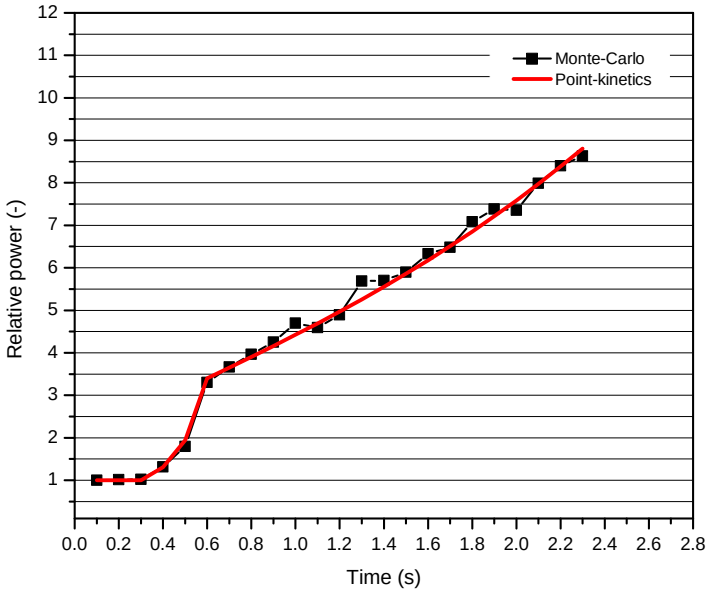

Figure 5.21: Test-case 5-6: Monte-Carlo calculated relative fission-rate vs PK.

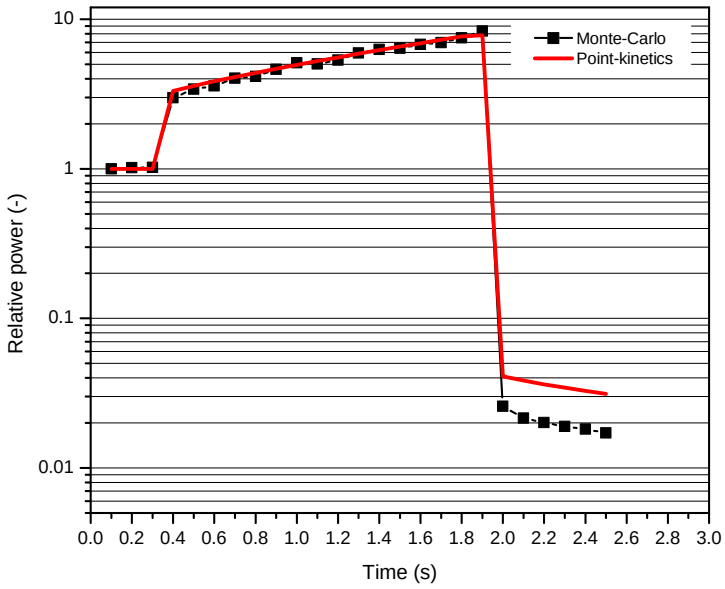

Figure 5.22: Test-case 5-6: Monte-Carlo calculated relative fission-rate vs PK.

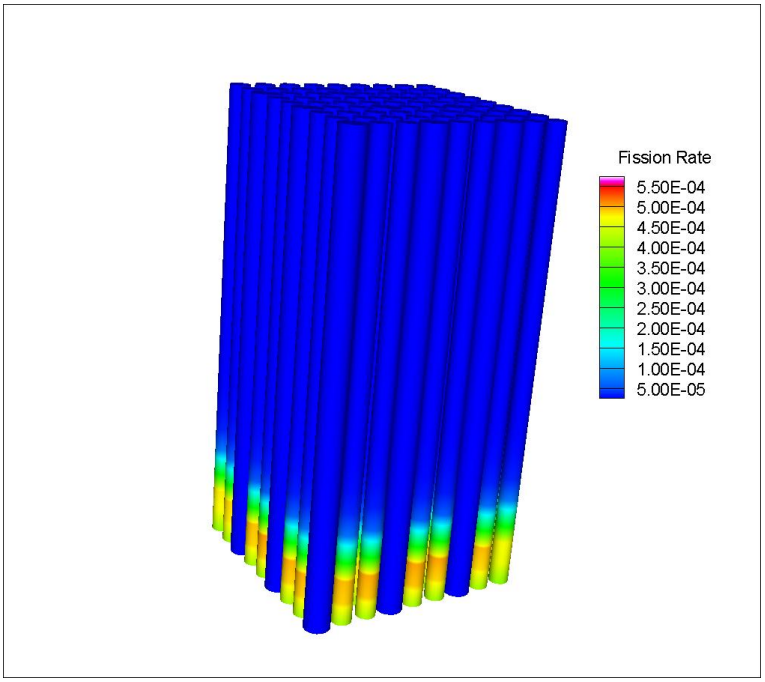

Figure 5.23: Test-case 5-6: Fission-rate (power) distribution $\left[\frac{fissions}{starting\ particle}\right]$ for t=0.1 s.

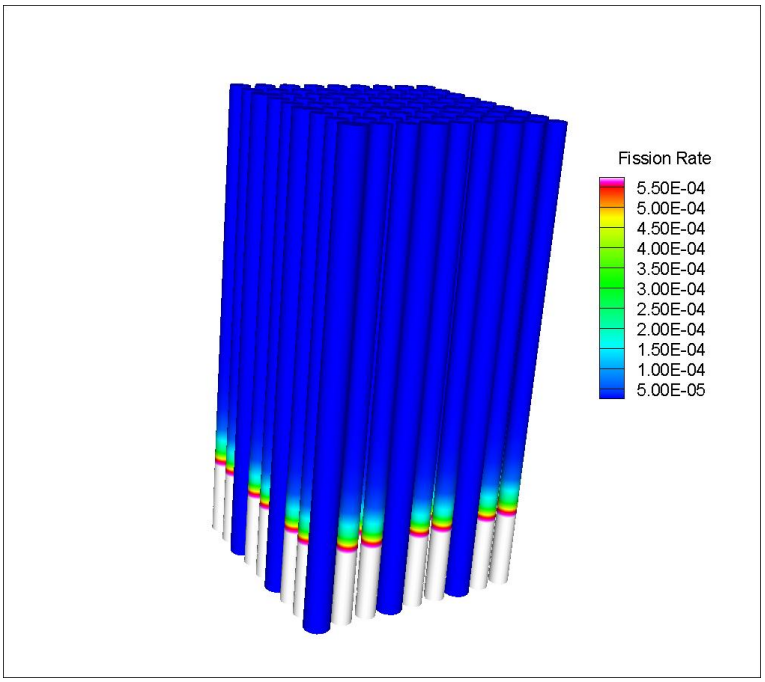

Figure 5.24: Test-case 5-6: Fission-rate (power) distribution $[\frac{fissions}{starting\ particle}]$ for t=0.4 s.

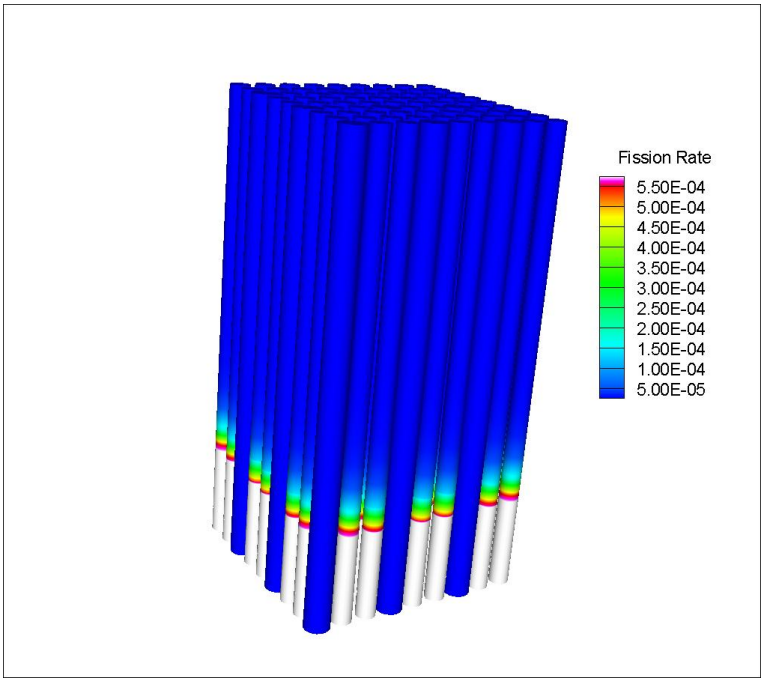

Figure 5.25: Test-case 5-6: Fission-rate (power) distribution $\left[\frac{fissions}{starting\ particle}\right]$ for t=1.9 s.

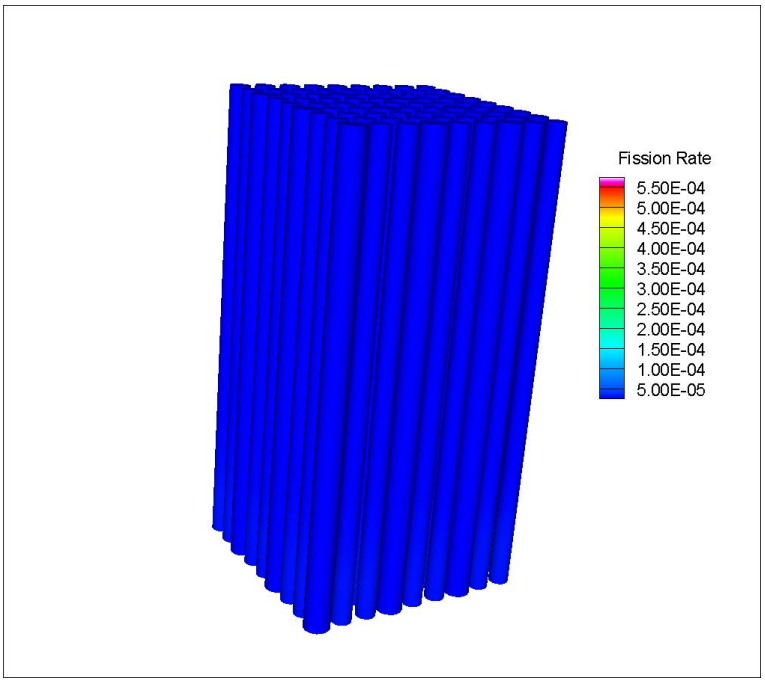

Figure 5.26: Test-case 5-6: Fission-rate (power) distribution $[\frac{fissions}{starting\ particle}]$ for t=2.0 s.

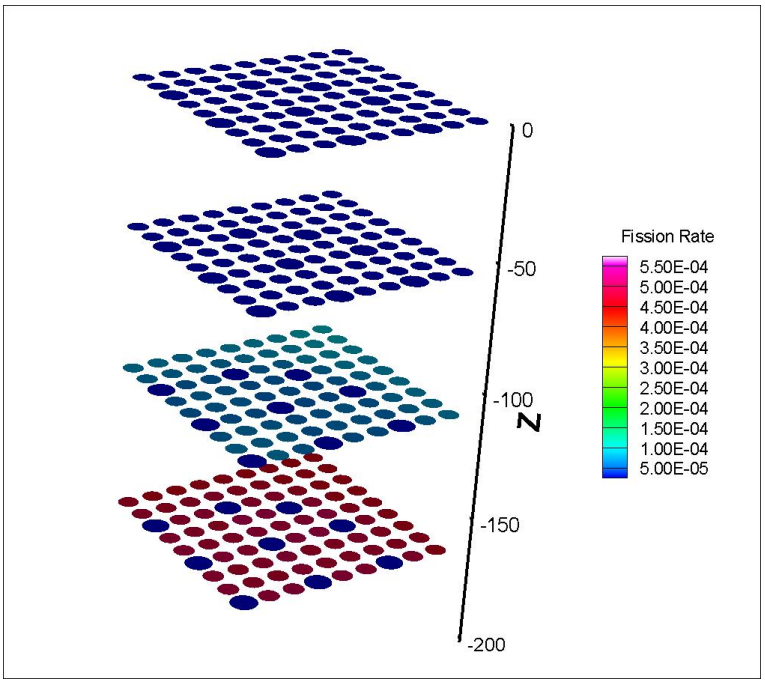

Figure 5.27: Test-case 5-6: Fission-rate (power) distribution $\left[\frac{fissions}{starting\ particle}\right]$ for t=0.1 s.

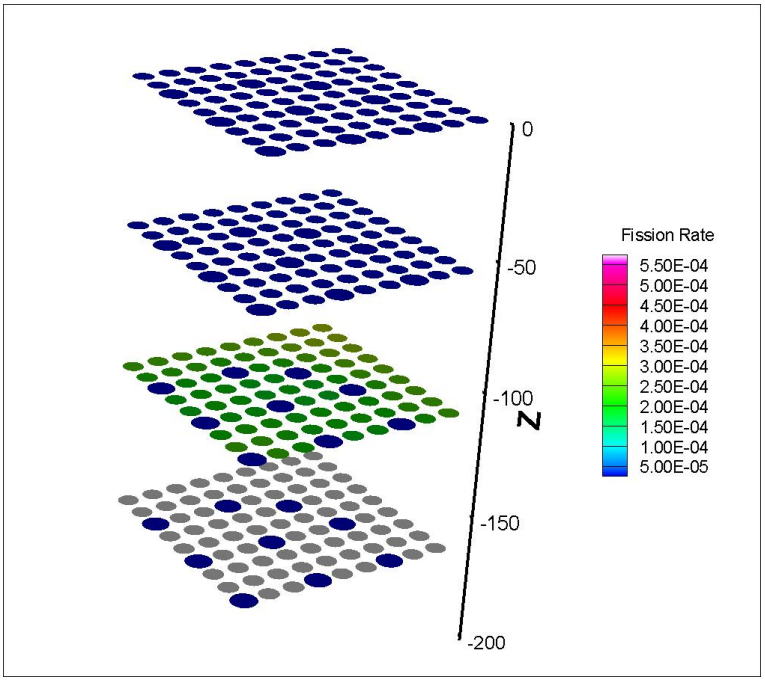

Figure 5.28: Test-case 5-6: Fission-rate (power) distribution $\left[\frac{fissions}{starting\ particle}\right]$ for t=0.4 s.

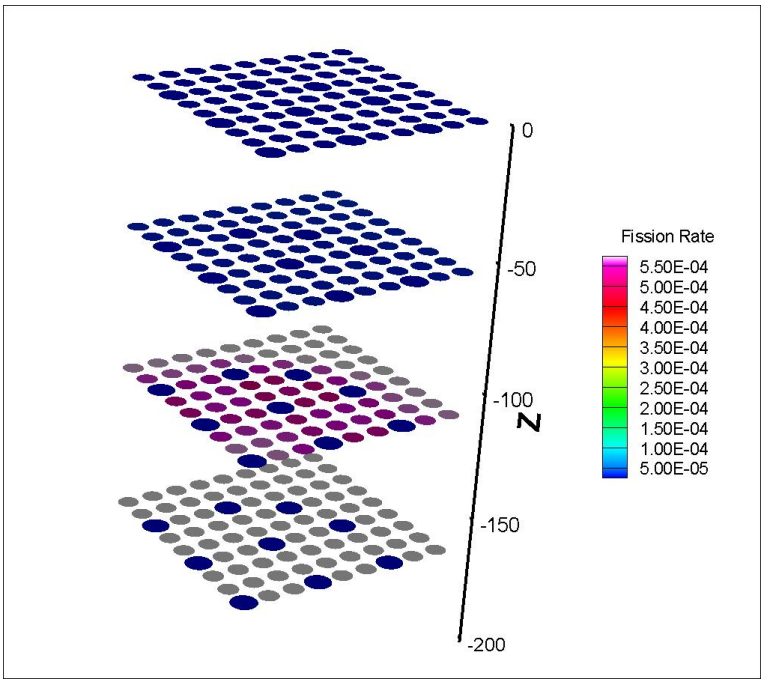

Figure 5.29: Test-case 5-6: Fission-rate (power) distribution $\left[\frac{fissions}{starting\ particle}\right]$ for t=1.9 s.

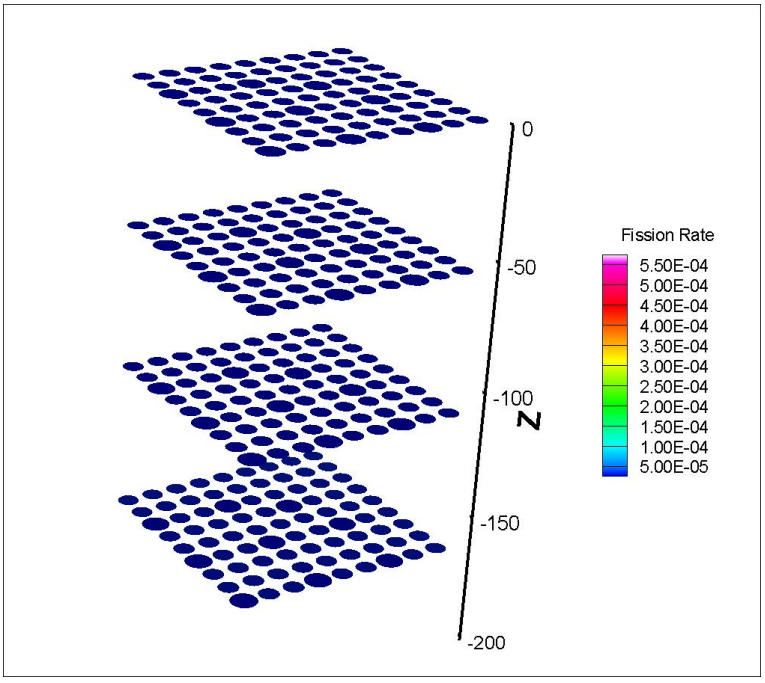

Figure 5.30: Test-case 5-6: Fission-rate (power) distribution $\left[\frac{fissions}{starting\ particle}\right]$ for t=2.0 s.

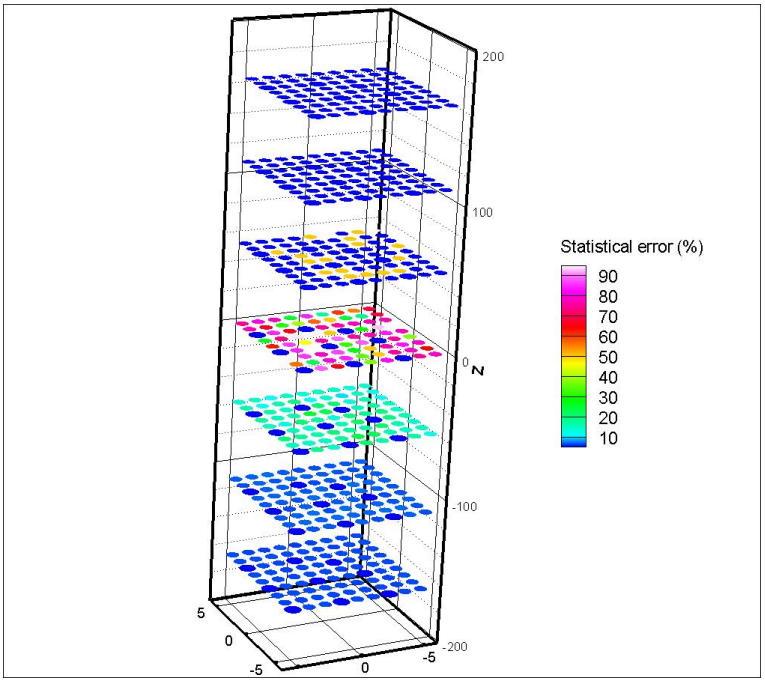

Figure 5.31: Test-case 5-6: Fission-rate statistical-error distribution for t=0.1 s.

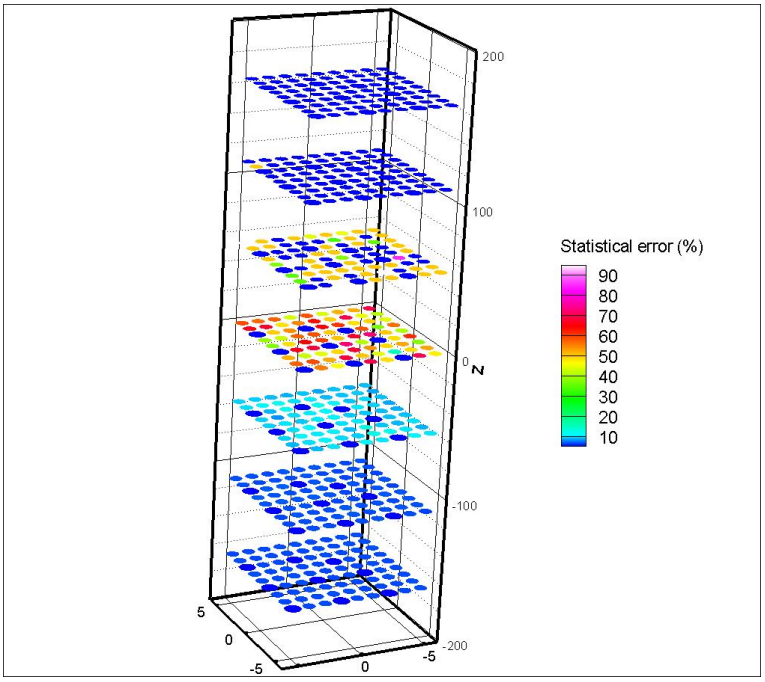

Figure 5.32: Test-case 5-6: Fission-rate statistical-error distribution for t=0.4 s.

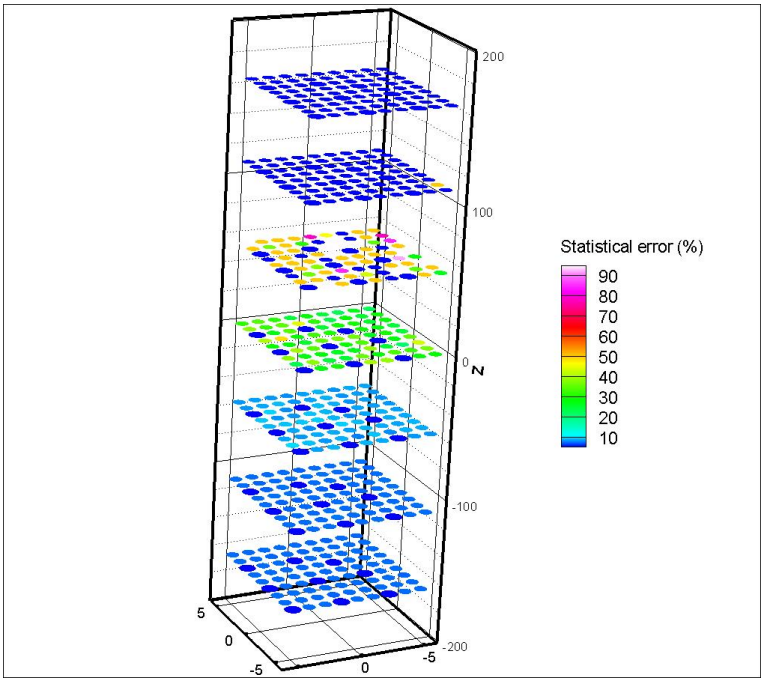

Figure 5.33: Test-case 5-6: Fission-rate statistical-error distribution for t=1.9 s.

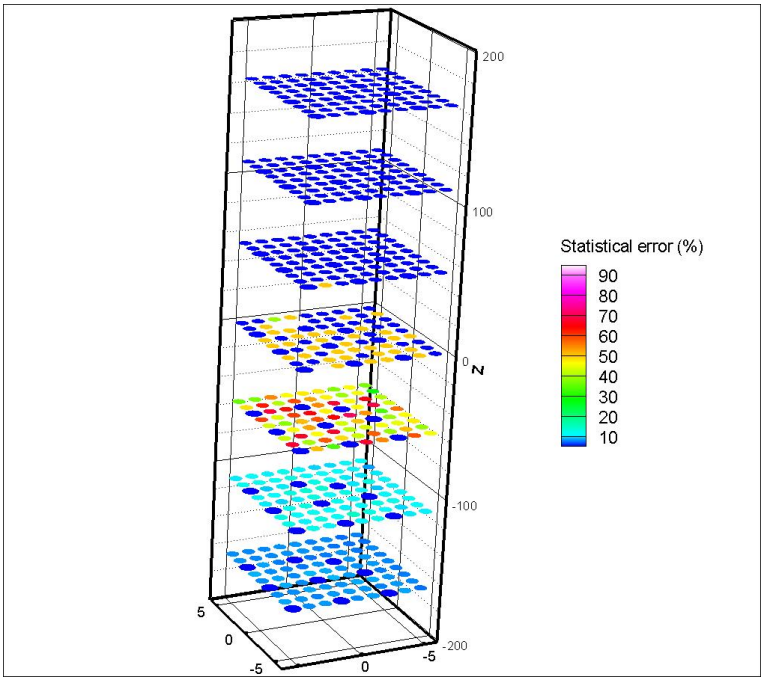

Figure 5.34: Test-case 5-6: Fission-rate statistical-error distribution for t=2.0 s.

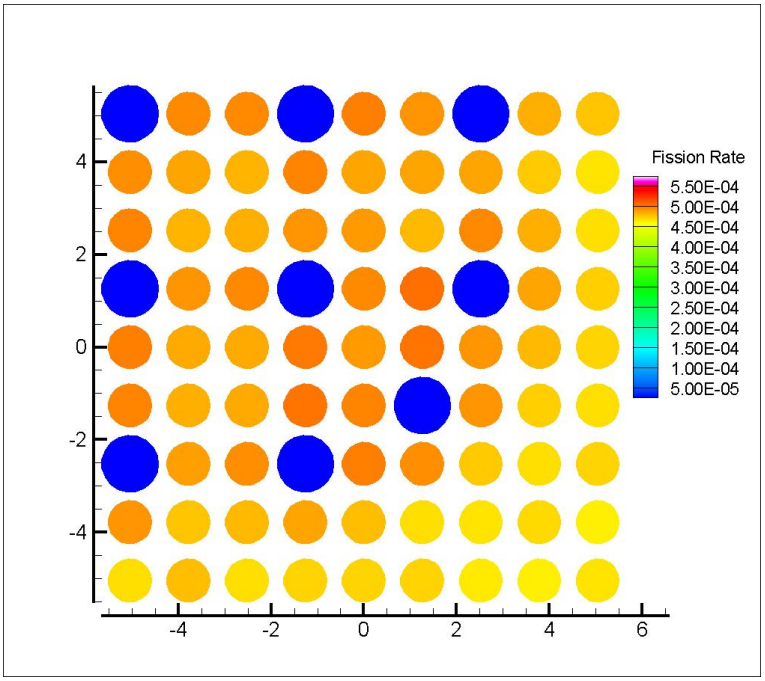

Figure 5.35: Test-case 5-6: Fission-rate (power) distribution $\left[\frac{fissions}{starting\ particle}\right]$ for z=-152.99 and t=0.1 s.

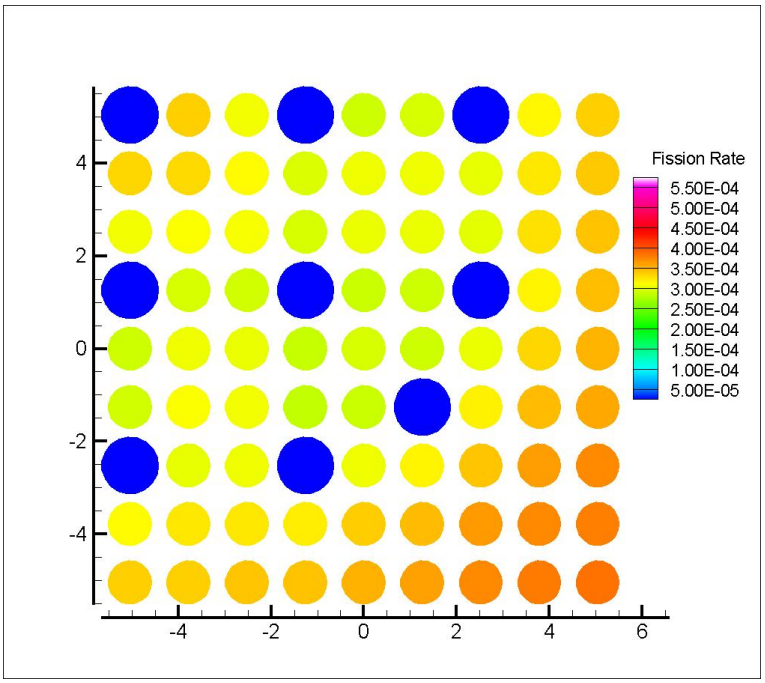

Figure 5.36: Test-case 5-6: Fission-rate (power) distribution $\left[\frac{fissions}{starting\ particle}\right]$ for z=-112.73 and t=1.9 s.

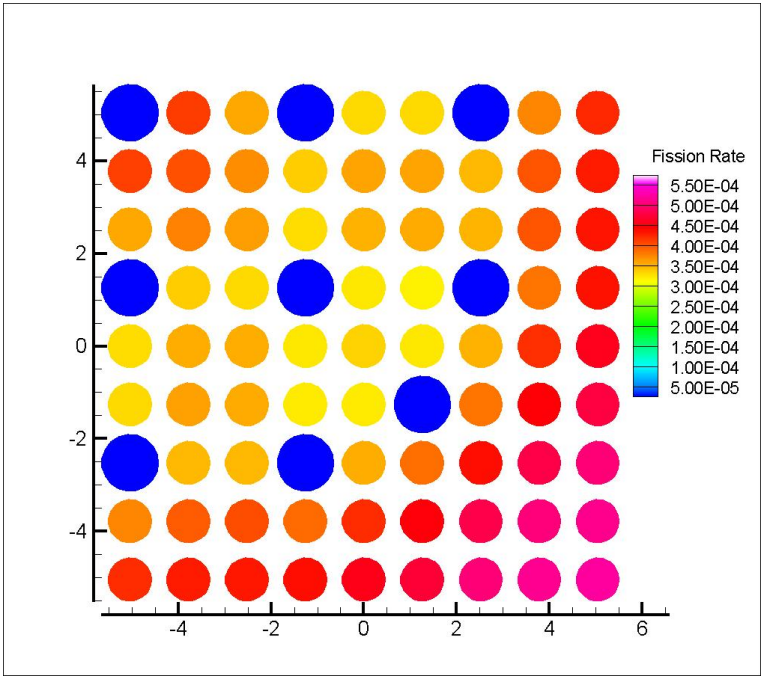

Figure 5.37: Test-case 5-6: Fission-rate (power) distribution $\left[\frac{\text{fissions}}{\text{starting particle}}\right]$ for z=-100.65 and t=2.0 s.

5.4.3 *Test-case 5-7: A pin-by-pin 17×17 FA transient induced by control-rod movement - with vacuum boundaries*

This test case aims to support the need for Monte-Carlo dynamic reactor analysis since PK can fail in many realistic cases. The Test-case 5-6 concerns a FA configuration where reflective boundary conditions have been used in the periphery of the configuration. Since neutron leakage is very low, a minimal extraction of the control rods can lead to a relatively large insertion of positive reactivity. This can lead to a better agreement between Monte-Carlo and PK because the neutron flux shape is not significantly distorted. For this reason the FA configuration is analysed again but now the reflective boundaries are replaced with vacuum boundaries and the material density of the fuel is modified. A transient induced by the extraction of the control rods is simulated. Now a much larger extraction or the control rods is required to achieve a comparable reactivity insertion to the previous case. The rods were extracted from z=-100 cm to z=-80 cm inducing a positive reactivity of ~520 pcm. This dynamic calculation has been performed using 60 batches and 10^6 initial neutrons per batch. Utilising 48 MPI-tasks on 48 physical processors the total wall-clock computational time was 15.79 h. The temporal evolution of the total fission-rate along with the standard deviation and the PK solution is illus-

trated in Fig. (5.38). The maximum statistical error is 3.68%. It can be seen that the two solutions differ significantly. This fact underlines the deficiency of simple PK models to treat transients with significant distortion of the neutron flux shape.

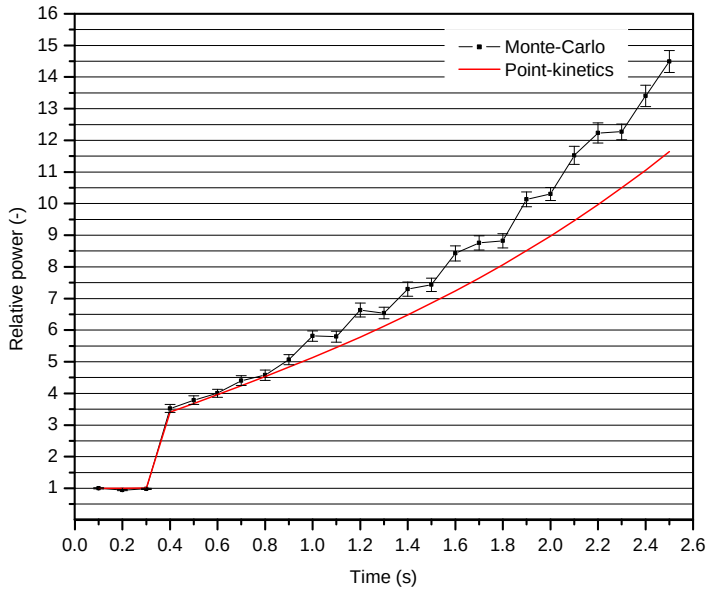

Figure 5.38: Test-case 5-7: Monte-Carlo calculated relative fission-rate vs PK.

5.5 THERMAL-HYDRAULIC FEEDBACK

Many physical phenomena are described by Partial Differential Equations (PDEs). When a problem is defined by a set of PDEs there are mainly two ways to solve it numerically. With the first one the whole set of the PDEs is solved simultaneously achieving high levels of accuracy. In the second way each physical field is solved separately and the information exchange among the solutions of the involved fields is kept minimum. This method, called Operator Splitting (OS) method, is the easiest way to solve a multi-physical problem. It implies that the impact of an operator which describes the physics of the analysed phenomenon is approximated by the impact of more different operators, each of them representing a different, "artificially" separated physical field. Practically one form of the OS approximation is implemented by solving sequentially in time the involved physical fields using distinct solvers and considering the output of the one as the input of the other, as illustrated in Fig. (5.39).

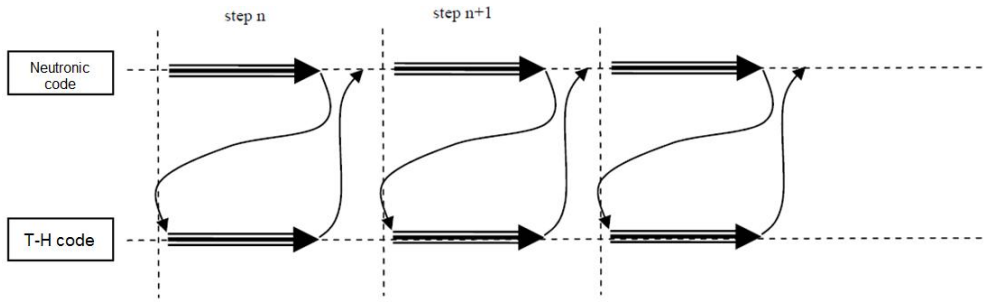

Figure 5.39: An OS (low-order) scheme for coupled neutronic/T-H analysis.

For the purposes of this study, OpenMC$^+$ is coupled with SUBCHANFLOW (SCF) (Imke et al., 2010), a T-H subchannel solver. SCF is based on the family of COBRA solvers (Basile et al., 1999). The old-fashioned programming methods of COBRA have been replaced by modern ones resulting in a tool that can be easily compiled and used. In addition SCF provides utilities for coupling with other codes and post-processing of the results. All these features are the reasons that led to the selection of SCF in the present research.

5.5.1 *Coupling algorithm*

In this study the OS method for coupling OpenMC$^+$ and SCF is adopted, since it constitutes the easiest way to couple two distinct solvers without the requirement of extensive modifications induced by the coupling itself.

The idea behind OS techniques is briefly described in this paragraph. Usually a physical phenomenon is the combined effect of several processes. For example the neutron flux is determined by neutronics, T-H, phenomena related to structural mechanics, etc. Thus the temporal behaviour of a physical quantity is described by a partial differential equation in which the local time derivative depends on the sum of the sub-operators corresponding to the different processes. These sub-operators can be of different nature; first- and second-order differential operators, nonlinear operators, constant operators, etc. For each sub-problem, corresponding to each sub-operator, numerical methods which provide fast and accurate solutions may exist. However, for the sum of these sub-operators adequate methods cannot usually be found. Hence the application of OS procedures means that, instead of their sum, the sub-operators are handled separately. The solution of the original problem is then obtained from a combination of the sub-problem numerical solutions (Csomos, 2007).

The dynamic neutronic problem has the following form:

$$\frac{\partial \phi}{\partial t} = L(T)\phi \tag{5.15}$$

Here it is considered that the transport process described by the operator L is performed by the neutronic solver N that is OpenMC$^+$. The vector $\boldsymbol{x}$ is considered as the OpenMC$^+$ output containing the scalar fluxes. Similarly, a T-H solver N, SCF in this case, is employed to solve the T-H sub-problem. The vector $\boldsymbol{y}$ contains the output of SCF including temperatures and densities. Then the integrated problem can take the following explicit form:

$$\frac{\partial \boldsymbol{x}}{\partial t} = N(\boldsymbol{x}, \boldsymbol{y}) \tag{5.16}$$

$$\frac{\partial \boldsymbol{y}}{\partial t} = T(\boldsymbol{x}, \boldsymbol{y}) \tag{5.17}$$

where $\boldsymbol{\chi}(0) = \boldsymbol{\chi}_0$ and $\boldsymbol{y}(0) = \boldsymbol{y}_0$. The symbols N and T represent the neutronic and the T-H solver of each time-step and not for the whole problem in time. After temporal discretization, a staggered OS coupling can be written as:

$$\frac{\boldsymbol{x}^{n+1} - \boldsymbol{x}^n}{\Delta t} = N(\boldsymbol{y}^n, \boldsymbol{x}^n) \tag{5.18}$$

$$\frac{\boldsymbol{y}^{n+1} - \boldsymbol{y}^n}{\Delta t} = T(\boldsymbol{y}^n, \boldsymbol{x}^{n+1}) \tag{5.19}$$

where the index n refers to the time-step. Thus the solution updates are generated by the following relations:

$$\boldsymbol{x}^{n+1} = (\Delta t \cdot N(\boldsymbol{y}^n, \boldsymbol{x}^n) + \boldsymbol{x}^n \tag{5.20}$$

$$\boldsymbol{y}^{n+1} = (\Delta t \cdot T(\boldsymbol{y}^n, \boldsymbol{x}^{n+1})) + \boldsymbol{y}^n \tag{5.21}$$

This strategy is non-iterative and the non-linearities due to the coupling in between the physics components are not resolved over a time step reducing the overall accuracy to first-order $O(\Delta t)$. For this reason such a coupling scheme is called *weak* or *loose*. *Loose* systems of PDEs usually require very small time-steps (Grandi, 2009). Since here neutronics is solved by Monte-Carlo, some questions arise. For each time step OpenMC$^+$ calculates the integral of the desired quantities, e.g., for a time-interval $[t_1, t_2]$ a Monte-Carlo flux tally calculates $\phi = \int_{t_1}^{t_2} \phi(t)dt$. However, as also highlighted by Sjenitzer et al. (2015), Monte-Carlo should, somehow, estimate the flux at each time point n, n+1,... in order to communicate with T-H. For this reason the flux at the middle of each time-step is calculated by averaging the flux over the time interval. Afterwards the flux at t=n+1, i.e. the upper boundary of the current time-step, is calculated using linear extrapolation.

As mentioned above an implementation of a *loose* OS coupling algorithm (Fig. (5.39)) does not treat the non-linearities of the system (Ragusa and Mahadevan, 2009). The non-linearities could be treated by iteratively converging the coupled solution in each time step. However, in the case of Monte-Carlo neutronics this would create an extraordinary increase of the computational cost. Therefore more sophisticated methods should

be investigated. However it is out of the scope of this work to optimise the coupling algorithm between dynamic Monte-Carlo and dynamic T-H and no further attention is paid.

The second question concerns the coupling programming approach that will be followed, i.e., internal or external coupling. This option mainly concerns the way that the data are exchanged between the two solvers. An internal coupling approach considers the two solvers as subparts of the main solver. In this case the two solvers could be compiled together and the information between the involved physical fields would be exchanged through programming variables, i.e., through memory. The second option concerns the execution of the involved solvers separately and the data exchange is usually done through data files. In this work the external coupling approach is selected mainly because it is the easiest way to couple two single-physics solvers keeping the required modifications of the original source codes as less as possible.

Another important question is how OpenMC$^+$, a stochastic solver, will be algorithmically connected with SCF, a typical deterministic solver. The answer is derived by the fact that the Monte-Carlo solvers consider independent realisations of the random variable in order to extract statistically averaged results. The current structure of OpenMC$^+$ implies that the easiest way is to apply the T-H feedback within each statistical batch affecting each independent realisation of the random variable. An alternative approach would require the T-H feedback directly on the statistically averaged random variable. However this would require the time-step loop to be external of the batch loop (see Algorithm 2). This would imply extensive modification of the source code of OpenMC$^+$ as well as of OpenMC, and for this reason the first approach is adopted (Fig. (5.40)).

In the present study T-H has an assisting role to neutronics. For this reason OpenMC$^+$ acts as the driver solver. More specifically if the T-H feedback is activated a new OpenMC$^+$ subroutine is called after the end of each time-step. This subroutine serves as the "main" subroutine of the T-H feedback and performs the following actions:

1. Management of the power profile calculation at the required time-point.
2. Reading of the power profile (neutronic feedback) from a data file.
3. Sending of a message to T-H to start the calculation of the current time-step.
4. Reading of the T-H feedback files written by the T-H solver.
5. Receipt of the message to proceed to the next time-step Monte-Carlo calculation.
6. Upgrade of the neutronic input file.
7. Reading of the updated neutronic input file.

In case of a parallel neutronic calculation the master process of OpenMC$^+$ handles the T-H feedback procedure. When the upgraded neutronic input file is ready, it is re-read by all the MPI-processes. For the calculation of the power distribution per batch and per

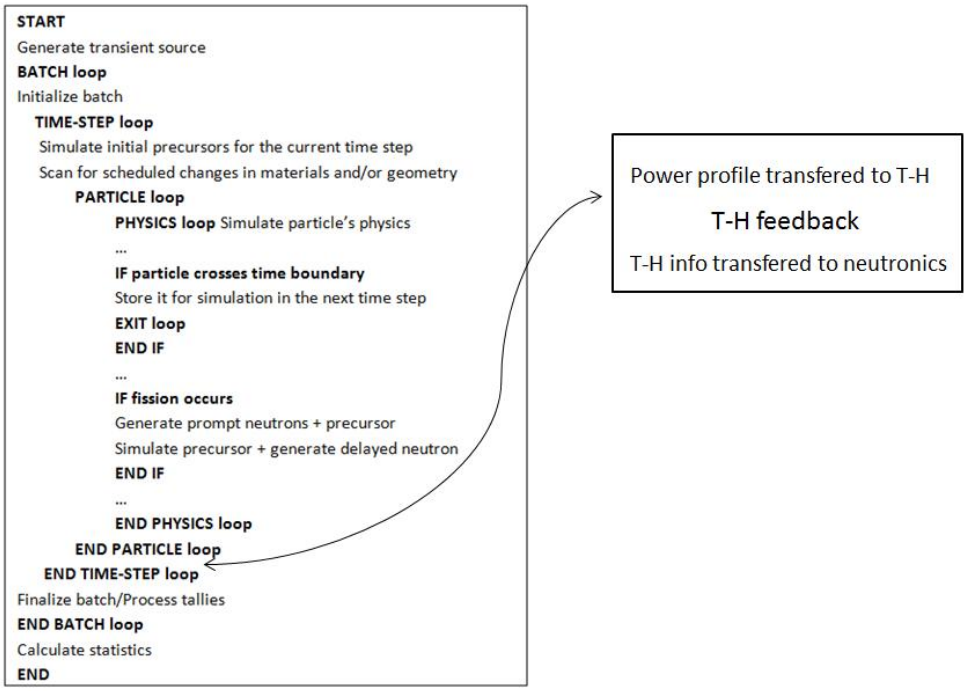

Figure 5.40: The approach for T-H feedback to dynamic Monte-Carlo followed in this research.

time-step, a tally that calculates the fission-generated energy is utilized. Here it should be mentioned that in a parallel neutronic calculation this tally is synchronized and reduced to the master in each time-step of each batch. This is necessary in order to link each time-step of each batch with a single T-H calculation. This ensures reproducibility of the results, i.e. results independent of the number of the utilized processors, that is always desired (§ 5.2.6). These algorithmic extensions are illustrated in Fig. (5.41).

In addition the source code of SCF should be modified for coupling purposes. The required modifications concern mainly the output format as well as the communication with OpenMC$^+$. The current version of SCF does not provide a restarting capability for transient analysis. Consequently this capability should be developed. The developed restarting capability is illustrated in Fig. (5.42).

The integrated coupling scheme is described by the simplified flowchart illustrated in Fig. (5.43). In the beginning both solvers are launched by a standard script. The synchronisation of the two solvers is performed simply by reading and writing messages in two different temporary files. For example when OpenMC$^+$ is going to stay inactive until T-H feedback is calculated, the following procedure is followed: firstly OpenMC$^+$ writes an arithmetic value in a temporary file. For SCF that value means to continue its execution. In the meantime OpenMC$^+$ is inserted in a "do-while" loop where the exit

condition is to read a particular value from another temporary file. That value will be written by SCF after the successful calculation and communication of the T-H-feedback.

5.5.2 *Critical boron search*

Many transient phenomena are induced by the distortion of a reactor steady-state. Thus it is desirable to analyse models which are initially in a steady-state. Reactor steady-states can be found by suitably modifying the boron concentration within the coolant. This can be done by properly extending the iterative algorithms that perform static coupled analysis. More specifically, the concentration of boron is modified in each iterative step until $k_{eff} \simeq 1$. Such an iterative process continues until the convergence of the T-H conditions as well as $k_{eff} \simeq 1$. In this thesis such an algorithm has been developed supplementary to the algorithm developed in § 4.3.

5.5.3 *Test-case 5-8: Proof of principle - A T-H induced transient in a single fuel pin model*

In this section a Boiling Water Reactor (BWR) single-pin model is analysed by OpenMC$^+$ with T-H feedback. The key features of the model are presented in Table (4.2). However the total power is reduced from 70 to 20 kW in order to achieve a smoother T-H feedback with lower temperatures. Also, boron is added to the coolant composition to generate an initial critical state (see § 5.5.2).

An initial static Monte-Carlo/T-H coupled calculation with critical boron search is performed to generate the initial conditions. Afterwards a dynamic calculation is performed. A transient behaviour is induced by a change of the coolant pressure. Initially, for a time interval of 0.5 s, the model remains in the steady-state. For t=0.5 s the pressure of the coolant reduces from 7.01 MPa to 6.99 MPa inducing a positive reactivity insertion. The evolution of the transient phenomenon is monitored for the remaining time interval. The transient calculation runs with a time-step Δt=0.05 s.

Selecting 10 batches and $1.6{\cdot}10^6$ initial neutrons per batch the total wall-clock time was 3.47 h when 96 MPI-tasks have been utilised. Fig. (5.44) shows the evolution of k_{eff} during the iterative calculation of the initial steady-state. The convergence at $k_{eff} \approx 1$ can be easily noticed. Figs (5.45, 5.46 and 5.47) illustrate the calculated initial T-H steady-state conditions. The dynamic behaviour of the model with a time-step of 0.1 s can be seen in Fig. (5.48). The pressure reduction induces a positive reactivity insertion due to the high initial boron concentration. The reason is that the pressure reduction causes a drop of the coolant density and the boron concentration, reducing thus the capture of neutrons by boron. In other words, the initially high boron concentration results in a

dominant positive reactivity feedback that overshadows the negative reactivity feedback from the reduction of the coolant density, i.e. the reduction of the moderation rate. For the confirmation of this hypothesis a static calculation runs using the average density profile for t = 1.0 s instead of the steady-state's one. Then the multiplication factor increases from k=1.00009 to k=1.00303 ($\rho \approx 294$ pcm) confirming the hypothesis.

The main goal of this section, i.e. § 5.5, was to develop a dynamic T-H feedback mechanism to the dynamic Monte-Carlo neutronic solution and verify its functionality. The Test case 5-8 confirms that the coupling mechanism works correctly. However validation is needed. Also Fig. (5.48) depicts that the statistical error is very high (max error$\approx$ 30%). It is clear that this is due to the small number of neutron batches selected for this calculation. For the reduction of the statistical and the numerical error an optimisation of the Monte-Carlo statistics together with the time-step length is needed. These tasks are out of the scope of this work and constitute a matter of future research.

5.6 CONCLUSION

This chapter presents the development of a module for dynamic neutronic analysis. This module is incorporated in the open-source Monte-Carlo code OpenMC. The developed module follows the logic of the fixed-source Monte-Carlo algorithm. Various new features have been developed to insert the dimension of time, to encapsulate the impact of precursors as a source of neutrons, to achieve dynamic changes of the analysed model, etc. The module was parallelized based on the MPI. An initial validation and investigation of its performance show encouraging results. More specifically some test-cases of progressively increased complexity are analysed. The results show good agreement with simple PK models. Thus the feasibility of pure Monte-Carlo dynamic analysis for small scale and pin-by-pin FA-scale problems is verified.

Additionally the dynamic Monte-Carlo module was coupled successfully with the T-H subchannel solver SCF in an OS context. The analysis of a small problem showed that the coupled dynamic computational scheme works correctly; however the validation of the dynamic T-H feedback is pending.

The main weak point of this algorithm is the high computational cost. This is attributed to the fact that the proper treatment of the two, entirely different, involved time scales demands a high Monte-Carlo statistics. The analysis of more complex and larger scale problems constitutes a topic of further research. Also the more in-depth investigation of the parameters that contribute to the increase of the statistical variance and the computational cost is another important matter of future research.

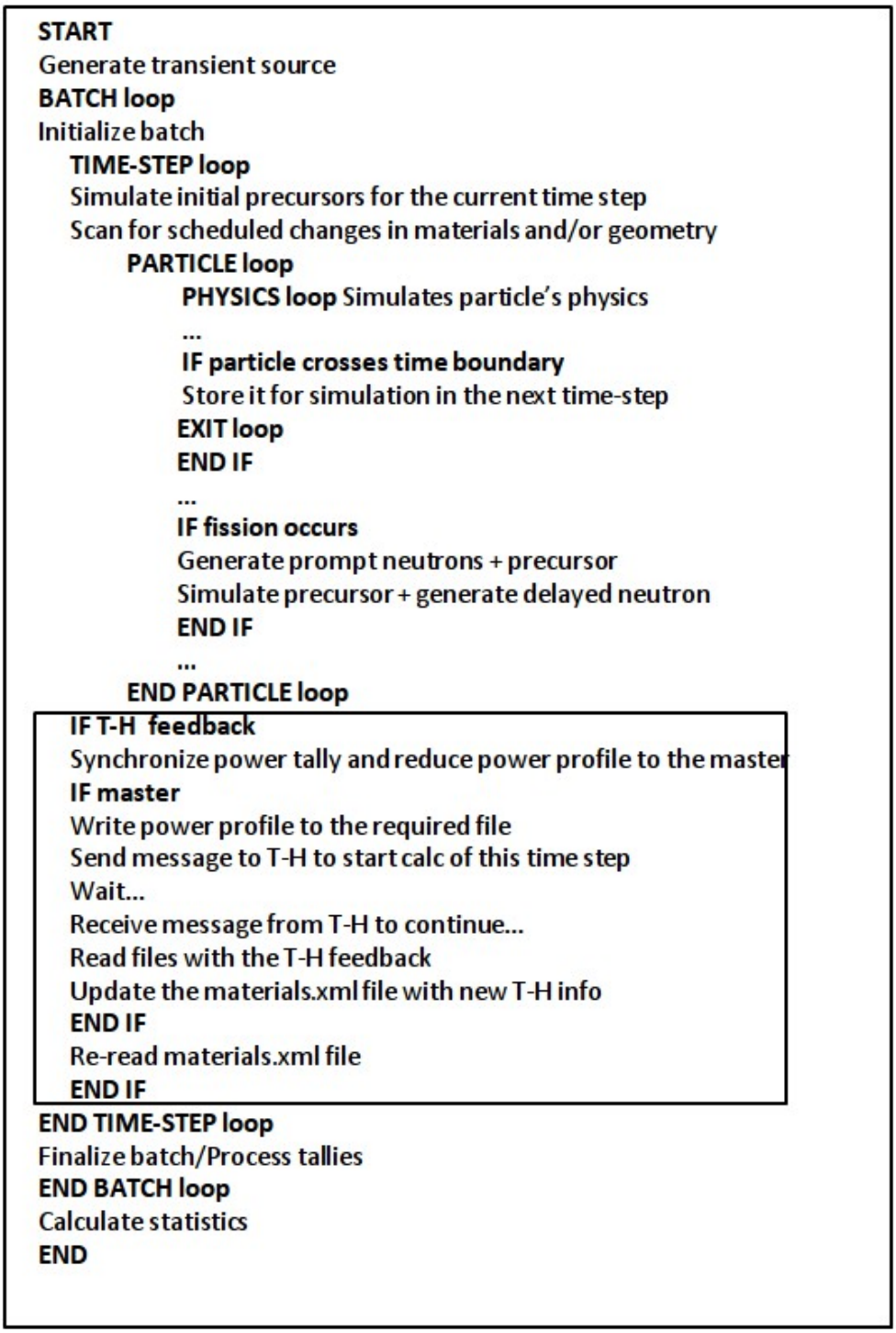

Figure 5.41: OpenMC's flowchart after the insertion of T-H feedback capability.

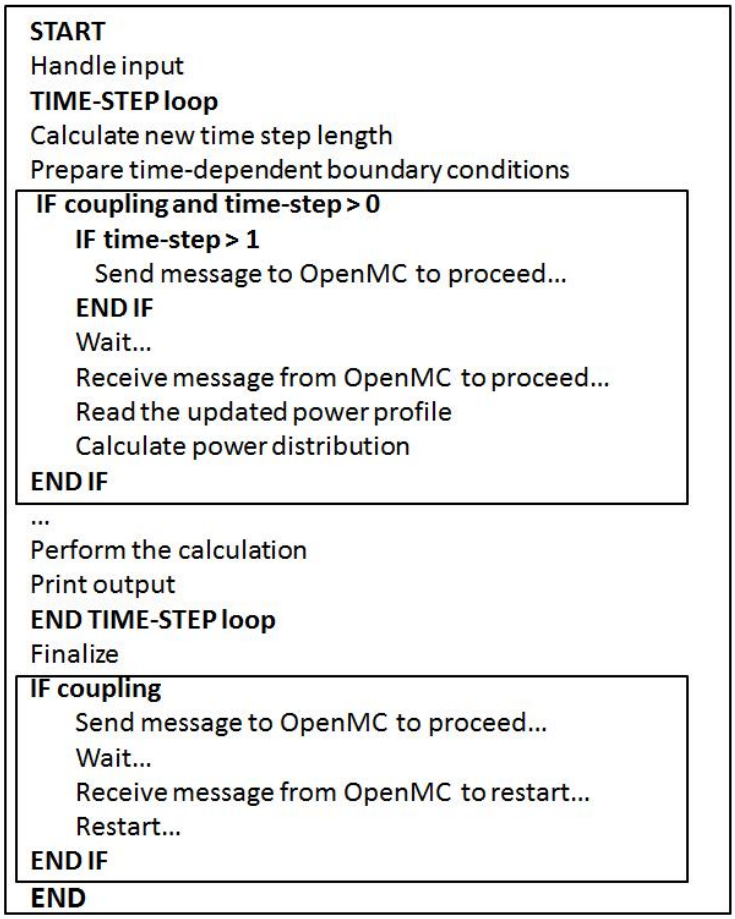

Figure 5.42: SCF's modified simplified flowchart.

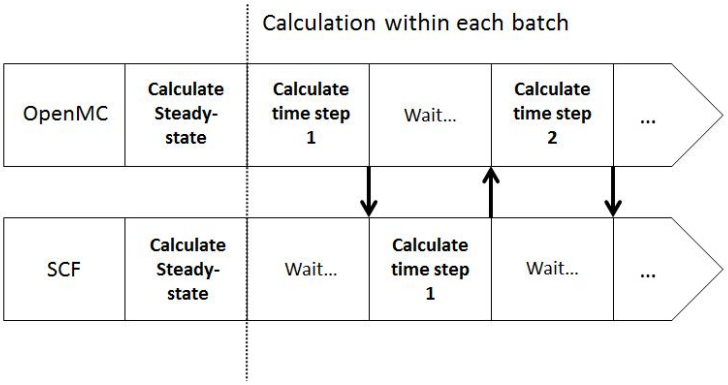

Figure 5.43: Integrated OpenMC^{+}/SCF dynamic scheme.

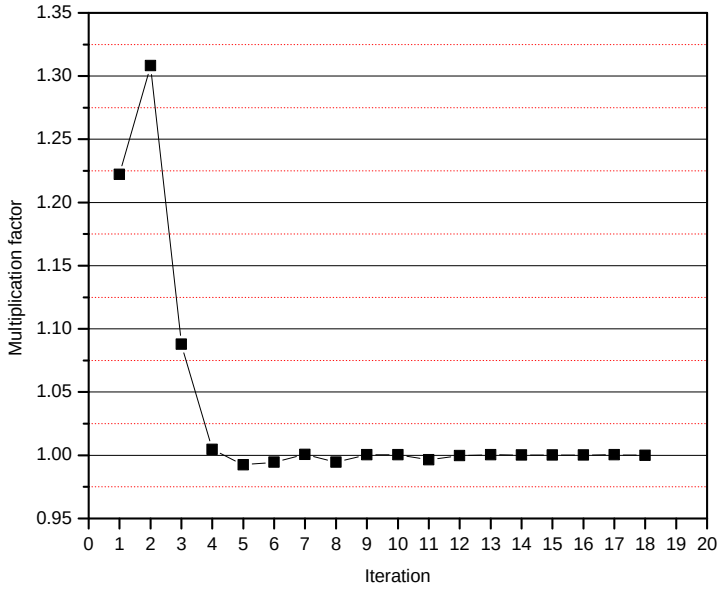

Figure 5.44: Test-case 5-8: k_{eff} evolution during the iterative calculation of the initial steady-state.

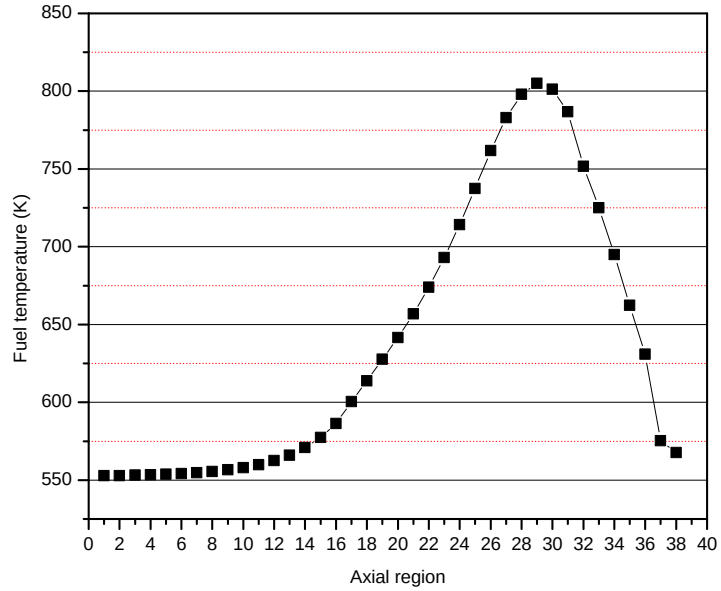

Figure 5.45: Test-case 5-8: Steady-state fuel temperature axial profile.

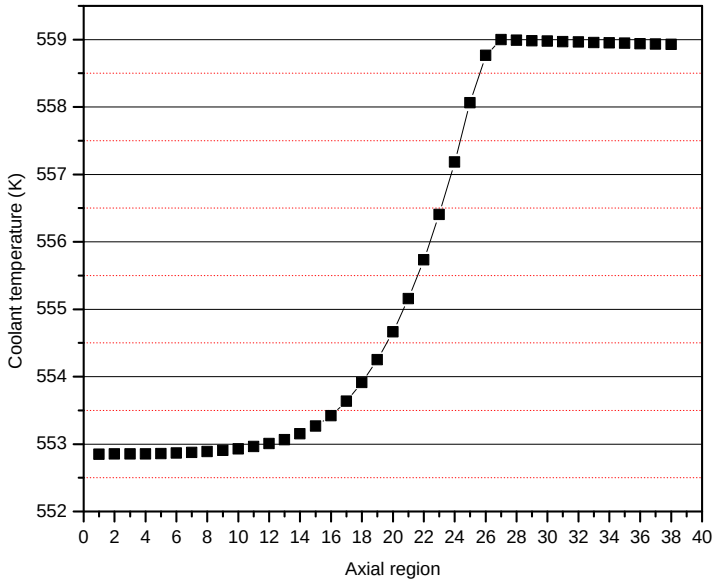

Figure 5.46: Test-case 5-8: Steady-state coolant temperature axial profile.

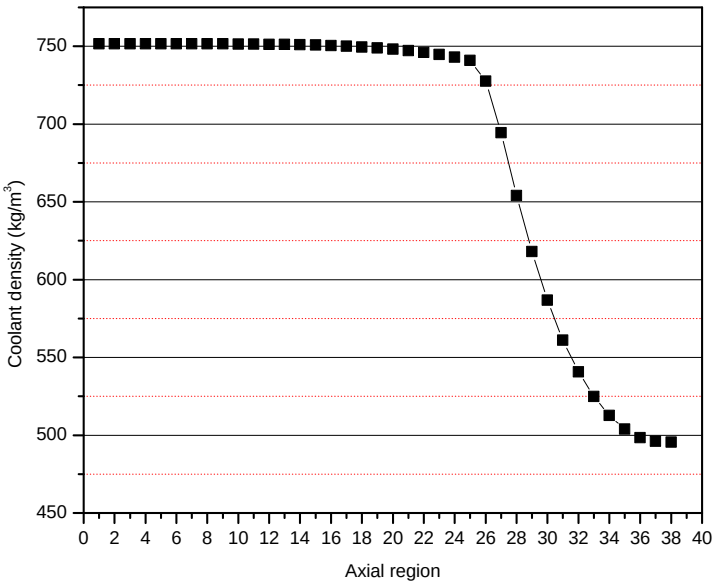

Figure 5.47: Test-case 5-8: Steady-state coolant density axial profile.

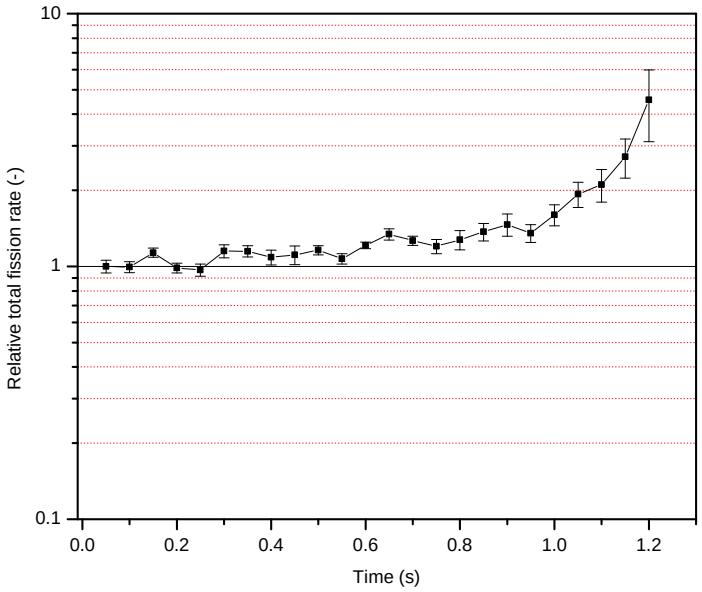

Figure 5.48: Test-case 5-8: Transient power profile.

6

CONVERGENCE ACCELERATION OF THE MONTE-CARLO SOURCE ITERATION

The main aim of this chapter is to present the first steps towards an alternative, numerically accelerated Monte-Carlo *k*-eigenvalue algorithm. A Newton-based, matrix-free numerical method for solving non-linear systems, the Jacobian Free Newton Krylov (JFNK) method described by Knoll and Keys (2004) (also see chapter 4), is adapted to a Monte-Carlo *k*-eigenvalue context aiming to accelerate the convergence. JFNK has been implemented in the deterministic solution of the Neutron Transport Equation (NTE) (Gill and Asmy, 2009). However the stochastic and computationally burdensome nature of a Monte-Carlo algorithm complicates the problem significantly and makes a straightforward implementation of JFNK rather impossible. For example, JFNK requires the execution of some linear iterations per Newton iteration that would increase the computational cost significantly. Another important question is how the Monte-Carlo calculated quantities affect the global behaviour of the JFNK algorithm since they are associated with statistical noise. In this work the proposed method is developed in the Monte-Carlo solver OpenMC and a step-by-step evaluation on simplified test-cases is performed.

6.1 STATE-OF-THE-ART

The Monte-Carlo criticality (or *k*-eigenvalue) analysis is performed utilising the power/Source Iteration (SI) iteration that calculates the *k*-eigenvalue and the eigenvector of the NTE eigenvalue form. This method guarantees the convergence to the fundamental eigenmode but very often the convergence is slow; when the Dominance Ratio (DR) is near one (see § 2.3.2). Typically this situation is met in loosely coupled multi-component systems and large symmetric systems (Dufek, 2007). For this reason the improvement of the convergence of the Monte-Carlo *k*-eigenvalue iterative process is listed among the most important and challenging problems in computational neutron transport analysis as stated by Cho and Chang (2009) and Martin (2012) .

The convergence of the neutron source is a crucial point because it affects the accuracy of the results of a *k*-eigenvalue calculation. The source convergence should be confirmed to avoid the contribution to the statistics of cycles [1] that do not correspond to the

1 The terms batch, cycle and iteration are used interchangeably in this work to denote the Monte-Carlo *k*-eigenvalue iteration.

converged region. The Shannon entropy, a concept from information theory, has been shown to be a useful diagnostic measure for characterising the convergence of the neutron source (Ueki and Brown, 2003, Ueki and Brown, 2005, Brown, 2006, and Brown, 2009). In practice, in every Monte-Carlo criticality calculation a problem-dependent number of cycles is skipped before the tallying starts (Brown, 2009). Another matter that is strongly bonded with the convergence of the source is the computational cost that imposes a constraint, especially when the problem requires a significant number of cycles. As a consequence it is of high interest to improve the convergence of the SI in order not only to increase the accuracy but also to reduce the computational cost.

One method that has been used for this purpose is the Non-linear diffusion acceleration implemented using the Coarse Mesh Finite Difference (CMFD) technique. In this work that method will be called as CMFD accelerated Monte-Carlo. The CMFD acceleration has been proposed by Lee et al. (2010). According to this method the multigroup eigenvalue diffusion equation is solved per Monte-Carlo SI to find a better estimation of the current source distribution. This improved estimation is communicated it back to Monte-Carlo aiming to improve the current Monte-Carlo guess. Initially the CMFD methods were aiming to accelerate the neutron source convergence during the inactive cycles of a Monte-Carlo calculation. However the use of CMFD feedback in the active cycles has also been investigated and applied. Lee et al. (2014) found that the CMFD corrected fission source suffers less from the inter-cycle correlation effect; they conclude that CMFD can be an effective way to improve the global calculation.

6.2 THE INTRODUCED METHOD

The integral form of the NTE is presented in § 2.1.2 and § 2.3.2. The *k*-eigenvalue form of the NTE that is solved with Monte-Carlo is given by the following relation:

$$\chi_f = \frac{1}{k_{eff}} F\chi_f \tag{6.1}$$

It is clear that this is an eigenvalue problem. If Eq. (2.39) is integrated over dP k_{eff} is given by:

$$k_{eff} = \frac{\int dP \int dP' \chi_f(P') K_f(P', P)}{\int dP \chi_f} \tag{6.2}$$

Numerically this problem is classically solved utilising the SI. After spatial discretization the SI is written:

$$\boldsymbol{\chi}_f^{n+1} = \frac{1}{k_{eff}^n} \boldsymbol{F} \boldsymbol{\chi}_f^n \tag{6.3}$$

where:

$$k_{eff}^{n+1} = \frac{\int \boldsymbol{F} \boldsymbol{\chi}_f^n \, d\boldsymbol{r}}{\int \boldsymbol{\chi}_f^n \, d\boldsymbol{r}} = k_{eff}^n \frac{\int \boldsymbol{\chi}_f^{n+1} \, d\boldsymbol{r}}{\int \boldsymbol{\chi}_f^n \, d\boldsymbol{r}} \tag{6.4}$$

and n denotes the nth iterative step. In § 2.3.2 it has been showed that when DR $\simeq 1$ the convergence of the Monte-Carlo SI is slow. Aiming to accelerate the convergence speed of SI the idea implemented is as following: From a numerical point of view, the Monte-Carlo SI could be seen as a fixed-point iteration of the form:

$$\boldsymbol{u}^{n+1} = \boldsymbol{f}(\boldsymbol{u}^n) \tag{6.5}$$

which gives rise to the sequence $\boldsymbol{u}_0, \boldsymbol{u}_1, \boldsymbol{u}_2 \ldots$ which is hoped to converge to a point $\boldsymbol{u}^*$. $\boldsymbol{u}$ is the vector of the solution that contains also the eigenvalue:

$$\boldsymbol{u} = \begin{bmatrix} \boldsymbol{\chi}_f \\ \lambda \end{bmatrix} \tag{6.6}$$

where $\lambda = \dfrac{1}{k_{eff}}$. The function $\boldsymbol{f}$ denotes the fixed-point iteration as following:

$$\boldsymbol{f}(\boldsymbol{u}) = \begin{bmatrix} \lambda \boldsymbol{F} \boldsymbol{\chi}_f \\ \bar{\lambda}(\boldsymbol{u}) \end{bmatrix} \tag{6.7}$$

where $\bar{\lambda}(\boldsymbol{u})$ represents the updating procedure for λ. Using the fixed-point iteration function one can define an associated non-linear system of the form:

$$\boldsymbol{r}(\boldsymbol{u}) = \boldsymbol{u} - \boldsymbol{f}(\boldsymbol{u}) = \mathbf{o} \tag{6.8}$$

where $\boldsymbol{r}$ is the vector of the non-linear residual vector. This is a problem of finding the root $\boldsymbol{u}^*$, i.e. $u^* = \boldsymbol{f}(u^*)$. In other words this statement is nothing else than the requirement for convergence to the solution $\boldsymbol{u}^*$, i.e., when convergence is achieved there is no difference between successive updates of the solution ($\boldsymbol{f}(\boldsymbol{u}^*) = \boldsymbol{u}^*$ or $\boldsymbol{u}^* - \boldsymbol{f}(\boldsymbol{u}^*) = \mathbf{o}$). Thus Eq. (6.8) corresponds to the solution of the fixed-point problem.

However some remarks should be made about Eq. (6.8). The solution $\boldsymbol{u}$ is associated with statistical noise. Also, in some problems the function $\boldsymbol{r}(\boldsymbol{u})$ may be highly non-linear. These facts could pose questions about the performance of a Newton method.

Instead of Eq. (6.8), one could state the problem in an alternative way. Consider the non-linear function:

$$\boldsymbol{r}(\boldsymbol{u}) = \boldsymbol{u} - \boldsymbol{f}^*(\boldsymbol{u}) \tag{6.9}$$

where $\boldsymbol{f}^*$ is the converged fixed-point iteration $\boldsymbol{f}$, or, in practice, its successive application for a number of times. Since $\boldsymbol{f}^*(\boldsymbol{u})$ represents some consecutive SIs, the approach of a quite similar solution $\boldsymbol{u}$ independently of the initial guess is guaranteed. Thus the new function $\boldsymbol{r}(\boldsymbol{u})$ would be ideally linear, in practice much smoother than the one of the previous formulation. One could say that this non-linear function formulation means that the desired converged solution $\boldsymbol{u}^*$ is already known from the converged iteration $\boldsymbol{f}^*$. However, in practice, this is not the case due to the following reasons:

1. Numerical error: in practice a finite number of cycles is used. Thus the solution does not "perfectly" (mathematically) converge.
2. Statistical error: Monte-Carlo is associated with statistical error. Thus the statistical oscillation of the solution (fission source + eigenvalue) is always present.

The non-linear problem of Eq. (6.9) can be solved with a Newton method of the form:

$$\boldsymbol{J}\delta\boldsymbol{u}^{k} = -\boldsymbol{r}(\boldsymbol{u}^{k}) \tag{6.10}$$

$$\boldsymbol{u}^{k+1} = \boldsymbol{u}^{k} + \delta\boldsymbol{u}^{k} \tag{6.11}$$

where $\boldsymbol{u}$ is the vector of the unknowns, $\boldsymbol{u}^{0}$ is the initial guess, $\boldsymbol{r}(\boldsymbol{u}^{k})$ is the vector of the non-linear residuals, $\boldsymbol{J} = \frac{\partial r}{\partial u}$ is its associated Jacobian matrix, and $\delta\boldsymbol{u}$ is the Newton correction vector. The Jacobian matrix represents the sensitivity matrix of the residual, i.e.; it constitutes a sensitivity quantification of each residual vector element to a change of each solution vector element. Because the construction of the Jacobian matrix is costly, it can be avoided provided that the solution of the linear system is done with a method that allows for the absence of this matrix. The Krylov methods (see § 4.4.2) is a family of linear solvers that require only the construction of matrix-vector products of the form $\boldsymbol{J}\boldsymbol{v}$ where $\boldsymbol{v}$ denotes a Krylov vector. Therefore, the following relation can approximate these products:

$$\boldsymbol{J}\boldsymbol{\nu} = \frac{\boldsymbol{r}(\boldsymbol{u} + \varepsilon\boldsymbol{\nu}) - \boldsymbol{r}(\boldsymbol{u})}{\varepsilon} \tag{6.12}$$

where ε is a small perturbation parameter. The scheme described by the Eqs (6.10-6.12) constitutes a JFNK scheme.

So far the Monte-Carlo SI has been transformed in a Monte-Carlo JFNK iteration. However the implementation of the proposed approach would require:

1. Some Monte-Carlo SIs in order to calculate $\boldsymbol{u} - \boldsymbol{f}^{*}(\boldsymbol{u})$.
2. Some Krylov iterations per each Newton iteration. Each Krylov iteration needs the execution of some Monte-Carlo cycles in order to calculate $\boldsymbol{f}^{*}(\boldsymbol{u} + \varepsilon\boldsymbol{\nu})$ and thus $\boldsymbol{r}(\boldsymbol{u} + \varepsilon\boldsymbol{\nu})$.

Practically the implementation of this algorithm is not possible for the following reasons:

1. It is impossible to run more than one Monte-Carlo cycles per Newton step.
2. It is impossible to run Monte-Carlo cycles within the Krylov steps.
3. Such an implementation would lead to a significant distortion of a classical Monte-Carlo *k*-eigenvalue source algorithm. Thus it would cancel any attempt for easy application to an existing Monte-Carlo solver.

The first problem is overcome constructing the function $\boldsymbol{r}(\boldsymbol{u}) = \boldsymbol{u} - \boldsymbol{f}^{*}(\boldsymbol{u}) \simeq \boldsymbol{u} - \boldsymbol{f}(\boldsymbol{u})$. This approximation is considered reasonable because:

1. The JFNK acceleration can be activated after a small number of classical SIs. Therefore the result of $\boldsymbol{f}$ will be reasonably close to that of $\boldsymbol{f}^*$.
2. When $n \to \infty$ then it should be $k \to k_0$, $\boldsymbol{\chi}_f \to \boldsymbol{\chi}_{f,0}$ that is $\boldsymbol{u} \to \boldsymbol{u}^*$. Hence the error induced by the approximation mentioned above will progressively become negligible.

The second problem is overcome applying the following idea: Within each Newton iteration the performance of perturbed Monte-Carlo SIs for the calculation of the matrix-vector products will be replaced by SIs of a multigroup diffusion-based method with transport-equivalent physics. Such a diffusion model method has been utilized by Herman et al. (2015) within the context of CMFD acceleration. In matrix form this diffusion model can be written as follows:

$$\boldsymbol{Q}\boldsymbol{\Phi}^{k+1} = \frac{1}{k_{eff}^{k}}\boldsymbol{P}\boldsymbol{\Phi}^{k} \tag{6.13}$$

where $\boldsymbol{Q}$ is the neutron loss matrix operator, $\boldsymbol{P}$ is the neutron production matrix operator and $\boldsymbol{\Phi}$ is the group flux vector. These two operators are constructed by tallying the desired quantities within each Monte-Carlo cycle. As a consequence a diffusion SI, with physics constructed equivalently to the current Monte-Carlo SI, is solved in a deterministic way using some linear solver.

Because the execution of deterministic diffusion SIs is considerably cheaper than the Monte-Carlo ones regarding computational time, one could utilise a significantly large number of Krylov linear iterations per Newton iteration, in order to convergence.

6.2.1 *Some thoughts about the theoretical validity of the introduced method*

The Monte-Carlo method for reactor criticality is composed of two (2) sub-parts that are often got confused.

- A Monte-Carlo method for the solution of the linear integral Eq. (6.1) with unknown the fission source χ_f for a fixed value of k_{eff}.
- A numerical mechanism that aims to converge the total solution (χ_f and k_{eff}) to the fundamental solution of the problem.

In other words the Monte-Carlo method is used to solve an equation with unknown the expected value of the fission source in each step of a numerical iteration.

A numerical method, the SI, acts as the numerical mechanism. The proof of the convergence of the SI given in § 2.3.2 concerns a deterministic SI. Thus in a practical stochastic context the term "convergence" should be relaxed since the statistical noise imposes limits.

The main idea developed in this section lies in the replacement of the classical numerical mechanism, i.e. the SI, with another that is characterised by better convergence properties, i.e. the Newton iteration. From this point of view it is expected that this new method will not bring more questions regarding statistical biasing than the ones that have already been imposed by the SI. This means that when the JFNK correction becomes sufficiently small, there is an independence between successive cycles, analogous to the one of the Monte-Carlo SI, that leads to the validity of the Central limit theorem. Regarding convergence, it is expected that this method will be followed by all the advantages and drawbacks of the deterministic Newton iteration plus the statistical uncertainty.

A point that needs additional attention is that the Newton methods require an initial guess being sufficiently close to the solution. Otherwise they may diverge instead of converging. Another question is how sufficient is the approximation of the matrix-vector products with deterministic CMFD SIs.

Finally it should be mentioned that tests of the current formulation with the adopted approximations have confirmed its functionality, however a formal mathematical derivation/investigation is needed to prove the the general applicability of the method.

6.2.2 *Setting a Monte-Carlo Jacobian free Newton Krylov algorithm*

The introduced algorithm is suitable for a relatively simple implementation into an existing Monte-Carlo SI scheme. The evaluation of the vector of the non-linear residuals $\boldsymbol{r}(\boldsymbol{u})$ needs only the difference between two successive SIs. Consequently all the details that concern the normalisation and the update of the involved quantities will not be modified in this new context. It could be said that the new scheme acts as an acceleration of the traditional Monte-Carlo SI iteration. The GMRES Krylov solver from the PETSc library (*PETSc*) has been chosen to solve the linear systems inside the Newton iteration.

For the implementation of the proposed method a mesh for the discretization of space and neutron energy is required. In this work the CMFD mesh of OpenMC is used. Over that mesh the neutron source, the non-linear residuals, the matrix-vector products as well as the JFNK-corrections of the SI are evaluated. Also, a way for the communication between the Monte-Carlo particle distribution and the vector form of the information that is required by JFNK should be defined. For the transformation of a Monte-Carlo particle distribution to a mesh cell-based vector form, the particle-weight per mesh cell is counted. In order now to communicate the JFNK correction back to Monte-Carlo, the expected number of neutrons to be born in a given cell and energy group calculated

by JFNK is compared to the SI-calculated source distribution. This strategy results in the generation of suitable weight adjusted factors ($f^{g}_{l,m,n}$) of the following form:

$$f^{g}_{l,m,n} = \frac{\sum\limits_{s}^{JNFK} w_s}{\sum\limits_{s}^{SI} w_s}; \quad s \in (g, l, m, n) \tag{6.14}$$

where w_s is the neutron's weight in a given cell (l, m, n) and energy group (g). Therefore the correction is communicated to the current neutron source by modifying the neutron weights per spatial cell and energy group as following (*OpenMC website*):

$$w'_s = w_s \times f^{g}_{l,m,n}; \quad s \in (g, l, m, n) \tag{6.15}$$

It should be noted that each particle's local coordinates and energy remain constant throughout this procedure. The algorithm developed in this research is summarised in Algorithm (3).

Algorithm 3 The introduced algorithm

do $k = 1$, Number of SI with active JFNK-acceleration
  Run the kth Monte-Carlo cycle
   -Calculate $\boldsymbol{u}' = f(\boldsymbol{u}^{k-1})$
   -Tally the CMFD-required quantities
  Construct the residual: $\boldsymbol{r}^k = \boldsymbol{u}^{k-1} - \boldsymbol{u}'$
  Solve the linear system: $\boldsymbol{J}\delta\boldsymbol{u}^k = -\boldsymbol{r}^k$ (Krylov solver)
  - - - - - - - - - - - - - *Internal operation of the Krylov solver*- - - - - - - - - - - - -
   do $j = 1$, Number of Krylov iterations
    ...
    Perturb the solution (source and k_{eff}) : $\boldsymbol{u}_{per} = \boldsymbol{u}^{k-1} + \varepsilon\boldsymbol{v}$
    Run the diffusion based SI
    Calculate: $\boldsymbol{r}(\boldsymbol{u} + \varepsilon\boldsymbol{\nu}) = \boldsymbol{u}^{k-1} - \boldsymbol{u}_{per}$
    Calculate the matrix-vector product: $\boldsymbol{J}\boldsymbol{\nu} = \frac{\boldsymbol{r}(\boldsymbol{u}+\varepsilon\boldsymbol{\nu}) - \boldsymbol{r}(\boldsymbol{u})}{\varepsilon}$
    ...
   end do
  -
  Update the global/Newton solution: $\boldsymbol{u}^k = \boldsymbol{u}^{k-1} + \delta\boldsymbol{u}^k$
  Communicate the new solution to the source bank
end do

As mentioned above, the main aim of this chapter is to initially evaluate the performance of the introduced method (SI-JFNK) in the analysis of some simplified models. As a first step, only the JFNK-corrected neutron fission source is communicated back to Monte-Carlo as an improved guess for the next Monte-Carlo cycle. The JFNK-modified k_{eff} is tested only in the last test-case. Initially the effect of SI-JFNK on the quality of the source is evaluated. Afterwards its effect in complete calculations will be examined. Finally the SI-JFNK performance is compared with that of the classical SI as well as the OpenMC's in-house CMFD accelerated SI (SI-CMFD). At this point it should be stated that the following test-cases are fictitious models with the purpose to scout the performance of the introduced method.

6.3.1 *Test-case 6-1: A bare U-235 1-D slab*

The first test case is a simple 1-D slab with length 200 cm composed by only U-235 (1-D slab-1). This problem is quite easy in numerical terms since it is characterised by a very low DR. A spatial mesh of 100 cells and 1 energy group have been utilised for this preliminary case (Table (6.1)). In the beginning the effect of one SI-JFNK cycle on the neutron source is evaluated. More specifically after 19 skipped SI cycles, with 50*k* neutrons per cycle, the classical SI source of the 20th step is compared with the source generated by SI-JFNK for the same cycle. Observing Fig. (6.1) it is obvious that SI-JFNK improves the neutron source distribution making the curve smoother and more similar to the well-converged source (Fig. (6.2)) compared with the one generated by the classical SI.

Now the impact of SI-JFNK on the convergence of the average eigenvalue, i.e. k_{eff}, is evaluated in comparison with SI and SI-CMFD. These calculations are performed with 50k neutrons per cycle and 20 inactive cycles. For the SI-JFNK case a maximum number of 30 linear iterations are performed per Newton step. Additionally the converged eigenvalue of an SI with high statistics, that acts as a reference calculation, has been used for comparison. Fig. (6.3) shows that SI-JFNK improves the convergence of the average k_{eff} since it seems that this method generates a more stable, around the reference value, sequence of estimations of the average k_{eff} than that of the other two methodologies. Table (6.2) shows the final calculated k_{eff}; SI-JFNK gives the closest eigenvalue to the reference value.

Fig. (6.4) illustrates the behaviour of the Krylov iterative linear solver within some specific Newton iterations. It can be seen that the magnitude of the linear residual

converges to a continuously lower value ensuring that the global problem gradually converges. Also, it seems that a lower number of Krylov linear iterations could be selected since the convergence of the linear residual is achieved between the 10th and the 15th linear iteration with no significant improvement in the remaining iterations.

The converged neutron source generated by SI-JFNK is illustrated in Fig. (6.2); the very good quality of the calculated neutron source is confirmed.

Table 6.1: Test cases 6-1 & 6-2: Slab models.

	1-D slab-1	**1-D slab-2**
Length (cm)	200	200
# mesh cells	100	100
# energy groups	1	1
w_{235}	1	0.21
w_{238}	-	0.68
w_{16}	-	0.11
Density $(\frac{atoms}{b-cm})$	0.00155	0.121597
Dominance ratio	0.11	0.987

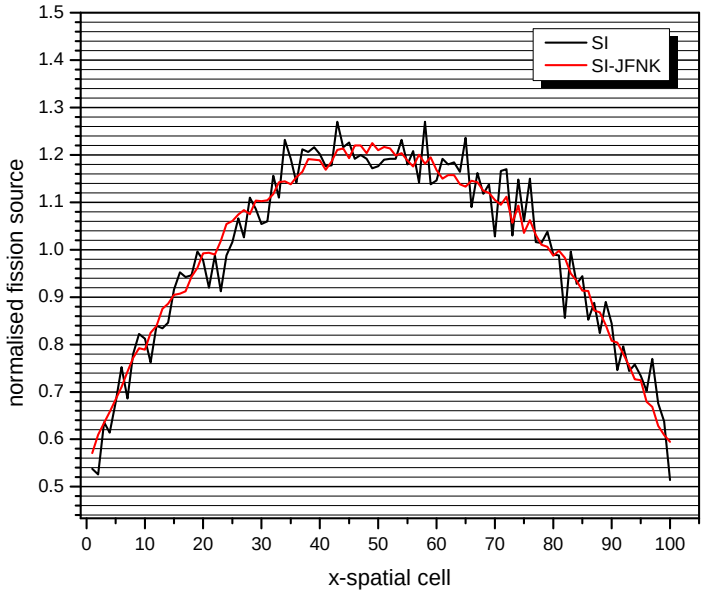

Figure 6.1: Test-case 6-1: Fission source for the 20th cycle.

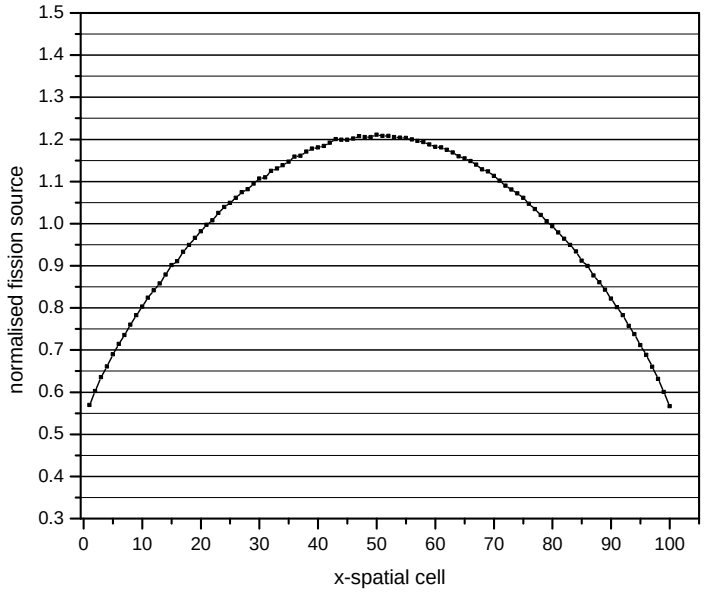

Figure 6.2: Test-case 6-1: Converged fission source with SI-JFNK.

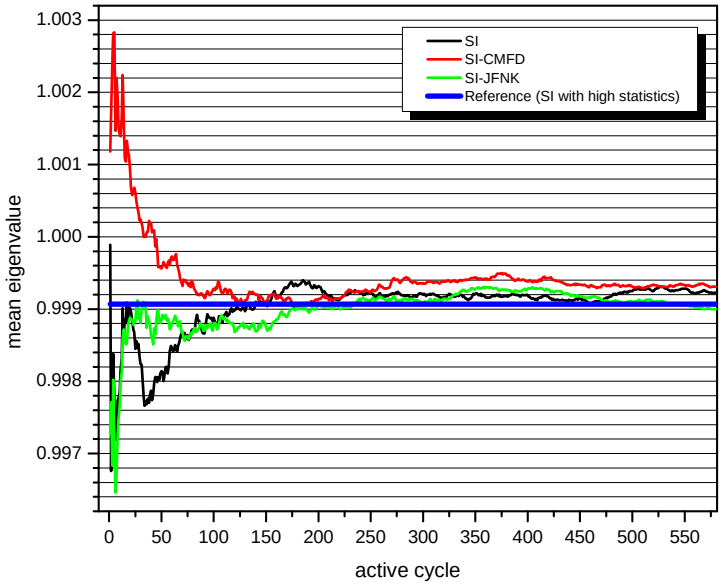

Figure 6.3: Test-case 6-1: Monte-Carlo calculated eigenvalue.

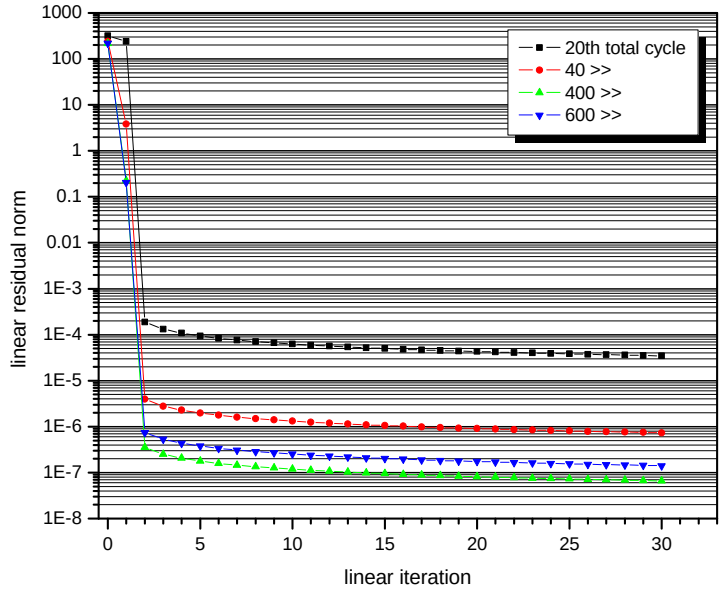

Figure 6.4: Test-case 6-1: Convergence of linear solver within some specific cycles.

6.3.2 *Test-case 6-2: A bare UO_2 1-D slab*

For the transformation of the previous problem to a more difficult one regarding numerics, the material properties of the 1-D slab-1 fuel were modified obtaining a dominance ratio closer to unity. More specifically the slab now contains UO_2; the atom densities, the material density and the DR are listed in Table (6.1). This configuration is called 1-D slab-2.

Initially three (3) calculations are performed; one SI, one SI-CMFD and one SI-JFNK, all of them with 100k neutrons per cycle and 10 inactive cycles. Concerning SI-CMFD and SI-JFNK, the CMFD and JFNK corrections are activated after 10 inactive cycles. For the SI-JFNK case a maximum number of 40 linear iterations are performed per Newton step. Fig. (6.5) shows the evolution of the Shannon entropy for these three cases. It can be seen that SI needs around 100 cycles in order to achieve convergence. However even so it is characterised by a quite oscillatory Shannon entropy. On the other hand, the sources that correspond to SI-CMFD and SI-JFNK converge almost immediatelly after their activation; the SI-CMFD source seems that converges somewhat faster than the one of SI-JFNK. As Fig. (6.5) suggests an extra SI calculation is performed with 100, instead of 10, inactive cycles. The evolution of the average k_{eff} is depicted in Fig. (6.6). It can be seen that after 700 active cycles the average eigenvalues given by SI (100 inactive), SI-CMFD and SI-JFNK (both with 10 inactive) have converged to the same value approximately. However it is illustrated that the SI-JFNK average k_{eff} converges faster than both the SI and SI-CMFD ones. All methods diverge slightly (~ 25-35 pcm) from the reference value (SI with high statistics) but it is expected that after some extra cycles they would converge to that value. In addition, the selection of higher Monte-Carlo statistics would improve the convergence of all methods.

Fig. (6.7) shows the calculated fission sources in some specific cycles, before and after the JFNK correction within the same cycle. For cycle 11 it can be noticed that the neutron source has not converged at all. For both cycles 40 and 100 the general shape has converged. A less noisy source is shown for cycle 100 as expected. It can be said that the JFNK correction achieves its goal; it improves the pure SI guess within the same cycle. It is notable that the SI-JFNK seems to have a filtering action on the fission source removing the statistical noise. The filtering action can be attributed to the formulation of the method. Since the non-linear residual represents the difference between the current guess and the converged solution, after some initial iterations the non-linearity seems to be caused just by the statistical noise. Thus, a part of it can be removed by the JFNK acceleration. Fig. (6.7) can support this statement. It illustrates that the JFNK corrected fission source becomes smoother than the Monte-Carlo uncorrected one only when it has obtained its final shape. The converged fission source is illustrated in Fig. (6.8).

Fig. (6.9) illustrates the behaviour of the Krylov iterative linear solver within some specific cycles. It can be seen that the magnitude of the linear residual converges to a continuously lower value ensuring again that the global problem gradually converges. It should be mentioned that the higher numerical difficulty of this problem compared with 1-D slab-1 is also reflected in the lower convergence levels of the linear solver (convergence to higher values) which are noticed in this case. Also in this case it seems that a significantly lower number of Krylov iterations could be selected since the convergence of the linear residual is achieved quite early with no significant improvement in the remaining iterations.

Table 6.2: Test-case 6-1 & 6-2: Calculated average eigenvalues.

	1-D slab-1	**1-D slab-2**
SI (20 inact.)	$0.99922 \pm 18pcm$	-
SI (100 inact.)	-	$1.60431 \pm 17pcm$
SI-CMFD	$0.99932 \pm 17pcm$	$1.60427 \pm 17pcm$
SI-JFNK	$\mathbf{0.99900 \pm 17}\boldsymbol{pcm}$	$\mathbf{1.60424 \pm 17}\boldsymbol{pcm}$
Reference (SI)	$\mathbf{0.99907 \pm 03}\boldsymbol{pcm}$	$\mathbf{1.60398 \pm 05}\boldsymbol{pcm}$

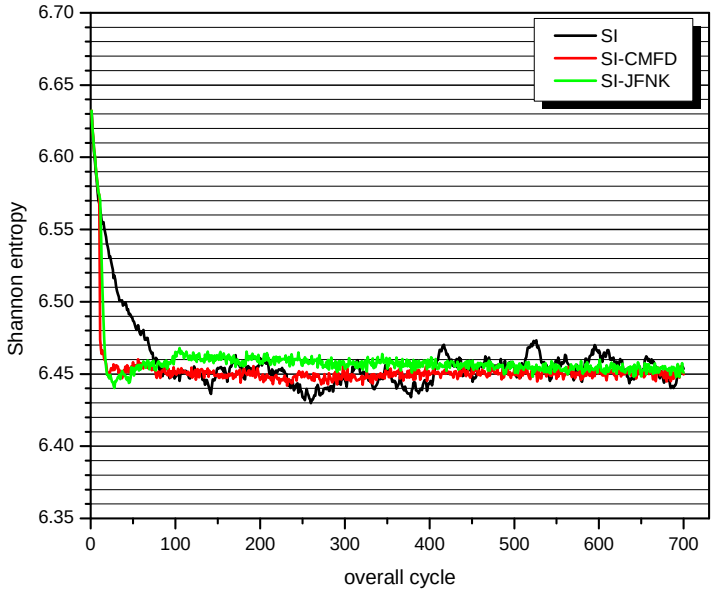

Figure 6.5: Test-case 6-2: Shannon entropy of the source.

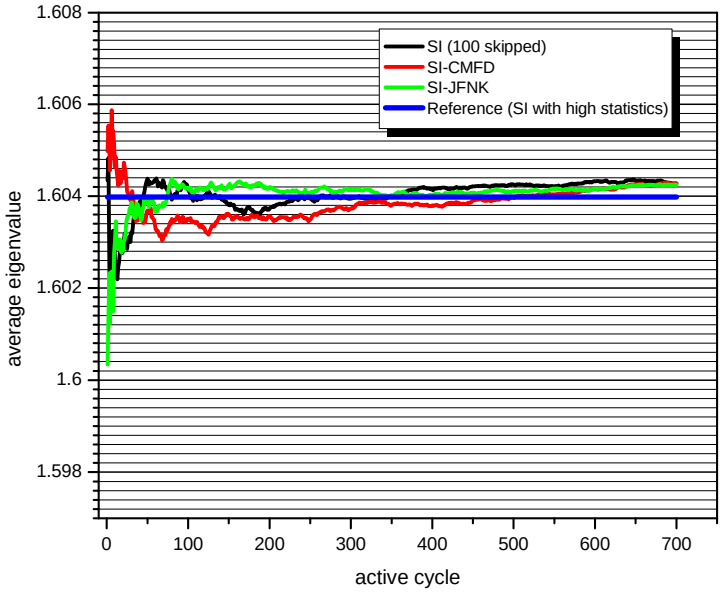

Figure 6.6: Test-case 6-2: Monte-Carlo calculated eigenvalue.

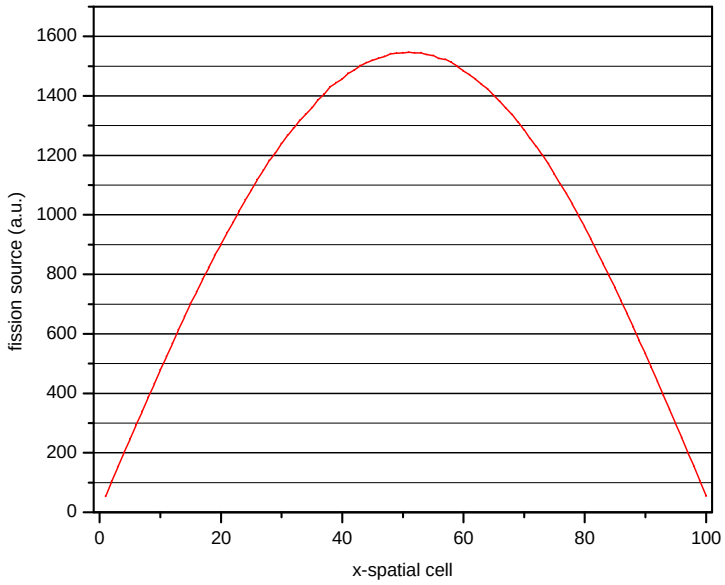

Figure 6.8: Test-case 6-2: Converged fission source.

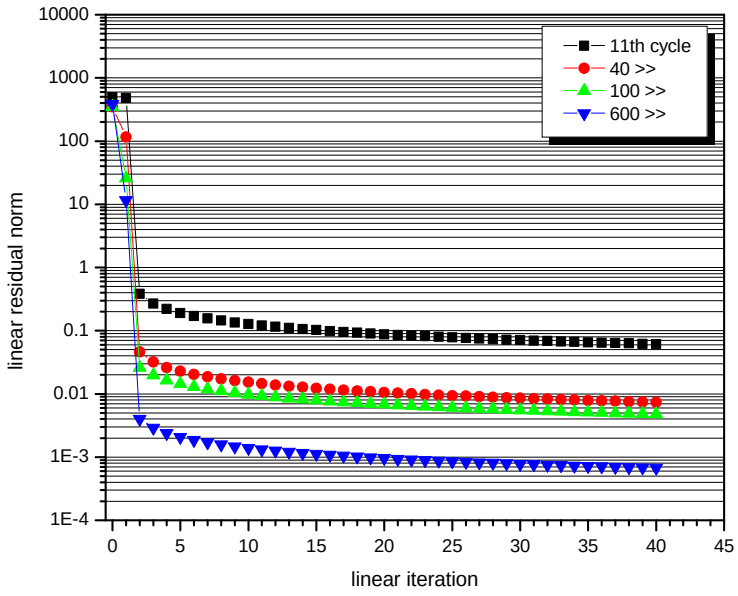

Figure 6.9: Test-case 6-2: Convergence of linear solver within some specific cycles.

6.3.3 *Test-case 6-3: A single multi-region fuel pin*

The third test case concerns a single-pin model with an axial variation of the fuel composition. This is the same model analysed in § 4.3.1. The main features can be seen in Table (6.3). The fuel pin is surrounded by coolant-moderator. A reflector exist at the pin top and bottom. In the radial direction reflective boundary conditions have been utilised whereas at the axial edges vacuum boundaries have been implemented. The fuel/moderator temperature, as well as the moderator density profile, have been calculated by some iterations of a coupled neutronic/Thermal-Hydraulics (T-H) calculation (see § 4.3.1) with 38 axial levels in the fuel region. The resulting high-density gradient is considered as a factor that complicates the solution of the Monte-Carlo k-eigenvalue calculation. Fig. (6.10) shows the coolant density profile that is used by this model.

In this case three (3) calculations are performed; one SI, one SI-CMFD and one SI-JFNK. The spatial mesh that is used in SI-CMFD and SI-JFNK consists of $1\times1\times420$ cells. In both SI-CMFD and SI-JFNK 10 inactive cycles are used and the acceleration feedback is activated in the 10th cycle. The classical SI is performed with 150 inactive cycles. In all cases 100k neutron histories per cycle have been simulated. One SI reference calculation with high statistics, i.e. 500k neutron histories per cycle, has also been carried out. In all cases the initial neutron source guess is a spatially flat neutron distribution.

Table 6.3: Test case 6-3: Single pin model.

	Single multi-region pin
Active length (cm)	380
Total length (cm)	420
Pellet radius (cm)	0.5225
Pin radius (cm)	0.6125
Fuel enrichment (%)	0.71/3.3/7.7

Fig. (6.11) shows that SI needs around 100 cycles to converge the source. However even then, the SI neutron source is characterised by a somewhat oscillatory Shannon entropy. On the other hand, the SI-CMFD and SI-JFNK neutron sources converge almost immediately after the correction activation. More specifically, SI-JFNK converges faster than SI-CMFD; SI-JFNK converges after ~70 overall cycles whereas SI-CMFD converges after ~100 overall cycles. Fig. (6.12) illustrates the evolution of the average k_{eff}. The converged eigenvalue calculated by the SI with high statistics is used as a reference. It can be seen that SI-JFNK converges after less than 100 active cycles, whereas SI (with 150 inactive cycles) converges after ~700 active cycles. SI-CMFD converges after ~200 active cycles. In addition Table (6.4) shows that the SI-JFNK eigenvalue is the closest to the reference value. Fig. (6.14) confirms the filtering action of the JFNK correction noticed in Test-case 6-2. It illustrates that the JFNK corrected fission source becomes smoother than the Monte-Carlo uncorrected one only when it has obtained its final shape. Fig. (6.15) presents the SI fission source for some specific cycles without any acceleration.

The introduced method is also tested having activated the k_{eff} feedback additionally to the neutron source one. Two calculations run with a spatial mesh of 105 cells, one with only source feedback and one with both source and k_{eff} feedbacks. Figs (6.16 and 6.17) show the evolution of the Shannon entropy. In the case where the k_{eff} feedback is activated, the Shannon entropy converges faster, i.e. in less than 75 cycles. The case without k_{eff} feedback needs about 150 cycles to converge.

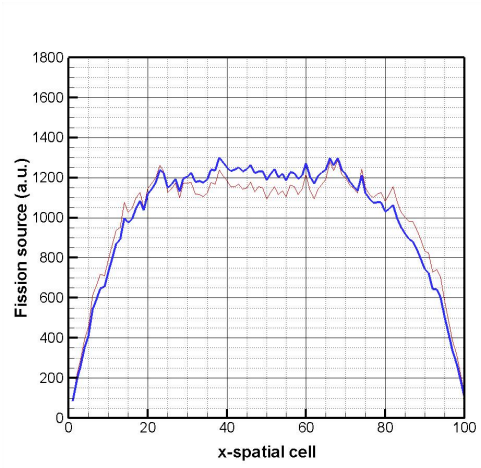

(a) cycle: 11

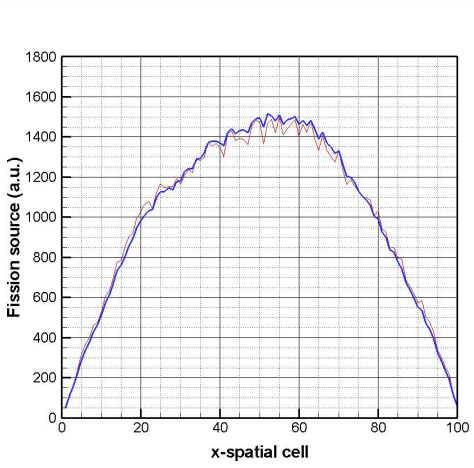

(b) cycle: 16

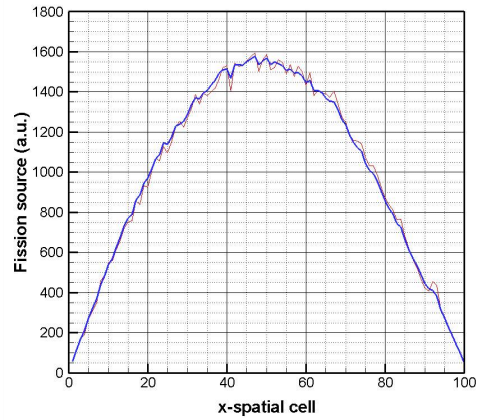

(c) cycle: 21

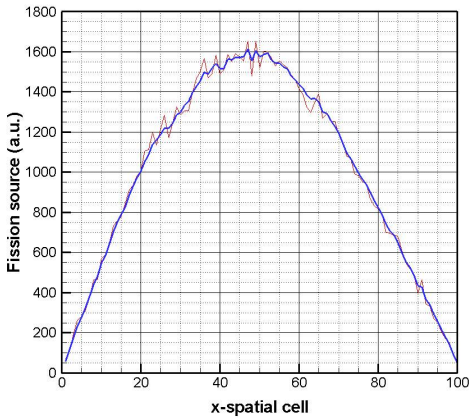

(d) cycle: 26

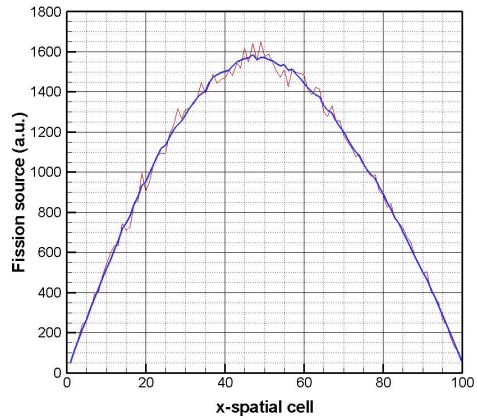

(e) cycle: 51

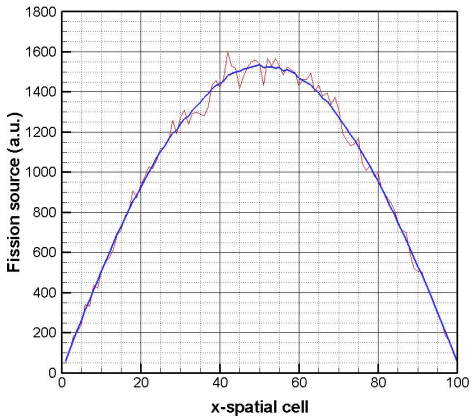

(f) cycle: 131

Figure 6.7: Test-case 6-2: Fission source for some specific cycles (blue: JNFK-corrected, red: before JFNK-correction).

Table 6.4: Test-case 6-3: Calculated average eigenvalues.

	Single multi-region pin
SI (150 inact.)	$1.25800 \pm 17\text{pcm}$
SI-CMFD	$1.25804 \pm 16\text{pcm}$
SI-JFNK	$\mathbf{1.25820 \pm 17}\boldsymbol{pcm}$
Reference (SI)	$\mathbf{1.25815 \pm 08}\boldsymbol{pcm}$

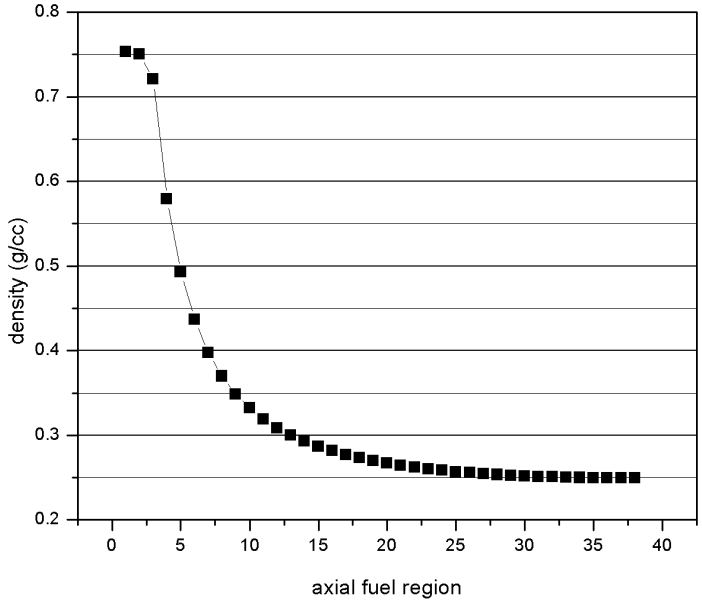

Figure 6.10: Test-case 6-3: Moderator density profile (bottom to top).

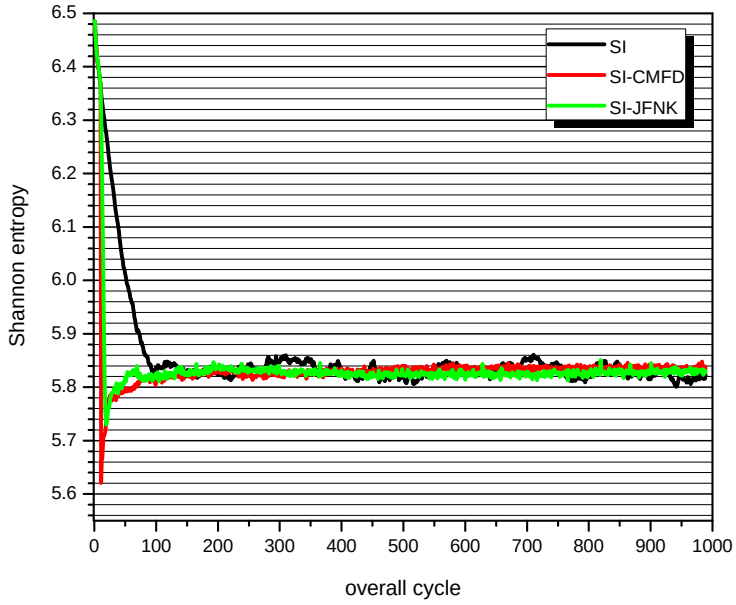

Figure 6.11: Test-case 6-3: Shannon entropy of the source.

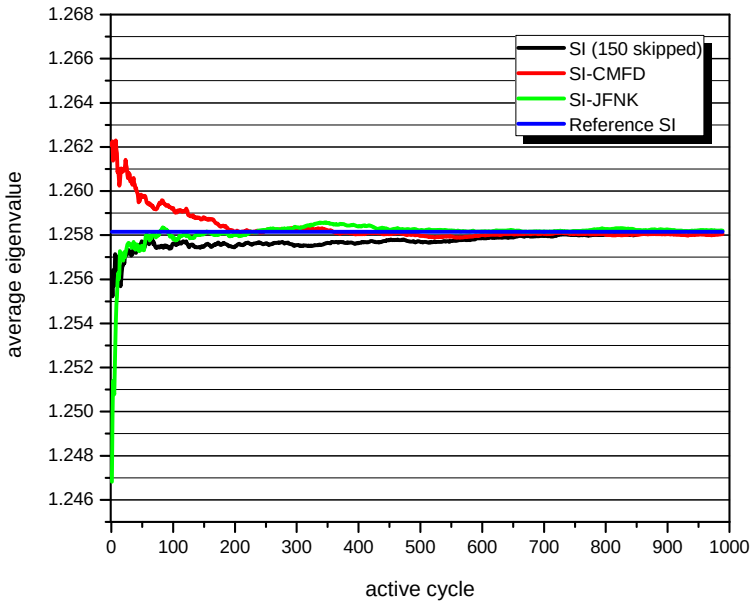

Figure 6.12: Test-case 6-3: Monte-Carlo calculated eigenvalue.

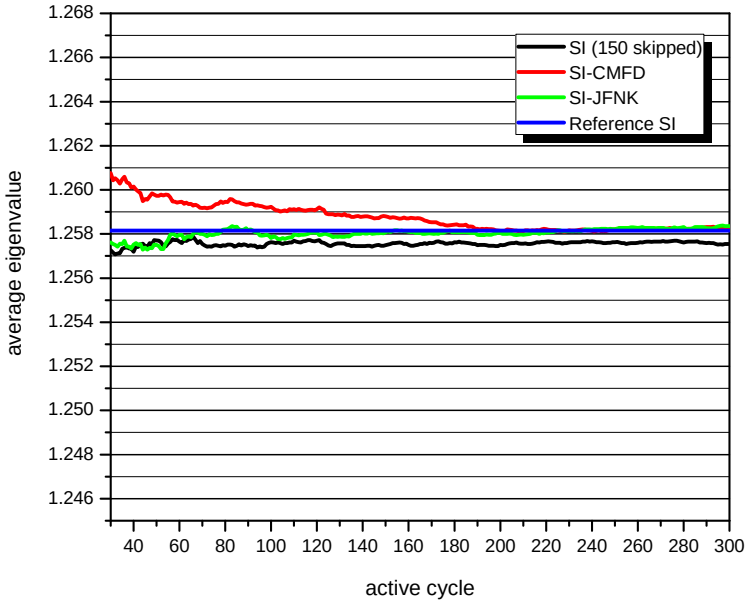

Figure 6.13: Test-case 6-3: Monte-Carlo calculated eigenvalue (zoom in).

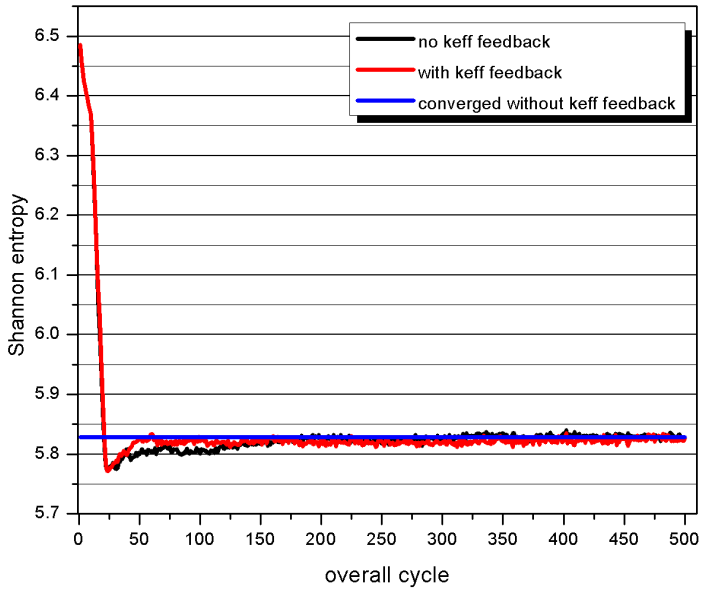

Figure 6.16: Test-case 6-3: Shannon entropy of the source; SI-JFNK without and with k_{eff} feedback.

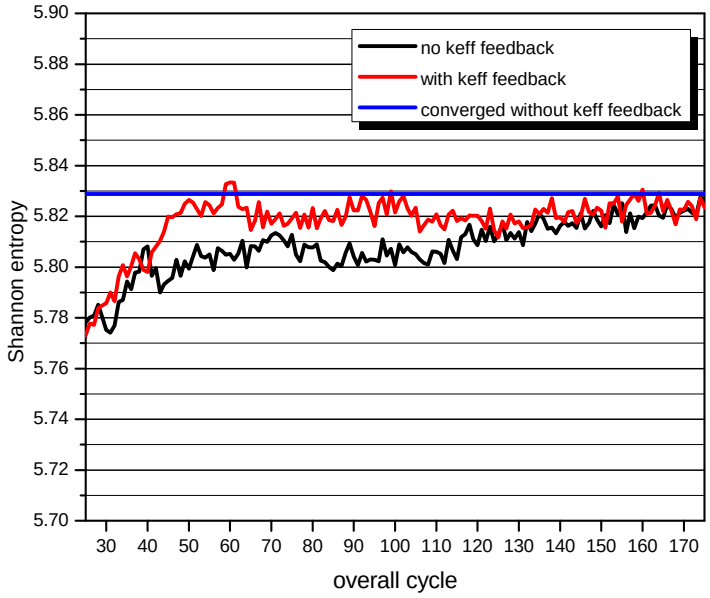

Figure 6.17: Test-case 6-3: Shannon entropy of the source; SI-JFNK without and with k_{eff} feedback (zoom in).

6.4 CONCLUSION

This research introduces a new method that aims to accelerate the convergence of the classical Monte-Carlo SI. This new method is based on the JFNK numerical technique. Because a straight-forward implementation of JFNK in a Monte-Carlo context is rather impossible due to the high computational cost, the CMFD diffusion technique was combined, as an approximation, with JFNK to alleviate this problem. Testing in three (3) simplified test cases shows that the introduced method accelerates the convergence of the fission neutron source to the final shape. Also it improves the quality of the fission neutron source by filtering some of the statistical noise. The improved update of each SI results in the global convergence acceleration (eigenvalue + eigenvector). The evaluation shows that the introduced method improves significantly the convergence compared with the classical SI. Furthermore, it seems that it behaves in a very competitive way compared even with CMFD; however further investigation is required.

A formal mathematical derivation/investigation of the proposed technique is needed. Also, since JFNK involves a set of various numerical parameters, their optimal combination with the Monte-Carlo statistics should be investigated. For example the comments about the Newton vs. the Krylov linear iteration made in § 4.6.2.1 are applied in this

case as well. The performance of the method in problems of larger scale should also be examined and evaluated. Finally, the computational cost of this method should be investigated and compared with that of the other methods. These issues constitute a subject for future research.

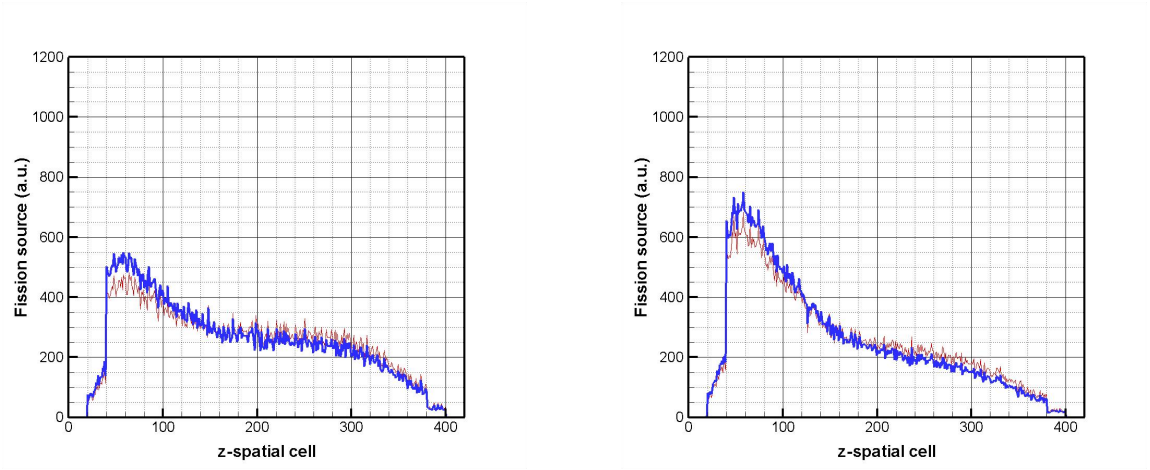

(a) cycle: 11

(b) cycle: 13

(c) cycle: 15

(d) cycle: 20

(e) cycle: 970

(f) cycle: 975

Figure 6.14: Test-case 6-3: Fission source for some specific cycles (blue: JNFK-corrected, red: before JFNK-correction).

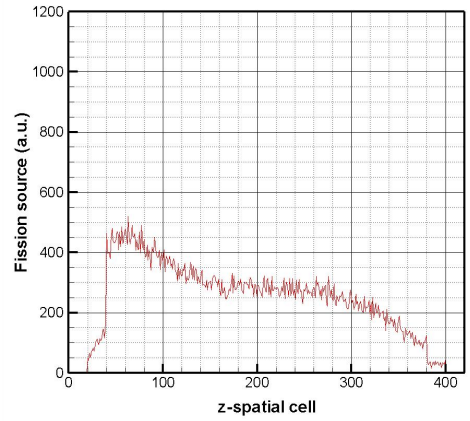

(a) cycle: 11

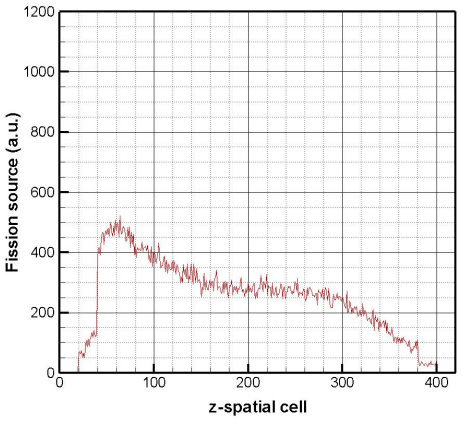

(b) cycle: 13

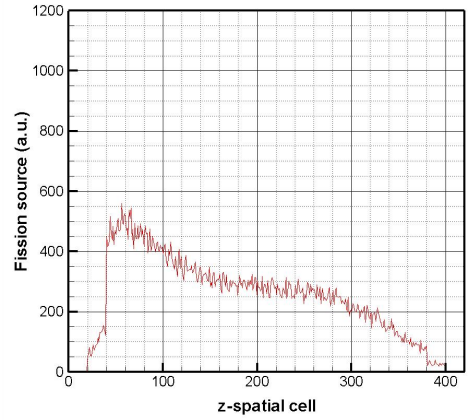

(c) cycle: 15

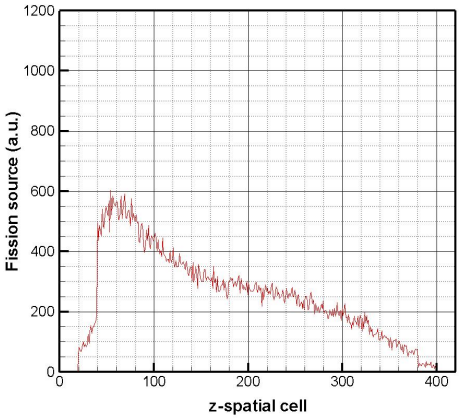

(d) cycle: 20

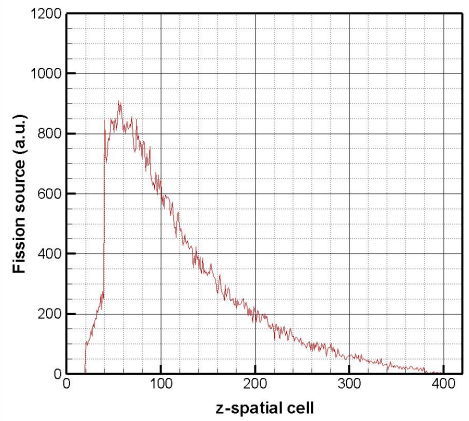

(e) cycle: 790

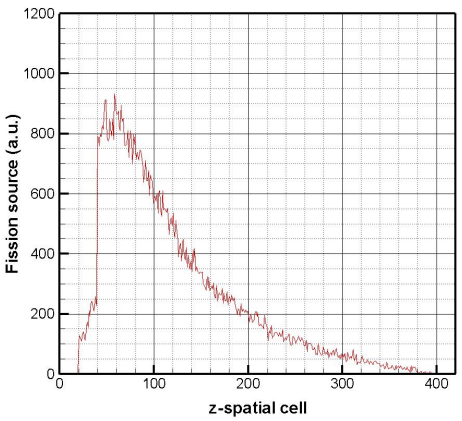

(f) cycle: 800

Figure 6.15: Test-case 6-3: Fission source for some specific cycles of SI with no acceleration.

Part IV

EPILOGUE

7

SUMMARY, CONCLUSION & PERSPECTIVE

7.1 SUMMARY

With this thesis an effort was made to answer some challenging questions faced by the Monte Carlo-based computational reactor core physics. More specifically it was sought to deal with the inclusion of efficient Thermal-Hydraulics (T-H) feedback to the Monte-Carlo transport solution, the extension of Monte-Carlo transport in reactor core dynamics and the convergence acceleration of the algorithm utilised in reactor criticality.

The first part of this thesis handles the problem of T-H feedback to the Monte-Carlo transport solution. Initially, a classical "serial" coupling scheme between the Monte-Carlo neutronic solver OpenMC and the COBRA-EN subchannel T-H solver was developed. This coupling scheme was used to scout the nature of the neutronic/T-H coupled transport solution procedure and mainly to validate the solution against numerical results from the bibliography. Afterwards the first attempt, according to the author's knowledge, was made to develop a Monte Carlo-neutronic/T-H coupling scheme based on a Newton-type methodology, aiming to improve the numerical performance. The Approximate Block Newton (ABN) algorithm was adapted in a reactor core physics context and the corresponding computational coupling scheme between OpenMC and COBRA-EN was developed. Three (3) reactor physics problems were analysed and the results were compared with those of a transport solution with T-H generated with the traditional methodology.

The second part was devoted to the development of a dynamic Monte-Carlo module based on the OpenMC code. The main aim was to develop and investigate a pure Monte-Carlo numerical tool able to analyse the kinetic neutronic behaviour of a nuclear system. The approach that was followed includes the stochastic simulation of all the physical neutronic phenomena that determine the reactor core dynamics. An important goal was the optimum embodiment of the developed module in the OpenMC code following its features and achieving as fewer modifications of the original source code as possible. The developed module was parallelized using the Message Passing Interface (MPI). The analysis of seven (7) test-cases shows satisfactory results and reveals space for future research. Also an Operator Splitting (OS) based coupling of the developed module with the T-H subchannel solver SUBCHANFLOW (SCF) was achieved. For the calculation

of critical initial conditions an iterative critical boron search capability was developed supplementary to the OpenMC/COBRA coupled algorithm.

The third part of the thesis regarded the development of an innovative method for the numerical acceleration of the Monte-Carlo Source Iteration (SI). More specifically a Newton-based, matrix-free numerical method for solving non-linear systems, the Jacobian Free Newton Krylov (JFNK) methodology, was adapted to a Monte-Carlo k-eigenvalue context aiming to accelerate the convergence of the algorithm to the fundamental eigenpair. The stochastic and computationally burdensome nature of a Monte-Carlo algorithm complicates the problem significantly and makes a straight-forward implementation of JFNK into Monte-Carlo rather impossible. To overcome this problem JFNK was combined with the method of the Nonlinear diffusion acceleration via a Coarse Mesh Finite Difference (CMFD) approximation.

7.2 ACHIEVEMENTS & FINDINGS

A "serial" coupling scheme based on the Picard Iteration (PI) between the OpenMC Monte-Carlo solver and the COBRA-EN subchannel T-H solver was successfully developed. This system was validated against results located in the bibliography. It was found that the numerical convergence meets higher difficulties in Boiling Water Reactor (BWR)-type problems due to the higher density gradients. Also it was verified that the use of numerical under-relaxation might alleviate the numerical oscillations in this kind of schemes.

Afterwards an innovative algorithm based on the ABN methodology was designed and successfully developed between the solvers mentioned above. More specifically the ABN algorithm was adapted to a Monte Carlo-neutronic/T-H coupling context and then the OpenMC Monte-Carlo solver was coupled with the COBRA-EN T-H solver using the introduced approach. The performance of the developed scheme was tested in three (3) reactor physics problems and was compared with that of the traditional "serial" coupling methodology, called PI. The results showed that ABN outperforms the PI method increasing the convergence speed and thus reducing the computational cost. The improvement was reflected in the convergence of the unified problem, including the fission-rate distribution, the T-H parameters and the multiplication factor. Besides it was concluded that the observed PI numerical oscillations may lead to the inefficiency of simple drop-based convergence criteria. It should be noted that the improvement occurred by the comparison with the traditional PI scheme was more significant in BWR-type problems, probably because they are characterised by larger moderator density gradients which might complicate the numerical solution of the problem. The validation against the results of the already validated "serial" scheme was successful. Concluding, the main

finding was that the introduced approach achieves the reduction of the number of the required Monte-Carlo transport solutions until convergence. Also the accuracy of the solution is probably higher since the numerical oscillations can induce error.

A Monte-Carlo module for dynamic neutronic analysis based on OpenMC was successfully developed. The module was parallelized based on the MPI. An initial validation against an analytical Point-Kinetics (PK) solution using only one precursor group was successful for four (4) small-scale configurations. Consequently the feasibility of pure Monte-Carlo dynamic analysis for small scale problems was verified. As a next step the validation of a multi-group precursor version was initially performed in a small-scale test-case against a numerical PK solution. Subsequently a pin-by-pin Fuel Assembly (FA) case was analysed for three (3) different scenarios. Good agreement with a numerical solution of the PK equations was found; the only exemption constitutes the stage after scram in the third scenario. This deviation from PK was expected and highlights the deficiency of PK, even in more detailed approximations according to the bibliography, in cases of rapid changes of the flux shape. Aiming to support this statement the FA model was modified; the reflective boundaries were replaced by vacuum ones. Then a larger control rod movement is required to insert a comparable amount of reactivity with the previous case. This induces a larger change of the flux shape; thus the PK did not agree with the Monte-Carlo solution. The main weak point of the developed algorithm regards the high computational cost. This is attributed to the consideration of two quite different time scales with demands for high Monte-Carlo statistics to achieve good accuracy for both of them.

The parallelism pattern was successfully verified. The initialization of the solution is performed in a master-worker context. This fact in combination with the proper treatment of the random number generation results in the reproducibility of the results, i.e. independence of the number of the employed processors. The verification of the reproducibility was also performed. This automatically results in the validation of the parallel version of the solver, i.e. if a non-parallel solution is validated, the parallel one is also validated.

Additionally, the dynamic Monte-Carlo module was coupled successfully with the the T-H subchannel solver SCF in an OS context. For this reason SCF was also modified. The coupling algorithm maintained the already developed structure of the algorithm. The analysis of a small-scale problem showed that the coupled dynamic computational scheme works correctly; however the validation of the dynamic T-H feedback is pending.

A new method for the acceleration of the Monte-Carlo k-eigenvalue transport solution was developed. Firstly, the k-eigenvalue form of the integral Neutron Transport Equa-

tion (NTE) was reformulated in a fixed-point iteration. This iteration was considered as a non-linear problem and the JFNK methodology was employed for its solution. The stochastic and computationally burdensome nature of a Monte-Carlo algorithm complicates the problem significantly and makes a straight-forward implementation of JFNK rather impossible. To overcome this problem a matrix-vector product approximation employing a CMFD diffusion method was developed. The first results showed very satisfying performance.

The testing of three (3) simplified cases, two (2) slab and one (1) single pin configuration indicates that the introduced methodology improves the quality of the neutronic solution update within each Monte-Carlo iteration compared with the classical SI. The improved SI update results in the acceleration of the global convergence. Initially, the introduced method was validated against the traditional Monte-Carlo methodology, with high statistics, in the problems mentioned above. Afterwards its performance was compared with the traditional method as well as the CMFD-accelerated one. It was found that the introduced methodology improves significantly the convergence of the fission neutron source and the mean eigenvalue in comparison with the classical SI. Furthermore, it seems that it behaves in a very competitive way even comparing with CMFD. In the beginning only the JFNK-correction of the source (eigenvector) was activated. In the last test-case the eigenvalue JFNK-correction was also activated imposing further numerical improvement.

The main scientific contribution of this work can be summarised in the following:

1. A classical "serial" coupling algorithm between OpenMC and COBRA-EN was successfully developed.
2. A novel method for coupling Monte-Carlo neutronics with T-H was developed based on the ABN numerical algorithm. According to the author's knowledge this was the first attempt to couple Monte-Carlo with T-H utilising a Newton-based coupling method.
3. This method was implemented in the coupling of OpenMC with COBRA-EN.
4. The evaluation of the introduced methodology in comparison with the "serial" coupling scheme showed clear convergence acceleration. This can be translated into the need for fewer transport solutions.

5. A pure Monte-Carlo module for dynamic neutronic analysis was developed in OpenMC following the host code's features. An attempt made to keep the required source-code modifications minimum. The methodology is based on previous work presented in bibliography.

6. A successful initial step-by-step validation against PK results was performed.
7. An initial evaluation of the parallelism pattern's performance was carried out.
8. The Monte-Carlo module for dynamic neutronic analysis was coupled with the T-H solver SCF.

9. A novel method for acceleration of the Monte-Carlo SI used for criticality analysis was developed. The introduced method combines JFNK and the Non-linear diffusion acceleration.
10. The introduced method was implemented in OpenMC.
11. The results were successfully validated. The initial evaluation showed clear superiority over the traditional SI and very good performance over the CMFD acceleration.

    This method can lead to:

    - Faster convergence of the fission source.
    - Faster convergence of the mean eigenvalue.

    These features can potentially be translated into:

    - Need for fewer inactive Monte-Carlo cycles.
    - Need for fewer active Monte-Carlo cycles.
    - Lower computational cost.

7.3 PERSPECTIVES

Testing the performance of the introduced ABN-based coupling methodology in larger scale problems is one of the main future tasks. The performance of this method is determined by a set of numerical parameters. Thus the investigation of the role of the various numerical parameters appears to be interesting; the optimisation of their combination could accelerate the convergence. Also, the implementation of numerical preconditioning could be investigated aiming to a further improvement of the method's numerical performance. The introduced approach could be combined possibly with the progressive increase of the used neutron histories per Newton step or the usage of relaxation schemes to reach arbitrarily large drop of norms and/or to further stabilise the solution. Last but not least a comparison between neutronic-based and T-H-based set-ups could be performed.

The analysis of more complex and larger scale problems constitutes the main topic of further research regarding the developed dynamic Monte-Carlo module. However a number of various additional tasks could be interesting and useful; e.g. the deeper

investigation of the parallelism pattern performance and the identification of improvements. Also, research on Variance Reduction Technique (VRT) that could improve the performance of the module is an important matter of further investigation.

A formal mathematical derivation of the introduced methodology for the Monte-Carlo SI acceleration is needed. Also this method should be investigated and tested in additional problems. The analysis of its performance in problems of larger scale would be interesting. JFNK involves a set of various numerical parameters. Therefore their role as well as their optimal combination with the Monte-Carlo statistics should be investigated. Finally the computational cost of the introduced method should be investigated and compared with that of other methods.

8

PUBLICATIONS

Journal articles

1. Antonios G. Mylonakis, M. Varvayanni, N. Catsaros, "A Newton-based Jacobian-free Approach for Neutronic-Monte Carlo/Thermal-Hydraulic Static Coupled Analysis", Annals of Nuclear Energy, vol. 110, pp. 709-725, 2017.
2. Antonios G. Mylonakis, M. Varvayanni, D.G.E Grigoriadis, N. Catsaros, "Developing and investigating a pure Monte-Carlo module for transient neutron transport analysis", Annals of Nuclear Energy, vol. 104, pp. 103-112, 2017.
3. A.G. Mylonakis, M. Varvayanni, N. Catsaros, P. Savva, D.G.E Grigoriadis, "Multi-physics and multi-scale methods used in nuclear reactor analysis", Annals of Nuclear Energy, vol. 72, pp. 104-119, 2014.

Peer-reviewed int. conference full articles

1. Antonios G. Mylonakis, M. Varvayanni, N. Catsaros, "Accelerating The Monte-Carlo Power Iteration Utilizing The Jacobian-Free Newton Krylov Methodology", M&C 2017 - Int. Conf. Mathematics & Computational Methods Applied to Nuclear Science & Engineering, Jeju, Korea, April 16-20, 2017.
2. A.G. Mylonakis, M. Varvayanni, N. Catsaros, "Adopting the Monte-Carlo methodology in dynamic reactor core analysis", RERTR 2016 - 37th International Meeting on Reduced Enrichment for Research and Test Reactors, Antwerp, Belgium, October 23-27, 2016.
3. A.G. Mylonakis, M. Varvayanni, N. Catsaros, "On-the-fly towards pure Monte-Carlo transient neutronic analysis", Proc. Int. Conf. Nuclear Energy for New Europe 2015, Portoroz, Slovenia, September 5-8, 2016.
4. T. Xenofontos, A.G. Mylonakis, P. Savva, M. Varvayanni, N. Catsaros, J. Maillard, J. Silva, "The ANET code: From High Energy Physics to stochastic Neutronics with Thermal Hydraulic Feedback", Proc. European Research Reactor Conference 2016, Berlin, Germany, 13-17 March, 2016.
5. A.G. Mylonakis, M. Varvayanni, N. Catsaros, "Investigating a Matrix-free, Newton-based, Neutronic-Monte Carlo/Thermal-Hydraulic Coupling Scheme", **Awarded Article**, Proc. Int. Conf. Nuclear Energy for New Europe 2015, Portoroz, Slovenia, September 14-17, 2015.

6. A.G. Mylonakis, M. Varvayanni, D.G.E. Grigoriadis, P. Savva, N. Catsaros, "Optimization of an Integrated Neutronic/Thermal-Hydraulic reactor core analysis model", Proc. Int. Conf. Nuclear Energy for New Europe 2014, Portoroz, Slovenia, September 8-11, 2014.

ENEN PhD contest 2017 (finalist)

1. A.G. Mylonakis, M. Varvayanni, A. Clouvas, "Extending the Monte-Carlo Methodology for complete reactor core analysis", European Nuclear Education Network PhD-thesis contest, PETRUS-ANNETTE PhD and Early-Stage Researchers Conference 2017.

Other conference papers

1. Antonios G. Mylonakis, M. Varvayanni, N. Catsaros, A. Clouvas, "Developing a Monte-Carlo Solver for the Simulation of the Reactor Core Dynamics", 26th Symposium of the Hellenic Nuclear Physics Society, 9-10 June, Anavyssos, Greece, 2017.

Part V

APPENDICES

a

TEST-CASE 5-6: MATERIAL COMPOSITION

Each fuel rod consists of the fuel pellet, the gap and the cladding. Around each fuel rod there is coolant/moderator. Above and bellow the active part of the fuel assembly there are reflectors. The material compositions are presented in the following Table (a.1). The gap consists of O_{16} with atom density 3.79450E-05 atom/b-cm. The control rods are semi inserted in the guide tubes. The part of the guide tubes located below the control rods is filled with coolant.

Table a.1: Test-case 5-6: Material properties (atoms/b-cm)

	Fuel	Clad	Coolant	Control rods	Top reflector	Bottom refl.
Total atom density	7.53032E-03	3.80967E-02	7.43208E-02	0.105133	3.46967E-02	0.159576
U_{235}	7.45045E-04	-	-	-	-	-
U_{238}	2.21225E-03	-	-	-	-	-
O_{16}	4.57302E-03	-	2.48798E-02	-	3.13919E-03	3.63934E-02
Zr_{90}	-	1.96006E-02	-	-	-	-
Zr_{91}	-	4.27452E-03	-	-	-	-
Zr_{92}	-	6.53375E-03	-	-	-	-
Zr_{94}	-	6.62108E-03	-	-	-	-
Zr_{96}	-	1.06667E-03	-	-	-	-
H_1	-	-	4.93025E-02	-	6.27838E-03	7.27867E-02
B_{10}	-	-	2.89100E-05	6.93964E-02	1.80700E-06	2.34900E-05
B_{11}	-	-	1.09619E-04	1.57032E-02	-	-
C_0	-	-	-	2.00331E-02	-	-
Fe_{54}	-	-	-	-	1.47684E-03	2.93862E-03
Fe_{56}	-	-	-	-	1.47684E-03	4.61296E-02
Fe_{57}	-	-	-	-	1.47684E-03	1.06547E-03
Fe_{58}	-	-	-	-	1.47684E-03	1.41541E-04

b

ΠΕΡΙΛΗΨΗ

Η παρούσα Διδακτορική Διατριβή (ΔΔ) αποτελείται από επτά (7) κύρια κεφάλαια αριθμημένα από το ένα (1) έως το επτά (7), τη βιβλιογραφία και το παράρτημα. Ακολουθεί συνοπτική περιγραφή του κάθε κεφαλαίου.

Κεφάλαιο 1

Στο Κεφάλαιο 1 παρατίθεται σύντομη εισαγωγή η οποία περιλαμβάνει την περιληπτική περιγραφή του περιεχομένου της ΔΔ. Πιο συγκεκριμένα στο κεφάλαιο αυτό γίνεται αρχική μνεία των προς επίλυση προβλημάτων και προσδιορίζεται η σκοπιά από την οποία μελετώνται. Τα προς επίλυση προβλήματα είναι τα ακόλουθα:

1. Ανάλυση αλληλεπιδρώντων φυσικών φαινομένων σε Πυρηνικό Αντιδραστήρα (ΠΑ) - ανάδραση κατά την επίλυση της Εξίσωσης Μεταφοράς Νετρονίων (ΕΜΝ) από την επίλυση του πεδίου της θερμοϋδραυλικής.
2. Δυναμική στοχαστική μεταφορά νετρονίων - πλήρως στοχαστική προσομοίωση της δυναμικής νετρονικής συμπεριφοράς του αντιδραστήρα. Με το όρο πλήρως στοχαστική εννοείται η απουσία υβριδικών αλγορίθμων αιτιοκρατικής - στοχαστικής ανάλυσης.
3. Επιτάχυνση της σύγκλισης του αλγορίθμου ανάλυσης κρισιμότητας - επιτάχυνση της σύγκλισης του αλγορίθμου επίλυσης της ΕΜΝ σε μορφή ιδιοτιμής.

Στο κεφάλαιο αυτό επεξηγείται επίσης η ανάγκη επίλυσης των παραπάνω προβλημάτων ως προκύπτουσα από την απαίτηση για στατική και δυναμική επίλυση των εμπλεκομένων φυσικών πεδίων ως αλληλεπιδρώντων. Δηλαδή η επίλυση πρέπει να λαμβάνει υπόψη την αλληλεπίδρασή τους αντί μεμονωμένης αντιμετώπισης του καθενός ξεχωριστά. Με την προσθήκη της απαίτησης για χαμηλό υπολογιστικό κόστος η ανάγκη επίλυσης των παραπάνω τριών (3) προβλημάτων καθίσταται προφανής. Τέλος στο Κεφάλαιο 1 παρατίθεται η λογική δομή ανάπτυξης του βασικού τμήματος της ΔΔ.

Κεφάλαιο 2

Στο Κεφάλαιο 2 αναπτύσσεται το θεωρητικό υπόβαθρο του αντικειμένου της ΔΔ. Πιο συγκεκριμένα αναφέρεται η βασική ολοκληρωτικο-διαφορική χρονοεξαρτώμενη μορφή της ΕΜΝ με

σύντομη περιγραφή των όρων της. Ακολούθως παρατίθενται και άλλες χρήσιμες μορφές της ΕΜΝ όπως η πλήρως ολοκληρωτική μορφή, η μορφή ιδιοτιμής της ολοκληρωτικο-διαφορικής ΕΜΝ και η χωρική-κινητική ολοκληρωτικο-διαφορική μορφή με θεώρηση και των πρόδρομων πυρήνων σαν πηγή νετρονίων. Στη συνέχεια περιγράφονται συνοπτικά οι κύριες προσεγγίσεις και παραδοχές που υιοθετούνται κατά τη αιτιοκρατική επίλυση της ΕΜΝ ώστε να στοιχειοθετηθεί η ανάγκη στοχαστικής επίλυσης της. Τέλος, αναφέρονται οι θεμελιώδεις αρχές της στοχαστικής μεταφοράς νετρονίων, οι αρχές των μεθόδων μείωσης της διακύμανσης, καθώς και ο αριθμητικός αλγόριθμος που απαιτείται για τη στοχαστική επίλυση του στατικού προβλήματος ιδιοτιμής της ολοκληρωτικής ΕΜΝ. Η δομή του παρόντος κεφαλαίου και η αλληλουχία των υπο-παραγράφων αποσκοπεί στην πληρέστερη αιτιολόγηση της αναγκαιότητας επίλυσης των προβλημάτων που μελετά η παρούσα ΔΔ. Επίσης γίνεται προσπάθεια να καταστεί το κείμενο όσο το δυνατόν αυτόνομο για τον αναγνώστη.

Κεφάλαιο 3

Στο Κεφάλαιο 3 τίθενται αναλυτικά τα προβλήματα τα οποία μελετώνται στην παρούσα ΔΔ καθώς και οι στόχοι της μελέτης αυτής. Πιο συγκεκριμένα, διατυπώνονται τα προβλήματα προς μελέτη και περιγράφονται οι γενικές κατευθύνσεις επίλυσης τους με βάση και το θεωρητικό υπόβαθρο το οποίο έχει δοθεί στο Κεφάλαιο 2. Επίσης συγκεκριμενοποιούνται οι στόχοι της επίλυσης των τεθέντων προβλημάτων.

Αρχικά τίθεται το πρόβλημα συζευγμένης νετρονικής/θερμοϋδραυλικής στατικής ανάλυσης ΠΑ. Η πιο συχνά χρησιμοποιούμενη μεθοδολογία αντιμετώπισης του προβλήματος αυτού περιλαμβάνει τη σειριακή επίλυση του νετρονικού και του θερμοϋδραυλικού πεδίου μέχρις ότου επιτευχθεί σύγκλιση της συνολικής ή ενός κατάλληλα επιλεγμένου μέρους της λύσης. Σύμφωνα με τη βιβλιογραφία, αυτή η μεθοδολογία «χαλαρής» σύζευξης συχνά παρουσιάζει προβλήματα σύγκλισης. Έτσι η εύρεση αποτελεσματικότερης μεθόδου η οποία θα συγκλίνει ταχύτερα και θα συνδυάζεται με λογικό υπολογιστικό κόστος παραμένει ανοιχτό πρόβλημα. Πρέπει να σημειωθεί ότι το υπολογιστικό κόστος αποτελεί κρίσιμο παράγοντα κατά την στοχαστική νετρονική ανάλυση ΠΑ.

Στη συνέχεια περιγράφεται το ερευνητικό πρόβλημα της επίτευξης πλήρους στοχαστικής δυναμικής νετρονικής ανάλυσης ΠΑ. Επεξηγείται ότι ενώ η στοχαστική νετρονική ανάλυση ΠΑ χρησιμοποιείται εκτενώς κατά τη στατική ανάλυση, αυτό δεν συμβαίνει στη δυναμική ανάλυση. Επιπροσθέτως τίθεται το πρόβλημα της συζευγμένης νετρονικής/θερμοϋδραυλικής δυναμικής ανάλυσης ΠΑ. Η στοχαστική νετρονική επίλυση εισάγει αλγοριθμικά ερωτήματα ως προς την επίτευξη σύζευξης.

Τέλος εισάγεται το πρόβλημα της επιτάχυνσης σύγκλισης του αλγορίθμου στοχαστικής επίλυσης της στατικής μορφής της ΕΜΝ. Για την στοχαστική επίλυση της ΕΜΝ σε μορφή

ιδιοτιμής χρησιμοποιείται η Μέθοδος Δυνάμεων ή Επανάληψη Πηγής η οποία εγγυάται τη σύγκλιση στο βασικό ιδιοζεύγος. Σύμφωνα με τη βιβλιογραφία η μέθοδος αυτή συγκλίνει πολύ αργά στην επίλυση συγκεκριμένων τύπων προβλημάτων τα οποία συναντώνται συχνά στον τομέα της πυρηνικής τεχνολογίας. Έτσι το πρόβλημα της επιτάχυνσης σύγκλισης της μεθόδου επανάληψης πηγής παραμένει μία σημαντική ερευνητική πρόκληση.

Κεφάλαιο 4

Το Κεφάλαιο 4 μελετά το πρόβλημα εισαγωγής θερμοϋδραυλικής ανάδρασης στη στοχαστική επίλυση της στατικής ΕΜΝ σε μορφή ιδιοτιμής. Αρχικά παρατίθεται βιβλιογραφική ανασκόπηση των συνηθέστερων μεθοδολογιών αντιμετώπισης του προβλήματος αυτού. Προκύπτει ότι η συνηθέστερη μέθοδος σύζευξης χρησιμοποιεί αλγόριθμο σειριακής επίλυσης του νετρονικού και θερμοϋδραυλικού πεδίου μέχρις ότου επιτευχθεί σύγκλιση της συνολικής ή ενός μέρους της λύσης.

Ακολούθως περιγράφεται η ανάπτυξη του εν λόγω σειριακού αλγορίθμου για την επίτευξη σύζευξης του νετρονικού Monte-Carlo κώδικα OpenMC με τον θερμοϋδραυλικό επιλύτη COBRA-EN. Το συζευγμένο σχήμα πιστοποιήθηκε με βάση αριθμητικά αποτελέσματα της βιβλιογραφίας. Επίσης διερευνήθηκε η επίδραση της χρήσης αριθμητικής υποχαλάρωσης η οποία φαίνεται ότι πράγματι βελτιώνει την αριθμητική συμπεριφορά. Λόγω της πολύ συχνά προβληματικής σύγκλισης του αλγορίθμου αυτού διερευνήθηκε η αντικατάσταση του με άλλη μεθοδολογία. Σε αυτό το πλαίσιο προσαρμόστηκε ο προσεγγιστικός αλγόριθμος Newton Τμήματος Μητρώου στην επίλυση συζευγμένων νετρονικών/θερμοϋδραυλικών προβλημάτων φυσικής αντιδραστήρα. Ο αλγόριθμος αυτός αναπτύχθηκε προγραμματιστικά ώστε να επιτευχθεί σύζευξη του νετρονικού Monte-Carlo κώδικα OpenMC και του θερμοϋδραυλικού επιλύτη COBRA-EN. Στη συνέχεια αξιολογήθηκε η συμπεριφορά του κατά την επίλυση κατάλληλα σχεδιασμένων προβλημάτων φυσικής αντιδραστήρα. Η προτεινόμενη μεθοδολογία εισαγωγής θερμοϋδραυλικής ανάδρασης στη στοχαστική επίλυση της ΕΜΝ είναι καινοτόμα καθώς εμφανίζεται για πρώτη φορά στη βιβλιογραφία.

Αρχικά επιλύεται πρόβλημα μεμονωμένης ράβδου καυσίμου αντιδραστήρα ζέοντος ύδατος. Η επίλυση του προβλήματος αυτού οδήγησε στα εξής συμπεράσματα: Η προτεινόμενη μεθοδολογία υπερτερεί της κλασσικής όσον αφορά την ακρίβεια και το υπολογιστικό κόστος. Φαίνεται ότι χαρακτηρίζεται από λιγότερες και ηπιότερες αριθμητικές ταλαντώσεις. Συνεπώς, η τελική λύση σταθεροποιείται και συγκλίνει ταχύτερα. Οι δύο (2) μεθοδολογίες συγκλίνουν στην ίδια συνολική λύση. Οι διαφορές που προκύπτουν αποδίδονται μετά από διερεύνηση στις αριθμητικές ταλαντώσεις του σειριακού αλγορίθμου που οδηγούν σε σημαντική διαφοροποίηση της λύσης από επανάληψη σε επανάληψη.

Στη συνέχεια επιλύεται πρόβλημα ολόκληρης δέσμης ράβδων πυρηνικού καυσίμου αντιδραστήρα πεπιεσμένου ύδατος. Και στην περίπτωση αυτή η προτεινόμενη μέθοδος οδηγεί σε ταχύτερη και σταθερότερη σύγκλιση. Το πρόβλημα αυτό επιλύεται ταχύτερα του προηγουμένου πιθανώς λόγω των μικρότερων διαφορών πίεσης μεταξύ ανώτερων και κατώτερων αξονικών τμημάτων. Για το λόγο αυτό το πρόβλημα αναπροσαρμόζεται με στόχο την αύξηση της αριθμητικής του δυσκολίας και επιλύεται ξανά. Πιο συγκεκριμένα η πίεση επανακαθορίζεται σε αντίστοιχη αυτής που ισχύει σε πρόβλημα αντιδραστήρα τύπου ζέοντος ύδατος. Επίσης η πυκνότητα ατόμων του σχάσιμου υλικού αυξάνεται ώστε να επιτευχθεί αύξηση της ισχύος. Για την επίλυση του πραγματοποιείται και ένας επιπλέον υπολογισμός με τον σειριακό αλγόριθμο επίλυσης σε συνδυασμό με αριθμητική υποχαλάρωση. Η επίλυση του προβλήματος αυτού οδηγεί στα εξής συμπεράσματα. Όντως η πυκνότητα ψυκτικού/επιβραδυντή παίζει σημαντικό ρόλο στην αριθμητική δυσκολία επίλυσης προβλημάτων τέτοιου τύπου. Η προτεινόμενη μεθοδολογία υπερτερεί της κλασικής με και χωρίς υποχαλάρωση. Η σύγκλιση της νόρμας της νετρονικής λύσης είναι ταχύτερη και σταθερότερη. Επίσης τονίζεται η ανάγκη θέσπισης κριτηρίων σύγκλισης πέραν των συχνά χρησιμοποιούμενων τα οποία φαίνεται ότι μπορεί να οδηγήσουν ακόμα και σε εσφαλμένα συμπεράσματα.

Συνοψίζοντας, το Κεφάλαιο 4 ασχολείται με το εξής πρόβλημα:

- Θερμοϋδραυλική ανάδραση κατά τη στοχαστική επίλυση της EMN σε μορφή ιδιοτιμής.

Τα κυριότερα αποτελέσματα-συμπεράσματα που προκύπτουν είναι τα εξής:

1. Η προτεινόμενη μεθοδολογία επιτυγχάνει επιτάχυνση της σύγκλισης της λύσης.
2. Οι διαδοχικές εκτιμήσεις της λύσης χαρακτηρίζονται από σημαντικά ηπιότερες αριθμητικές ταλαντώσεις σε σχέση με την κλασική σειριακή μεθοδολογία.
3. Η βελτίωση είναι σημαντικότερη σε προβλήματα αντιδραστήρων ζέοντος ύδατος όπου υπάρχει ισχυρότερη μεταβολή/μείωση καθ' ύψος της πυκνότητας του ψυκτικού/επιβραδυντή ύδατος.
4. Υπάρχει ανάγκη προσεκτικής θέσπισης κριτηρίων σύγκλισης διότι τα κριτήρια που βασίζονται αποκλειστικά σε μεταβολή της τιμής μίας νόρμας μεταξύ δύο επαναλήψεων μπορεί να οδηγήσουν σε εσφαλμένα συμπεράσματα.

Κεφάλαιο 5

Το Κεφάλαιο 5 περιγράφει την ανάπτυξη στοχαστικού κώδικα ανάλυσης της δυναμικής νετρονικής συμπεριφοράς ΠΑ. Αρχικά παρατίθεται βιβλιογραφική μελέτη η οποία δείχνει ότι πράγματι η μεθοδολογία Monte-Carlo χρησιμοποιείται σχεδόν αποκλειστικά για την στατική ανάλυση αντιδραστήρα. Η δυναμική ανάλυση αντιδραστήρα συνήθως γίνεται με αιτιοκρατικές μεθόδους οι οποίες όμως κάνουν χρήση πολλών και ποικίλων απλουστεύσεων και προσεγγίσεων, όπως έχει περιγραφεί στο Κεφάλαιο 2. Για τον λόγο αυτό κρίνεται σκόπιμη η προσπάθεια

ανάπτυξης πλήρως στοχαστικών αριθμητικών «εργαλείων» τα οποία θα μπορούσαν πιθανώς να συμβάλλουν στην ακριβέστερη ανάλυση ΠΑ. Στη βιβλιογραφία βρέθηκε μία τέτοια προσπάθεια ανάπτυξης μεθοδολογίας πλήρους στοχαστικής δυναμικής νετρονικής ανάλυσης. Η μέθοδος αυτή αποτέλεσε βασική αναφορά στην παρούσα μελέτη. Μετά τη βιβλιογραφική ανασκόπηση περιγράφεται η ανάπτυξη αριθμητικού κώδικα επίλυσης νετρονικών δυναμικών προβλημάτων ο οποίος ενσωματώνεται στον κώδικα επίλυσης στατικών προβλημάτων OpenMC. Για την παρούσα εργασία αποτελεί επιπλέον στόχο η βέλτιστη αλγοριθμική/προγραμματιστική ανάπτυξη η οποία θα οδηγήσει στην ελάχιστη δυνατή μεταβολή του αρχικού πηγαίου κώδικα και στην μέγιστη εκμετάλευση των ήδη υπαρχουσών δυνατοτήτων του κώδικα OpenMC.

Στο κεφάλαιο αυτό περιγράφεται επίσης η σταδιακή πιστοποίηση του υπό-ανάπτυξη κώδικα σε διάφορα προβλήματα αυξανόμενης πολυπλοκότητας. Στα προβλήματα αυτά η χρονοεξαρτώμενη συμπεριφορά εισάγεται είτε αλλάζοντας δυναμικά την σύσταση κάποιου υλικού του προβλήματος είτε μεταβάλλοντας δυναμικά τη γεωμετρία του. Επίσης γίνεται αρχική αξιολόγηση της παραλληλοποίησης του δυναμικού κώδικα αναλύοντας μικρής κλίμακας πρόβλημα με προοδευτικά αυξανόμενο αριθμό επεξεργαστών. Στη συνέχεια περιγράφεται η προσθήκη δυναμικής θερμοϋδραυλικής ανάδρασης σύμφωνα με την αριθμητική τεχνική Διαχωρισμού Τελεστή και ο έλεγχος της σε απλουστευμένο πρόβλημα. Η επίλυση του θερμοϋδραυλικού πεδίου γίνεται με τον επιλύτη SUBCHANFLOW. Για την ανάγκη προσδιορισμού αρχικών κρίσιμων νετρονικών-θερμοϋδραυλικών συνθηκών αναπτύχθηκε και δυνατότητα αριθμητικού προσδιορισμού της συγκέντρωσης βορίου στο ψυκτικό/επιβραδυντή η οποία επιτυγχάνει αρχικές συνθήκες κρισιμότητας.

Συνοψίζοντας, το Κεφάλαιο 5 ασχολείται με το εξής πρόβλημα:

- Πλήρως στοχαστική επίλυση δυναμικών νετρονικών προβλημάτων με προσθήκη θερμοϋδραυλικής ανάδρασης.

Τα κυριότερα αποτελέσματα-συμπεράσματα που προκ είναι τα εξής:

1. Επιτυχής ανάπτυξη ενός αμιγώς στοχαστικού κώδικα επίλυσης δυναμικών νετρονικών προβλημάτων.
2. Επιτυχής πιστοποίηση του κώδικα στην ανάλυση προβλημάτων αυξανόμενης δυσκολίας μετά από σύγκριση των αποτελεσμάτων του με αυτά δυναμικού μοντέλου σημειακού αντιδραστήρα.
3. Ανάδειξη της έλλειψης δυνατότητας των απλοποιημένων σημειακών μοντέλων να περιγράψουν τη δυναμική συμπεριφορά νετρονικών συστημάτων όπου η χρονοεξαρτώμενη συμπεριφορά συνοδεύεται από σημαντική μεταβολή της μορφής της κατανομής νετρονίων.
4. Επίτευξη προσθήκης δυναμικής θερμοϋδραυλικής ανάδρασης.

Κεφάλαιο 6

Το Κεφάλαιο 6 περιγράφει την ανάπτυξη καινοτόμου αλγορίθμου επιτάχυνσης της σύγκλισης της αριθμητικής επίλυσης της στατικής ΕΜΝ σε μορφή ιδιοτιμής. Αρχικά περιγράφονται οι αιτίες του προβλήματος. Ακολούθως περιγράφεται μέθοδος αντιμετώπισης του η οποία έχει προταθεί σχετικά πρόσφατα στη διεθνή βιβλιογραφία. Η μέθοδος αυτή ονομάζεται Επιτάχυνση Μη-γραμμικής Διάχυσης και εφαρμόζεται στον κώδικα OpenMC με χρήση της τεχνικής Πεπερασμένης Διαφοράς Αραιού Πλέγματος. Η μεθοδος αυτή χρησιμοποιεί ταυτόχρονη αιτιοκρατική απλουστευμένη επίλυση του νετρονικού προβλήματος σε κάθε στοχαστική επανάληψη. Λόγω της απλουστευμένης αιτιοκρατικής επίλυσης το υπολογιστικό κόστος είναι μικρό επιτρέποντας αιτιοκρατική επίλυση έως τη σύγκλιση για κάθε στοχαστική επανάληψη. Η συγκεκλιμένη αιτιοκρατική λύση χρησιμοποιείται για τη διόρθωση της στοχαστικής λύσης σε κάθε επανάληψη.

Στη συνέχεια γίνεται περιγραφή της μεθοδολογίας που αναπτύσσεται στην παρούσα ΔΔ. Σύμφωνα με αυτήν, το επαναληπτικό πρόβλημα εύρεσης ιδιοζεύγους αναδιαμορφώνεται σε πρόβλημα Newton το οποίο επιλύεται με την αριθμητική τεχνική Ελεύθερης Ιακωβιανού πίνακα Newton Krylov (JFNK) επίλυσης μη-γραμμικών εξισώσεων. Η εν λόγω τεχνική αποφεύγει την υπολογιστικά «δαπανηρή» κατασκευή του Ιακωβιανού πίνακα. Ωστόσο η στοχαστική επίλυση της ΕΜΝ καθιστά την ευθεία εφαρμογή της μεθόδου JFNK πρακτικά αδύνατη καθώς απαιτείται κατασκευή προσεγγιστικών γινομένων πίνακα-διανύσματος. Το πρόβλημα αυτό αντιμετωπίζεται με ανάπτυξη αλγορίθμου αιτιοκρατικής κατασκευής προσεγγιστικών γινομένων πίνακα-διανύσματος.

Στη συνέχεια περιγράφεται η εφαρμογή της προτεινόμενης μεθόδου σε τρία προβλήματα αυξανόμενης δυσκολίας. Τα προβλήματα αυτά αναλύονται με την προτεινόμενη μέθοδο, την επανάληψη πηγής χωρίς επιτάχυνση, και την επανάληψη πηγής με επιτάχυνση μη-γραμμικής διάχυσης. Σαν μέθοδος αναφοράς χρησιμοποιείται η κλασική επανάληψη πηγής με υψηλό αριθμό σωματιδίων και επαναλήψεων για την επίτευξη μικρού στατιστικού σφάλματος. Η απόδοση των μεθόδων συγκρίνεται ως προς τη σύγκλιση της πηγής νετρονίων και της μέσης ιδιοτιμής. Το πρώτο πρόβλημα αφορά τη στατική νετρονική επίλυση γεωμετρίας άπειρης ομογενούς πλάκας όπου φαίνεται η σημαντική βελτίωση στην απόδοση έναντι της κλασικής μεθόδου. Το δεύτερο πρόβλημα αφορά και αυτό γεωμετρία άπειρης πλάκας ομογενούς υλικού. Όμως στην περίπτωση αυτή η σύσταση του υλικού έχει διαμορφωθεί κατάλληλα ώστε να καταστήσει το πρόβλημα σημαντικά δυσκολότερο αριθμητικά. Εδώ η υπεροχή της προτεινόμενης μεθόδου είναι εμφανέστερη. Το τρίτο πρόβλημα αφορά μία μεμονωμένη ράβδο πυρηνικού καυσίμου με αξονικά μεταβαλλόμενη σύσταση καυσίμου περιβαλλόμενη από ψυκτικό νερό. Και στην περίπτωση αυτή επιβεβαιώνεται η υπεροχή της προτεινόμενης μεθόδου σε σχέση με τις υπόλοιπες. Συνοψίζοντας, το Κεφάλαιο 6 ασχολείται με το εξής πρόβλημα:

- Επιτάχυνση της σύγκλισης του αλγορίθμου επίλυσης της ΕΜΝ σε μορφή ιδιοτιμής.

Τα κυριότερα αποτελέσματα-συμπεράσματα που προκύπτουν είναι τα εξής:

1. Επιτυχής ανάπτυξη μεθόδου αριθμητικής επιτάχυνσης της σύγκλισης της Επανάληψης Πηγής. Η προτεινόμενη μεθοδολογία συνδυάζει αριθμητική τεχνική επίλυσης μη-γραμμικών συστημάτων και αλγόριθμο επιτάχυνσης μη-γραμμικής διάχυσης.
2. Εφαρμογή της παραπάνω μεθόδου σε στοχαστικό στατικό κώδικα.
3. Επιτυχής πιστοποίηση των αποτελεσμάτων της προτεινόμενης μεθόδου. Ακολούθως, η αρχική αξιολόγηση της απόδοσης της έδειξε σημαντική βελτίωση έναντι της κλασικής επανάληψης πηγής και της επανάληψης πηγής με χρήση επιτάχυνσης μη-γραμμικής διάχυσης. Η μέθοδος αυτή οδήγησε σε:
   - Ταχύτερη σύγκλιση της πηγής νετρονίων.
   - Ταχύτερη σύγκλιση της μέσης ιδιοτιμής.

   Συνεπώς μπορεί να οδηγήσει σε:
   - Μείωση των αναγκαίων ανενεργών στοχαστικών επαναλήψεων.
   - Μείωση των αναγκαίων ενεργών στοχαστικών επαναλήψεων.
   - Αύξηση ακρίβειας και χαμηλότερο υπολογιστικό κόστος.

Κεφάλαιο 7

Στο Κεφάλαιο 7 γίνεται σύντομη ανασκόπηση της ΔΔ, παρουσιάζονται τα συμπεράσματα και αναλύεται η συμβολή της στην επίλυση των τεθέντων προβλημάτων. Ακόμα, παρατίθενται προτάσεις μελλοντική έρευνας.

Η κύρια επιστημονική συνεισφορά της παρούσας ΔΔ συνοψίζεται στα παρακάτω:

1. Αναπτύχθηκε σειριακός αλγόριθμος σύζευξης μεταξύ στοχαστικού νετρονικού κώδικα και θερμοϋδραυλικού επιλύτη.
2. Αναπτύχθηκε καινοτόμα μέθοδος για τη σύζευξη στοχαστικού νετρονικού κώδικα και θερμοϋδραυκού επιλύτη η οποία βασίζεται σε αριθμητικό προσεγγιστικό αλγόριθμο επίλυσης μη-γραμμικών συστημάτων που προκύπτουν από τη σύζευξη επιλυτών.
3. Η μέθοδος αυτή χρησιμοποιήθηκε για τη σύζευξη στοχαστικού κώδικα και θερμοϋδραυλικού επιλύτη.
4. Η αξιολόγηση της προτεινόμενης μεθόδου σε σύγκριση με τον σειριακό αλγόριθμο σύζευξης έδειξε βελτίωση της σύγκλισης. Αυτό σημαίνει σταθερότερη σύγκλιση και λιγότερες απαιτούμενες νετρονικές επιλύσεις έως τη σύγκλιση.

5. Αναπτύχθηκε κώδικας πλήρους στοχαστικής δυναμικής νετρονική ανάλυσης επεκτείνοντας υπάρχοντα κώδικα στατικής στοχαστικής ανάλυσης. Η ανάπτυξη βασίστηκε σε μέθοδο η οποία έχει προταθεί πρόσφατα στη βιβλιογραφία.

6. Τα αποτελέσματα του κώδικα πιστοποιήθηκαν συγκρινόμενα με αποτελέσματα δυναμικού μοντέλου σημειακού αντιδραστήρα σε προβλήματα προοδευτικής δυσκολίας.
7. Πραγματοποιήθηκε αρχική αξιολόγηση του σχήματος παραλληλοποίησης.
8. Πραγματοποιήθηκε σύζευξη με θερμοϋδραυλικό επιλύτη με στόχο την προσθήκη θερμοϋδραυλικής ανάδρασης στην νετρονική λύση.

9. Αναπτύχθηκε καινοτόμα μέθοδος επιτάχυνσης της επανάληψης πηγής η οποία χρησιμοποιείται στην ανάλυση κρισιμότητας. Η προτεινόμενη μέθοδος συνδυάζει αριθμητική τεχνική επίλυσης μη-γραμμικών συστημάτων και αλγόριθμο επιτάχυνσης μη-γραμμικής διάχυσης.
10. Ο αλγόριθμος αυτός ενσωματώθηκε σε στοχαστικό στατικό κώδικα.
11. Τα αποτελέσματα της νέας μεθόδου πιστοποιήθηκαν επιτυχώς. Αρχική αξιολόγηση της απόδοσης του έδειξε σημαντική βελτίωση έναντι της επανάληψης πηγής, και της επανάληψης πηγής με χρήση επιτάχυνσης πεπερασμένης διαφοράς αραιού πλέγματος. Η μέθοδος αυτή οδήγησε σε:
    - Ταχύτερη σύγκλιση της πηγής νετρονίων.
    - Ταχύτερη σύγκλιση της μέσης ιδιοτιμής.

    Συνεπώς μπορεί να οδηγήσει σε:
    - Μείωση των αναγκαίων ανενεργών στοχαστικών επαναλήψεων.
    - Μείωση των αναγκαίων ενεργών στοχαστικών επαναλήψεων.
    - Αύξηση ακρίβειας και χαμηλότερο υπολογιστικό κόστος.

C

ΛΕΞΙΚΟ ΑΝΤΙΣΤΟΙΧΙΣΗΣ ΑΓΓΛΙΚΩΝ ΤΕΧΝΙΚΩΝ ΟΡΩΝ ΜΕ ΕΛΛΗΝΙΚΟΥΣ

Adiabatic approximation model: Μοντέλο αδιαβατικής προσέγγισης

Approximate block Newton algorithm: Προσεγγιστικός αλγόριθμος Newton τμήματος μητρώου

Boiling water reactor: Αντιδραστήρας ζέοντος ύδατος

Coarse mesh finite differences: Πεπερασμένες διαφορές αραιού πλέγματος

Combined precursor: Συνδυασμένος πρόγονος πυρήνας

Control rods: Ράβδοι ελέγχου

Critical boron search: Αναζήτηση συγκέντρωσης βορίου κρίσιμου συστήματος

Decay constant: Σταθερά διάσπασης

Delayed neutron fraction: Ποσοστό καθυστερημένων νετρονίων

Delayed neutrons: Καθυστερημένα νετρόνια

Diffusion coefficient: Σταθερά διάχυσης

Dominance ratio: Λόγος κυριαρχίας

Fission rate: Ρυθμός σχάσεων

Fixed-point iteration: Επανάληψη σταθερού σημείου

Fixed-source algorithm: Αλγόριθμος σταθερής πηγής

Fuel Assembly: Δέσμη ράβδων καυσίμου

Fuel pin: Ράβδος καυσίμου

Jacobian free Newton Krylov: Ελεύθερη Ιακωβιανού πίνακα μέθοδος Newton Krylov

Krylov solver: Επιλύτης Krylov

Linear congruential random number generator: Γραμμική αναλογική γεννήτρια τυχαίων αρ.

Linear solver: Γραμμικός επιλύτης

Mean generation time: Μέσος χρόνος ζωής νετρονίων

Macroscopic cross-section: Μακροσκοπική ενεργός διατομή

Microscopic cross-section: Μικροσκοπική ενεργός διατομή

Master-worker parallelism: Αλγόριθμος παράλληλης επεξεργασίας συντονιστή-εργαζόμενου

Multiphysics analysis: Ανάλυση αλληλεπιδρώντων φαινομένων

Multiplication factor: Συντελεστής πολλαπλασιαμού

Neutron batch: Δέσμη νετρονίων

Neutron current: Ρεύμα νετρονίων

Neutron diffusion equation: Εξίσωση διάχυσης νετρονίων

Neutron flux: Ροή νετρονίων

Neutron transport equation: Εξίσωση μεταφοράς νετρονίων

Neutron transport theory: Θεωρία μεταφοράς νετρονίων

Neutron spatial-kinetics equations: Χωρικές-κινητικές εξισώσεις νετρονίων

Non-linear diffusion acceleration: Επιτάχυνση μη-γραμμικής διάχυσης

Non-linear residual: Μη-γραμμικό υπόλοιπο

Nuclear reactor: Πυρηνικός αντιδραστήρας

Nuclear reactor core: Πυρήνας (καρδιά) πυρηνικού αντιδραστήρα

Operator-Splitting method: Μέθοδος διαχωρισμού τελεστή

Point kinetic model: Δυναμικό μοντέλο σημειακού αντιδραστήρα

Precursors: Πρόγονοι πυρήνες

Pressurized water reactor: Αντιδραστήρας πεπιεσμένου ύδατος

Prompt neutrons: Ακαριαία νετρόνια

Pseudo-random number: Ψευδο-τυχαίος αριθμός

Pseudo-random number generator: Γεννήτρια ψευδο-τυχαίων αριθμών

Pseudo-random number sequence: Σειρά ψευδο-τυχαίων αριθμών

Quasi-static approximation: Σχεδόν στατική προσέγγιση

Reaction rate: Ρυθμός αντιδράσεων

Reactivity: Αντιδραστικότητα

Reactor criticality: Κρισιμότητα αντιδραστήρα

Reflective boundary condition: Συνοριακή συνθήκη αντικατοπτρισμού

Neutron reflector: Ανακλαστής νετρονίων

Shannon entropy: Εντροπία Shannon

Slab geometry: Γεωμετρία απείρων πλακών

Source iteration: Επανάληψη πηγής

Subcritical reactor: Υποκρίσιμος αντιδραστήρας

Supercritical reactor: Υπερκρίσιμος αντιδραστήρας

Tally: Εικονικός ανιχνευτής

Vacuum boundary condition: Συνοριακή συνθήκη κενού

Variance reduction technique: Τεχνική μείωσης της διακύμανσης

Part VI

REFERENCES

BIBLIOGRAPHY

Balay, S., J. Brown, K. Buschelman, W.D. Gropp, D. Kaushik, M.G. Knepley, L.C. McInnes, B.F. Smith, and H. Zhang. *PETSc*. URL: www.mcs.anl.gov/petsc (cit. on pp. 55, 146).

Basile, D., M. Beghi, R. Chierici, E. Salina, and E. Brega (1999). *COBRA-EN: an upgraded version of the COBRA-3C/MIT code for thermal hydraulic transient analysis of light water reactor fuel assemblies and cores*. Tech. rep. 1010/1. Milano: ENEL-CRTN (cit. on pp. 41, 53, 59, 68, 129).

Bell, G.I. and S. Glasstone (1970). *Nuclear Reactor Theory*. New York, USA: Van Nostrand Reinhold Company (cit. on pp. 10, 11, 13, 16).

Bernnat, W., M. Matters, J. Keinert, and A. Conti (2000). *Application of the Monte Carlo Method for the Calculation of Safety Related Reactor Physics Parameter for Power Reactor with Consideration of Detailed Burn-up Distributions*. Tech. rep. IKE-6-2000. University of Stuttgart (cit. on p. 42).

Bernnat, W., M. Mattes, N. Guilliard, J. Lapins, W. Zwermann, I. Pasichnyk, and K. Velkov (2014). «Monte Carlo Neutronics and Thermal Hydraulics Analysis of Reactor Cores with Multilevel Grids.» In: *Conf. Supercomputing in Nuclear Applications and Monte Carlo (SNA & MC 2013)*. Paris, France (cit. on p. 39).

Bettencourt, M.E. (2013). «Fluidic and Neutronic Coupling of the Space Molten Salt Reactor Concept.» PhD thesis. The Ohio State University (cit. on p. 39).

Brown, F.B. (2008). *Fundamentals of Monte-Carlo Particle Transport*. URL: green.lanl.gov/resources.html (cit. on pp. 20, 22, 94–96).

Brown, F.H. (2006). «On the Use of Shannon Entropy of the Fission Distribution for Assessing Convergence of Monte Carlo Criticality Calculations.» In: Vancouver, British Columbia, Canada (cit. on p. 142).

Brown, F.H. (2009). «A Review Of Best Practices For Monte Carlo Criticality Calculations.» In: *Nuclear Criticality Safety Topical Meeting*. American Nuclear Society. Richland, WA (cit. on p. 142).

Cardoni, J. N. (2011). «Nuclear Reactor Multi-Physics Simulations with Coupled MCNP5 and STAR-CCM+.» PhD thesis. University of Illinois at Urbana-Champaign (cit. on p. 39).

Chaudri, K.S., Y. Su, R. Chen, W. Tian, G. Su, and S. Qiu (2012). «Development of Sub-Channel Code SACoS and Its Application in Coupled Neutronics/Thermal Hydraulics System for SCWR.» In: *Ann. Nucl. Energy* 45, pp. 37–45 (cit. on p. 39).

Cho, N.Z. and J. Chang (2009). «Some outstanding problems in neutron transport computation.» In: 41.4. Special issue, pp. 381–340 (cit. on pp. 33, 141).

Csomos, P. (2007). «Theoretical and Numerical Analysis of Operator Splitting Procedures.» PhD thesis. Eotvos Lorand University, Faculty of Science (cit. on p. 129).

Dahlquist G., Bjorck A. (1974). *Numerical methods*. Englewood, Cliffs, NJ: Prentise-Hall (cit. on p. 40).

Davison, B. (1958). *Neutron Transport Theory*. Great Britain: Oxford University Press (cit. on pp. 10, 11).

Dembo, R.S., S.C. Eisenstat, and T. Steihaug (1982). «Inexact Newton methods.» In: *SIAM J. Numer. Anal.* 19.400-408 (cit. on p. 84).

Duderstadt, J.J. and L. J. Hamilton (1976). *Nuclear Reactor Analysis*. New York (cit. on p. 97).

Duderstadt, J.J and W.R. Martin (1979). *Transport Theory*. New York, USA: Wiley (cit. on pp. 9, 10, 92).

Dufek, Jan (2007). «Accelerated Monte Carlo Eigenvalue Calculations.» In: *XIII Meeting on Reactor Physics Calculations in the Nordic Countries*. Vasteras, Sweden (cit. on pp. 33, 141).

Dulla, S., E.H. Mund, and P. Ravetto (2008). «The Quasi-Static Method Revisited.» In: *Prog. Nucl. Energy* 50, pp. 908–920 (cit. on p. 87).

Espel, F.P., M. N. Avramova, K.N. Ivanov, and S. Misu (2013). «New Developments of the MCNP/CTF/NEM/NJOY Code System-Monte Carlo Based Coupled Code for High Accuracy Modeling.» In: *Ann. Nucl. Energy* 51, pp. 18–26 (cit. on p. 39).

Gill, D.F. and Y.Y. Asmy (2009). «A Jacobian-Free Newton-Krylov Iterative Scheme For Criticality Calculations Based On The Neutron Diffusion Equation.» In: *Int. Conf. on Mathematics,Computational Methods and Re- actor Physics*. Saratonga Springs, New York (cit. on p. 141).

Gill, D.F., D.P. Griesheimer, and D.L. Aumiller (2017). «Numerical methods in coupled Monte Carlo and Thermal-Hydraulic calculations.» In: *Nuclear Science and Engineering* 185 (cit. on p. 31).

Goluoglu, K.L., C.L. Bentley, R.V. Demeglio, S. Goluoglu, R.E. Pevey, I. Suslov, and H.L. Dodds (1998). «Application of TDKENO for the analysis of criticality excursion experiments.» In: *Trans. Am. Nucl. Soc.* 77, pp. 145–146 (cit. on p. 87).

Grandi, G. M. (2009). «Effect of the Discretization and Neutronic Thermal Hydraulic Coupling on LWR Transients.» In: *The 13th International Topical Meeting on Nuclear Reactor Thermal Hydraulics (NURETH-13)*. Kanazawa City, Ishikawa Prefecture, Japan (cit. on p. 130).

Grieshemer, D. P., D.L. Aumiller, D.F. Gill, and J.W. Lane (2008). «An Integrated Thermal Hydraulic Feedback Method for Monte Carlo Reactor Calculations.» In: *Int. Conf. Physics of Reactors (PHYSOR 2008)*. Interlaken, Switzerland (cit. on p. 39).

Guoa, Z., J. Zhoua, D. Zhanga, K.S. Chaudri, W. Tiana, G. Sua, and S. Qiu (2013). «Coupled Neutronics/Thermal-Hydraulics for Analysis of Molten Salt Reactor.» In: *Nucl. Eng. Des.* 258, pp. 144–156 (cit. on p. 39).

Herman, B.R., B. Forget, and K. Smith (2015). «Progress toward Monte Carlo-thermal hydraulic coupling using low-order diffusion acceleration methods.» In: *Ann. Nucl. Energy* 84, pp. 63–72 (cit. on p. 145).

Hoogenboom, J.E., W.R. Martin, and B. Petrovic (2011). «The Monte-Carlo performance benchmark test-aims specifications and first results.» In: *Int Conf. Mathematics and Computational Methods Applied to Nuclear Science and Engineering*. Rio de Janeiro, Brazil (cit. on pp. 68, 115).

Hu, J. and Rizwan-Uddin (2008). «Coupled Neutronics and Thermal-Hydraulics Simulations Using MCNP and FLUENT.» In: *Trans. Am. Nucl. Soc.* 98, p. 606 (cit. on p. 39).

Imke, U., V. Sanchez, and R. Gomez (2010). «SUBCHANFLOW: an empirical knowledge based subchannel code.» In: Berlin, Germany, pp. 4–6 (cit. on p. 129).

Ivanov, A., V. Sanchez, and J.E. Hoogenboom (2012). «Single Pin Benchmark problem for coupled Monte Carlo-Thermal Hydraulics Analysis.» In: *PHYSOR 2012-Advances in Reactor Physics-Linking Research, Industry, and Education*. Knoxville, Tennessee, USA (cit. on pp. 43, 58).

Ivanov, A., V. Sanchez, R. Stieglitz, and K. Ivanov (2013). «High fidelity simulation of conventional and innovative LWR with the coupled Monte-Carlo thermal-hydraulic system MCNP-SUBCHANFLOW.» In: *Nucl. Eng. Des.* 262, pp. 264–275 (cit. on p. 42).

Ivanov, K. and M. Avramova (2007). «Challenges in Coupled Thermal-Hydraulics and Neutronics Simulations for LWR Safety Analysis.» In: *Ann. Nucl. Energy* 34.6, pp. 501–513 (cit. on p. 39).

Jeff-3.1.2. NEA data bank. URL: http://www.oecd-nea.org/dbforms/data/eva/evatapes/jeff_31 (cit. on pp. 57, 97, 113).

Joo, H.G., J.Y. Cho, K.Y. Kim, M.H. Chang, B.S. Han, and C.H. Kim (2004). «Consistent Comparison of Monte Carlo and Whole-Core Transport Solutions for Cores with Thermal Feedback.» In: *PHYSOR 2004 - The Physics of FuelCycles and Advanced Nuclear Systems: Global Developments*. American Nuclear Society. Chicago, Illinois (cit. on p. 39).

Knoll, D.A. and D.E. Keys (2004). «Jacobian-free Newton-Krylov methods: a survey of approaches and applications.» In: *J. Comput. Phys.* 193, pp. 357–397 (cit. on pp. 49, 51, 141).

Kotlyar, D., Y. Shaposhnik, E. Fridman, and E. Shwageraus (2011). «Coupled neutronic thermo-hydraulic analysis of full PWR core with Monte-Carlo based BGCore system.» In: *Nucl. Eng. Des.* 241, pp. 3777–3786 (cit. on p. 39).

Krane, K.S. (1988). *Introductory Nuclear Physics*. John Wiley and Sons (cit. on p. 9).

Lamarsh, J.R. (1966). *Nuclear Reactor theory*. Addison-Wesley Publishing Company (cit. on p. 9).

Lee, M.J., H.G. Joo, D. Lee, and K. Smith (2010). «Investigation of CMFD Accelerated Monte Carlo Eigenvalue Calculation with Simplified Low Dimensional Multigroup Formulation.» In: *International Conference on the Physics of Reactors*. American Nuclear Society. Pittsburgh, PA (cit. on p. 142).

Lee, M.J., H.G. Joo, D. Lee, and K. Smith (2014). «Coarse mesh finite difference formulation for accelerated Monte Carlo eigenvalue calculation.» In: *Ann. Nucl. Energy* 65, pp. 101–113 (cit. on p. 142).

Legrady, D. and J.E. Hoogenboom (2008). «Scouting the feasibility of Monte-Carlo Reactor Dynamics simulations.» In: *Topical Meeting on Reactor Physics*. American Nuclear Society. Interlaken, Switzerland (cit. on p. 93).

Lewis, E.E. and W.F. Miller (1993). *Computational Methods of Neutron Transport*. American Nuclear Society (cit. on pp. 14, 16).

Li, L. and K. Wang (2012). «The First-Principle Coupled Calculations Using TMCC and CFX for the Pin-Wise Simulation of LWR.» In: American Nuclear Society. Knoxville, Tennessee (cit. on p. 39).

Li, L., H. Yuan, and K. Wang (2012). «Coupling of RMC and CFX for Analysis of Pebble Bed-Advanced High Temperature Reactor Core.» In: *Nucl. Eng. Des.* 250, pp. 385–391 (cit. on p. 39).

Lux, I. and L. Koblinger (1991). *Monte Carlo Particle Transport Methods: Neutron and Photon Calculations*. CRC Press (cit. on pp. 19, 21, 22, 25, 26, 31).

MPI website. URL: http://www.mcs.anl.gov/research/projects/mpi/ (cit. on p. 96).

MacFarlane, R.E. and D.W. Muir (1999). *NJOY99.0 Code System for Producing Pointwise and Multigroup Neutron and Photon Cross Sections from ENDF/B Data*. Tech. rep. PSR 480/NJOY99.00. Los Alamos National Laboratory (cit. on p. 57).

Martin, W.R. (2012). «Challenges and prospects for whole-core Monte Carlo analysis.» In: *Nuclear Engineering and Technology* 44.2 (cit. on pp. 33, 87, 141).

Meulekamp, R. Klein and S.C. van der Marck (2006). «Calculating the effective delayed neutron fraction with Monte Carlo.» In: *Nucl. Sci. Eng.* 152 (cit. on p. 97).

OpenMC website. URL: https://mit-crpg.github.io/openmc/methods/random_numbers.html (cit. on pp. 96, 147).

Petit, O., F.X. Hugot, Y.K. Lee, C. Jouanne, and A. Mazzolo (2008). *TRIPOLI-4 User Guide*. Tech. rep. Report CEA-R-6169. Code available from OECD/NEA Data Bank. CEA (cit. on p. 97).

Ragusa, J. C. and V. S. Mahadevan (2009). «Consistent and accurate schemes for coupled neutronics thermal-hydraulics reactor analysis.» In: *Nucl. Eng. Des.* 239, pp. 566–579 (cit. on p. 130).

Romano, P.K. and B. Forget (2013). «The OpenMC Monte Carlo particle transport code.» In: *Ann. Nucl. Energy* 51, pp. 274–81 (cit. on pp. 40, 53).

Rowlands, G. (1962). «Resonance Absorption and NonUniform Temperature Distributions.» In: *Journal of Nuclear Energy* 16, pp. 235–236 (cit. on p. 59).

Saad, Y. and M.H. Schultz (1986). «GMRES: a generalized minimal residual algorithm for solving nonsymmetric linear systems.» In: *SIAM J. Sci. Stat. Comput.* 7, pp. 856–869 (cit. on pp. 51, 53, 56).

Seker, V., J. W. Thomas, and T. J. Downar (2007). «Reactor Simulation with Coupled Monte Carlo and Computational Fluid Mechanics.» In: *Joint Int. Topl. Mtg. Mathematics and Computation and Supercomputing in Nuclear Applications (M&C and SNA 2007)*. American Nuclear Society. Monterey, California (cit. on p. 39).

Shadid, J.S., R.S. Tuminaro, and H.F. Walker (1997). «An inexact Newton method for fully coupled solution of the Navier-Stokes equations with heat and mass transport.» In: *J. Comput. Phys* 137, pp. 155–185 (cit. on p. 84).

Sjenitzer, B.L. (2013). «The Dynamic Monte Carlo method for Transient Analysis of Nuclear Reactors.» PhD thesis. TU Delft (cit. on pp. 87–89, 91–94).

Sjenitzer, B.L. and J.E. Hoogenboom (2011). «A Monte-Carlo method for calculation of the dynamic behaviour of nuclear reactor.» In: *Prog. Nucl. Sci. Technol.* 2, pp. 716–721 (cit. on p. 87).

Sjenitzer, B.L. and J.E. Hoogenboom (2013). «Dynamic Monte-Carlo method for Nuclear Reactor Kinetics Calculations.» In: *Nucl. Sci. Eng.* 175, pp. 94–107 (cit. on pp. 87, 88).

Sjenitzer, B.L., J.E. Hoogenboom, and V.S. Espinoza J.J. Escalante (2015). «Coupling of dynamic Monte-Carlo with thermal-hydraulic feedback.» In: *Ann. Nucl. Energy* 76, pp. 27–39 (cit. on p. 130).

Truchet, G., P. Leconte, A. Santamarina, E. Brun, F. Damian, and A. Zoia (2015). «Computing adjoint-weighted kinetics parameters in Tripoli-4 by the Iterated Fission Probability method.» In: *Ann. Nucl. Energy* 85, pp. 17–26 (cit. on p. 97).

Tuminaro, R.S., H.F. Walker, and J.N. Shadid (2002). «On backtracking failure in Newton-GMRES methods with a demonstration for the Navier-Stokes equations.» In: *J. Comput. Phys.* 180, pp. 549–558 (cit. on p. 84).

Ueki, T. and F.H. Brown (2003). «Stationarity and Source Convergence in Monte Carlo Criticality Calculations.» In: ANS Topical Meeting on Mathematics & Computation (cit. on p. 142).

Ueki, T. and F.H. Brown (2005). «Stationarity Modeling and Informatics-Based Diagnostics in Monte Carlo Criticality Calculations.» In: *Nucl. Sci. Eng* 149, pp. 38–50 (cit. on p. 142).

Vazquez, M. (2014). «Monte Carlo Neutronics and Thermal-hydraulics coupling applied to Fast Reactors.» PhD thesis. Universidad Politechnica de Madrid (cit. on pp. 43–46, 87).

Waata, C.L. (2005). «Coupled Neutronics Thermal-Hydraulics Analysis of a High Performance Light-Water Reactor Fuel Assembly.» PhD thesis. University of Stuttgart (cit. on p. 39).

Walker, A. (2014). *FoX-A Fortran XML Library*. URL: `github.com/andreww/fox` (cit. on p. 55).

Wu, X. and T. Kozlowski (2015). «Coupling of System Thermal-Hydraulics and Monte-Carlo Code: Convergence Criteria and Quantification of Correlation Between Statistical Uncertainty and Coupled Error.» In: *Ann. Nucl. Energy* 75, pp. 377–387 (cit. on p. 39).

X-5 Monte Carlo Team, MCNP. *A general Monte Carlo N-Particle Transport Code, Version 5. Volume I: Overview and Theory*. la-ur-03-1987 ed. Los Alamos National Laboratory (cit. on p. 43).

Yeckel, A., L. Lun, and J.J. Derby (2009). «An approximate block Newton method for coupled iterations of nonlinear solvers: theory and conjugate heat transfer applications.» In: *J. Comput. Phys.* 228, pp. 8566–8588 (cit. on pp. 31, 51, 60).

Yeckel, A., L. Lun, and J.J. Derby (2010). «Multi-scale crystal growth computations via an approximate block Newton method.» In: *J. Cryst. Growth* 312, pp. 1463–1467 (cit. on pp. 31, 56, 60).

Zerkak, O., T. Kozlowski, and I. Gajev (2015). «Review of multi-physics temporal coupling methods for analysis of nuclear reactors.» In: *Ann. Nucl. Energy* 84, pp. 225–233 (cit. on p. 87).